Identification and understanding the mode of actions of inhibitors against *Vibrio Cholerae* pathogenesis

Thesis submitted for the degree of
Doctor of Philosophy (Science)
in
Life Science & Bio-technology

By

SUSHMITA KUNDU, M.Sc.
(JU Index No.: 141/21/Life Sc./27)

Department of Life Science and Biotechnology
Jadavpur University
Kolkata, India

2025

to...

Baba & Maa

आई. सी. एम. आर. - राष्ट्रीय जीवाणु संक्रमण अनुसंधान संस्थान
ICMR - NATIONAL INSTITUTE FOR RESEARCH IN BACTERIAL INFECTIONS
Formerly. ICMR-National Institute of Cholera and Enteric Diseases (ICMR-NICED)
स्वास्थ्य अनुसंधान विभाग, स्वास्थ्य एवं परिवार कल्याण मंत्रालय, भारत सरकार
Department of Health Research, Ministry of Health & Family Welfare, Govt. of India
WHO COLLABORATING CENTRE FOR RESEARCH AND TRAINING ON DIARRHOEAL DISEASES

CERTIFICATE FROM THE SUPERVISOR

This is to certify that the thesis entitled **"Identification and understanding the mode of actions of inhibitors against *Vibrio Cholerae* pathogenesis"** submitted by ~~Sri~~ / Smt. **SUSHMITA KUNDU** who got ~~his~~ / her name registered on **08.12.2021** for the award of Ph. D. (Science) Degree of Jadavpur University, is absolutely based upon her own work under the supervision of **Dr. SUSHMITA BHATTACHARYA** and that neither this thesis nor any part of it has been submitted for either any degree / diploma or any other academic award anywhere before.

Sushmita Bhattacharya 10.6.25

(Signature of the Supervisor date with official seal)

Dr. Sushmita Bhattacharya
Scientist C
Division of Biochemistry
ICMR - National Institute for Research in Bacterial Infections
Beliaghata, Kolkata - 700010

पी-33, सी.आई.टी. रोड, स्किम - XM, बेलियाघाटा, कोलकाता -700 010, पश्चिम बंगाल, भारत
P-33, C.I.T. Road, Scheme - XM, Beliaghata, Kolkata - 700 010, West Bengal, India
+91-33-2363 3373 (निदेशक/Director), +91-33-2370 1176, 5533 (प्रशासन/Administration) www.niced.org.in

DECLARATION

I do, hereby, declare that the work embodied in this thesis entitled **"Identification and understanding the mode of actions of inhibitors against *Vibrio Cholerae* pathogenesis"** submitted for the award of Doctorate of Philosophy (Science) in Life Science and Bio-technology, is the completion of work carried out under the supervision of Dr. Sushmita Bhattacharya, Scientist C, at the Division of Biochemistry, ICMR - National Institute for Research in Bacterial Infections, Kolkata. Neither this thesis nor any part of it has been submitted for either any equivalent degree/diploma or any other academic award elsewhere.

Date: 10/06/2025
Place: Kolkata

Sushmita Kundu

Signature of the candidate

(Sushmita Kundu)

Contents

Acknowledgement

Acknowledgement

As I approach the completion of my doctoral research, words fall short in expressing the depth of my gratitude to all those who have supported me, professionally and emotionally, throughout this journey.

I am profoundly grateful to my esteemed guide, Dr. Sushmita Bhattacharya of the Biochemistry Division at ICMR-National Institute for Research in Bacterial Infections (ICMR-NIRBI), Kolkata. Her unwavering support, insightful guidance, and encouragement have been instrumental in shaping my research and academic growth. Her mentorship has not only refined my research skills but also inspired me to explore beyond the confines of my immediate work, fostering a holistic scientific perspective.

I extend my sincere thanks to Dr. Santasabuj Das, Director of ICMR-NIRBI, for granting me the opportunity to pursue my research within this esteemed institution. I also appreciate the assistance and laboratory facilities provided by Dr. Nabendu Sekhar Chatterjee, Dr. Asish Kumar Mukhopadhyay, Dr. Hemanta Koley, Dr. Sandipan Ganguly, Dr. Provash Chandra Sadhukhan, Dr. Amit Pal, Dr. Ranjan Kumar Nandy, Dr. Mamta Chawla Sarkar, Dr. Moumita Bhowmick, and Dr. Sulagna Basu.

My heartfelt appreciation goes to my seniors, colleagues, and friends whose camaraderie and support enriched my research experience. Special thanks to Dr. Suman Das, Dr. Debjyoti Bhakat, Dr. Indranil Mondal, Dr. Anusuya Debnath, Dr. Deotima Sarkar, Dr. Priyanka Basak, and Dr. Uzma Khan for imparting invaluable knowledge in microbiology and molecular biology. Their continuous encouragement, especially during challenging times, was a beacon of motivation.

I am grateful to Dr. Prolay Halder, Dr. Sanjib Das for their assistance in animal experiments and to my lab friends, juniors and technical assistant, Ms. Priyanka Maitra, Mr. Sourin Alu, Mr. Abhishek Singh, Ms. Samhati Bhukta, Mr. Mrinmoy Das and Ms. Tarnima Basak, for their unwavering support and collaboration.

I deeply appreciate the contributions of our lab interns, Pritha, Mou, Gourab, and Ditam, whose enthusiasm and dedication were invaluable.

I would also like to acknowledge the support of my other seniors and colleagues, including Prosenjit da, Bipul da, Tanmoy da, Gautam da, Subhankar da, Subhoshree di, Tanushree di, Sraborni di, Tania di, Shreya di, Rituparna di, Punam di, Rudra Narayan da, Sangita di, Debjani di, Sreeja di, Puja di, Sanjeeb da, Tapas da, Maruf da, Ajanta di, Amrita di, Suparna di, Sohini, Bani di, Payel di, Sagnik da, Urbi di, Raina di and Deboleena. Their collective support and encouragement were pivotal in overcoming the challenges encountered during my research.

I am thankful to Animesh, Arpita di, Bibhas da and Anaswara for their technical assistance, particularly in confocal microscopy, electron microscopy sample preparations, and histological slide preparations.

The administrative staff of ICMR-NIRBI, Ananda da, Alam da, Malay da, Dipak da, Subho da, Prosenjit da, and Gouri di, have been consistently helpful, and I extend my sincere thanks to them for their support.

I gratefully acknowledge the Indian Council of Medical Research, Government of India, and Dr. Shin-ichi Miyoshi of Okayama University, Japan, for their financial support and assistance to our lab.

I am indebted to all the authors whose works I reviewed; their research provided the foundation upon which my thesis is built. I hope they will excuse any use of their illustrations, which have been appropriately cited and acknowledged for academic purposes.

I extend my gratitude to all my teachers from school, college, and university who have guided and inspired me throughout my educational journey.

Finally, I owe my deepest thanks to my family, my father, Mr. Jayanta Kundu, and my mother, Mrs. Meghna Kundu, whose sacrifices and unwavering support have been my pillars of strength. I also

cherish the blessings of my grandparents, Dadu and Dida, whose love and guidance continue to inspire me.

To everyone mentioned above and to those I may have inadvertently omitted, I offer my heartfelt thanks. Your contributions have been instrumental in helping me reach this significant milestone in my academic career.

I owe my deepest gratitude to all the authors of literatures reviewed, as their work provided me information and knowledge to carry out my thesis work.

I earnestly appeal them to please excuse me for using some of their illustrations with proper citation and acknowledgement in my writing for academic purpose only.

I would like to thank all my teachers in school, college and university who have allowed me to grow and learn with them.

This dissertation would not have been possible without the generous support, encouragement and patience of my family members during the course of this journey. I pay my sincere respect to my Baba, Mr. Jayanta Kundu and Maa, Mrs. Meghna Kundu who had to sacrifice a routine life in order to accommodate my long hour at the laboratory and who have been the unequivocal pillars of strength throughout my life. I thank the almighty and the departed souls of my grandparents, Dadu, Dida, for their eternal love and blessings which helped me sail through the tumultuous journey.

Finally, thank you everybody (including all the people I have mentioned above and if I have forgotten anyone else to talk about) for your help and cooperation, what made me reach this height in my career.

Dated: **Sushmita Kundu**

Place: Kolkata

Abbreviations

Abbreviations

°C	Degree Celsius
µg	Microgram
µl	Microlitre
µM	Micromolar
µm	Micrometre

A

A_{260}	Absorbance at 260 nm
A_{280}	Absorbance at 280 nm
Amp^R	Ampicillin resistant
APS	Ammonium Persulphate
ATP	Adenosine triphosphate
ATCC	American Type Culture collection

B

bp	Base pairs
BSA	Bovine serum albumin
BLAST	Basic local alignment search Tool

C

CFU	Colony forming unit
cm	Centimetre
CT	Cholera toxin
cDNA	Complementary DNA

D

DNA	Deoxyribonucleic acid
DMSO	Dimethyl sulphoxide
DMEM	Dulbecco's modified eagle's medium

E

EDTA	Ethylenediaminetetraacetic acid
ELISA	Enzyme-linked immunosorbent assay

F

FBS	Fetal Bovine Serum
FIC	Fractional inhibitory concentration

F (contd.)

FPKM	Fragment Per Kilobase Per Million Mapped Fragments

G

g	Gram
GM1	Monosialoganglioside
GFP	Green Fluorescent Protein

H

h	Hour
HRP	Horseradish peroxidase
HT-29	Human colorectal adenocarcinoma cell line

I

IPTG	Isopropyl-β-Dthiogalactopyranoside
IL	Interleukin

K

kb	Kilobase pairs

L

LA	Luria agar
LB	Luria-Bertani Broth
LDH	Lactate dehydrogenase

M

M	Molar
MeOH	Methanol
mg	Milligram
min	Minutes
ml	Millilitre
mm	Millimeter
mM	Millimolar
mRNA	Messenger RNA

M (contd.)

MIC	Minimum Inhibitory Concentration
MBC	Minimum Bactericidal Concentration
MHB	Mueller Hinton Broth
mA	milliampere

N

Ng	Nanogram
Ng	Nanometer
NBT	Nitro Blue Tetrazolium
NCBI	National Centre for Biotechnology Information
nM	Nanomolar

O

OD	Optical density

P

PAGE	Polyacrylamide gel electrophoresis
PBS	Phosphate buffer saline
PBS-T	Phosphate buffer saline-Tween 20
PCR	Polymerase chain reaction
PVDF	Polyvinylidene fluoride
PMSF	Phenylmethane sulphonylfluoride

Q

qRT-PCR	Quantitative RT-PCR

R

RNA	Ribonucleic acid
rpm	Revolution(s) per minute
RT	Reverse transcriptase

S

sec	Second(s)
SD	Standard deviation
SDS	Sodium dodecyl sulfate
Str	Streptomycin

T

TAE	Tris-HCl-acetate-EDTA
TBS	Tris Buffer Saline
TE	Tris-HCl-EDTA
TCBS	Thiosulphate-Citrate-Bile salt-Sucrose
TEMED	N, N, N', N'-tetramethyl ethylene diamine
TMB	3,3',5,5'-tetramethylbenzidine
TNF	Tumor necrosis factor

U

UV	Ultraviolet

V

V	Volt

W

w/v	weight by volume
WT	Wild-type

Chapter 1

Review of Literature

Review of Literature

1.1. Vibrio cholerae

Vibrios are Gram-negative, facultative anaerobes with non-spore-forming curved rods ranging from 1.04 to 2.06 µm in length and a single polar flagellum for motility (Syed &Klose et al., 2011) (***Fig.1.1***). The term '*vibrio*' refers to the characteristic vibratory motility, derived from the word 'vibrare' (meaning to vibrate). They are heterotrophic and they require several nutrients. They are non-encapsulated and are commonly found as saprophytic forms in saltwater, freshwater, and soil and can also occur as parasites and pathogens. In 1854, Italian anatomist Filippo Pacini identified *Vibrio cholerae* as the cause of cholera which was further established as the causative agent of cholera by Robert Koch (***Fig.1.2***). Koch isolated the bacteria from the rice water stools of cholera patients and termed them as "comma bacilli" because of their unique shape. The name *Vibrio comma* was used for several decades before being changed to *V. cholerae* (Lippi et al., 2014).

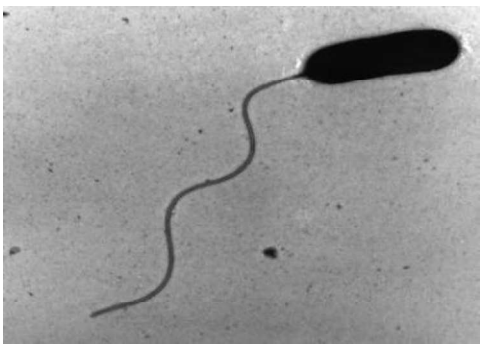

Fig.1.1. *V. cholerae* with its single polar flagellum [Source: (Syed &Klose et al., 2011)]

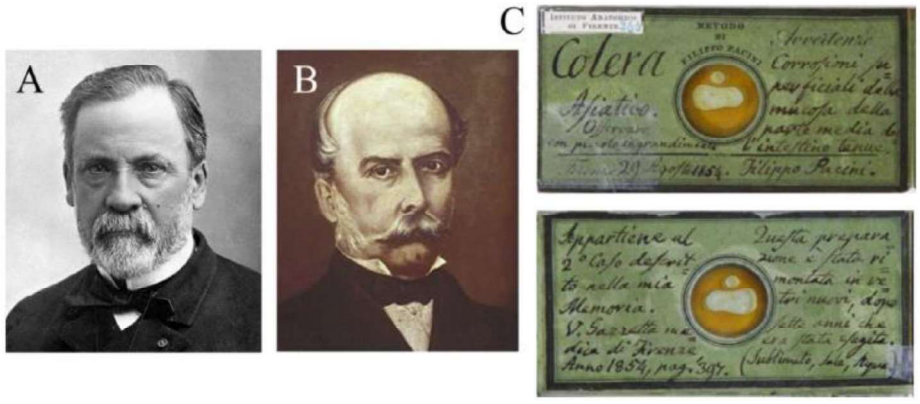

Fig.1.2. Early scholars whose contribution played a pivotal role in the discovery of the etiological agent of cholera. (A) Robert Koch (B) Filippo Pacini (C) Unpublished memoirs of Pacini's observation where the discovery of Vibrions was described step by step (University of Florence, Museum of natural History, Biomedical section).

1.2. Microbiology

V. cholerae (Type strain: ATCC 14035) belongs to the Vibrionaceae family, that also includes *Plesiomonas spp, Aeromonas, and Photobacterium* (Farmer, 2006; Watnick et al., 1999). The bacterium is oxidase-positive, reduces nitrate and it has a single, sheathed, polar flagellum that provides motility to it. *V. cholerae* is Gram-negative and non-acid fast and it stains readily with aniline dyes. *V. cholerae* thrives in temperature range between 16 °C to 40 °C and it is strongly aerobic organism. The organism can tolerate high alkalinity; with an ideal pH range of 7.6 to 8.2, which is helpful for *V. cholerae* selective culture in alkaline peptone water. It grows well in standard laboratory conditions. After overnight growth on nutrient agar, colonies appear as moist, translucent, round discs with a diameter of 1-2 mm. *V. cholerae* colonies and liquid culture had a distinctive odour. Addition of 1% sodium chloride (NaCl) stimulates the growth of *V. cholerae*. However, there is a distinction of *V. cholerae* from other *Vibrio* spp is that it can grow in nutritional broth without added NaCl, while the growth is inhibited by 7% NaCl.

1.3. V. cholerae Genome

The entire genomic sequence of *V. cholerae* El Tor N16961, a Gram-negative γ-Proteobacterium, is 4,033,460 base pairs (bp). *V. cholerae* has two circular chromosomes; chromosome I is 2.96×10^6 bp, while chromosome II has 1.07×10^6 bp (***Fig.1.3***). The genome of *V. cholerae* has 3885 putative open reading frames distributed in its two chromosomes. The majority of the genes required for growth and viability are located on chromosome I, however some genes found only on chromosome II are also regarded to be essential for normal cell function. The genomic sequence study of *V. cholerae* identified a large integron island (a gene capture system) on chromosome II (Baker-Austin et al., 2018; Hall et al., 1991). Chromosome 1 encodes DNA replication, repair, transcription, translation, cell wall biosynthesis, and core catabolic and biosynthetic processes. Again, most genes necessary for bacterial pathogenicity,

including those encoding the toxin co-regulated pilus, cholera toxin, lipopolysaccharide, and extracellular protein secretion machinery, are found on chromosome I.

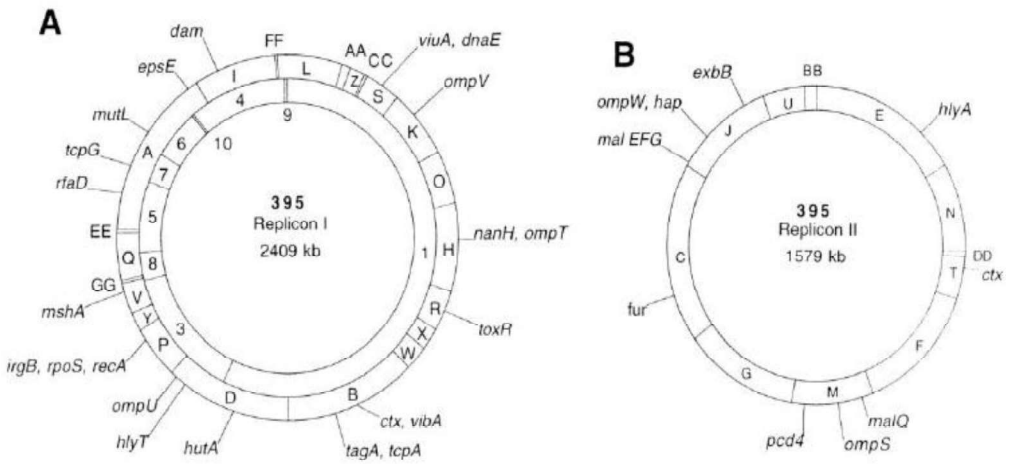

Fig.1.3. *V. cholerae* genome showing two (large and small) chromosomes. [Source: (Trucksis et al., 1998)]

1.4. Comparative Genomics

The majority of *V. cholerae* genes are similar to *E. coli* genes (1,454 ORFs). 499 *V. cholerae* ORFs exhibit the highest similarity to other *V. cholerae* genes, indicating duplication. The majority of duplicated ORFs encode products involved in regulatory functions, chemotaxis, transport, adhesion, transposition, pathogenicity, or unknown functions encoded by conserved hypothetical proteins. There are several duplications, with at least one of each ORF on each chromosome, indicating chromosome crossover. The duplication of genes related to scavenging (chemotaxis and solute transport) highlights the significance of these genes in *V. cholerae* biology, particularly its adaptability to various environments. El Tor strain N16961 has only one copy of the cholera toxin prophage, while other *V. cholerae* strains have several copies of this element (Davis et al., 1999; Mekalanos et al., 1983). Strains of the classical biotype include a second copy of the prophage that is localized on chromosome II (Trucksis et al., 1998). Thus, virulence genes are thought to be under selective pressure, affecting copy number and chromosomal location.

1.5. Genome evolution of choleragenic V. cholerae

The origin and evolution of many bacterial diseases are directly linked to genome fluidity. Bacterial evolution is mostly driven by horizontally acquired genetic elements that carry fitness traits. The genome of *V. cholerae* includes mobile genetic elements (MGEs) that are essential for disease progression and survival (Faruque et al.,2003; Vale et al.,2022). Only the O1 and O139 isolates of *V. cholerae* have been reported to be choleragenic out of 206 different serovers. Surprisingly, their two main virulence factors are encoded within mobile genetic components acquired through horizontal gene transfer. CT is encoded by the filamentous phage CTXϕ (Das et al., 2011). The CTXϕ phage can be transferred across *V. cholerae* strains, using TCP as the phage receptor. TCP is encoded on the *Vibrio* pathogenicity island-1. *V. cholerae* isolates harbouring other mobile genetic elements such as the SXT integrative conjugative element, VPI-2, and *Vibrio* seventh pandemic island-1 and -2 have been linked to virulence (Dalsgaard et al.,2000). The self-transmissible SXT element confers *V. cholerae* isolates resistance to streptomycin, sulfamethoxazole, and trimethoprim (Dalsgaard et al.,2000) (***Fig.1.4***).

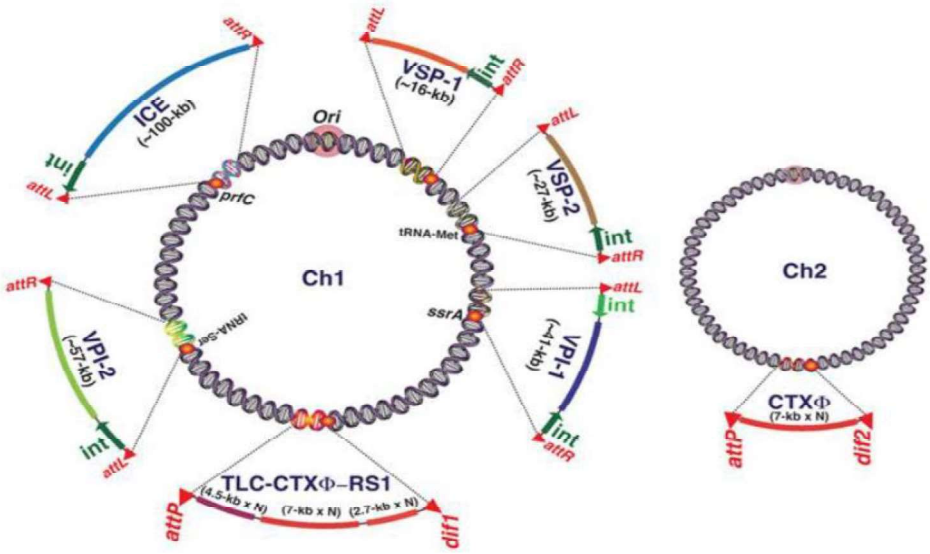

Fig.1.4. Distribution of genomic islands (GIs), prophages, and integrative conjugative element (ICE) in the genome of *V. cholerae* clinical isolates. Each of the genetic elements except prophages is linked with different mobility functions like integrase and repeat sequences. VPI-1, *Vibrio* pathogenicity island-1; VPI-2, *Vibrio* pathogenicity island-2; VSP-1, *Vibrio* seventh pandemic island-1; VSP-2, *Vibrio* seventh pandemic island-2; int, integrase [Source: (Pant et al., 2020.)].

VPI-2, is present only in pathogenic *V. cholerae* isolates, encodes genes for sialic acid transport and catabolism. Choleragenic vibrios have a competitive advantage

in the mouse intestine due to their ability to utilize sialic acid as a carbon source. VSP-1 encodes the transcription factor VspR, which is regulated by a ToxT small RNA (Faruque et al.,2003). VspR controls the expression of various VSP-1-encoded genes, including DncV, which encodes a new kind of dinucleotide cyclase. DncV produces a hybrid cyclic AMP-GMP molecule that promotes successful intestinal colonization and inhibits *V. cholerae* chemotaxis, which is associated with hyperinfectivity (Dalsgaard et al.,2000). VSP-2 has yet to be associated with a putative function. The four pathogenicity islands encoded by choleragenic *V. cholerae*, VPI-1, VPI-2, VSP-1, and VSP-2, can excise from their host's genome and form circular intermediates, potentially allowing virulence genes to be transferred to non-pathogenic *V. cholerae* strains (Banerjee et al., 2014).

Interestingly, some non-O1, non-O139 environmental isolates have been identified to have virulence genes. These strains may serve as reservoirs of virulence genes for non-choleragenic *V. cholerae* strains. The discovery that *V. cholerae* becomes naturally competent when it grows on chitin, and the existence of hybrid strains of *V. cholerae* that encode mobile genetic elements associated with virulence, suggest that the shell of copepods is a critical location for genetic material exchange, potentially leading to the emergence of novel pathogenic isolates (Dalsgaard et al.,2000; Vale et al.,2022).

1.6. Taxonomy

The genus *Vibrio* has many different species, only a few of which are pathogenic. *V. cholerae* is the classical example of a pathogenic species in this genus, with others including *V. parahaemolyticus, V. alginolyticus, V. mimicus, V. vulnificus*, and various non-agglutinable vibrios (Sakazaki, Gomez, 1967) (previously termed as NAG vibrios). The present systematic position of *V. cholerae* shown in ***Table 1.1*** (alongside),

Domain	Bacteria
Phylum	Proteobacteria
Class	Gamma proteobacteria
Order	Vibrionales
Family	Vibrionaceae
Genus	*Vibrio*
Species	*V. cholerae*

Table 1.1. Systematic position of *V. cholerae* [Source: (Garrity et al., 2005)].

1.7. Phenotypic fingerprinting and classification of V. cholerae

The phenotypic fingerprinting and classification scheme of *V. cholerae* can be divided into five major types, which include biochemical tests, serological classification, biotyping, phage typing, and anti-microbial susceptibility testing **(*Fig.1.5*).**

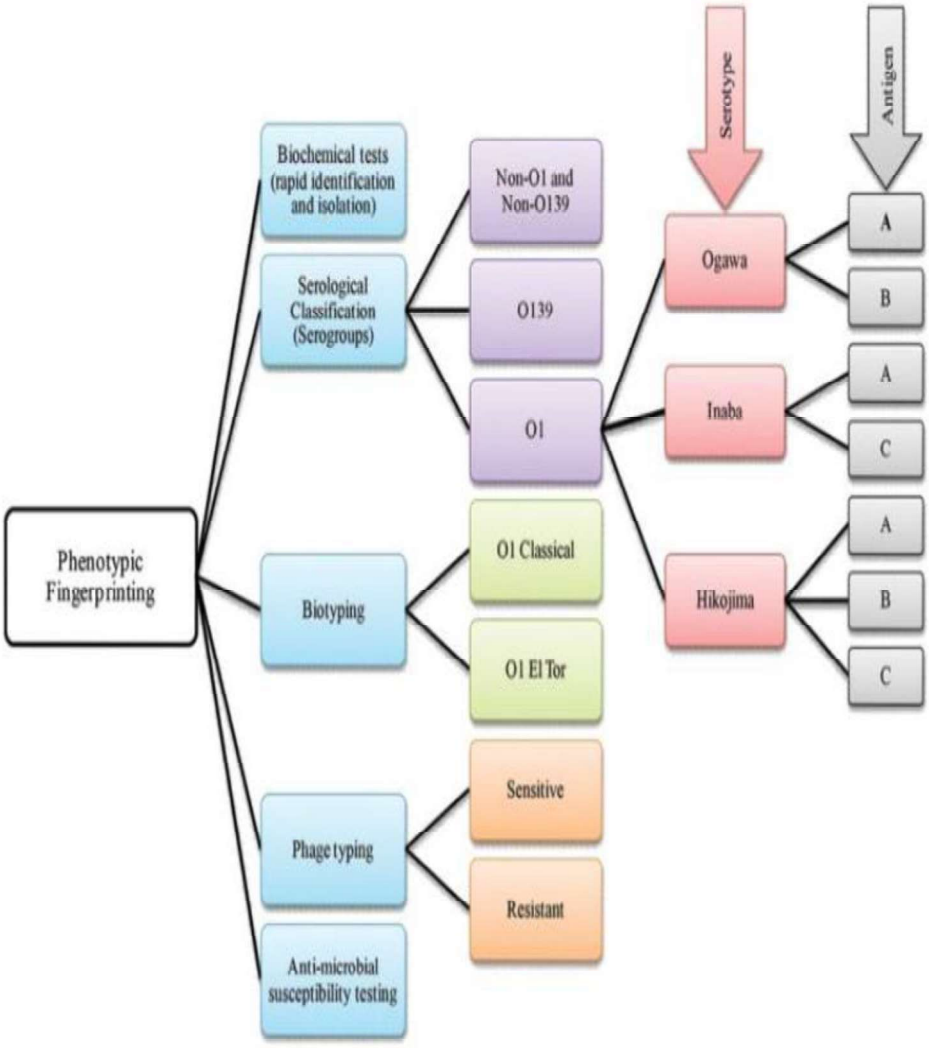

Fig.1.5. Scheme of classification of *V. cholerae* [Source: (Rahaman et al., 2015)].

1.7.1. Biochemical tests

V. cholerae and the other species belonging to the *Vibrio* and related genera can be differentiated for all practical purposes by a variety of simple tests as shown in *Table 1.2* (below) (Chatterjee et al., 2003; Kaper et al., 1995).

Tests	*V. cholerae*	Other Vibrio species	Enterobacteriaceae
Oxidase[1]	+	+ a	–
String test[2]	+	+/–	–
Acid from mannitol[3]	+	+/–	+/–
Acid from sucrose[3]	+	+/–	+/–
Lysine decarboxylase[4]	+	+/–	+/–
Ornithine decarboxylase[4]	+	+/–	+/–
Growth in 0% NaCl[5]	+	– b	–
Mol % G+C[6]	47-49	38-51	38-60

Table 1.2. Differentiation of *V. cholerae* from related species. **a**, except for *V. metchnikovii*; **b**, except for *V. mimicus*; positive response means: **1**, test for the presence in bacteria of certain oxidase that will catalyze the transport of electrons between donors in bacteria and a redox dye which is reduced to a deep purple colour; **2**, a mucoid string is formed when an inoculating loop is drawn slowly away from a drop of 0.5% aqueous solution of sodium deoxycholate in which a 24-h growth of the organism is suspended. The string is formed because the organisms are lysed, DNA released and the mixture made viscous; **3**, the ability of the organism to ferment the particular sugar added to the growth medium and produce acid which changes colour of an indicator (phenol red, bromothymol blue, etc.); **4**, the ability of the organism to decarboxylate a particular amino acid added to the growth medium with the liberation of carbon dioxide and change of colour of the medium to violet; **5**, the ability of the organism to grow in the absence of NaCl in the medium; **6**, DNA base composition given in terms of mol% G+ C [Source: (Garrity et al., 2005)].

1.7.2. Serological classification (Serotyping)

V. cholerae is classified based on the type of O-antigen present. O-antigen is a homopolymer formed of amino acid sugar D-perosamine (4-amino-4, 6-dideoxy-D-mannose), with the amino groups acetylated by 3-deoxy L-glycero-tetronic acid (Redmond, 1979; Kenne et al, 1982; Manning et al, 1994). Sakazaki and Shimada developed the most extensively used classification method for *V. cholerae* O-antigen (Sakazaki & Shimada, 1977). This typing system consists of 138 O-groups, which

includes the recently discovered O139 group (Shimada et al., 1994). The different O groups are referred to as serogroups or serovars *(Fig.1.6)*.

The O1 serogroup is divided into three antigenic forms: Inaba, Ogawa, and Hikojima. These antigenic types are referred to as serotypes or subtypes. *V. cholerae* O1's O antigen consists of three factors: A, B, and C. The A factor is likely a D-perosamine homopolymer, but the nature of the B and C factors is unknown (Martínez-Govea et al., 2001).

The differences among the subtypes are mainly quantitative; Ogawa strains produce A, B, and a small amount of C antigen, while Inaba strains exclusively produce A and C antigens (Shimada et al., 1994). The Hikojima subtype contains all three factors. The O139 strain combines O1 and non-O1 strains. This strain lacks O1 LPS production and some O1 antigen-related genes, but shares similarities with O1 El Tor strains in terms of cholera enterotoxin and toxin co-regulated pilus (TCP).

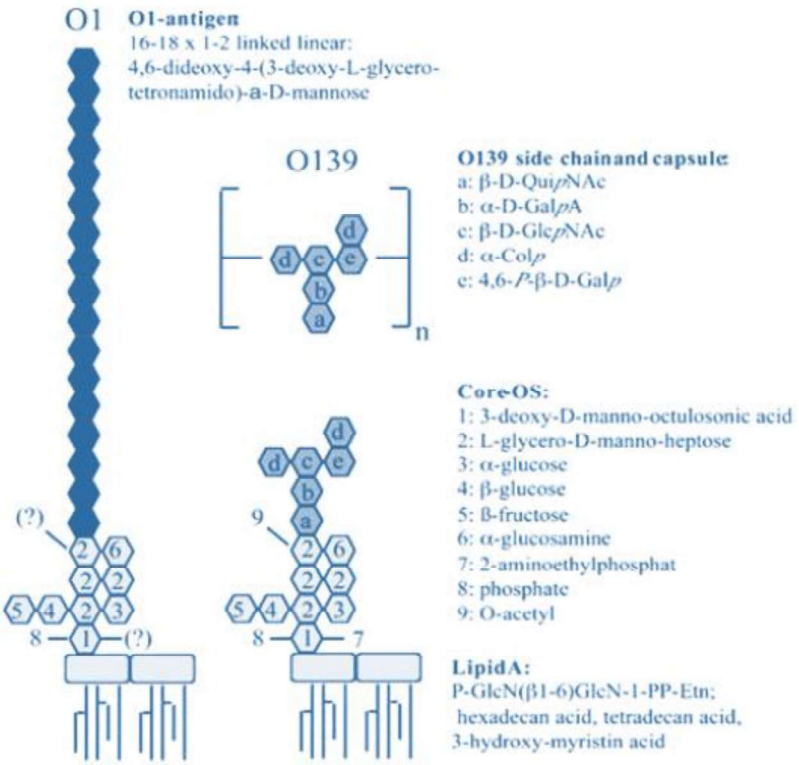

Fig.1.6. LPS structure of *V. cholerae* serogroup O1 and O139. The deduced structure of *V. cholerae* serogroup O1 (left) and O139 (right); shown are the different O antigen and capsule structures, and the similar core-OS and lipid A structures [Source: (Villeneuve et al., 2000)].

1.7.3. Biotyping

There are two biotypes of *V. cholerae* O1 strains: Classical and El Tor. The two biotypes are distinguished by hemolysis, hemagglutination, phage and polymixin B sensitivity, the Voges-Proskauer reaction, and genetic methods including multiplex PCR and RFLP (Alm & Manning, 1990) as shown in ***Table 1.3*** (below). Isolates from the sixth pandemic were classified as classical biotype. The seventh pandemic has primarily involved isolates of the El Tor biotype.

Tests used	Responses of the Two biotypes	
	Classical	El Tor
Hemolysis of sheep erythrocytes	−	+/ −
Agglutination of chicken erythrocytes	−	+
Voges-Proskauer reaction	−	+
Inhibition of Polymixin B (50-µg disk)	+	−
Lysis by Gr IV cholera phage	+	−
Lysis by FK cholera phage	+	−

Table 1.3. Differential characteristics of *V. cholerae* biotypes [Source: (Alm et al., 1990)].

1.8. Isolation and identification of V. cholerae

The Cary-Blair medium is utilized for transporting *V. cholerae* in stool samples. Alkaline peptone water (APW) is generally used as enrichment broth, while TCBS agar is the preferred plating medium for *V. cholerae* (***Fig.1.7***). TCBS agar is green when prepared. *V. cholerae* grows overnight (18-24 hours) and forms large (2-4 mm) yellow colonies with opaque centers and translucent peripheries. The yellow colour results from sucrose fermentation in the medium. *V. parahaemolyticus* and other organisms that are sucrose nonfermenting organisms, from green to blue-green colonies. Taurocholate Tellurite Gelatin Agar (TTGA), also known as Monsur's agar, can be used to isolate *V. cholerae* bacteria (Kaper et al., 1995). *V. cholerae* grows overnight on TTGA agar to form small opaque colonies with slightly dark centers. After 24 hours, the centers of the colonies darken and eventually turn "gunmetal" grey. In addition to the dark coloration caused by tellurite reduction, colonies have an opaque zone surrounding them that resembles a halo.

Refrigerating the plate for 15-30 min can intensify the halo effect caused by production of enzyme gelatinase. *Vibrio* colonies on MacConkey's agar initially appear colourless but turn reddish after prolonged incubation due to lactose fermentation. On blood agar, colonies are initially surrounded by a green zone that eventually clears due to hemolysis. *V. cholerae* can be detected using biochemical testing, direct specimen examination, agglutination in antisera against the O1 antigen, and DNA probes/PCR (Chakraborty et al.,2000).

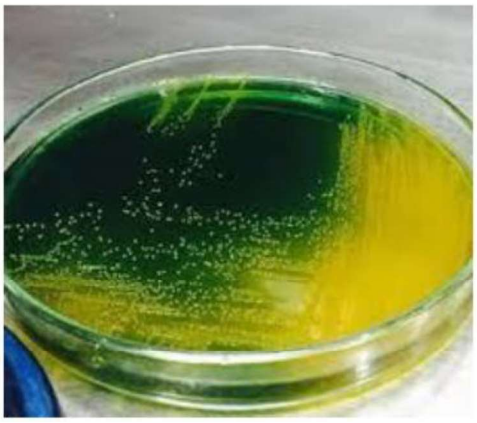

Fig.1.7. *V. cholerae* grown on TCBS agar, selective media for *V. cholerae*. Overnight colonies of *V. cholerae* on TCBS agar are large (2-4 mm) and yellow because of the fermentation of sucrose. They are characteristically round, smooth, glistening. and slightly flattened

1.9. Ecology and environmental reservoirs of V. cholerae

The ecology of *V. cholerae* plays an essential role in developing virulent and toxic variants. The salt requirement for *V. cholerae* development indicates that it originated at sea. The similarities between *Vibrio spp*. isolated from deep-sea hydrothermal vents in the East Pacific region indicate that this species is native to the deep sea (Colwell et al., 2004). Later *V. cholerae* genome sequencing investigations confirmed that *V. cholerae* is a versatile bacterium that can live in various habitats and infects the human gastro-intestinal tract (Vezzulli et al., 2010).

Virulence genes in *V. cholerae* strains from various serogroups disperse in aquatic habitats due to lateral movement of genetic material, creating an environmental reservoir for these genes (De et al., 2004). Phage infection causes *V. cholerae* to acquire antibiotic resistance genes, leading to new toxigenic variants and multi-drug resistance. Chitin, a major component of crustacean shells, has recently been found to induce the natural competence of *V. cholerae* (Lipp et al., 2002; Colwell et al., 2004).

V. cholerae, an aquatic pathogen, can be found in brackish, marine, and fresh waters. It can live for months or years in some aquatic habitats by interacting with zooplankton and other aquatic animals (Huq et al., 1983) (***Fig.1.8***). *V. cholerae* form

biofilms on the chitinous surface of copepods in its natural environment. Colwell and colleagues were the first to identify *V. cholerae* symbiotic relationship with aquatic planktons(Huq et al., 1983; Vezzulli et al., 2010). *V. cholerae* O1 and non-O1 serogroups were found on live copepods, primarily colonizing the mouth and egg sac. Low temperature and nutritional conditions can cause the Viable but Non-Culturable (VBNC) state, which can be resuscitated under favourable conditions. *V. cholerae* can bind to autotrophic species like phytoplankton and macroalgae, which can serve as a carbon source. Attachment to chitinous zooplankton and gelatinous egg masses (e.g., chironomids) provides nutrition and also promotes horizontal gene transfer (HGT). Fish and birds eat plankton or mussels that may contain *V. cholerae*, which might possibly spread the bacterium over long distances. In aquatic habitats, *V. cholerae* outcompetes other bacterial taxa associated with zooplankton such as γ-proteobacteria and *Vibrio* photobacterium, and it is commensal with copepods (Vezzulli et al., 2010). *V. cholerae* associated with zooplankton lives longer in seawater than free-living cells (Alam et al., 2017).

Relationship of *V. cholerae* with copepods provides benefits such as increased food availability, adaptation to environmental nutritional gradients, stress tolerance, and predator protection. The presence of Cladocerans, *Monia spp., Diphanosoma spp*., and the rotifer *Brachionus angularies* is linked to *V. cholerae* prevalence and cholera outbreaks. *V. cholerae* is associated with the copepod *Acatina tonsa*, which has a higher amount of *V. cholerae* than other co-occurring copepods (Alam et al., 2017).

1.10. Environmental factors that influence V. cholerae growth

The occurrence of *V. cholerae* in the environment is dependent on a number of environmental factors such as temperature, pH, salinity, and phyto- as well as zooplanktons (Lutz et al., 2013; Turner et al., 2014).

1.10.1. Abiotic factors

V. cholerae thrives in warm water (above 15°C), high pH (8-8.6), and 25 ppt salinity. Elevated temperature and pH enhance attachment to chitinous surfaces, while high salinity triggers melanin production for UV protection. Sunlight supports its spread via phytoplankton, but excessive evaporation raises salinity, limiting growth. While, heavy rainfall responsible for 51% of water-borne outbreaks, reduces salinity and alters ocean circulation, boosting *V. cholerae* growth, though excessive rain may sometimes lower cases. Huq et al, in the year 2005 mentioned increased cases of cholera with a decrease in pond or estuarine water depth. *V. cholerae* persistence is influenced by water conductivity, with higher conductivity in lakes and estuaries linked to increased cholera cases. Its adaptive traits allow survival without soluble iron by producing siderophores to absorb insoluble iron (Fe_2O_3).

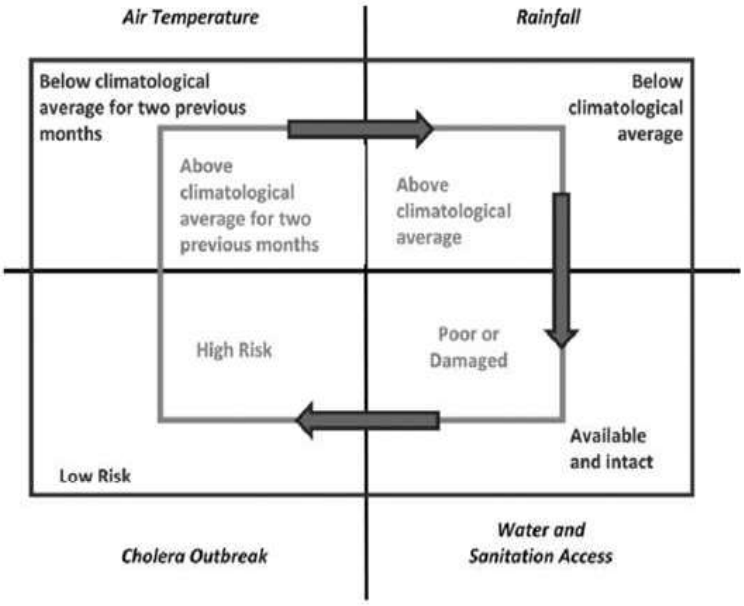

Fig.1.9. Environmental Factors Influencing Epidemic Cholera

[Source: Jutla et al., 2013].

Access to Fe^{3+} ions enhance survival, boosts proliferation, and affects cholera toxin (CT) expression (Castro-Rosas and Escartin 2000; Turner et al., 2009) (*Fig.1.9*)

1.10.2. Biotic factors

In spring and autumn, abundant phytoplanktons and zooplanktons provide chitinous surfaces for bacteria like *V. cholerae* to thrive. This could allow the organism's overall population to increase in the environment despite the presence of more bacterivorous predators (Huq et al., 2005; Lobitz et al., 2000).

1.11. Different roles played by V. cholerae in the environment

V. cholerae plays multiple functional roles in order to survive and adapt to their environment. Majority of these features are initiated or activated in the presence of chitin in the exoskeleton of zooplanktons in aquatic reservoirs. As already mentioned, *V. cholerae* uses them as an adhesion matrix, the other functions are interconnected to each other.

1.11.1. Chemotaxis

V. cholerae exhibits chemotaxis toward chitin oligosaccharides. Starving cells secrete chitinase, which breaks down chitin into (GlcNAc)n, creating a gradient that guides the cells to the chitin surface. Once attached, *V. cholerae* absorbs carbon and nitrogen from chitin (Cottingham et al., 2003).

1.11.2. Surface colonization

V. cholerae uses multiple attachment mechanisms to survive in nutrient-limited aquatic environments and acquire nutrients from biotic surfaces. It binds to surfaces like ship hulls, zooplankton, macroalgae, and floating aggregates. When near chitin, *V. cholerae* attaches via hydrophobic and ionic bonds. Key surface proteins involved in chitin binding include MSHA, GbpA, and ChiRP (Huq et al., 2005; Tamplin et al., 1990) (***Fig.1.10***).

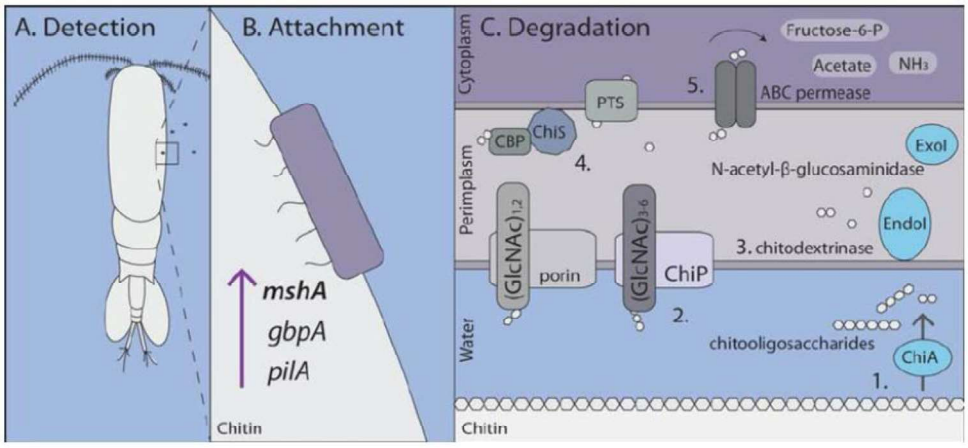

Fig.1.10. Utilization of chitin by *Vibrio spp.* (A) Chemotaxis towards chitin occurs when chitin oligosaccharides are detected by two independent receptors. (B) Attachment to chitin occurs via GbpA, MshA pilus, or chitin-regulated pilus encoded by pilA. (C) Attachment to chitin leads to extracellular secretion of chitinases such as ChiA, which degrade chitin polymer to chito oligosaccharides creating a gradient that guides the cells to the chitin surface [Source: (Erken et al., 2015)]

1.12. Motility

Vibrio spp. use flagella for motility, which is essential for chemotaxis, colonization, biofilm formation, and pathogenicity. *V. cholerae* and *V. alginolyticus* are monotrichous with a single polar flagellum, while other *Vibrio spp*. can be peritrichous or lophotrichous (Butler & Camilli, 2005; McCarter, 2004; Yildiz & Visick, 2009). The flagellum consists of the basal body, hook, and filament, assembled sequentially. In *V. cholerae*, over 50 genes regulate flagellar synthesis through a four-tier transcriptional hierarchy (Echazarreta & Klose, 2019). FlrA, the master regulator, activates class II genes with RpoN (σ54), while FlrB and FlrC regulate class III genes that encode structural components like FlaA, FlgB/G, FlgT, FlgP, FlgK, and MotY (Klose & Mekalanos, 1998; Syed et al., 2009) ***(Fig.1.11)***.

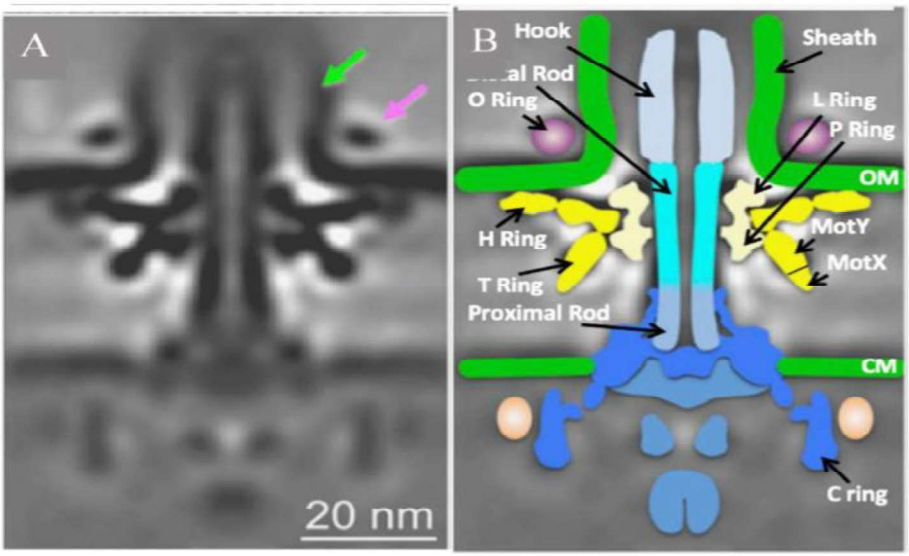

Fig.1.11. Structure of *V. cholerae* flagellar complex. (A) Electron microscopy rendering of the sheathed *Vibrio* flagellar complex. *Vibrio* specific attributes are depicted by arrows: the sheath (green arrow) and the O ring (purple arrow). **(B)** Schematic of the sheathed *Vibrio* flagellar complex [Source: (Echazarreta & Klose, 2019)].

1.13. Quorum sensing

Quorum sensing in *V. cholerae* regulates gene expression based on cell density through autoinducers (AIs), CAI-1 and AI-2. These AIs are detected by two-component receptors. At high cell density (HCD), quorum sensing activates hapR, which

promotes flagellum biosynthesis and represses biofilm and virulence factor production, allowing *V. cholerae* to disperse (Z. Liu et al., 2007). At low cell density (LCD) (Higgins et al., 2007; Ng et al., 2011; Wei et al., 2012), hapR is repressed, leading to biofilm formation and virulence factor expression for host attachment. Quorum sensing also promotes natural competence and horizontal gene transfer (HGT), enhancing survival and adaptation **(*Fig.1.12*).**

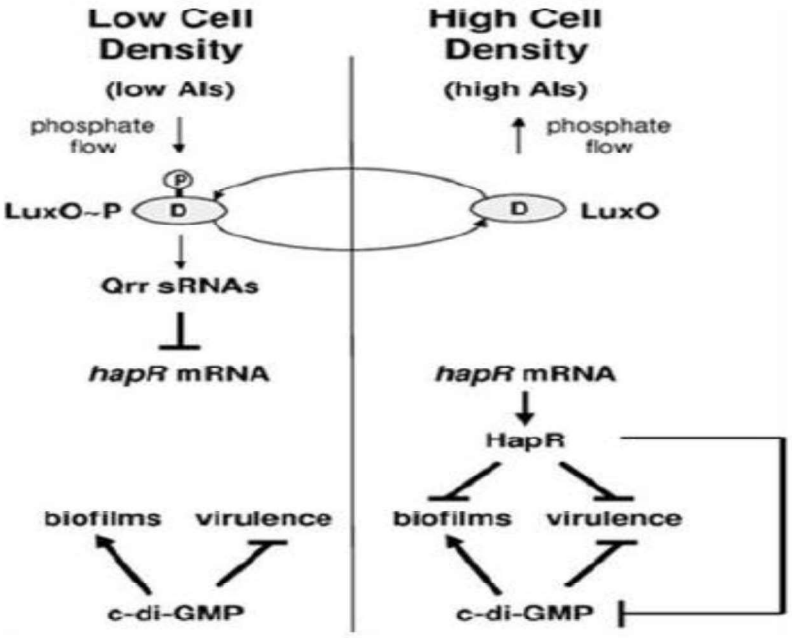

Fig.1.12. Simplified model of the interaction between Quorum sensing and c-di-GMP in the regulation of gene expression in *V. cholerae*. When concentrations of AIs are low (left side), the response regulator LuxO is phosphorylated, resulting in expression of multiple genes encoding the Qrr sRNAs that repress translation of the master transcriptional regulator, HapR. When concentrations of AIs are high (right side), LuxO is dephosphorylated which leads to termination of qrr expression. In the absence of the Qrr sRNAs, HapR is produced. HapR represses both biofilm formation and virulence factor expression. Like HapR, c-di-GMP also represses virulence factor expression, but unlike HapR, c-di-GMP activates biofilm formation. Here, HapR is shown to repress biofilm formation both directly (via controlling vpsT) and indirectly by reducing the levels of c-di-GMP [Source: (Waters et al., 2008)]

1.14. Biofilm formation

V. cholerae forms biofilms for survival in aquatic environments and host colonization. Biofilms enhance nutrient uptake, aid in acid resistance, and are regulated by

VpsR and VpsT (Watnick et al., 1999). Rugose colonies, with high VPS production, resist stress, phages, and protists ***(Fig.1.13)***.

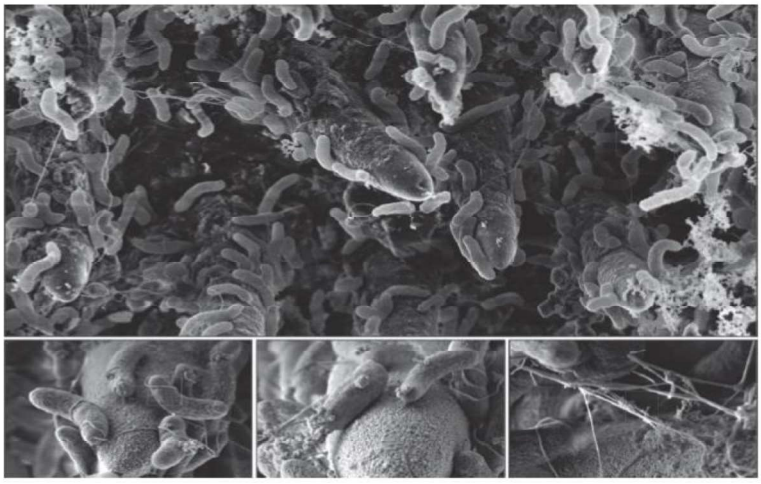

Fig.1.13. *V. cholerae* forms biofilms on chitinous surfaces. Biofilm forming *V. cholerae* cells bound to chitinous surfaces are illustrated in these scanning electron micrographs. In the lower row bacteria that are attached to chitinous spikes (porous-looking surface) are shown at higher magnification, which allows the visualization of detailed structures such as the polar flagellum, unidentified pili/fibers, and biofilm matrix components [Source: (Echazarreta & Klose, 2019)].

1.15. Transmission of V. cholerae from the environment to the host

Toxigenic strains of *V. cholerae* coexist with nontoxigenic strains in aquatic environments, a situation facilitated by biofilm formation on biological surfaces and the utilization of chitin as a source of carbon and nitrogen ***(Fig.1.14)***. When these bacteria, adapted to aquatic environments, are ingested through contaminated food or water, the toxigenic strains can colonize the small intestine. They then multiply and secrete cholera toxin, which is expelled back into the environment through the host's secretory diarrhea. The pathogens shed in the stool are in a transient hyper infectious state, which enhances the outbreak by facilitating transmission to subsequent hosts (Antonova et al., 2012; Lo Scrudato & Blokesch, 2012, 2013; Meibom et al., 2004).

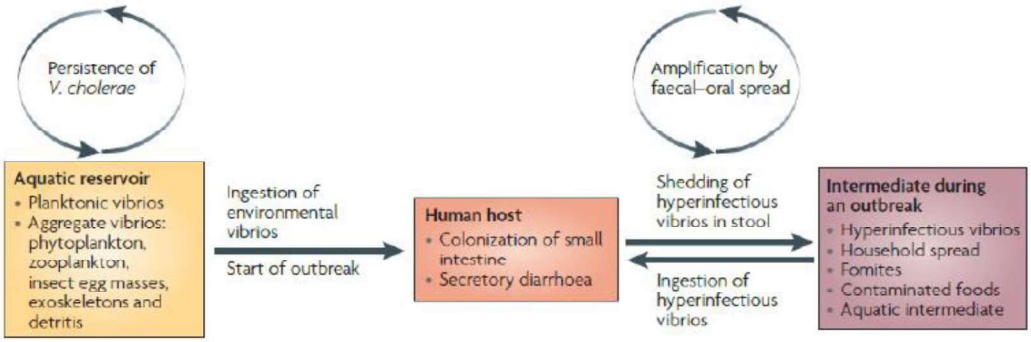

Fig.1.14. The life cycle of pathogenic *V. cholerae*. Toxigenic strains of *V. cholerae* persist in aquatic environments alongside non-toxigenic strains, aided by biofilm formation on biological surfaces and the use of chitin as a carbon and nitrogen source. On ingestion of these aquatic-environment adapted bacteria in contaminated food or water, toxigenic strains colonize the small intestine, multiply, secrete cholera toxin, and are shed back into the environment by the host in secretory diarrhoea. The stool-shed pathogens are in a transient hyper-infectious state that serves to amplify the outbreak through the transmission to subsequent hosts [Source: (Nelson et al., 2009)]

1.16. V. cholerae Pathogenesis

Cholera causes severe, watery diarrhoea that can quickly lead to dehydration and death in untreated patients. *V. cholerae* of the O1 and O139 serotypes cause epidemic cholera in humans. All other serotypes are classified as "non-O1" strains and are linked with sporadic cases of gastroenteritis (Taylor, Miller, et al., 1987) (*Fig.1.15*).

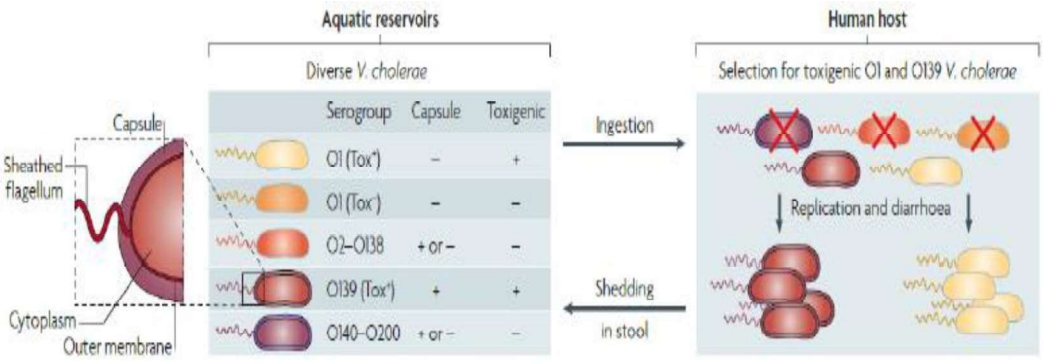

Fig.1.15. Phylogenetic relationship of *V. cholerae* strains. On the basis of the antigenicity of the O antigen component of the outer membrane lipopolysaccharide, more than 200 serogroups (O1–O200) of *V. cholerae* exist in aquatic environments. Only a subset of O1 and O139 serogroup strains are toxigenic (Tox+) and therefore capable of causing cholera when ingested; such strains are selected in the host environment, while the non-toxigenic (Tox–) strains are selected against. Different O antigen types are indicated by the colour of the outer membrane and sheathed flagellum. Capsules are present in a subset of strains [Source: (Boucher et al., 2016)].

V. cholerae infection occurs after consuming contaminated water or food. After passing through the stomach acid barrier, the organism colonizes the epithelium of the small intestine using toxin-coregulated pili and other colonization factors, such as haemagglutinins, accessory colonization factor, and core-encoded pilus, which are thought to play a role in pathogenesis **(*Fig.1.16*).**

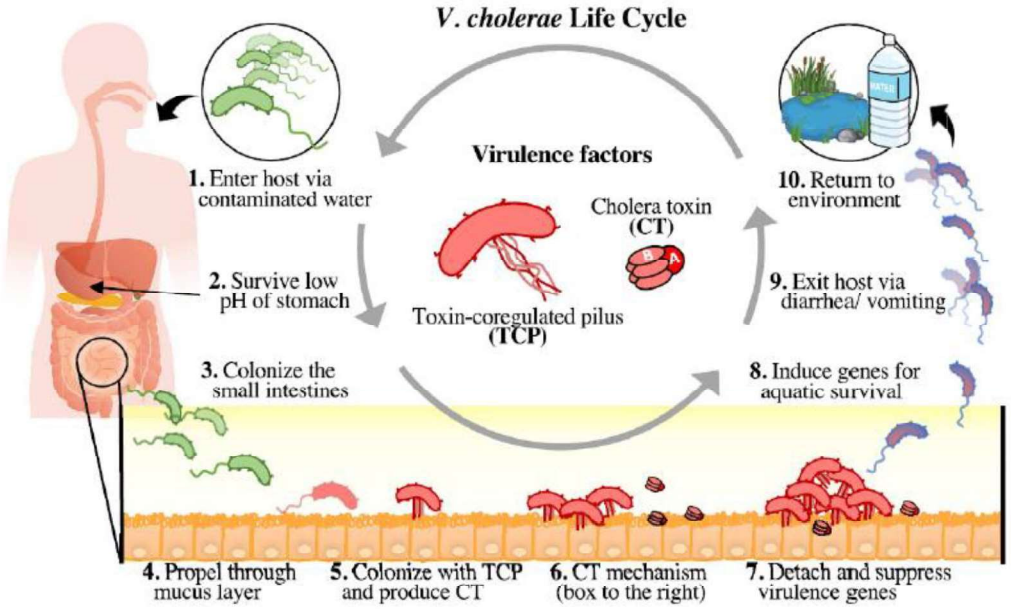

Fig.1.16. *V. cholerae* life cycle and pathogenesis. *V. cholerae* is a waterborne disease that causes cholera and is a human-restricted pathogen. (1) *V. cholerae* is introduced to the human host through contaminated water. (2) In the stomach, *V. cholerae* encounters a low pH environment. (3) To induce disease, *V. cholerae* colonizes the small intestine. (4) *V. cholerae* uses a single flagellum to propel through the mucus and reaches the epithelial surface. *V. cholerae* responds to host signals including bile, mucins, pH, and oxygen availability to induce virulence factors such as toxin coregulated pilus (TCP) and cholera toxin (CT). (5) TCP facilitates the colonization of the epithelial surface, and CT is produced, binding GM1 on the host cells. (6) CT is then endocytosed and induces cyclic AMP (cAMP). High cAMP levels cause the efflux of electrolytes and water, resulting in the characteristic watery diarrhea of cholera. (7) Microcolonies form and *V. cholerae* produces extracellular matrix components including Vibrio polysaccharides, biofilm proteins, and extracellular DNA. At high cell density, *V. cholerae* represses virulence genes through quorum sensing. (8) At this high density, *V. cholerae* detaches from the epithelial surface and migrates to the lumen. Genes required for transitioning into the aquatic environment are upregulated. (9) *V. cholerae* is excreted from the host in diarrheal stool and vomitus. (10) *V. cholerae* returns to the environment, where contamination of drinking water may infect another host. [Source: (Chac et al., 2021)]

1.17. Cholera: The fearsome waterborne infection

Cholera is an acute enteric infection caused by the bacterium *V. cholerae*, found in fecally contaminated water or food, often associated with insufficient access to safe water and proper sanitation. The World Health Organization estimates that 3-5 million people worldwide are afflicted with cholera each year, resulting in 100,000-120,000 deaths (WHO,2023).

Cholera is characterized by a sudden onset of acute watery diarrhoea, resulting in substantial fluid loss, sunken eyes, blue-grey skin, and death (***Fig.1.17***). The short incubation time (two hours to five days) can lead to explosive outbreaks, with a rapid increase in case numbers. Approximately 75% of those infected with cholera show no symptoms. However, the pathogens can remain in their faeces for 7-14 days before being released into the environment and potentially infecting others (Nelson et al.,2009).

1.18. Epidemiology of V. cholerae

Cholera originally appeared in India's Ganges Delta in the 19th century. Seven well-defined pandemics have been reported over the centuries, with an eighth pandemic suspected to have occurred since 1992 (***Table 1.4).*** The seventh pandemic, induced by the El Tor biotype of *V. cholerae* serogroup O1, started in Indonesia in 1961 and spread to Africa and the America in 1970 and 1991, respectively. In 1992, a new serotype, O139, emerged in India and spread rapidly to Bangladesh and other surrounding Asian countries. Recent cholera outbreaks have occurred in countries that have been free of the disease for decades.

Cholera Pandemics	Years	Countries
First	1817-1823	The first pandemic originated in the Ganges River delta in India. the disease spread to Southeast Asia, central Asia, Middle East, eastern Africa, and the Mediterranean coast.
Second	1829-1849	It started also in India and reached Russia by 1830 and spread in countries Finland, Poland, Europe, North America.
Third	1852-1859	Originated once again in India. It devastated large swaths of Asia, Europe, North America and Africa. In 1854, the worst year, 23,000 died in Britain alone.
Fourth	1863-1879	The fourth pandemic began in the Bengal region from which Indian Muslim pilgrims visiting Mecca spread the disease to the Middle East. From there it migrated to Europe, Africa and North America. Cholera claimed 90,000 lives in Russia in 1866.
Fifth	1881-1896	Again, originated in the Bengal region of India and swept through Asia, Africa, South America and parts of France and Germany.
Sixth	1899-1923	The sixth pandemic killed more than 8,00,000 people in India before moving into the Middle East, northern Africa, Russia and parts of Europe.
Seventh	1961 to present	Unlike other pandemics the seventh pandemic originated in Indonesia then spread to Italy, Africa and ravaged populations across Asia and the Middle East. Later an outbreak among Rwandan refugee in 1994, Zimbawe in 2008, Haiti in 2010 took many lives.

Table 1.4. History of cholera pandemics [Source: (Momba et al., 2018)].

In 2022, the World Health Organization (WHO) reported a near doubling of global cholera cases, with a total of 923,037 cases compared to 499,447 in 2021. While this increase might seem like a setback in cholera control, there is some positive news: the total number of reported cholera-related deaths fell by 36%, decreasing from 2,990 in 2021 to 1,911 in 2022. Notably, Africa recorded its lowest annual numbers of cases and deaths in the 21st century, and America reported the fewest cases and deaths since cholera was introduced to Haiti in 2010. In 2022, there was a significant rise in reported cholera cases, mainly attributed to the surge in Yemen (861,096 cases) (*Fig.1.19*), the Democratic Republic of the Congo (30,304 cases), and Mozambique (7,010 cases). These three countries together accounted for 97% of the globally reported cases that year (WHO, 2022) (*Fig.1.18*)

"Yemen has been devastated by a brutal war which started in early 2015. Twenty-one million people (75% of the total population) require humanitarian assistance, 7.3 million are severely food insecure, and 3.3 million are internally displaced. Moreover, the healthcare system is on the brink of collapse as more than 55% of health

facilities are partially functioning or destroyed. This situation, which is already a complex web of challenges, is exacerbated by the airport closures, severe shortages of fuel, food, drinking water and medication, and non-payment of public employees for 15 months since September 2016. In addition, sewage and drainage systems are clogged and rubbish is piled high in the streets. The underground water in all Yemeni cities is contaminated with sewage and treatment plants are not functioning because of lack of fuel and maintenance."

-excerpt from *Al-Mekhlafi Hesham*, 2018 on Recent cholera outbreak in Yemen.

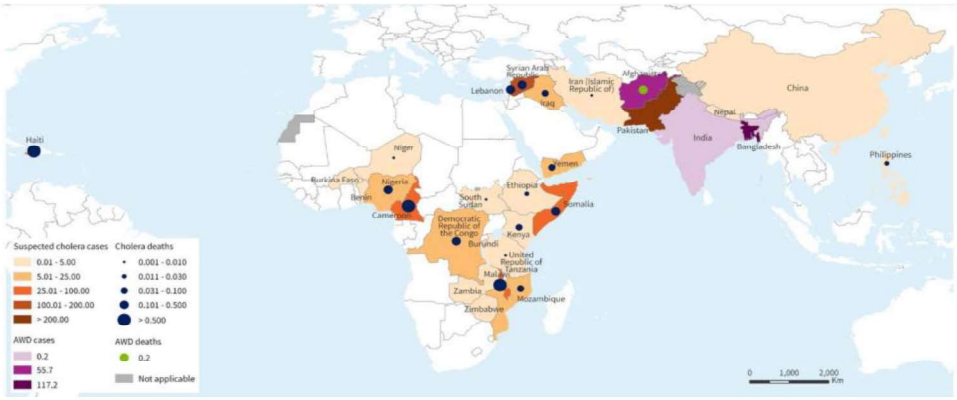

Fig.1.18. Countries reporting cholera cases and deaths in 2022 [Source: Weekly Epidemiological Record, WHO cholera report 2022]

Fig.1.19. (A) People gather to collect drinking water from a charity tanker truck in the midst of the cholera epidemic in Taiz governorate, **(B)** rubbish piles up on the main street in Sana'a city, and **(C)** cholera-infected patients lie on the ground while receiving treatment at a temporary health station in Hajjah governorate, Yemen. [Source: (Al-Mekhlafi, 2018)]

1.19. V. cholerae and human intestine

Ingestion of water or food contaminated with *V. cholerae* is the primary route by which humans acquire this bacterium. After ingestion, *V. cholerae* must survive the harsh acidic conditions of the stomach to establish an infection. It then needs to penetrate the mucus lining that protects the intestinal epithelial cells. Because *V. cholerae* is sensitive to acid, a relatively high infectious dose is necessary to cause an infection in humans, typically ranging from 10^6 to 10^{11} CFU/ml. Once in the human intestine, *V. cholerae* adheres to and colonizes the intestinal epithelial cells, eventually producing cholera toxin (CT), which leads to the symptoms of cholera (Cash et al., 1974). During the transition from aquatic environment to the human intestine, *V. cholerae* encounters low pH conditions of gastric juice (Cash et al., 1974). The cells that overcome the gastric barrier further colonize the intestinal epithelial cells, eventually producing CT and causing cholera.

1.20. Mechanisms of intestinal colonization

V. cholerae pathogenesis is complex and involves interactions between both host and bacterial factors. Once *V. cholerae* is introduced into the intestinal lumen, it must attach to the intestinal lining (Valiente et al.,2018; Chiang et al.,1999). This initial attachment is essential for the bacteria to establish disease. Various colonization factors have been identified as important adhesion molecules that interact with the surface of host cells. For *V. cholerae* to successfully cause disease, it must colonize the small intestinal epithelium. Several components contribute to this colonization process, including bacterial pili, hemagglutinins, an accessory colonizing factor, porin-like proteins, rfb-encoded enzymes, and a chitin-binding protein (Lloyd et al.,2023).

1.21. Impact of host factors

To survive and cause infection, *V. cholerae* must pass certain barriers after ingestion. Additionally, several factors assist the bacterium in colonizing and causing cholera. For infection, *V. cholerae* must survive the acidic gastric barrier (pH 2), requiring a high infectious dose (10^6 to 10^{11} CFU/ml). It thrives in the small intestine

(pH 7.6), where GbpA, a chitin-binding protein, helps it to bind mucin, a glycoprotein coating the intestinal epithelium. This GbpA-mucin interaction enhances colonization. However, recent studies show that mucins can restrict *V. cholerae* colonization, especially in the proximal small intestine, where the mucus layer is thicker (Kaper et al., 1995).

According to previous reports, control of *V. cholerae* virulence gene expression is mediated by two opposing ToxT effectors *in vivo*. Bicarbonate enhances ToxT activity, whereas the unsaturated fatty acid components of bile, such as linoleic acid, inhibit ToxT activity. The concentrations of these two effectors differ between the luminal fluid and within the mucus layer that protects the epithelium. Bile and its components are at high concentrations in the lumen but, due to their relatively large size, are at very low concentrations within the mucus layer (A. Chatterjee et al., 2007; Gupta & Chowdhury, 1997). Bicarbonate is present both in the lumen, where it buffers stomach acid, and within the mucus layer, via secretion by the epithelial cells. ToxT of *V. cholerae* is inactivated by bile in the lumen, which permits the bacteria to retain motility and enter the mucus layer so that they can colonize the epithelial surface (Abuaita & Withey, 2009). The production of TCP and CT prior to entry into the mucus layer would be deleterious, as the bacteria would aggregate in the lumen and will be unable to colonize. Thus, these two signals that act inversely on the binding affinity of ToxT for its DNA binding sites are able to direct *V. cholerae* to the optimal site for colonization (Kaper et al., 1995) **(*Fig.1.20*).**

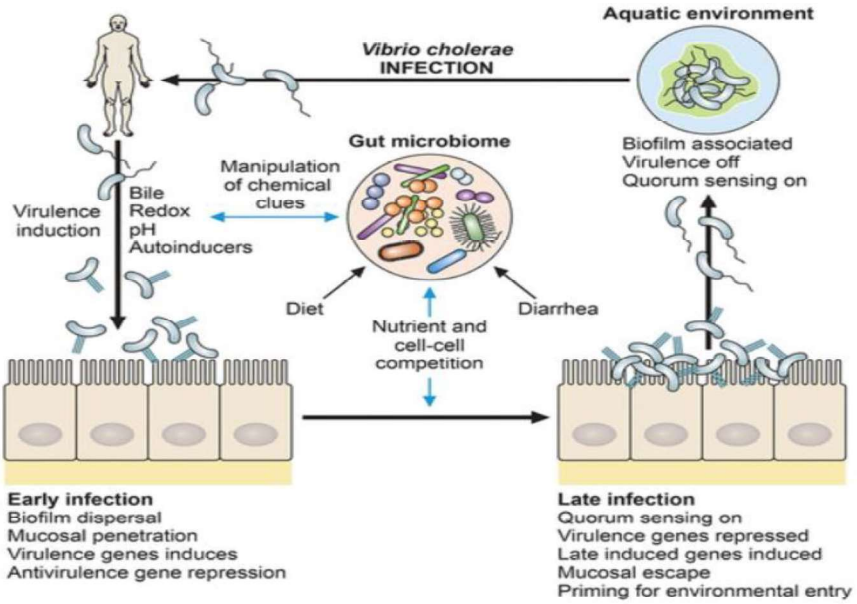

Fig.1.20. Interaction of the gut microbiome with environmental signalling during *V. cholerae* life cycle. The microbiome is shaped on individual basis by diet, microbial exposure, and history of gut insults such as diarrhoea, malnutrition, and inflammation. Commensal microbial functions influence chemical cues used by *V. cholerae* to time gene expression during early vs late infection states [Source: (Hsiao et al., 2020)].

1.22. Virulence factors of V. cholerae

In *V. cholerae*, the two main factors responsible for cholera disease are cholera toxin (CT) and the toxin co-regulated pilus (TCP). A filamentous bacteriophage, known as CTXΦ, carries genes that encode cholera toxin (Spangler et al.,1992). Additionally, a 41-kb pathogenicity island located on the chromosome encodes the toxin co-regulated pilus (TCP). Cholera toxin, which is encoded by the *ctxAB* genes found in the lysogenic CTXΦ, is a potent enterotoxin that belongs to the A-B toxin type (Cassel et al.,1978). The toxin consists of one enzymatic A subunit and five receptor-binding B subunits. It is secreted by a bacterial type II secretion system. After secretion, the B subunit (CT-B) binds to ganglioside GM1 receptors located in lipid rafts on the plasma membrane of target cells. The entire toxin complex is then endocytosed by the cell and transported through the Golgi apparatus to the endoplasmic reticulum. Here, the A subunit (CT-A) dissociates from the toxin complex. CT-A is subsequently transported to the cytoplasm of the target cell, where it ADP-ribosylates a GTP-binding protein that activates adenylate cyclase. The event causes an increase in intracellular cAMP levels, which disrupts the movement of electrolytes in the epithelial cells

(Field et al.,2003). This disruption results in increased secretion of NaCl, which further drives the osmotic movement of water into the intestinal lumen. As a result, this leads to watery diarrhea, a hallmark of cholera (Field et al.,2003).

1.23. Regulation of Virulence factors

Many virulence genes of *V. cholerae* are regulated co-ordinately in response to environmental signals. While the specific conditions affecting toxin production in the human intestine are not fully understood, research studies have identified several factors that increase toxin production. These factors include low temperatures (between 25ºC and 30ºC), osmolarity (with NaCl concentrations of 50 to 60 mmol), high aeration, acidic pH (around 6.5), and the presence of certain amino acids (such as asparagine, serine, glutamate, and arginine), as well as phosphate and trace elements

1.23.1. ToxR regulon

The transcription of virulence genes from both the CTXφ and VPI is meticulously orchestrated by a regulatory cascade known as the "ToxR Regulon." Despite the historical reference to ToxR as the primary regulator, it does not directly control the expression of cholera toxin (CT) and toxin-coregulated pilus (TCP) (Taylor et al., 1987). Instead, this role is fulfilled by the transcriptional activator ToxT. Various regulatory proteins and factors modulate the cascade to ensure ToxT is expressed only under optimal environmental conditions (Dirita et al., 1992)

ToxR, along with TcpP, regulates the transcription of *toxT*. The *toxR* gene is present in all *Vibrio* species as part of the ancestral genome and is constitutively expressed. In contrast, *tcpP* is located on the *Vibrio* pathogenicity island (VPI), found only in pandemic strains, and is expressed solely under virulence-inducing conditions. ToxR is an integral membrane regulatory protein belonging to the OmpR family, characterized by a cytoplasmic winged helix-turn-helix DNA-binding domain (Matson et al., 2007).

ToxS, another integral membrane protein, enhances ToxR dimerization, which is essential for full ToxR activity and subsequent initiation of *toxT* transcription. At the *toxT* promoter, ToxR is thought to act as an enhancer of TcpP binding (Morgan et

al., 2011). Although TcpP can directly interact with RNA polymerase, ToxR is necessary for activating *toxT* transcription. DNase I footprinting has shown that ToxR/S binds to the *toxT* promoter between -100 and -69 relative to the transcriptional start site (Krukonis et al.,2000).

ToxR also regulates the transcription of the outer membrane porins OmpU and OmpT. It upregulates *ompU*, which encodes a porin that protects against the harmful effects of bile, and this regulation is further enhanced in the presence of bile. Conversely, ToxR downregulates *ompT*, which is expressed in environmental and nutrient-limited conditions (Goss et al.,2013; Beck et al., 2004).

TcpP, in collaboration with ToxR/S, regulates *toxT* transcription through its interaction with TcpH, another membrane protein. TcpH stabilizes TcpP, preventing its rapid degradation by the metalloprotease YaeL. However, in non-permissive conditions for virulence, TcpP degradation occurs even in the presence of TcpH. YaeL targets the periplasmic domain of TcpP and remains active in non-virulence inducing environments (Njoroge et al.,2012).

Taurocholate, a bile salt found in the intestine, induces TcpP dimerization, thereby enhancing its activation potential for *toxT*. TcpP/H binds to the *toxT* promoter between -51 and -32 relative to the transcriptional start site (Manneh-Roussel et al.,2018). TcpP alone can activate *toxT* expression when overexpressed due to its DNA-binding specificity. However, *tcpPH* expression is not constitutive. Instead, it is regulated by the transcriptional regulators AphA and AphB. AphA binds to the *tcpPH* promoter between -101 and -71, while AphB binds between -78 and -43 (Bogard et al., 2012; Behari et al.,2001).

AphA is a dimer and a member of the winged helix transcription factor superfamily, while AphB is a LysR-type regulator protein. AphB directly interacts with AphA on the DNA to activate *tcpPH* and changes conformation in response to pH and oxygen level changes (Bogard et al., 2012). TcpPH is also negatively regulated by the cAMP receptor protein (CRP) and PepA. CRP, typically involved in metabolism, can bind to the promoter and repress expression by competing for the same binding sites as AphA and AphB (Bogard et al., 2012). The mechanism of PepA repression remains unclear, but it is known that PepA responds to changes in pH and temperature. Under

non-permissive conditions for virulence, PepA represses *tcpPH* transcription (Skorupski et al.,1997) (*Fig.1.21*)

.

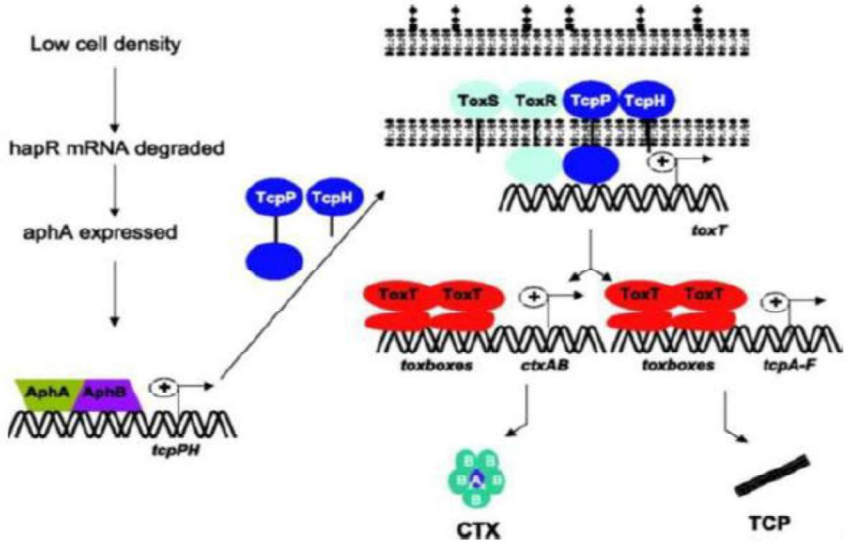

Fig.1.21. Schematic representation of ToxR regulon showing the different components regulating the production of two major virulence determinants CT and TCP [Source: (Matson et al., 2007)]

1.24. The Virulence Gene Transcriptional Activator ToxT

ToxT is a 32 kDa protein composed of 276 amino acids and serves as the primary virulence gene regulator for *ctxAB* and *tcp* (Champion et al., 1997; Hulbert & Taylor, 2002). It belongs to the AraC/XylS family of proteins, with homology observed in the C-terminal domain (CTD). The CTD, spanning amino acids 170-276, is approximately 100 amino acids long and contains two helix-turn-helix DNA-binding motifs. A small linker region of ten amino acids separates the CTD from the N-terminal domain (NTD), which extends from amino acids 1-160 (Lowden et al., 2010). While the NTD lacks sequence similarity to other members of the AraC/XylS family, the crystal structure of ToxT reveals secondary structural homology to AraC, despite minimal amino acid identity.

ToxT not only activates transcription of the genes encoding cholera toxin (CT) and toxin-coregulated pilus (TCP), but also other virulence genes, including *acfA, acfD, aldA, tagA, tcpI*, and the regulatory RNAs *tarA* and *tarB* (Withey et al., 2005).

ToxT achieves this by binding to 13 base pair degenerate sequences called toxboxes, each containing a poly-T tract at the 5' end of the binding site. These toxboxes are located upstream of the -35-promoter element, which is part of the RNA polymerase binding site. This positioning suggests that ToxT directly interacts with the RNA polymerase α subunits to stimulate transcription (Matson et al., 2007).

The arrangement of toxboxes varies depending on the target gene. For *tcpA, ctxAB,* and *tarA*, there are two toxboxes arranged as direct repeats (Richard et al., 2010; Withey et al., 2006). For *acfA, acfD, tagA,* and *tcpI*, the toxboxes are arranged as inverted repeats, with the divergently transcribed *acfA* and *acfD* sharing the same toxboxes. In contrast, *aldA* contains only a single toxbox (Withey et al., 2005). Additionally, ToxT can activate its own transcription through its role in activating the *tcp* operon, where the *toxT* gene is located. This self-regulation allows for finer control over virulence gene expression.

Members of the AraC/XylS family can function as either dimers or monomers. For example, AraC, RhaS, and RegA act as dimers, while MarA, SoxS, and Rob act as monomers. The ability of ToxT to function as either a monomer or a dimer remains controversial. Since most ToxT-activated promoters contain two toxboxes, it is hypothesized that ToxT functions as a homodimer. However, *aldA*, which contains only a single toxbox, suggests that dimerization is not required for ToxT to activate transcription (Richard et al., 2010; Withey et al., 2006).

Studies using the LexA dimerization assay and bacterial two-hybrid systems indicate that the NTD of ToxT is involved in dimerization (Wood et al., 1999). However, full-length, intact ToxT has never been observed to dimerize, and the crystal structure of ToxT depicts a monomeric protein. Virstatin, a small molecule inhibitor of virulence gene expression, is proposed to reduce ToxT dimerization (Shakhnovich et al., 2007). Interestingly, ToxT can bind to promoters as a monomer, as demonstrated in DNA-footprinting experiments at the *tcpA* promoter (Withey et al., 2005). Even when the spacing between toxboxes was increased, ToxT could still protect the DNA. However, when the spacing was significantly altered, ToxT failed to activate transcription, indicating that the distance between toxboxes is critical for full activation. Despite extensive research, further studies are needed to fully understand the role of dimerization in ToxT function **(*Fig.1.22*).**

.

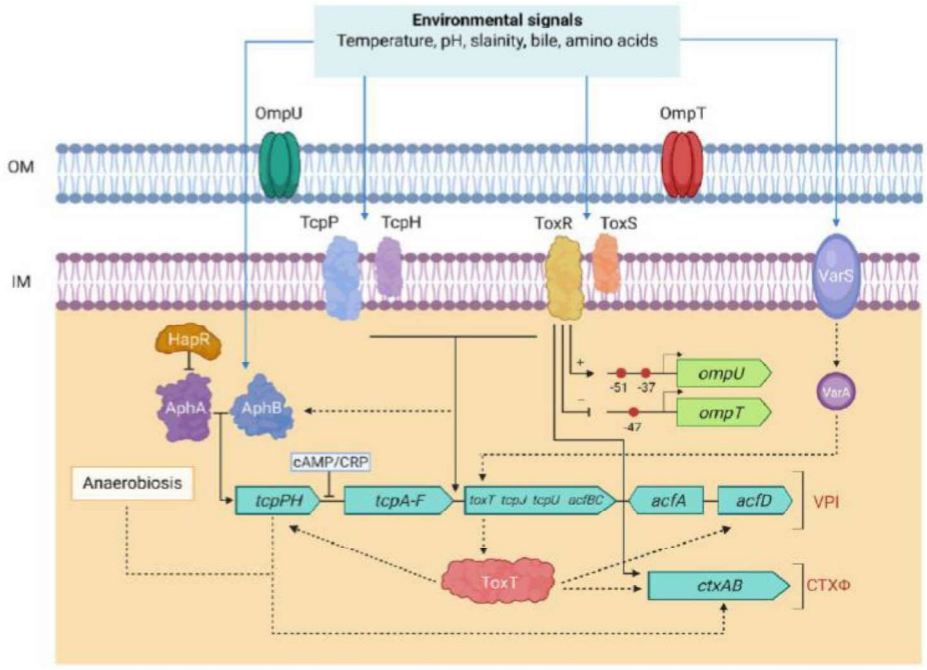

Fig.1.22. Regulation model of ToxT-mediated virulence genes in *V. cholerae*. TcpP/TcpH and ToxR/ToxS function together in activating transcription of *toxT*. ToxR and TcpP need accessory proteins (ToxS and TcpH, respectively) for maximal activity. ToxT initiates transcription of the full *tcp* operon, *ctxAB*, and *acf*. AphA and AphB activate transcription of the *tcpPH* operon in response to environmental conditions. *tcpPH* promoter is negatively influenced by the global regulator, CRP. ToxR/ToxS, and AphA/AphB also regulate genes other than *ctx* and *acf*. ToxRS, AphAB, TcpPH, and ToxT coordinately regulate the transcription of *ctx* and *tcp*. AphA and AphB activates the expression of the *tcpPH*. TcpPH and ToxRS regulate *ctx* and *tcp* genes through ToxT. AphB has been linked to the expression of *tcpPH* for anaerobiosis that enhances the production of CT. The direct activator and the second activator are differentiated by black solid and dotted arrows, respectively. Blue arrows indicate different environmental conditions sensed by the ToxRS and TcpPH, AphAB, and VarS regulatory systems. The two component VarS-VarA system responds to environmental factors and signals *toxT*. ToxR, independently activates and represses transcription of *ompU* and *ompT*. ToxR modulation was shown by an arrow (*ompU*) and line with base (*ompT*) through (+) for the transcription of *ompU* and (-) for repressing the transcription of *ompT*. Red circles in *ompU* and *ompT* indicate the ToxR binding sites and the transcriptional start sites are marked with arrows for each promoter [Source: (Ramamurthy et al., 2020)].

1.25. Major virulence factors of V. cholerae

1.25.1. Cholera enterotoxin (CT)

Cholera toxin, also known as choleragen (PDB ID: 1XTC), is the primary factor responsible for the clinical manifestations of cholera (*Fig.1.23*). This potent exotoxin stimulates enterocytes to increase the secretion of electrolytes, particularly chloride ions (Cl–), leading to passive water loss and resulting in severe diarrhea. The cholera enterotoxin, produced by adherent *V. cholerae*, is secreted across the bacterial outer membrane into the extracellular environment, where it disrupts ion transport in intestinal epithelial cells. The existence of cholera enterotoxin (CT) was first hypothesized by Robert Koch in 1884 and was experimentally demonstrated 75 years later by S. N. De and Chatterjee in 1953, followed by the work of Dutta et al. in 1959. Many strains of *V. cholerae* O1 harbour multiple copies of the *ctx* operon, which encodes the cholera toxin.

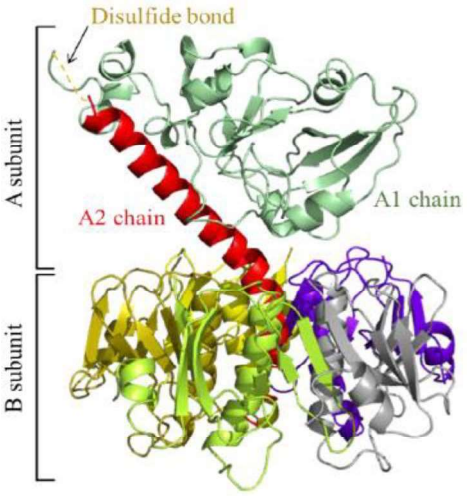

Fig.1.23. Crystallographic structure of Cholera enterotoxin [Source: (Odumosu et al., 2010)].

Cholera toxin is classified as an AB toxin, comprising one A subunit and five identical smaller B subunits (Finkelstein & LoSpalluto, 1969). The B subunits are responsible for binding the toxin to the eukaryotic cell receptor, ganglioside GM1, facilitating the entry of the A subunit into the host cell. Once inside, the A1 subunit activates the alpha subunit of Gs, a guanylnucleotide-binding protein involved in regulating adenylate cyclase activity. The ADP-ribosylation of Gs results in elevated levels of cyclic AMP (cAMP), leading to alterations in ion transport in the villous and crypt cells of the intestinal mucosa. This causes an increase in chloride secretion into the intestinal lumen and inhibition of sodium absorption, resulting in significant fluid and electrolyte loss.

The A and B subunits of cholera toxin are encoded by the *ctx* operon located within a region of DNA known as the CTX genetic element (Waldor et al., 1996). Originally thought to be a compound transposon associated with toxigenic strains of *V. cholerae*, it is now understood that the *ctx* genes reside within the genome of alysogenic filamentous phage (CTXφ) (Davis & Waldor, 2003). The single-stranded CTXφ infects *V. cholerae* by binding to the toxin-coregulated pilus (TCP), the major colonization determinant of *V. cholerae*. Upon infection, the CTXφ genome integrates into the *V. cholerae* genome to form a prophage. The 6.9-kb CTXφ genome has a modular structure composed of two functionally distinct domains: the core and the RS2 regions. The core region encodes cholera toxin and phage morphogenesis genes, while the RS2 region encodes genes required for replication, integration, and regulation of CTXφ (Waldor & Mekalanos, 1996). Based on the distinct GC content of *ctxAB* compared to the rest of the CTXφ genome, it has been suggested that the *ctxAB* genes were likely acquired by a precursor form of CTXφ. Comparative analysis of CTXφ from various *V. cholerae* strains indicates that the acquisition of this phage by *Vibrio* species has occurred multiple times and involved several CTXφ genotypes (Boyd et al., 2000). The binding of cholera toxin to epithelial cells is enhanced by the enzyme neuraminidase. An alternative mechanism of cholera toxin action suggests that prostaglandins and the enteric nervous system (ENS) play a role in response to CT. Additionally, cholera toxin serves as a potent oral antigen, both independently and in combination with unrelated antigens. The B subunit of CT exhibits an adjuvant-like effect, likely due to its binding with GM1 ganglioside (Czerkinsky et al., 1989) **(*Fig.1.24*).**

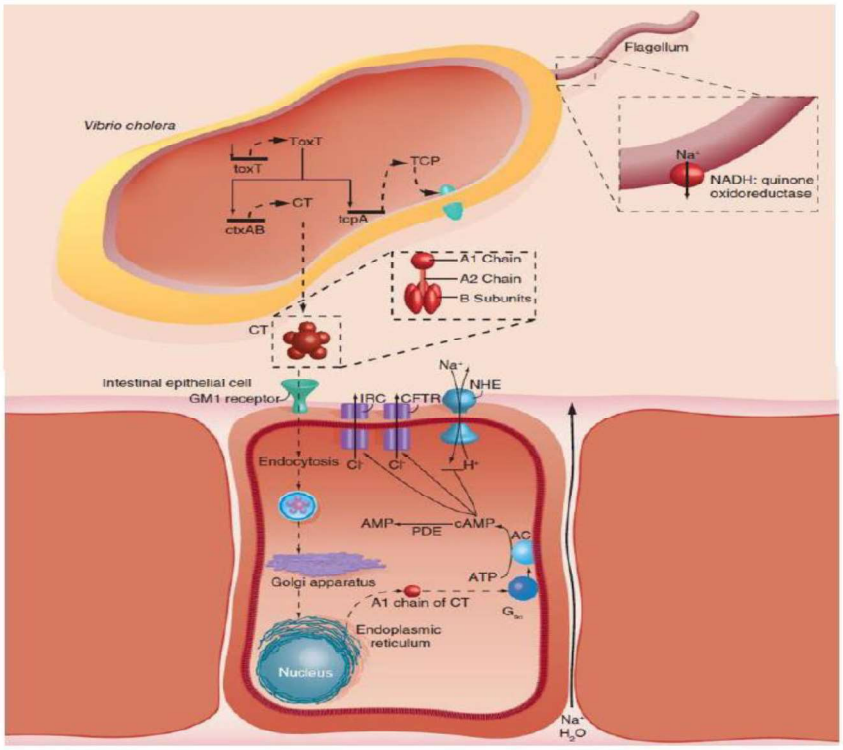

Fig.1.24. Schematic overview of mode of action of cholera enterotoxin (CT). Cholera toxin approaches target cell surface. B subunits bind to oligosaccharide of GM1 ganglioside (the first-ever structurally defined mammalian cell receptors). Conformational alteration of holotoxin occurs, allowing the presentation of the A subunit to cell surface. The A subunit enters the cell. The disulfide bond of the A subunit is reduced by intracellular glutathione, freeing A1 and A2. NAD is hydrolyzed by A1, yielding ADP-ribose and nicotinamide. One of the Gs proteins of adenylate cyclase is ADP-ribosylated, inhibiting the action of GTPase and locking adenylate cyclase (AC) in the "on" mode (Fishman,1980) and elevation of intracellular cAMP occurs. Increased intracellular cAMP then causes stimulation of cystic fibrosis transmembrane conductance regulator and/or inwardly rectifying Cl-channel-dependent Cl- secretion and inhibition of Na+ absorption through NHE, resulting in effluxes of Na+ and water and, hence, secretory diarrhea. CFTR: Cystic fibrosis transmembrane conductance regulator; CT: Cholera toxin; IRC: Inwardly rectifying Cl- channel; NHE: Na+–H+ exchanger; TCP: Toxin-coregulated pilus [Source: (Muanprasat et al., 2013)].

1.25.2. Zonula occludens toxin (Zot)

V. cholerae produces a range of extracellular products, including zonula occludens toxin (Zot). The *zot* gene, along with other virulence factor genes such as *ctxA, ctxB*, and *ace*, is integrated into the chromosomal genome of a filamentous phage known as CTXØ. The Zot protein appears to play a role in CTXØ morphogenesis, as

mutagenesis studies have shown that CTX elements lose their ability to self-transmit under appropriate conditions when the zot gene is disrupted (Fasano et al., 1991).

In addition to its role in phage morphogenesis, Zot increases the permeability of the small intestine by disrupting the structure of intercellular tight junctions (TJ). This effect was first observed in rabbit ileal tissues mounted in Ussing chambers using filtered supernatants from *V. cholerae* O1 strains, suggesting that Zot is secreted (Fasano et al., 1991). Zot exhibits cell specificity due to its interaction with a specific receptor whose surface expression varies across different cell types. Zot induces cytoskeletal reorganization, leading to the opening of TJ through transmembrane phospholipase C activation and subsequent protein kinase Cα-dependent polymerization of actin filaments, which strategically regulate the paracellular pathway (Pierro et al., 2001). *In vivo* experiments indicate that this effect on TJ can cause intestinal secretion by enabling the permeation of the intercellular space. This modulation is reversible, time- and dose-dependent, and confined to the small intestine, as Zot does not affect colon permeability. Furthermore, the number of Zot receptors decreases along the intestinal villous axis (Baudry et al., 1992).

The strong correlation between the presence of the zot gene and the *ctx* genes across *V. cholerae* strains suggests that Zot may synergistically contribute to the acute dehydrating diarrhea characteristic of cholera. Additionally, the complete genomic sequence of the *V. cholerae* El Tor N16961 strain has revealed that the CTXØ filamentous phage is integrated into one of the bacterium's two circular chromosomes.

1.25.3. Accessory cholera toxin (Ace)

The Ace protein of *V. cholerae* was first identified by Trucksis et al. in 1993. The open reading frame of the ace gene is located directly upstream of the zot gene. Unlike Zot, but similar to cholera toxin (CT), Ace increases the potential difference across the membrane rather than tissue conductivity.

The ace gene encodes a peptide composed of 96 residues with a predicted molecular weight of 11.3 kDa. This peptide alters ion transport, leads to fluid accumulation in ligated rabbit ileal loops, and induces mild diarrhea. The amino acid sequence of Ace shares similarities with a group of eukaryotic ion-transporting ATPases, including the human plasma membrane calcium pump, the calcium-transporting ATPase

from rat brain, and the Cystic Fibrosis Transmembrane Conductance Regulator (CFTR) (Bear et al., 1992).

In a colonic carcinoma T84 monolayer cell model, Ace stimulates Ca^{2+}-dependent Cl^-/HCO_3^- symporters, thereby generating a potential difference across the membrane.

1.25.4. Hemolysin/ *V. cholerae* cytolysin (VCC)

In the early 1960s, it was observed that strains of the El Tor biotype of *V. cholerae* exhibited hemolytic activity toward sheep erythrocytes. This characteristic was used as a phenotypic marker to differentiate them from strains of the classical biotype (Kaper et al., 1995). Classical strains of *V. cholerae* lack this hemolytic toxin due to an 11-base pair deletion in the structural gene responsible for producing the toxin. The toxin was purified from cultures of *V. cholerae* grown in brain heart infusion broth (BHI) and was partially characterized. The structural gene comprises an open reading frame that is 2,223 nucleotides long, which encodes a protein known as pre-prohemolysin. This protein is 741 amino acids long, with a molecular weight of 81,961. The pore-forming toxin hemolysin was first purified by Honda and Finkelstein. Hemolysin exhibits cytolytic activity against various erythrocytes and mammalian cells in culture, and it is highly lethal to mice. The premature protein is an 82 kDa protein that undergoes two processing steps to become a mature 65 kDa active cytolysin (Yamamoto Shigeo et al, 1993) (*Fig.1.25*). The gene *hlyA*, which codes for hemolysin, is found in classical, El Tor, and non-O1 strains of *V. cholerae*. VCC can cause fluid accumulation in ligated rabbit ileal loops. In contrast to the watery fluid produced in response to CT, the fluid accumulated due to hemolysin was found to be bloody and mixed with mucus.

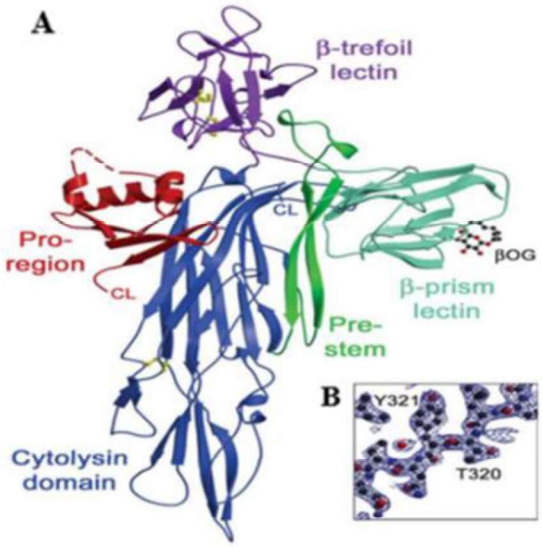

Fig.1.25. Crystallographic structure of Cytolysin [Source: (Podobnik et al., 2016)].

1.25.5. Toxin Coregulated Pilus

After attachment to the intestinal epithelium, the bacterium decreases motility, begins to proliferate, and initiates the virulence cascade. *V. cholerae* forms TCP-mediated clusters of bacterial cells called microcolonies (*Fig.1.26*). It was recently shown that microcolonies originate from single cells after reaching the intestinal epithelium. To date, several roles of the pilus have been determined: TCP enhances attachment to intestinal epithelial cells and facilitates bacteria-bacteria interactions, visualized *in vitro* as autoagglutination, by tethering the cells together; the ability to form microcolonies correlates with the ability to colonize the infant mouse and humans. TCP acts as the receptor of the CTX phage, a filamentous bacteriophage that encodes CT (Chang et al., 2017). Interestingly, an in-frame deletion mutant for *tcpA* shows highly reduced expression of the gene encoding the major subunit of CT *in vivo*, indicating that the presence of an intact TCP apparatus is essential for effective regulation of the virulence cascade (Almagro-Moreno et al., 2015). TCP is also required for the secretion of the soluble colonization factor TcpF. *In vivo*, a *tcpF* mutant is severely defective for colonization, a reduction equivalent to the effect seen with a *tcpA* mutant, which encodes the major pilin subunit. Although TcpF mutants are still able to form microcolonies, they are loosely packed and have decreased adherence around the edges; thus, it appears that TcpF functions as an enhancer of microcolony formation *in vitro* (Almagro-Moreno et al., 2015). As is the case for the *ctxAB* genes, *V. cholerae tcpA* and TCP biogenesis genes are encoded by a genetic element (TCP-ACF pathogenicity island) with the characteristics of a phage. Thus, it appears that the two major virulence determinants of *V. cholerae*, which are co-ordinately expressed in response to a regulatory cascade that is influenced by *in vivo* signals. They are encoded by genetic elements that have been acquired by horizontal transmission (*Fig.1.27*).

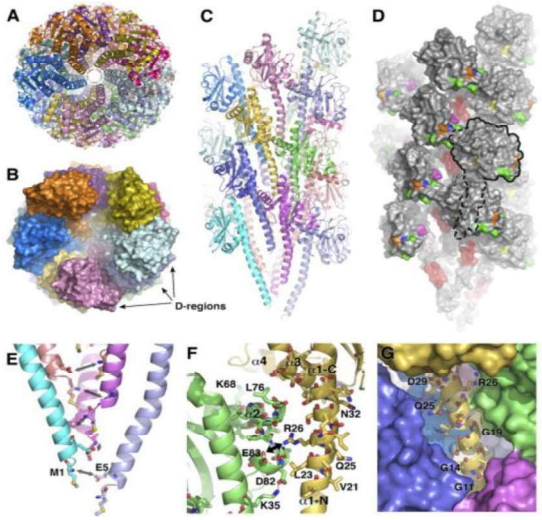

Fig.1.26. Crystallographic structure of Toxi Coregulated Pilus [Source: (Oki et al., 2022)]

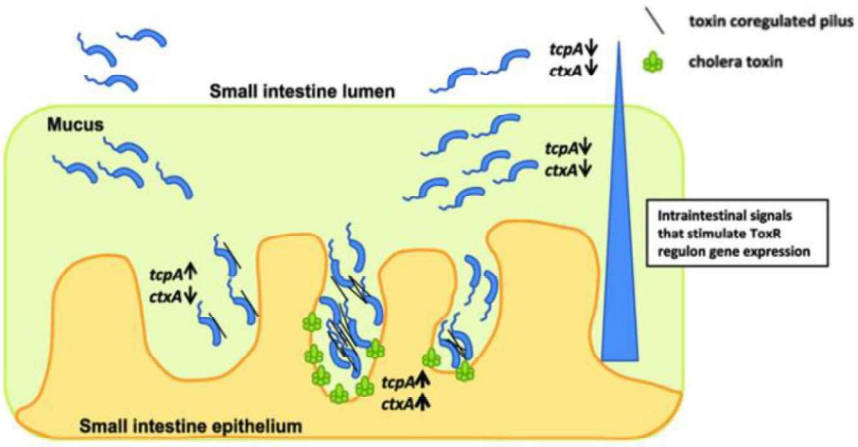

Fig.1.27. Synthesis of cholera toxin and toxin coregulated pilus in the small intestine [Source: (Peterson et al., 2018)]

Forming microcolonies within the host may also be beneficial to *V. cholerae* for other reasons, including more efficient nutrient uptake and protection from antimicrobials like bile or bactericidal compounds produced near the intestinal epithelium. Furthermore, it is thought that microcolonies might protect *V. cholerae* from shedding. In strains with functional quorum-sensing systems, virulence is repressed at high cell density. However, quorum sensing does not seem to play an essential role in virulence, as various toxigenic strains of *V. cholerae* have a naturally occurring frameshift mutation in the *hapR* gene, which encodes the master regulator of quorum sensing.

1.25.6. Accessory Colonization Factor

Intestinal mucus serves as a chemotactic signal for *V. cholerae*, guiding the bacteria toward the intestinal surface. This directed motility, combined with the ability of *vibrio* to secrete enzymes such as mucinase, lipases, and proteinases, enhances their capacity to penetrate the mucus layer and reach the intestinal epithelial cells. Disruption of accessory colonization factor (ACF) genes leads to altered swarm plate phenotypes, a hallmark of genes involved in chemotaxis (Valiente et al., 2018). Furthermore, amino acid alignment algorithms reveal a close similarity between AcfB and enteric methyl-accepting chemotaxis proteins, supporting the hypothesis that ACF proteins play a role in host-specific chemotaxis system that responds to intestinal mucus (Valiente et al., 2018).

The TCP and ACF gene clusters are physically linked with *V. cholerae* chromosome and are flanked by bacteriophage attachment (*att*) half-sites. Together, these two

loci form over 25 Kb of chromosomal DNA, encoding an environmentally regulated "pathogenicity island." Genomic analysis of *V. cholerae* strains indicates that only *vibrios* capable of causing epidemic cholera possess this "pathogenicity island." A recent study suggests that the "pathogenicity island" carrying the TCP/ACF genes functions as a prophage (VPIφ). Notably, the genes encoding CTX are located on CTXφ, with TCP serving as the receptor for CTXφ and the coat protein for VPIφ. Remarkably, maximum TCP expression presumably occurs only in the gastrointestinal tracts of humans. Indeed, CTXφ can efficiently convert TCP+ CTXφ- *V. cholerae* to CTXφ+ in experimentally infected mice (Valiente et al., 2018). These findings underscore the importance of understanding the role of intestinal signals in the pathogenesis and spread of Asiatic cholera.

1.25.7. Miscellaneous toxins

In addition to CT, Zot, Ace, hemolysin, and, TcpA which are commonly found in *V. cholerae*, several other toxins have been identified in this pathogen. These include Shiga-like toxin (ST), Cholix toxin, a new sodium channel inhibitor associated with cholera toxin, and thermo-stable direct hemolysin (*Fig.1.28*).

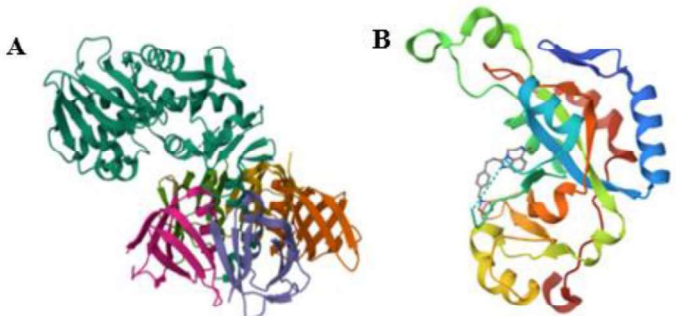

Fig.1.28. Crystallographic structure of (A) Shiga-like toxin and (B) Cholix toxin [Source: (Ling et al., 1998)]

1.26. Prevention and control of V. cholerae

A comprehensive approach is essential for preventing and controlling cholera, as well as reducing fatalities. This includes surveillance, water sanitation and hygiene, social mobilization, treatment, and the use of oral cholera vaccines.

1.26.1. Surveillance

Cholera cases are diagnosed on the basis of clinical symptoms in patients presenting like severe acute watery diarrhea. To confirm the diagnosis, *V. cholerae* is identified in stool samples from infected individuals. Local capacity to detect and monitor cholera cases, through the collection, organization, and analysis of data, is essential for an effective surveillance system and for planning control measures.

1.26.2. Water and Sanitation interventions

Economic development and universal access to safe drinking water and adequate sanitation are essential long-term solutions for controlling cholera, as well as for reducing other diseases spreading through the fecal-oral pathway (Taylor et al.,2015). To prevent both epidemic and endemic cholera, the following precautions are taken. Development of piped water systems with water treatment facilities, including chlorination, household-level interventions such as water filtration, chemical or solar water disinfection, and safe water storage, as well as the installation of safe sewage disposal systems, including latrines (D'Mello-Guyett et al.,2020).

1.26.3. Treatment

Noncommunicable diseases now dominate global health, but diarrheal disease remains a significant threat. In 2016, it was the eighth leading cause of death, claiming 7.6 million children under five. Oral rehydration solution (ORS), pioneered by Dr. Dilip Mahalanabis, revolutionized dehydration treatment, saving millions of lives, particularly in resource-limited areas. Cholera, a potentially deadly disease, can be successfully treated if ORS is administered promptly. The WHO/UNICEF ORS sachet is dissolved in 1 litre of clean water. Adult patients with mild dehydration may require up to 6 litres of ORS ***(Table 1.5)***.

New ORS	Grams/litre	%	New ORS	Mmol/litre
Sodium chloride	2.6	12.683	Sodium	75
Glucose, anhydrous	13.5	65.854	Chloride	65
Potassium chloride	1.5	7.317	Glucose, anhydrous	75
Trisodium citrate, dihydrate	2.9	14.146	Potassium	20
			Citrate	10
Total	20.5	100.00	Total Osmolarity	245

Table 1.5. Composition of the new ORS formulation

1.27. Vaccines – present and future

Oral Cholera Vaccines (OCVs) are now a cornerstone of the action plan titled "Ending Cholera: A Global Roadmap to 2030," which was launched in 2017 by the World Health Organization's Global Task Force on Cholera Control (GTFCC) along with 50 other organizations. The goal is to reduce cholera deaths by at least 90% and to eliminate cholera transmission in most of the currently affected countries by the year 2030. There are currently three WHO-approved oral cholera vaccines: Dukoral®, ShancholTM, and Euvichol® *(Table 1.6).*

Vaccine	Dukoral®	Shanchol™	Euvichol®
Manufacturer	Valneva, France	Shantha Biotechnics, (Hyderabad, India) Sanofi Company	Eubiologics, Seoul, Republic of Korea
Developer	SBL Vaccin (Solna, Sweden)	IVI, Shantha	IVI, Eubiologics
Type	Monovalent, killed whole-cell vaccine O1 serogroup and recombinant cholera toxin B subunit	Bivalent, killed whole-cell (O1 and O139 serogroups)	Bivalent, killed whole-cell (O1 and O139 serogroups)
Age range for vaccination	≥ 2 years	1 year and older	1 year and older
Regimen	2 doses given 7 to 14 days apart (3 doses for children 2 to 5 yrs old)	Two doses 14 days apart	Two doses 14 days apart
Booster	Every 2 years for individual ≥6 yrs (every 6 mo for children 2 to 5 yrs)	No recommendation from manufacturer	No recommendation from manufacturer
Route	Oral	Oral	Oral
Buffer	Sodium bicarbonate buffer	No buffer required	No buffer required
Duration of protection	2 years (6 months in children 2 to 5 yrs)	At least 3 years Up to 5 yrs	Not available
Storage	+2°C to +8°C	+2°C to +8°C	+2°C to +8°C
Shelf Life	36 months	24 months	24 months
Licensure	60 countries	28 countries	Zambia, Nepal and Pakistan
WHO prequalification	25 Oct 2001	29 Sep 2011	23 Dec 2015

Table 1.6. WHO-approved oral cholera vaccines

Dukoral™ (Valneva, France): The first effective oral cholera vaccine (OCV) developed was the inactivated whole-cell/ cholera toxin B subunit vaccine, Dukoral™. This vaccine contains a mixture of formalin- and heat-killed *V. cholerae* O1 bacteria, which includes both the Ogawa and Inaba serotypes, as well as the classical and El Tor biotypes. Additionally, it contains a recombinantly produced cholera toxin B subunit. Dukoral is widely used as a vaccine for travellers to prevent both cholera and entero-toxigenic *Escherichia coli* (ETEC) diarrhea. It provides approximately 65% protection against cholera for a duration of 2 years.

Shanchol™ (Sanofi-Shantha Biotechnics, India): In the late 1980s, Sweden supplied Vietnam with the technology to manufacture an orally killed whole-cell cholera vaccine (OCV). This vaccine included the same components of *V. cholerae* O1 found in Dukoral, but it excluded the cholera toxin B subunit to reduce production costs and simplify the manufacturing process. A two-dose immunization against cholera has been shown to provide 66 percent protection for both adults and children as young as one year old. Following the development of O139 in India and Bangladesh in 1992, the vaccine was modified to include killed *V. cholerae* O139 cells and was subsequently approved for use, first as OrcVax™ and later as mOrcvax™. In endemic areas, individuals vaccinated with Shanchol™ or Euvichol® can expect approximately 65 percent protection against cholera for up to five years after immunization.

Euvichol™/Euvichol-Plus™ (Eubiologics, S. Korea): To meet the growing demand for OCVs, IVI transferred the reformulated OCV technology to Eubiologics in Seoul, Republic of Korea. This has resulted in the successful production of Euvichol™ OCVs, which share an identical composition with Shanchol™. ICMR-NIRBI successfully conducted a mass vaccination program using the Euvichol-Plus oral cholera vaccine in South 24 Parganas, Kolkata, covering approximately 30,000 people.

Other nationally licensed OCVs: The mOraVax™ from Vietnam, Cholvax™ from Bangladesh (produced by Incepta), OraVacs™ from China (produced by Shanghai United Cell Biotechnology), and Vaxchora™ from the United States (produced by PaxVax) consist of lyophilized *V. cholerae* "CVD 103-HgR" O1 bacteria. These bacteria are derived from a classical Inaba strain (569B).

1.28. The emergence of drug resistance in V. cholerae

In recent decades, *V. cholerae*, the bacteria responsible for acute watery diarrheal disease cholera, has become important multidrug-resistant (MDR) enteric pathogen (Kitaoka et al., 2011). While chromosomal mutations can contribute to antimicrobial resistance (AMR), a significant factor in the drug resistance of *V. cholerae* is its frequent acquisition of extrachromosomal mobile genetic elements (MGEs) from both closely and distantly related bacterial species. The antimicrobial resistance genes

identified in *V. cholerae* can lead to antibiotic resistance through one of three mechanisms: (i) reduced permeability or active efflux of the antibiotics, (ii) alteration of antibiotic targets via post-transcriptional or translational modifications, and (iii) hydrolysis or chemical modification of the antibiotics (***Fig.1.29***).

Antibiotic treatment for cholera patients is recommended after restoring initial fluid loss and controlling vomiting. The emergence of multi-drug resistant (MDR) and extremely drug-resistant (XDR) *V. cholerae* serves as significant evidence of recent bacterial evolution (Verma et al., 2019). Recent research suggests that horizontal gene transfer (HGT) through self-transmissible, autonomously replicating plasmids, or integrative mobile genetic elements (IMGEs), such as integrating conjugative elements (ICEs), insertion sequences (IS), and transposable genetic elements, primarily contributes to the development of MDR and XDR *V. cholerae*.

During the 1960s, resistance to one or more antibiotics was mainly due to spontaneous mutations in the drug's target, which includes DNA gyrase, topoisomerase, the beta-subunit of RNA polymerase (RpoB), and the small subunit of ribosomal protein. Multidrug-resistant (MDR) *V. cholerae* isolates from serogroup O1 that were resistant to tetracycline, streptomycin, and chloramphenicol were first reported in 1970. Since the early 1990s, resistance to ampicillin, nalidixic acid, chloramphenicol, and tetracycline has rapidly increased. Currently, most clinical isolates of *V. cholerae* exhibit resistance to nearly all commonly used antibiotics (Verma et al., 2019).

The emergence of multi-drug resistant (MDR) *V. cholerae* serogroup O139 was first reported in 1996. This resistance is attributed to the SXT element, a 100-kb integrative conjugative element (ICE) that harbours multiple resistance genes against sulfamethoxazole, trimethoprim, and streptomycin (Das et al., 2020).

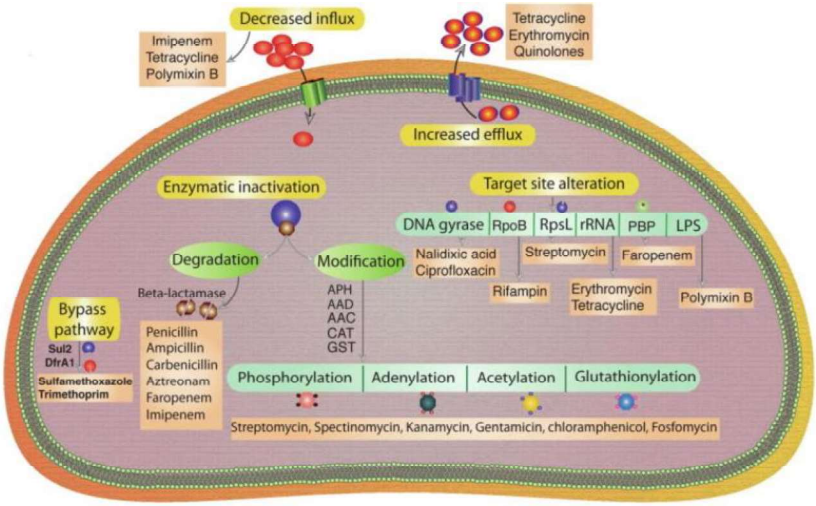

Fig.1.29. Mechanisms of antibiotic resistance in *V. cholerae*. Bacteria can develop resistance to antimicrobials by two simple mechanisms; by altering the target sequence (vertical transmission) or by acquiring resistance-encoding genes from other bacterial species (horizontal gene transfer). The acquired resistance traits can provide resistance by changing membrane permeability, enzymatic degradation or modification of antimicrobial drugs or by modifying the drug targets. They may also provide an alternative metabolic pathway or actively pump out antimicrobial compounds from the cytosol [Source: (Das et al., 2020)].

1.29. Anti-bacterial vs Anti-virulence approach

Antimicrobial resistance (AMR) is one of the top global public health and development threats. According to WHO report, bacterial AMR was directly responsible for approximately 1.27 million deaths worldwide in 2019 and contributed to an additional 4.95 million deaths. The primary factors driving the emergence of drug-resistant pathogens are the misuse and overuse of antimicrobials in humans, animals, and plants. AMR affected countries across all regions and income levels. The drivers and consequences of antibiotic resistance (AMR) are exacerbated by poverty and inequality, with low- and middle-income countries being the most affected. AMR jeopardizes many of the advancements in modern medicine. It complicates the treatment of infections and increases the risks associated with medical procedures, such as surgeries, caesarean sections, and cancer chemotherapy. The world is facing a crisis regarding the antibiotic pipeline and access to medications. There is lack of new antibiotics in the pipeline, alongside a pressing need for equitable access to both new and existing vaccines, diagnostics, and treatments, all against the backdrop of rising resistance levels.

Bacteria secrete various virulence factors to cause disease in humans. These factors include adhesins, which allow bacteria to bind to host cells and facilitate colonization, as well as the production of toxins that can kill cells or disrupt signal transduction in mammalian cells. Anti-virulence therapeutic strategies aim to inhibit essential virulence components, thus preventing bacterial pathogenesis without killing the bacteria. This approach in treating bacterial infections may be more effective than standard antibiotics since it targets specific factors involved in pathogenesis. As a result, it may exert less evolutionary pressure on the development of antibiotic resistance and also minimize collateral damage to the resident microbiota (Dehbanipour et al.,2022) (*Fig.1.30*).

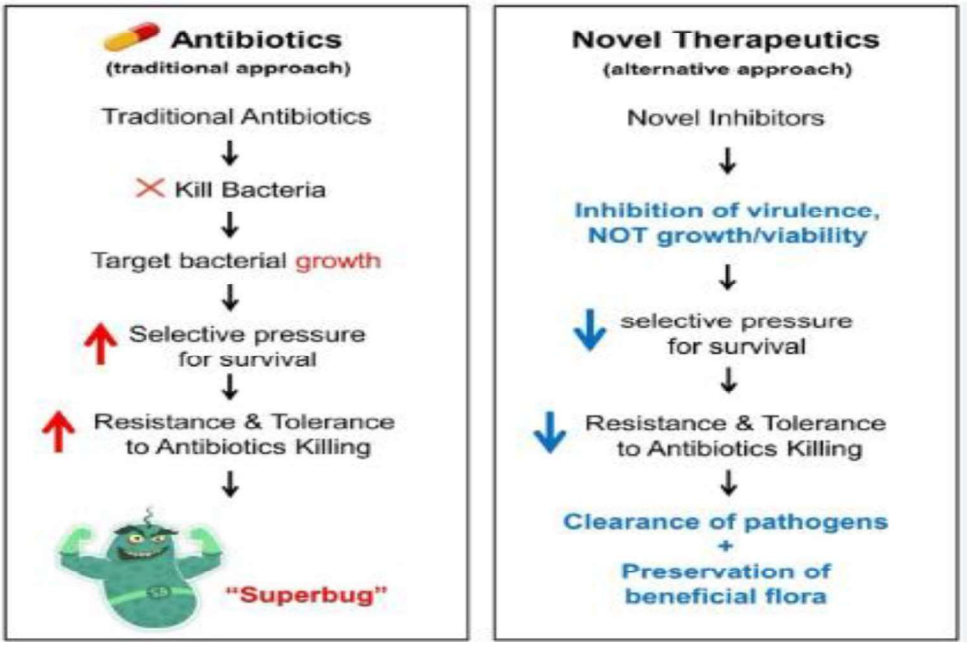

Fig.1.30. A graphical summary of the anti-bacterial vs anti-virulence approach [Source: (Dehbanipour et al.,2022)].

1.30. Anti-virulence Therapeutic Strategies Targeting Bacterial Pathogenicity

Antimicrobial resistance (AMR) has become a critical threat to human health. In addition to approximately 700,000 deaths caused by drug-resistant pathogens annually, this number is projected to rise to around 10 million by 2050. Furthermore, essential medical procedures such as organ transplantation, cancer chemotherapy, and surgery are increasingly compromised due to AMR. Since antimicrobial resistance is

a multifactorial phenomenon, addressing this issue requires a multifaceted approach (WHO, 2018).

One promising strategy in the fight against AMR is the development of innovative antimicrobial compounds that operate through mechanisms different from those of conventional antibiotics (Munguia & Nizet, 2017). Among these strategies, anti-virulence therapy has emerged as a potential alternative. Unlike traditional antibiotics that aim to kill pathogens, anti-virulence therapy focuses on depriving pathogens of their virulence factors. This approach is expected to exert lower selective pressure on pathogens, thereby reducing the emergence and spread of resistant mutants (Johnson et al., 2018; Langeveld et al., 2014; Rasko & Sperandio, 2010).

Virulence factors are microbial components that enable pathogens to colonize, invade, and persist within a host. Production of these factors is regulated by complex mechanisms; interfering with these regulatory pathways is a viable strategy to inhibit virulence. In this context, quorum-sensing systems (QS), which control the production of various virulence factors, are considered one of the most promising targets for anti-virulence drug development (Aminov, 2010; Aminzare et al., 2018; Burt, 2004).

In addition, the proper folding and oligomerization of virulence factors are essential for their biological activity. Consequently, targeting the bacterial machinery responsible for virulence factor assembly is another effective approach. Recent research has highlighted the role of bacterial functional membrane microdomains (FMMs) in the assembly of several virulence factors, making FMMs an attractive target for drug development.

Anti-virulence strategies also aim to interfere with the functions of virulence factors. One effective method is toxin neutralization, as pathogens often secrete toxins to colonize the host and evade the immune system. Furthermore, biofilm formation is a common strategy used by pathogens to resist the host immune response. Anti-virulence therapies targeting biofilms focus on disrupting bacterial adhesion, interfering with extracellular matrix production, or disintegrating existing biofilms (***Fig.1.31***).

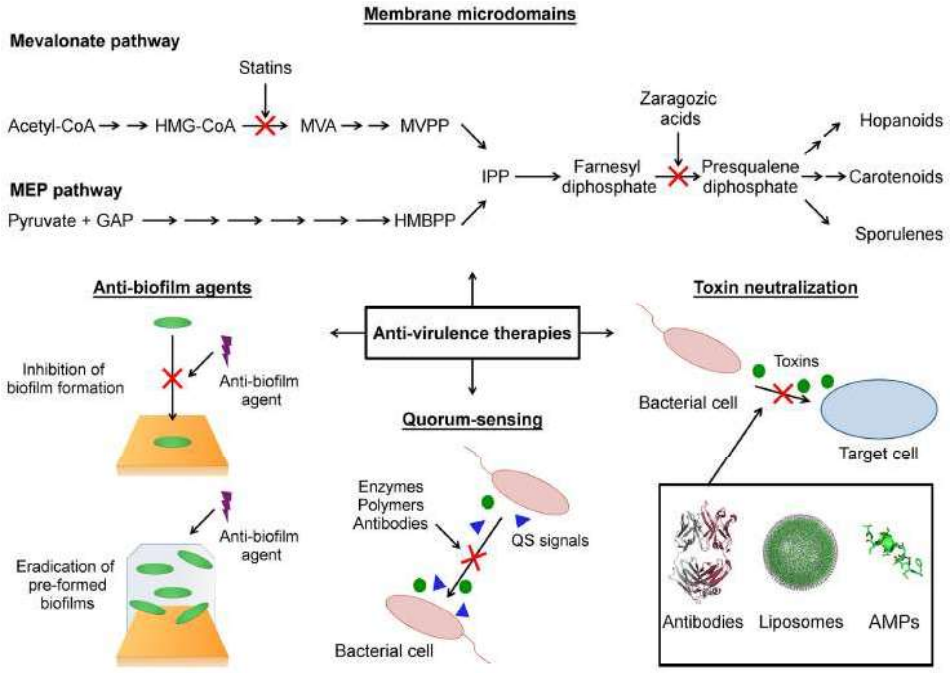

Fig.1.31. Schematic representation of anti-virulence strategies. Membrane microdomains: The functional membrane microdomains (FMMs) are targeted by small molecules (statins, zaragozic acid) that inhibit the biosynthesis of their major constituent lipids (hopanoids, carotenoids). Anti-biofilm agents: This strategy focused on the use of agents that block the initial bacterial attachment to surface during biofilm formation and agents that destroy preformed biofilm. Quorum-sensing: The anti-virulence strategy that seeks modulate the production of virulence factors through interference with the quorum-sensing networks. Toxin neutralization: A strategy focused on block the action of toxins on host target cells. HMG-CoA (3-hydroxy-3-methylglutaryl-CoA), MVA (mevalonic acid), MVPP (5-diphosphomevalonate), GAP (D-glyceraldehyde-3-phosphate), HMBPP (4-hydroxy-3-methylbut-2-enyl-diphosphate), IPP (isopentenyl diphosphate), QS (quorum sensing), AMPs (antimicrobial peptides) [Source: Martínez et al., 2019].

1.30.1. Different anti-virulence strategies to combat bacterial infections

- **Destroying bacterial membrane microdomains**

Disrupting functional microdomains (FMMs) in bacterial membranes hinders biofilm formation and virulence in *Bacillus subtilis*, *Campylobacter jejuni*, and *Staphylococcus aureus*, making FMMs a promising anti-virulence target with low resistance potential**.** For eg., drugs such as statins can disrupt bacterial membrane microdomains, potentially rendering antibiotic-resistant bacteria like MRSA more susceptible to antibiotics.

- **Interference with quorum-sensing signal biosynthesis**

Small molecule inhibitors disrupt quorum sensing (QS) without affecting bacterial growth or causing resistance. MTAN inhibitor 5′-methylthio-DADMe-Immucillin-A blocks autoinducer production in *V. cholerae* and *E. coli* O157:H7. Innovative quorum quenching strategies, such as CRISPRi targeting LuxS and bacteriophage-based CRISPRi delivery, effectively disrupt *E. coli* biofilms

- **Preventing biofilm formation and affecting the biofilm structure without killing bacteria**

Biofilms protect bacteria from antibiotics and immune responses, often forming on implants and catheters. Anti-virulence compounds like Higrocin C, Coumarin, and DNAse I prevent adhesion, inhibit matrix production, and disrupt biofilms without harming bacteria.

- **Bacterial toxin neutralization**

Pathogenic bacteria produce toxins like *S. aureus* alpha-toxin and *C. difficile* TcdB to evade immunity and cause damage. Anti-virulence therapies target these toxins without affecting bacterial viability, reducing resistance and preserving the microbiome. Promising approaches include using bioactive compounds (e.g., pinoresinol, guineensine) monoclonal antibodies (e.g., MEDI4893, ASN100), nanoparticles, liposomes, engineered *Lactobacillus* strains, and multi-antigenic nano toxoids for vaccine development.

Inhibitors of functional membrane microdomains assembly, quorum-sensing systems, biofilm formation, and toxin production and function are listed in ***Table 1.7.***

Inhibitors	**Inhibitory Activity**	**Bacterial species**	**Virulence factors affected**
Miltefosine	Anti-FMM	*S. aureus*	• Rny oligomerization
5-DSA	Anti-FMM	*S. aureus*	• Rny oligomerization • T7SS system assembly
Simvastatin	Anti-FMM	*S. aureus*	• T7SS system assembly

CRISPR-Cas9	Anti-QS Anti-biofilm	*E. coli SE15*	• Reduced biofilm formation • Down-regulation of *mqsR, pgaB, pgaC, csgE,* and *csgF*
CRISPR interference	Anti-QS Anti-biofilm	*E. coli AK-117*	• Reduced biofilm formation
2-(methylsulfonyl)-4-(1H-tetrazol-1-yl) pyrimidine	Anti-QS Anti-biofilm	*P. aeruginosa*	• Reduced biofilm formation • Reduced production of pyocyanin and pyoverdine
AHL-nitric oxide hybrids	Anti-QS	*P. aeruginosa* PA14 *P. aeruginosa* PAO1	• Reduced pyocyanin and elastase production
Flavonoids	Anti-QS	*P. aeruginosa* PA14	• Reduced pyocyanin production and swarming motility • *rhlA* transcription inhibition
T315 compound	Anti-biofilm	*S. enterica serovar Typhimurium* *S. enterica serovar Typhi* *A. baumannii*	• Reduced biofilm production
2-aminobenzimidazole derivatives	Anti-biofilm	*S. enterica serovar Typhimurium*	• Reduced biofilm production
Kaempferol	Anti-biofilm	*S. aureus*	• Reduced biofilm production (inhibition of initial attachment) • Inhibition of sortase A activity • Downregulation of *clfA, clfB, fnbA* and *fnbB* expression
3F1 compound	Anti-biofilm	*S. mutans*	• Biofilm dispersion
2-aminoimidazole derivatives	Anti-toxin	*Clostridium difficile*	• Reduced toxin activity
Peptides	Anti-toxin	*Aggregatibacter actynomycetemcomitans*	• Inhibition of LtxA-mediated cytotoxicity

Galloylated catechins	Anti-toxin	*A. actynomycetemcomitans*	• Inhibition of LtxA-mediated cytotoxicity

Table 1.7. Inhibitors of functional membrane microdomains assembly, quorum-sensing systems, biofilm formation, and toxin production and function [Source: (Martínez et al., 2019)].

In conclusion, anti-virulence therapy represents a promising approach to combat antimicrobial resistance. By targeting virulence factors and their regulatory mechanisms, this strategy can potentially reduce the selective pressure on pathogens and limit the emergence of resistant mutants. Extensive research and development in this field are essential to mitigate the growing threat of antimicrobial resistance. The potential use of small molecules, and other bioactive compounds were also studied here.

1.31. Combination therapy

Combination therapy is the tailored use of two or more therapeutic agents and/or methods to combat the increasing problem of multidrug-resistant (MDR) pathogens, which is a significant global health concern. Antibiotics, once the most effective defence against life-threatening infections, are becoming less effective. As a result, we are left with a limited selection of antibiotics to treat MDR infections. Researchers are actively seeking new antibiotics, but combination therapy is also gaining recognition in the treatment of multidrug-resistant (MDR) infections (N. Wang et al., 2022). This approach involves using two or more therapeutic agents that work through different mechanisms. By doing so, it can create a synergistic effect that effectively kills MDR pathogens. When pathogens utilize significant resources to defend against one agent, they often become more vulnerable to another. Combination therapy offers a wider antimicrobial spectrum, enhances the synergistic effects, and helps in reducing development of drug resistance (Tamma et al.,2012). In recent years, non-antibiotic compounds have played an important auxiliary role in improving the efficacy of antibiotics and promoting the treatment of drug-resistant bacteria (Bollenbach T et al.,2015). Combining non-antibiotic compounds with antibiotics is considered a promising strategy against multidrug-resistant (MDR) bacteria (Wolska et al., 2012).

1.31.1. Bacterial Resistance Mechanisms Against Antibiotics and Potential Resistance-Reversing Agents

- **Enzymatic Modification of Antibiotics**

  The most common mechanism of bacterial resistance to aminoglycoside antibiotics (AGAs) is through aminoglycoside modifying enzymes (AMEs). β-lactams enhance AGA entry by damaging the bacterial cell wall, aiding in treating resistant infections. β-lactams antibiotics are often combined with beta-lactamase inhibitors like clavulanic acid, sulbactam, or tazobactam which prevent enzymatic degradation of antibiotics.

- **Decreased Drug Accumulation**

  Bacteria resist aminoglycosides through active efflux pumps (e.g., MexXY-OprM in *P. aeruginosa*, AcrAD-TolC in *E. coli*, and EmrD-3 in *V. cholerae*) that expel AGAs, reduced membrane permeability due to porin mutations (e.g., OmpF in *E. coli*), membrane protease activity (e.g., FtsH in *P. aeruginosa*) that degrades misfolded proteins, and biofilm formation, which blocks AGA penetration and triggers stress responses via PhoPQ and PmrAB systems in *P. aeruginosa*. Combining tetracycline/minocycline with a lipopeptide designed to improve membrane targeting and accumulation has shown promising results. L-leucine has been shown to increase the sensitivity of drug-resistant *Salmonella* to salafloxacin.

- **Modification of Drug Targets**

  16S rRNA methyltransferases (16S-RMTases) confer high-level aminoglycoside resistance by adding methyl groups to 16S rRNA using S-adenosylmethionine (SAM), reducing AGA binding.

  Artemisinin derivative DHA27 in combination with the AG antibiotic tobramycin enhances the antibacterial effect of aminoglycosides against *Pseudomonas aeruginosa* by inhibiting the activity of 16S rRNA methyltransferases.

- **Changes of Bacterial Metabolism**

  In *P. aeruginosa*, the Crc-Hfq complex and small RNA CrcZ regulate carbon metabolism and contribute to gentamicin resistance. Combination of carbenicillin and gentamicin or piperacillin-tazobactam and gentamicin can improve efficacy against *P. aeruginosa*. Polymyxin B and amikacin disrupt *P. aeruginosa* metabolism, while AMPs like PMAP-36 and PRW4 increase membrane permeability, enhancing gentamicin's effect on *E. coli* and *S. aureus.*

Examples of synergy between novel antimicrobials and antibiotics are listed in *Table 1.8.*

Novel antimicrobial	Antibiotic	Bacterial species
Plant		
thymol	Nisin	*L. monocytogenes*
EGCg	Ampicillin + sulbactam	*MRSA*
EGCg	Penicillin	*S. aureus*
Baicalein	tetracycline	*MRSA*
7-methyljuglone	Isoniazid	*M. tuberculosis*
Carnosol	Aminoglycosides	VRE
Asiatic acid, corosolic acid	Tobramycin	*P. aeruginosa*
Ellagic acid, tannic acid	Novobiocin	*A. baumanii*
Kaempferol glycosides	Fluoroquinolones	MRSA
Galangin	Cefazidime	PRSA
Oleanolic acid	Rifampicin	*M. tuberculosis*
Betulic acid	Methicillin, vancomycin	*S. aureus*
Oleanolic acid, ursolic acid	Ampicillin, oxacillin	*S. aureus, S. epidermidis*
green tea catechin, Triphala, Brazilian red propolis	gentamicin	*E. coli, S.aureus*
Other antibiotics		
gentamicin	azithromycin	*P. aeruginosa*
ciprofloxacin	trimethoprim	*V. cholerae, E. coli*
Ag+ and AgNPs		
Ag+	Vancomycin, amoxicillin, penicillin G	*S. aureus*
AgNPs	Polymyxin B	Gram– bacteria
AgNPs	Ampicillin	Gram+ bacteria

Photosensitizers		
PACT	Gentamicin	*S. aureus*, MRSA
Bacteriophages lytic enzymes		
Cpl -1	Cefotaxime, moxifloxacin	*S. pneumoniae*
LysK	Lysostaphin	MRSA
ClyS	Oxacillin, vancomycin	MRSA
LysH5	Nizin	*S. aureus*

Table 1.8. **Examples of synergy between novel antimicrobials and antibiotics** [Source: (Wolska et al., 2012)].

In this work, we evaluated the combined effects of bioactive compounds with the conventional antibiotics and examined the effect of this strategy in enhancing the efficacy of existing antibiotics.

Chapter 2

Objectives

Objectives

The overall goal of this thesis work is to identify potential inhibitors targeting the virulence factors of *V. cholerae* and to elucidate their mechanisms of action. The specific objectives are:

1. Screening of potential inhibitors against Vibrio Cholerae growth, motility, adhesion, virulence, and toxin production.

The successful colonization of *Vibrio cholerae* in the host is facilitated by its motility, which allows the organism to penetrate the thick mucus layer. This penetration is followed by the induction of virulence factors that aid in colonization and the release of toxins. Therefore, targeting these virulence factors with potential inhibitors will be an important aspect of the study.

2. Elucidation of possible mode of action of these inhibitors.

After screening the inhibitors, our next objective is to identify and understand the mechanism of inhibition.

3. Investigate the effect of these inhibitors in combination with known drugs in vitro and in vivo models.

Combinatorial therapy is becoming increasingly important in the treatment of diseases. Combining multiple drugs to address a condition has demonstrated greater effectiveness than using a single drug, as it can help reduce the development of drug resistance. In this study, we investigated the effects of the potential inhibitor with antibiotics.

Chapter 3

Materials and Methods

Materials and Methods

3.1. Bacterial strains, their maintenance and culture conditions

The multidrug-resistant *V. cholerae* O1 El Tor Inaba strain N16961 was used as a standard strain (Heidelberg et al., 2000) and the list of all strains used in this study is included in the appendix. All strains were stored at -80 °C in Luria broth (LB) supplemented with 15% glycerol, in a total volume of 2 ml. To isolate the *V. cholerae* strains, aliquots from the -80 °C stock were streaked onto Thiosulfate Citrate Bile Salts Sucrose Agar (TCBS) agar plates and incubated overnight at 37 °C. The characteristic large, yellow, single colonies were then selected for further work. Strains were grown in Luria-Bertani (LB) medium (BD, Difco, Franklin Lake, NJ) at 37 °C with the necessary antibiotics, either streptomycin (100 µg/ml) or ampicillin (100 µg/ml), as needed, under constant shaking at 180 rpm. To study the expression of virulence genes, bacteria were grown in AKI media containing 0.4% yeast extract (BD Difco, San Diego, CA), 1.5% Bacto peptone (BD Difco, San Diego, CA), 0.5% NaCl, and 0.3% freshly produced $NaHCO_3$ (Merck, Burlington, MA) pH=7.2 and at 37 °C under static condition.

3.2. Medium additives for inhibitor study

For the inhibitor study, the following bioactive compounds were used, Sodium butyrate (Sigma-Aldrich, Saint Louis, Missouri, USA), NH125 (Calbiochem, San Diego, California),Cyclic-di-GMP (Sigma-Aldrich, Saint Louis, Missouri), Totarol (Cayman chemicals, Ann Arbor, Michigan), Quercetin (Sigma-Aldrich, Saint Louis, Missouri), Allylanisole (Sigma-Aldrich, Saint Louis, Missouri), Geraniol (Sigma-Aldrich, Saint Louis, Missouri), Ethyl gallate (Sigma-Aldrich, Saint Louis, Missouri), Camphor (Sigma-Aldrich, Saint Louis, Missouri), Basil oil (Sigma-Aldrich, Saint Louis, Missouri), Catechin hydrate (Sigma-Aldrich, Saint Louis, Missouri), Rosemarinic acid (Sigma-Aldrich, Saint Louis, Missouri), Melibiose (Sigma-Aldrich, Saint Louis, Missouri), Ribose (Sigma-Aldrich, Saint Louis, Missouri), 1,2 deoxywithastramonolide (Sigma-Aldrich, Saint Louis, Missouri), eugenol (Sigma-Aldrich,

Saint Louis, Missouri) Xylose (Sigma-Aldrich, Saint Louis, Missouri) ***(Table 3.1)***. Appropriate dilutions were made during stock preparations and during experiments by dissolving the compounds in DNAase/RNAase-free water or in polar solvent Dimethyl Sulfoxide (DMSO) and filter sterilizing it (0.2µm). Additives were supplemented in LB or AKI media in different concentrations. Media with no additive was used as control.

Bioactive compounds	**Uses**	**Structure**
Camphor	Anti-virulence	
Totarol	Anti-virulence	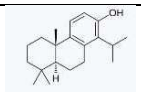
Cyclic-di-GMP	Anti-virulence	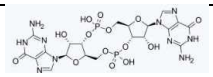
Basil oil	Anti-viral	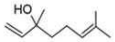
Catechin hydrate	Antimicrobial	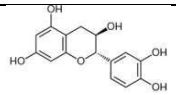
Rosemarinic acid	Anti-virulence	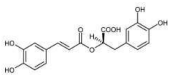
Ribose	Anti-virulence	
Melibiose	Anti-virulence	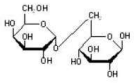
1,2 deoxywithstramon-olide	Anti-virulence	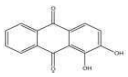
eugenol	Anti-virulence	
Xylose	Anti-inflammatory	
geraniol	Antioxidant	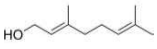
NH125	Antibacterial	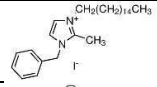
Ethyl gallate	Antioxidant	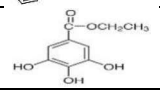

Sodium butyrate	Anti-inflammatory	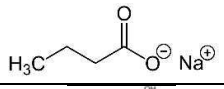
quercetin	Anti-inflammatory	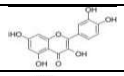
p-allylanisole	Antibacterial	

3.1. List of different compounds used for inhibitory study

3.3. Determination of Minimum Inhibitory Concentration (MIC) and Minimum Bactericidal Concentration (MBC) of inhibitor

The Minimum Inhibitory Concentration (MIC) of inhibitors was determined using the broth microdilution method in accordance with CLSI guidelines (Clinical Laboratory Standards Institute, 2000) ***(Fig 3.1)***. This was performed in 96-well flat-bottom polystyrene microtiter plates (Costar Corning, Arlington, Virginia). The bacterial suspension was adjusted to an optical density of 0.08-0.12 at 600 nm, which is equivalent to 0.5 McFarland standard turbidity, using a spectrophotometer. 200 µl of cell suspensions were inoculated into 96-well microplates. Inhibitors were dissolved in appropriate solvents and then mixed with Mueller Hinton Broth (MHB) as needed before being transferred to the microplate wells to achieve a 2-fold serial dilution. Wells containing only MHB served as negative controls, while wells containing MHB with bacteria were used as positive controls. Plates were incubated at 37 °C for 24 h, and bacterial growth was assessed by checking turbidity and the presence of pellet at the bottom of the plate. The concentrations of inhibitors that did not affect the bacterial growth were selected as sub-MICs. The minimum inhibitory concentration (MIC) value was recorded as the lowest concentration of the tested compound that showed no macroscopically visible growth of bacteria (Burt et al., 2004). To determine the minimum bactericidal concentration (MBC), 100 µl from each well that exhibited no visible growth was inoculated in Müller-Hinton Agar (MHA) plates. After incubating for 24 h at 37 °C, the number of surviving organisms was counted. The lowest concentration at which no colonies were identified on the plate after 24 h incubation was determined to be the MBC (Magina et al., 2009). Each experiment was repeated three times independently. To ensure that the antimicrobial effect was due to the inhibitors and not the solvent, we used solvents as negative controls, which did not inhibit bacterial growth.

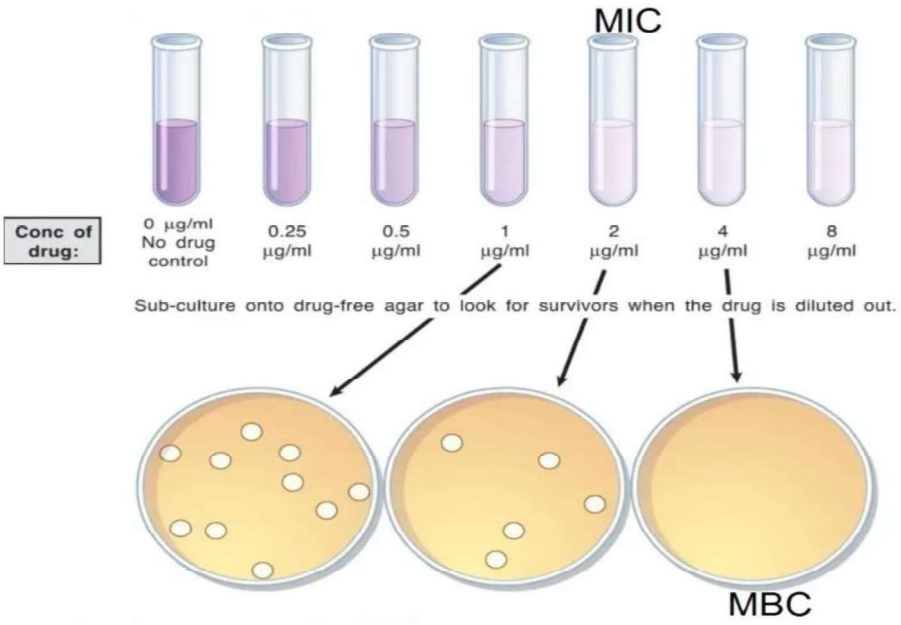

Fig 3.1. MIC/MBC test of a bactericidal drug [Source: (Alm et al., 2005)].

3.4. Generation of V. cholerae growth curve

The growth curves of *V. cholerae* El Tor strains were examined using an overnight culture in LB media, followed by the addition of inhibitors at or below the minimum inhibitory concentration (MIC) levels. Briefly, one colony was inoculated in 5 ml of LB broth and cultured overnight at 37 °C with shaking (Mondal et al., 2014). The cells in the stationary phase were collected, centrifuged, washed twice in phosphate buffered saline (PBS), and their concentration was adjusted to 1×10^9 cells per ml using LB medium. Subsequently, in fresh 25 ml of LB broth, an initial inoculum of 1×10^8 cells per ml was added. The cultures were then maintained at 37 °C for an additional 24 h under constant shaking conditions. Viability of the bacteria was assessed by performing dilution plating in streptomycin treated Luria Agar (LA) plates at various time intervals, followed by colony count (Vercruysse M. et al., 2014). For the combination study, the growth curve was analysed using the same protocol, except that the bacterial culture was challenged with sodium butyrate, antibiotics and combination of drugs.

3.5. Mucin penetration assay

The assay was conducted following a previously published method (Z. Liu et al., 2008). In brief, mucin columns were prepared using 1 ml syringes by adding varying concentrations of porcine mucin (1%, 1.5%, and 2%) (Sigma, Saint Louis, Missouri). During the inhibitor study, different concentrations of bioactive compounds were added to each mucin column, while an untreated mucin column served as the control. Bacteria were grown till mid-log phase and their concentration was adjusted to 5×10^8 cells per ml using PBS. Next, 0.1 ml of the bacterial culture was added to the top of the mucin columns. The columns were then allowed to settle for 1 h at 37 °C under static conditions. After settling, 100 µl fractions were collected from the bottom of the columns. The bacterial numbers were determined by serially diluting the samples, plating them in LA plates, and counting the colony-forming units (CFU).

3.6. ELISA

Levels of IL-8, IL-6, IL-1β, and TNF-were measured from fluid collected during rabbit ileal loop cultures after infection with wild-type *V. cholerae*, and treatment with and without sodium butyrate, using ELISA method. The ELISA was performed using ELISA Kits from Krishgen, Mumbai, India, following the manufacturer's protocol. In brief, 50 µl of ELISA diluent (composed of 12 ml of buffered protein base with 0.09% sodium azide as a preservative) was added to each well. Subsequently, 100 µl of the sample was added to the wells. The mixture was incubated for 2 h at room temperature, and then the wells were washed five times. After washing the wells, 100 µl of the working detector (enzyme concentrate + detection antibody) solution was added to each well and incubated for 1 h at room temperature. Following incubation, the wells were washed five times. Next, 100 µl of TMB substrate was added to each well, and the wells were incubated for 30 min at room temperature. After this incubation period, 50 µl of the stop solution was added to each well, and optical density (OD) was measured at 450 nm using a microplate reader (BioRad, Hercules, CA). A standard curve was generated using a 2-fold serial dilution of purified IL-8, IL-6, IL-1β, and TNF-α. This curve was then used to determine the unknown concentrations of IL-8, IL-6, IL-1β, and TNF-α.

3.6.1. GM1 ganglioside – Cholera toxin (CT) ELISA

Secretion of cholera toxin (CT) by *V. cholerae* strains was assessed using a GM1 enzyme-linked immunosorbent assay (ELISA) based on a previously described method (Holmgren et al., 1973), with minor modifications (Patra et al., 2012). CT expression was measured using cell-free culture supernatants from *V. cholerae* cultures grown in AKI media, which were harvested after 18 h of static incubation at 37 °C as well as from *in vivo* rabbit ileal loop cultures. The culture supernatants were then added to the wells of MaxiSorp ELISA plates, which had been coated with 1.5 µg/ml GM1 ganglioside in 60 mM Na_2CO_3 (Sigma, Saint Louis, Missouri). After incubating for 2 h at room temperature, the wells were washed five times with PBS. Next, 100 µl of polyclonal α-CT antibody (Sigma, Saint Louis, Missouri), diluted in Solution 1 [1× PBS, 2% BSA, 0.05% TWEEN-20] at 1:1000 ratio, was added to each well. Again after 1 h incubation at room temperature, the wells were again washed five times with PBS. Finally, 100 µl of HRP-conjugated anti-rabbit secondary antibody, diluted in PBS at 1:2000 ratio, was added to each well. After incubation for 1 h at room temperature, the plate was washed five times with PBST (PBS + 0.05% TWEEN 20). Next, 100 µl of TMB substrate (BD Biosciences, Franklin Lakes, New Jersey) was added to each well, using a 1:1 ratio of Kit solution 1 and 2. The plate was then incubated for a few minutes to allow colour development. Finally, 100 µl of 6N H_2SO_4 was added to each well to stop the reaction. In each set of assays, known amounts of purified CT were used at different concentrations to generate a standard curve. The amount of CT secreted by *V. cholerae* strains was determined by extrapolating the optical density values of the samples at 450 nm using this standard curve. The OD_{450} average obtained from triplicate wells of each experimental set was used to estimate the amount of CT present and expressed as ng of CT/ml.

3.7. Biofilm assay

Biofilm assay was performed using a previously described method (Zhu et al., 2003). In brief, 1:100 dilution of an overnight culture of *V. cholerae* was inoculated into LB broth present in 10 by 75 mm borosilicate glass tubes and incubated at 37 °C for 30 h. After incubation, the tubes were rinsed three times with PBS and then filled

with 1% crystal violet stain. After 5 min, the excess stain was rinsed off with deionized water. The crystal violet that was associated with biofilm was solubilized in DMSO, and the optical density at 595 nm (OD_{595}) of the resulting suspension was measured.

3.8. Cell culture

In this study, human intestinal cell line HT-29 (ATCC HTB-38) was used for the experiments (*Fig 3.2*). HT-29 cell line was maintained following the guidelines provided by the American Type Culture Collection (ATCC). The cells were cultured in Corning T-25 flasks using Dulbecco's Modified Eagle's Medium (DMEM) (Sigma, St. Louis, MO, USA), which contained 4.5 g/l of glucose, 110 mg/l of sodium pyruvate, and 10% heat-inactivated fetal bovine serum (FBS) (South American origin, PAN Biotech, Germany). The cells were incubated in an incubator (HERAcell® 150, Thermo Scientific, USA) containing 5% CO_2 at 37 °C to form a monolayer. Complete DMEM media, supplemented with 3.7 g/l sodium bicarbonate, 50 U/ml penicillin, and 50 mg/ml streptomycin (Sigma, St. Louis, CA), was used for maintaining the cell line and infection studies. Culture media was replaced with fresh media on alternate days, and the monolayer was used after reaching approximately 90% confluency. Stock was prepared by using 95% complete growth media and 5% DMSO (Sigma, St. Louis, MO, USA) and was stored in liquid nitrogen. To maintain the growth of anchorage-dependent cell lines in monolayers during exponential development, cells were sub-cultured at regular intervals. Cells were sub-cultured after reaching approximately 70% to 90% confluency, indicating they were nearing the end of exponential growth. First, media was discarded, and the cells were washed with PBS at 37 °C, without calcium or magnesium. Next, 2 ml to 3 ml of a 0.25% trypsin-EDTA solution (37 °C), was added to detach the cells. After a short incubation at 37 °C, complete growth medium was added to inactivate the trypsin. Following this, the cells were centrifuged, suspended in complete media, and seeded according to a routine split ratio of 1:3 to 1:8.

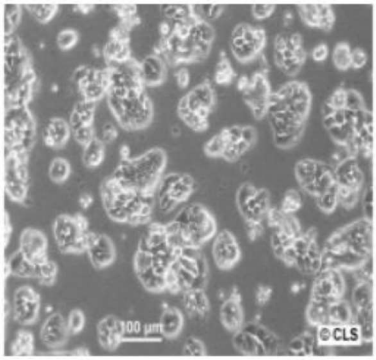

Fig 3.2. Microscopic image of HT-29 cell line

3.9. In vitro growth assay in HT-29 cell line

The mucin-secreting human intestinal cell lines HT-29 was maintained in Dulbecco's Modified Eagle's Medium (DMEM, Sigma, St. Louis, MO, USA). This medium was supplemented with 10% fetal bovine serum (FBS) (HiMedia, Mumbai, India), 1% (vol/vol) non-essential amino acids (DMEM, Sigma, St. Louis, MO, USA), and a 1% (vol/vol) mixture of penicillin and streptomycin (Sigma, St. Louis, MO, USA). Cells were cultured at 37 °C under 5% CO_2. Survival of *V. cholerae* in the presence of mucin-secreting HT-29 cells was analyzed using the established protocol (Mondal et al., 2014). Incomplete media, lacking penicillin-streptomycin and containing 0.5% FBS, was used for serum starvation. HT-29 cells, which were 80% confluent and serum-starved, were cultured in 12-well plates and infected with log phase cultures of *V. cholerae* N16961 strains (with or without drugs) at an infectious dose of 1×10^7 CFU/ml. After a varying period of incubation, unbound cells were collected from the supernatant. The bound bacteria were then detached by treating the cells with 0.1% Triton X-100 for 2-3 min. Both the unbound and bound bacteria were collected, washed in PBS, serially diluted, and plated on LA plates to determine the viable bacterial count.

3.10. HT-29 cell adhesion assay

Adhesion of *V. cholerae* (with or without drugs) to HT-29 cells was performed according to previously described methods (Chourashi et al., 2016). HT-29 cells were split into 12-well cell culture plates and maintained in DMEM supplemented with 10% fetal bovine serum (FBS). Once the cells reached 80% confluency, a freshly grown mid-log phase bacterial inoculum of 1.2×10^8 was prepared. This inoculum was washed in PBS and quantified using colony-forming unit (CFU) counting. The ratio of bacteria to HT-29 cells was set at 100:1 (MOI 100), and the inoculum was added to 1.2×10^6 HT-29 cells in DMEM culture medium containing 0.5% FBS and no antibiotics. Adhesion assay was performed by incubating the bacteria/cells at 37 °C for 1 h under conditions of 5% CO_2 and 90% relative humidity. Following incubation, the cells were washed three times with pre-warmed PBS (pH=7.4) and then detached using 0.1% Triton X-100. The adherent bacteria were counted after serial dilution by plating on LA plates that were supplemented with 100 μg/ml of streptomycin. For fluorescence

microscopy, *V. cholerae* strains were transformed with Ampicillin resistant GFP expressing plasmid, pGFPuv (Clontech, TaKaRa Bioscience) by electroporation. Confluent monolayers were infected with 1 ml of bacterial suspension (GFP expressing *V. cholerae* strain containing 1×10^6 bacteria/ml) and incubated at 37 °C for 4 h. Adhesion assay with this GFP expressing *V. cholerae* strain was done on a grease-free, sterile coverslip, washed in PBS, and mounted with VECTASHIELD antifade mounting medium (Vector laboratories, Newark, California) to view under a fluorescence microscope (Olympus AX-70, Hachioji, Tokyo, Japan).

3.11. In silico docking study

The 3D structure of the docking target ToxT was downloaded from the RCSB Protein Data Bank and visualized using UCSF Chimera version 1.11. Protein was prepared for docking using the Yasara engine and saved as a new PDB file with Chimera. The ligands used for docking were sourced from various published reports. These ligands were converted to PDB format using UCSF Chimera and energy minimized using universal force fields (UFF). The ligands were then docked into the binding pocket of ToxT using PyRx with AutoDock Vina, and energy values were computed for each ligand. Ligands that fit into the binding pocket were selected for further *in vitro* and *in vivo* studies.

3.12. Primer design for PCR

All the primers used in this study were designed based on the sequences of the *V. cholerae* El Tor strain N16961 (NCBI Reference sequence: NC_002505.1 for Chromosome 1 and NC_002506.1 for Chromosome 2), which is available in GenBank (https://www.ncbi.nlm.nih.gov/). The primers and the sequences were tested for potential primer dimer formation, degeneracy, and cross-reactivity with any other genes present in *V. cholerae* using the BLAST program (https://blast.ncbi.nlm.nih.gov/Blast.cgi). For Real-Time PCR, the primers were designed using IDT software (PrimerQuest™ Tool). A complete list of all the primers utilized in this study is included in the appendix section.

3.13. Total RNA isolation for expressional studies

Bacteria were harvested from log-phase cultures and centrifuged at 8000×*g* for 10 min at 4 ºC. The bacterial pellets were washed three times with PBS and then used for RNA isolation. Total RNA was extracted using TRIzol (Invitrogen, Carlsbad, CA) according to the manufacturer's protocol. In brief, TRIzol, a monophasic solution of phenol and guanidine isothiocyanate, was added to the cell pellet (0.5 ml) for every 5 ml of culture with an optical density (OD) of 1 at 600 nm. The cells were then resuspended through slow pipetting. Samples were incubated for 20 min at room temperature to ensure the complete dissociation of nucleoprotein complexes. Chloroform (0.2 ml per ml of TRIzol) was then added to the mixture, which was shaken vigorously for 15 sec and incubated for an additional 2 to 3 min at room temperature. Following this, the mixture was centrifuged at 12,000×*g* for 20 min at 4 °C, and the aqueous phase was carefully transferred to a DNase and RNase-free microcentrifuge tube (Axygen, Union City, CA). Isopropanol was added (0.5 ml per ml of TRIzol), and the mixture was incubated at room temperature for 10 min. Finally, RNA was precipitated by centrifugation at 12,000×*g* for 10 min at 4 °C. The pellet was washed with 0.5 ml (1 ml/ml of TRIzol) of 75% (v/v) ethanol, air dried, and then dissolved in nuclease-free water. Isolated RNA was treated with DNase of Ambion® DNAfree™ kit (Ambion, Texas, USA) to eliminate any contaminating genomic DNA, following the manufacturer's protocol. The total RNA isolated was stored at -80 °C until needed. Purity of the RNA was assessed spectrophotometrically at 260/280 nm.

3.14. Measurement of the RNA concentration and purity

Concentration of RNA was quantified by measuring the absorbance at 260 nm using the following formula: (A_{260} × DF × 40)/ 1000 µg/µl. In this formula, A_{260} represents the absorbance of the diluted RNA at 260 nm, while DF is dilution factor for the RNA in nuclease-free water. For RNA, A_{260} of 1.0 corresponds to 40 µg/ml concentration. The purity of RNA was determined from the ratio of absorbance at both 260 and 280 nm. Ideally, the purest form of RNA has a ratio of A_{260}/A_{280} equal to 2.

3.15. Reverse transcription reaction

First-strand cDNA synthesis was prepared using a Verso cDNA synthesis kit (Thermo, Waltham, MA). Initially, 1 µg of total RNA was heated at 70 °C for 10 min to denature secondary structures, then immediately cooled on ice. This RNA was mixed with the reaction components in a 0.2 ml PCR tube, as outlined in *Table 3.2*. The components were gently mixed and briefly spun down. The mixture was incubated at room temperature for 10 min, followed by incubation at 42 °C for 15 min. The enzymes were heat-inactivated by incubating at 95 °C for 5 min, and the sample was then kept at 4 °C for at least 5 min. The reverse transcription (RT) products were stored at -20 °C until further use.

Components	**Volume added**
5X cDNA synthesis buffer*	4 µl
dNTP mix	1 µl
RNA primer (Random hexamer)	1 µl
RT enhancer	1 µl
Verso Enzyme Mix	1 µl
Template (RNA)	1-5 µl
Nuclease Free Water	To make up the volume of 20 µl
Final volume	20 µl

Table 3.2. Composition of the reaction mixture for reverse transcriptase PCR

*The reverse transcriptase buffer contains 100 mM tris-HCl (pH 9.0 at 25°C), 500 mM KCl and 1% Triton X-100.

3.16. Quantitative Real Time PCR

V. cholerae was grown to the log phase in the presence or absence of inhibitors. Total RNA isolated from *V. cholerae* was converted to cDNA using the Reverse Transcription protocol (Promega, Madison, WI, USA). This cDNA was then used as a template to quantify mRNA transcript levels. Quantitative PCR (qPCR) was performed using 2× SYBR Green PCR Master Mix (Applied Biosystems, Foster City, California) along with 0.2 µM of specific forward and reverse primers. These primers were

designed using Primer Quest from Integrated DNA Technologies (IDT) for each transcript (appendix for details). The composition of the real-time PCR reaction mixture is shown in *Table 3.3* while the cycling conditions for real-time PCR are illustrated in *Fig. 3.3*. Data analysis was performed using the 7500 Real-Time PCR detection system (Applied Biosystems, Foster City, California). The process involved 40 cycles of a two-step cycle, followed by a melting curve. Relative expression of the target transcripts was calculated using Livak's $2^{-\Delta\Delta Ct}$ method (Livak et al., 2001), with *recA* (VC_0543) serving as an internal control.

Components	**Volume added**
SYBR Green Master Mix	10 µl
Real-Time Forward Primer (10µM)	1 µl
Real-Time Reverse Primer (10µM)	1 µl
Template (cDNA)	1-5 µl
Nuclease Free Water	To make up the volume of 20 µl
Final volume	20 µl

Table 3.3. Composition of the Real-Time PCR reaction mixture

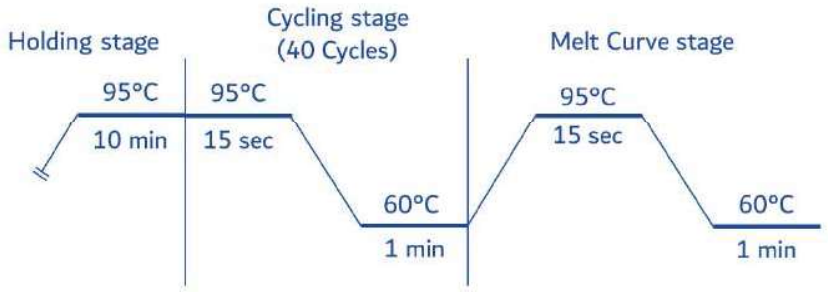

Fig.3.3. Schematic diagram of real time PCR conditions for all transcripts.

3.17. Polymerase Chain Reaction (PCR)

Polymerase chain reaction throughout the study wherever required was conducted in 0.2 ml PCR tubes with the following reaction mixture as described below (*Table 3.4*). The components were mixed gently and briefly spun, after which PCR was performed using a thermal cycler (Bio-Rad, Hercules, California). The annealing temperature for each set of forward and reverse primers was set 2 °C below the melting

temperature (T_m) of each primer. The extension time for the Taq DNA polymerase was calculated based on a synthesis rate of 1000 base pairs per min.

Components	Volume added
$MgCl_2$, 25mM	2 µl
5X Reaction Buffer	4 µl
Forward Primer (10µM)	0.4 µl
Reverse Primer (10µM)	0.4 µl
dNTP mix, 10mM	0.8 µl
Taq DNA polymerase, 5U/µl	0.2 µl
Template (DNA)	2 µl
Nuclease Free Water	To make up the volume of 20 µl
Final volume	20 µl

Table 3.4. Composition of the PCR reaction mixture (For each reaction)

3.18. Agarose gel electrophoresis

The amplified DNA fragments were resolved using 1.2% agarose gel electrophoresis. First, agarose was mixed with 1×TAE buffer (refer to the Appendix) and heated until fully dissolved. The melted agarose was then poured into a gel caster. Following this, the electrophoresis run was performed, and the PCR products were stained with either Ethidium Bromide (EtBr) or SYBR Safe DNA Gel Stain (Invitrogen). The stained gel was visualized under a UV transilluminator, and images were captured using a gel documentation system (Bio-Rad). Densitometric analysis of the agarose gel was conducted by measuring the band intensities of the amplified test samples using Bio-Rad QUANTITY 1 software.

3.19. Plasmid DNA isolation

Plasmids were isolated using the Wizard® Plus Minipreps DNA purification kit (Promega, USA) (*Fig. 3.4*). In summary, 1-10 ml of overnight-grown bacterial culture was pelleted by centrifugation at 1,400 × *g* for 10 min. The bacterial pellet was then resuspended in 400 µl of cell resuspension solution (50 mM Tris-HCl, pH 7.5; 10 mM EDTA; 100 µg/ml RNase A). Next, 400 µl of cell lysis solution (0.2 M NaOH; 1% SDS) was added, resulting in a clear cell suspension. After adding 400 µl of neutralization solution (1.32 M potassium acetate, pH 4.8), the lysate was centrifuged at 10,000 × *g* for 15 min. The supernatant was combined with 1 ml of resin, and a vacuum of 15 inches of Hg was applied to completely draw the resin and lysate through the mini column. Following this, the resin was thoroughly washed with a wash buffer consisting of 80 mM potassium acetate, 8.3 mM Tris-HCl (pH 7.5), 40 µM EDTA, and 55% ethanol. Finally, the plasmid bound to the membrane was recovered using nuclease-free water.

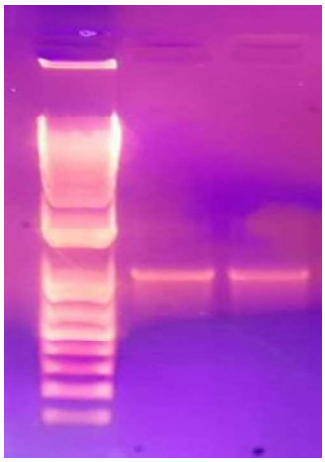

Fig.3.4. Agarose Gel of Extracted Plasmid DNA

3.20. Purification of PCR products

The PCR products and gel-cut products were purified using the Wizard SV Gel and PCR Clean-Up System (Promega, USA). Briefly, an equal volume of membrane binding solution (containing 4.5 M guanidine isothiocyanate and 0.5 M potassium acetate at pH 5.0) was mixed with the PCR product. For gel-cut products, a membrane-binding solution was added at 1 µl/mg and heated at 65 °C to dissolve the agarose gel. This prepared mixture was then poured into an SV mini column and incubated at room temperature for 1 min. A vacuum of at least 15 inches of Hg was applied to fully draw the solution through the membrane. Following this, the membrane was washed by adding 700 µl of wash solution, followed by 500 µl of a membrane wash solution containing 10 mM potassium acetate (pH 5.0), 80% ethanol, and 16.7 µM EDTA (pH 8.0). To eliminate any residual ethanol, the mini columns were centrifuged at 16,000 × *g* for 5 min. The membrane was subsequently incubated at room temperature with 30 µl of nuclease-free water for 1 min. DNA was eluted by centrifugation at 16,000 × *g* for 1

min into a fresh tube. The absorbance of the eluted product was then measured at 260 nm to determine its concentration.

3.21. Measurement of DNA concentration and purity

Concentration of DNA was quantified by measuring absorbance at 260 nm using the following formula: (A_{260} × DF × 50)/ 1000 µg/µl, where A_{260} is the absorbance of the diluted DNA at 260 nm and DF is dilution factor of DNA in nuclease-free water. For dsDNA, A_{260} of 1.0 corresponds to 50 µg/ml concentration. The purity of DNA was determined from the ratio of absorbance at both 260 and 280 nm. Ideally, the purest form of DNA has A_{260}/A_{280} ratio of 1.8.

3.22. Polyacrylamide gel electrophoresis (PAGE)

Protein samples were analysed by using SDS-PAGE (Raymond et al.,1959). Prior to loading, the samples were heated with loading dye at 100 °C for 5 min. The gel run was conducted at a voltage ranging from 80 to 120 V at room temperature, in an Atto gel running system (Atto, Japan) For the composition of the running buffer, refer to the appendix. The details of the SDS-PAGE gel composition can be found in *Table 3.5*.

	Separating gel (pH 8.8)						**Stacking gel (pH 6.8)**
	5%	**7.5%**	**10%**	**12.5%**	**15%**	**20%**	
A (ml)*	1.7	2.5	3.33	4.2	5	6.7	1.5
B (ml)*	2.5	2.5	2.5	2.5	2.5	2.5	-
C (ml)*	-	-	-	-	-	-	1.8
H_2O (ml)	5.8	5	4.2	3.33	2.5	0.8	
10% APS (µl)	23	23	23	23	23	23	10
TEMED (µl)	5.5	5.5	5.5	5.5	5.5	5.5	7.0

Table 3.5. Composition of the SDS-PAGE gel

*A, B, C denotes the composition of different solutions. Please see the appendix.

3.23. Coomassie staining

After performing SDS-PAGE, the gel was fixed in a solution of 50% methanol (MeOH) and 5% glacial acetic acid (AcOH) for 30 min. Subsequently, the gel was incubated at room temperature for another 30 min in a staining solution consisting of 50% MeOH, 50% AcOH, and 0.1% Coomassie Brilliant Blue R250. To visualize the protein bands, the gel was destained using a solution of 5% MeOH and 7.5% AcOH (Meyer et al., 1965).

3.24. Protein estimation by modified Lowry method

The concentration of the protein sample was measured using the modified Lowry method (Lowry et al., 1951). Three types of reagents were used for this estimation method:

Reagent A: 2% Na_2CO_3 in 0.1 M NaOH containing 0.16% Na-K tartrate + 0.1% SDS

Reagent B: 4% $CuSO_4$. $5H_2O$

Reagent C: 100: 1= A: B (10 ml + 100 µl)

A total of 200 µl of the protein sample was incubated with 600 µl of reagent C at room temperature for 15 min. Following this, 1 N Folin-Ciocalteu's reagent was added to the mixture, and it was further incubated at 37 °C for 30 min. Optical density (OD) was then measured at 660 nm. The protein concentration was estimated using the equation: concentration = OD_{660} / 0.0026, which was derived from a standard curve of bovine serum albumin (BSA).

3.25. Western blotting

For western blotting, the electrophoretic transfer of proteins from SDS-PAGE to a nitrocellulose or polyvinylidene fluoride (PVDF) membrane was performed. To transfer proteins from the polyacrylamide gel to the PVDF membrane (Towbin et al., 1979), the membrane, gel, and filter pads were kept in transfer buffer (48 mM Tris, 39 mM Glycine, 0.05% SDS, and 20% MeOH) for 30 min at room temperature. The set up for semi-dry transfer is illustrated in ***Fig. 3.5.A***, and the transfer was performed at 200 mA for 1 h. For wet transfer, the transfer cassette was assembled as shown in ***Fig. 3.5.B***, and the process was carried out at 100 V for 1 h under cold conditions.

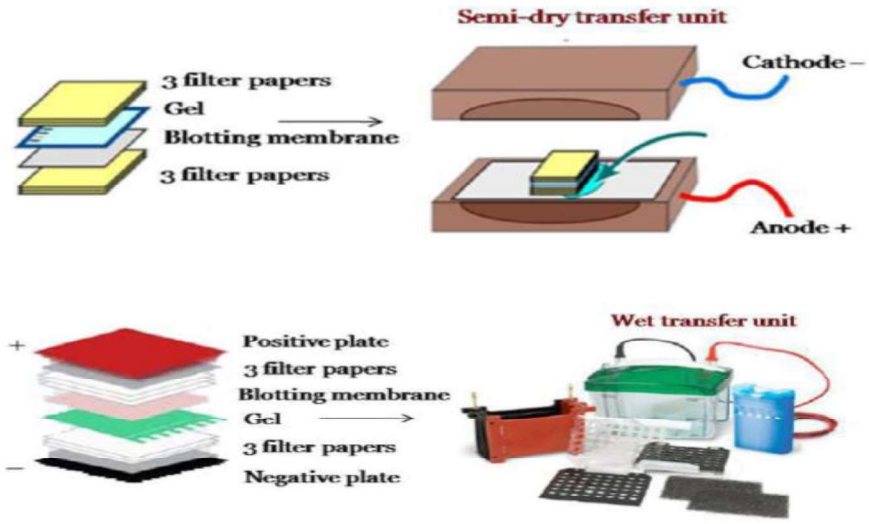

Fig.3.5. Arrangement of filter paper, gel, and membrane for western blot.
(A) Semi-dry transfer (B) Wet transfer [Source: (Alm et al., 2005)].

After the transfer, membrane was incubated in a blocking buffer containing 5% skimmed milk in TBST (20 mM Tris, pH 7.5; 50 mM NaCl; and 0.1% Tween 20) for 1 h at room temperature to block non-specific binding sites. Subsequently, the membranes were incubated with primary antibodies at appropriate dilutions for overnight at 4 °C. The primary antibodies used included rabbit polyclonal anti-ToxT (Cat# BB-SAP50), rabbit polyclonal anti-TcpA (Cat# BB-SAP50), and rabbit polyclonal anti-DnaK (Cat# BB-SAP50). Following primary antibody incubation, membranes were treated with goat anti-rabbit secondary antibody for 2 h at room temperature. Finally, the membranes were washed with TBST for 30 min. Bands were then developed using the ChemiDoc MP Imaging System (Bio-Rad, USA) with a chemiluminescent HRP substrate (Millipore, Burlington, Massachusetts, USA).

3.26. Expression and purification of Recombinant protein NBP-ToxT/CytR

Purification of the Nickel Binding Recombinant Protein Fusion (NBP-ToxT/CytR) was carried out as previously described (Plecha et al., 2015), using the *Escherichia coli* strain BL21(DE3) containing the pHIS-Tev plasmid that harbors the 6X His-recombinant protein fusion construct *(Fig.3.6)*. Initially, the cells were grown overnight at 37 °C. They were then sub-cultured into fresh LB broth at a 1:100 ratio

and allowed to grow until the optical density at 600 nm reached 0.5. Following this, the culture was induced with 0.5 mM of isopropyl-D-thiogalactopyranoside (IPTG) and incubated at 37 °C for 3 h. The NBP-ToxT/CytR protein was extracted as an insoluble protein from inclusion bodies by sonication and was then solubilized in 10 ml of buffer A, which consists of 25 mM Tris, 100 mM NaCl, 0.1% Triton X-100, and 7 M urea at pH 7.5. The denatured protein was initially loaded in Ni^{2+}-conjugated agarose beads that had been pre-equilibrated in buffer A. The column was then washed with 20 ml of buffer A, and the denatured protein was eluted using 10 ml of buffer A containing 250 mM imidazole. Fractions that contained the 6X His-recombinant protein fusion construct were collected and subsequently renatured by gradually removing urea through dialysis using a 10 kDa membrane. SDS-PAGE was performed to analyze the samples, and the protein concentration in each sample was quantified by Bradford Reagent and the purity was confirmed by SDS-PAGE, stained with Coomassie Brilliant Blue.

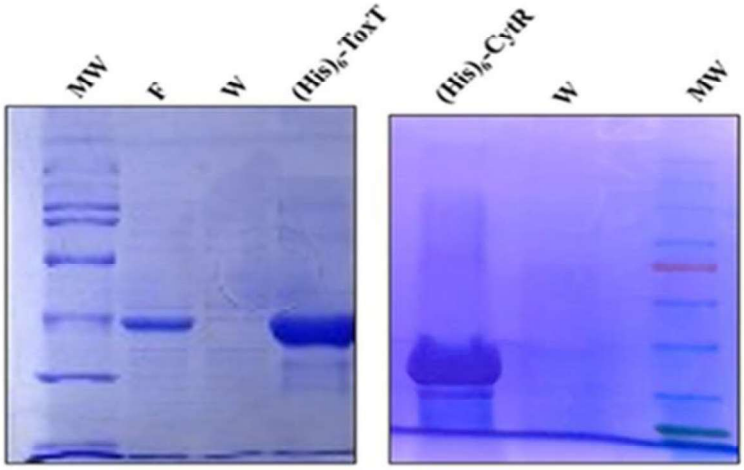

Fig.3.6. Coomassie blue staining of the purification of $(His)_6$-ToxT/$(His)_6$-CytR fusion protein using nickel chelated affinity chromatography. Mw, molecular weight marker; F, flow-through fraction; W, washed fraction

3.27. Fluorescence Quenching Analysis

Interaction between the ToxT protein and Sodium butyrate (SB) was analyzed by examining concentration-dependent effects of SB on the tryptophan fluorescence emission of ToxT. Emission spectra for ToxT were obtained from a solution of 0.1 µM of the protein dissolved in 25 mM Tris (pH 7.5) and 100 mM NaCl, both in the presence and absence of SB. The solution was excited at 280 nm, and intrinsic fluorescence emissions were scanned from 300 nm to 500 nm using a Hitachi Fluorescence Spectrophotometer F-7000 (Tokyo, Japan). Fluorescence quenching was evaluated using the classical Stern-Volmer equation, as previously described (Tükenmez et al., 2021).

3.28. Protein-DNA Binding Experiments

3.28.1. Chromatin immunoprecipitation

The effect of SB on ToxT occupancy at downstream promoter DNAs was examined through chromatin immunoprecipitation (ChIP). *V. cholerae* cells were grown in the presence of SB (20 mM) for 4 h. Following the incubation, the cells was crosslinked with 1% formaldehyde. Crosslinking was stopped by adding glycine to a final concentration of 125 mM, and the bacteria were washed three times with ice-cold PBS buffer. Cells were then resuspended in lysis buffer (10 mM Tris-HCl, pH 8.0; 50 mM NaCl, containing 20 ng/µl RNase A and 10^5 kU of ready lyse lysozyme) and incubated at 37 °C for 30 min. One volume of double-strength IP buffer (200 mM Tris HCl, pH 7.5; 600 mM NaCl; 4% Triton X-100), which also contained a protease inhibitor cocktail and 1 mM phenyl methyl sulfonyl fluoride (PMSF), was added to each lysate. DNA was then sonicated to achieve fragments ranging between 200 to 1000 base pairs. Cell debris was removed by centrifugation at 12,000 rpm for 10 min and 4 °C, and a portion of the supernatant was collected as the input sample for immunoprecipitation (IP) assays. The nucleoprotein complexes were immunoprecipitated by overnight incubation at 4 °C with 8 µg of anti-ToxT antibody. Salmon sperm DNA treated G agarose beads (Thermo Scientific), pre-washed with lysis buffer was used to pull down the antibody protein DNA complexes for 4 h at 4 ºC. The beads were washed sequentially: first with lysis buffer, then with wash buffer (500 mM NaCl lysis buffer), followed by LiCl immune complex buffer, which consists of 20 mM Tris-HCl (pH 8.0),

0.25 M LiCl, 1 mM EDTA, 0.5% (wt/vol) NP-40, 0.5% (wt/vol) DOC, and 1% (wt/vol) PMSF. Finally, the beads were washed with TE buffer (10 mM Tris-HCl, pH 8.0, 1 mM EDTA). The immunoprecipitated complexes (IP) were eluted from the beads by incubating at 65 °C for 30 min in TE buffer containing 1% SDS. Reversal of cross-linking was done by incubation with 20µg of proteinase K for 1 h at 65 °C. Both the control input and the immunoprecipitated DNA samples were then purified using a PCR purification kit (Qiagen, Hilden, Germany) and eluted in 30 µl of DNase-free water. Real-time quantitative PCR (qPCR) and agarose PCR gel electrophoresis were performed to quantify promoter occupancy by ToxT, as previously described using the primers for ChIP (Yan et al.,2023). Data were graphically represented as % of input. The schematic representation of chromatin immunoprecipitation (ChIP) assay in represented in ***Fig 3.7.***

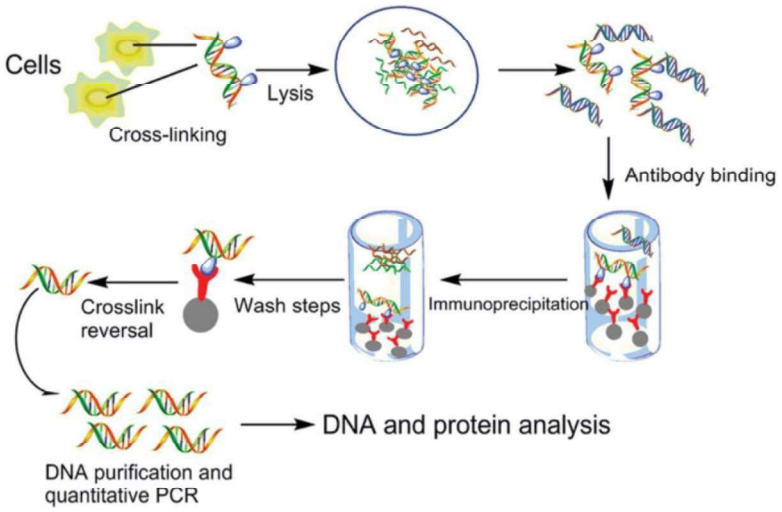

Fig 3.7. A schematic representation of ChIP assay [Source: (Song, C et al., 2015)].

3.28.2. Electrophoretic Mobility Shift Assay

Chromosomal DNA of *V. cholerae* N16961 was used as a template for PCR process to amplify a DNA fragment of 150 bp corresponding to the *tcpA* promoter region. This amplified product was then labelled with biotin at the 5' end and purified using the QIAquick removal kit (Qiagen). To assess the drug-protein interaction, binding reactions were set up in which purified His-tagged ToxT protein was pre-incubated with SB for 20 min in a binding buffer consisting of 10 mM Tris-HCl (pH 7.5), 100 mM KCl, 1 mM EDTA, 1 mM dithiothreitol, 200 µg of bovine serum albumin per ml,

and 10% glycerol. Next, a fixed amount of biotinylated DNA fragment (1 nM) was added, and the mixture was incubated for an additional 20 min. To demonstrate specificity, a non-specific protein (CytR), a 70-fold molar excess of unlabelled double-stranded *tcpA* fragment and a 70-fold molar excess of unlabelled non-specific DNA were used as controls. Additionally, another butyrate derivative, tributyrate (TB), was utilized to further assess the specificity of the interaction. To investigate potential drug-DNA interactions, labelled DNA (0.5 nM) was pre-incubated with SB for 20 min in a binding buffer. After this initial incubation, purified ToxT protein (4 µM) was added, and the incubation continued for an additional 20 min. The samples were then loaded onto a 4% native polyacrylamide gel and electrophoresed at 100 V at 4 °C using 0.5× Tris-borate-EDTA buffer. Following electrophoresis, DNA was transferred from the gel to a charged nylon membrane for nucleic acid blotting (Millipore). Cross-linking was performed using a UV Strata linker from Strata gene, and detection was achieved with the LightShift™ Chemiluminescent EMSA Kit (Thermo Scientific). The schematic representation of EMSA in represented in ***Fig 3.8.***

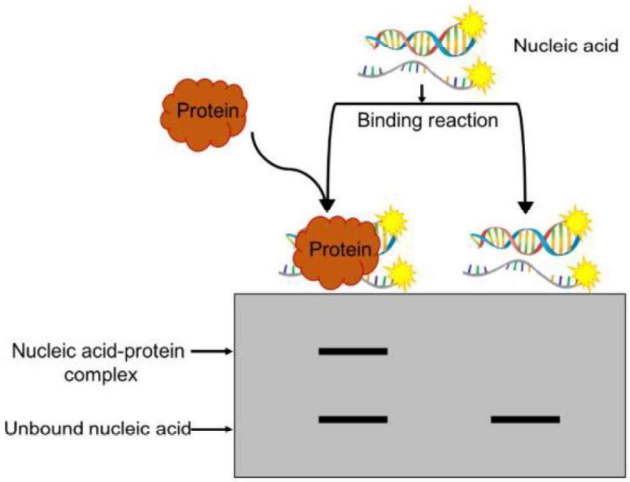

Fig 3.8. A schematic representation of EMSA [Source: (Hellman et al., 2007)].

To determine the equilibrium dissociation constant (K_D) for samples with and without SB, the percentage of labelled DNA bound to protein for each lane was measured. These data were then fitted to the following equation: percent bound=B_{max} *X [protein]*^{h}*/ (*K_D^h *+ [protein]*^{h}*),* where *h* is the Hill coefficient and B_{max} is the amount of bound DNA at which the curve plateaus, which was set to a constraint of 100% using GraphPad Prism 9 software. K_D values for each condition were compared to each other using the extra sum of squares F test to determine if the two values were statistically different.

3.29. RNA Sequencing

RNA sequencing was performed by Medgenome, Bangalore, India. *V. cholerae* strain N16961 samples were grown under toxin-inducing conditions, both in the presence and absence of SB, until they reached mid-log phase. Following this, the bacterial samples were harvested. Total RNA was isolated using Trizol method and processed for quality assessment. RNA samples were evaluated using a Nanodrop for quality and quantitated with the Qubit dsDNA BR assay (Thermo Scientific). Additionally, quality of RNA was verified using a 1% agarose TAE gel, and any degradation was checked with the Agilent Bioanalyzer RNA 6000 nano kit. The samples that passed quality control (QC) were further analyzed. To selectively enrich the mRNA, ribosomal RNA (rRNA) was depleted using a Ribo-Zero rRNA removal kit (Epicentre, Madison, WI). Subsequently, a cDNA library was constructed using a TruSeq stranded mRNA sample kit (Illumina, San Diego, CA). RNA sequencing was performed with Illumina HiSeq X system.

Library QC: 1) Illumina library: To achieve the highest quality of data on Illumina sequencing platforms, optimum cluster densities across every lane of each flow cell were created which required accurate quantification of library templates. So, to quantify prepared libraries, qPCR was done according to the Illumina qPCR Quantification Protocol Guide. 2) GS FLX library: To generate a standard curve of fluorescence readings and calculate the library sample concentration, Roche's Rapid library standard Quantification solution and calculator was used. The samples which had passed library QC were taken further for sequencing.

The raw data were processed using the HISAT2-StringTie pipeline. The raw sequencing reads were mapped against the genomic sequence of *V. cholerae* O1 biovar El Tor str. N16961 using the HISAT2 alignment tool. StringTie was used to assemble reads and generate FPKM (fragments per kilobase per million) values, as a normalization metric (Liu et al., 2022). After filtering undesirable contaminants (such as rRNAs), differentially expressed genes between different groups were identified by the package DESeq2 [20mM of SB over 0mM of SB treatment were determined as fold change (FC) by the formula $\log2(\text{mean FPKM}_{test}/ \text{mean FPKM}_{control})$], with thresholds of adjusted *P* values at ≤ 0.05 and an absolute fold change ≥ 2. The differentially expressed genes identified among the two groups were generated in a heatmap by the CIMminer program.

3.30. Antimicrobial Susceptibility Testing

Disc diffusion method: - Bacterial growth inhibition was assessed using the standard disc diffusion method as described previously (Bauer et al., 1966). First, Petri plates were prepared by pouring 25 ml of Nutrient Agar (Biomark Laboratories, Pune, India) and allowing it to solidify. The plates were then dried, and 100 µl of bacterial suspension containing 1×10^6 cells/ml was evenly spread over the surface of each plate. The plates were then allowed to dry for 5 min. Next, antibiotic discs (Oxoid Ltd., Hampshire, UK) were placed on the surface of the plates. The plates were incubated at 37 °C for 24 h, after which the zones of inhibition were observed and measured in mm *(Table 3.6)*.

Name of the antibiotics (Disc content µg/disk)	**Zone diameter interpretative criteria (CLSI guidelines) mm**		***V. cholerae* strains (zone size in mm)**			***E. coli* strains (zone size in mm)**	
	S	**R**	**N16961** (O1 El Tor)	**BCH13298** (O1 El Tor variant)	**Micro78** (O1 El Tor variant)	**B2**	**IDH15978**
Ampicillin (10)	≥ 17	≤ 13	6 (R)	6 (R)	6 (R)	0 (R)	0 (R)
Erythromycin (5)	≥ 17	≤ 12	7 (R)	7 (R)	7 (R)	6 (R)	6 (R)
Chloramphenicol (5)	≥ 18	≤ 12	6 (R)	6 (R)	6 (R)	19 (S)	19 (S)
Ciprofloxacin (5)	≥ 21	≤ 15	0 (R)	0 (R)	0 (R)	0 (R)	0 (R)
Tetracycline (5)	≥ 15	≤ 11	0 (R)	0 (R)	0 (R)	0 (R)	0 (R)
Streptomycin (10)	≥ 17	≤ 12	0 (R)	0 (R)	0 (R)	0 (R)	0 (R)
Nalidixic acid (30)	≥ 19	≤ 13	0 (R)	0 (R)	0 (R)	0 (R)	0 (R)
Trimethoprim / Sulfamethoxazole (1.25/23.75)	≥ 16	≤ 10	0 (R)	0 (R)	0 (R)	0 (R)	0 (R)
Norfloxacin (10)	≥ 17	≤ 12	8 (R)	8 (R)	8 (R)	9 (R)	9 (R)
Cefotaxime (30)	≥ 26	≤ 22	14 (R)	14 (R)	14 (R)	0 (R)	0 (R)
Gentamicin (10)	≥ 15	≤ 12	22 (S)	22 (S)	22 (S)	21 (S)	21 (S)

Table 3.6. Antibiogram profile of bacterial strains determined according to the CLSI guidelines

Broth microdilution method: - We have also determined the bacterial growth inhibition using the CLSI broth microdilution method. This test involved serially diluting the antibiotics in LB media containing bacterial suspension of 1×10^6 cells/ml and incubating them at 37 °C for 24 h. The minimum inhibitory concentration (MIC) indicates the lowest concentration of the antibiotics that prevents visible bacterial growth. The table below *(Table 3.7)* presents the MIC values (µg/ml) along with the cutoff values for resistance according to CLSI guidelines.

Antimicrobial Agent	MIC (g/ml) Interpretive Criteria			IDH1986	IDH07976	IDH14062	IDH13966	V32	V24	V100	Micro78
	S	I	R								
Streptomycin	8	16	32	64 (R)	64 (R)	32 (S)	128 (R)	8 (S)	8 (S)	16 (S)	64 (R)
Ampicillin	8	16	32	32 (R)	32 (R)	32 (R)	32 (R)	8 (S)	32 (R)	32 (R)	32 (R)
Azithromycin	2	-	-	64 (R)	64 (R)	64 (R)	8 (S)	64 (R)	8 (S)	8 (S)	64 (R)
Chloramphenicol	8	16	32	32 (R)	32 (R)	32 (R)	8 (S)	4 (S)	4 (S)	64 (R)	32 (R)
Tetracycline	4	8	16	16 (R)	16 (R)	8 (I)	8 (I)	2 (S)	4 (S)	8 (I)	16 (R)
Ciprofloxacin	1	2	4	4 (R)	4 (R)	2 (I)	4 (R)	8 (R)	1 (S)	1 (S)	4 (R)
Gentamicin	4	8	16	1 (S)	1 (S)	2 (S)	8 (I)	8 (I)	16 (R)	2 (S)	1 (S)

Table 3.7. MIC values (µg/ml) for resistance according to CLSI guidelines.

3.31. Checkerboard Assay

The combination of sodium butyrate with antibiotics and the determination of fractional inhibitory concentrations (FIC) indices were assessed using checkerboard assays *(Fig 3.9)*. In this procedure, 100 µl of Mueller-Hinton broth (MHB) was added to each well of a 96-well plate. Antibiotics were diluted along the abscissa while sodium butyrate was diluted along the ordinate. Overnight bacterial culture was standardized to 0.5 McFarland turbidity standard and then diluted at a ratio of 1:100 in MHB broth. After incubation at 37 °C for 24 h, the optical density of each well at 600 nm was measured using a Microplate reader (Tecan, Mannedorf, Switzerland).

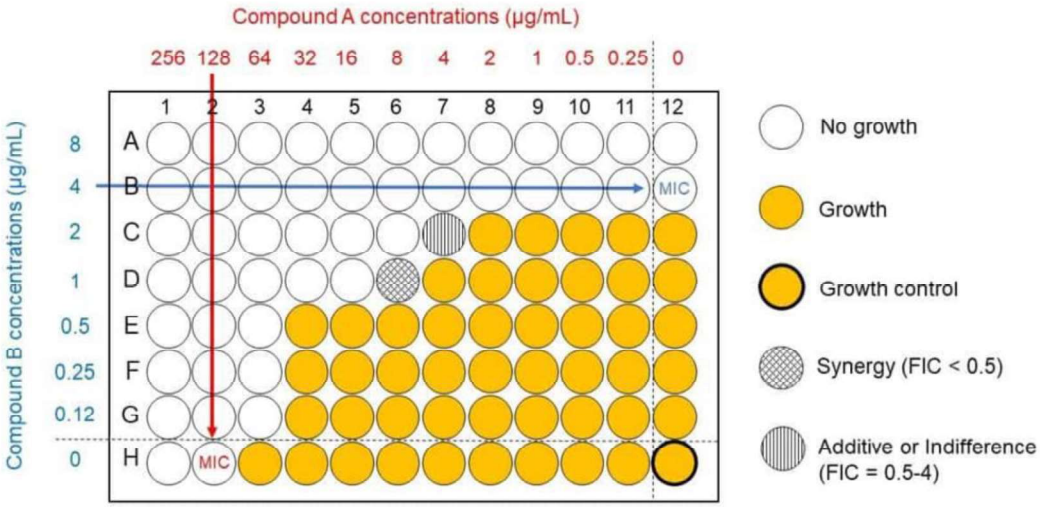

Fig 3.9. Synergy Checkerboard Assay [Source: (Prince et al., 2022)].

- **Evaluation of combination effects**

The FIC index (FICI) was calculated using the following formula:

FIC index = MIC_{ab} / MIC_a + MIC_{ba} / MIC_b = FIC_a + FIC_b

In this formula, MIC_a represents the minimum inhibitory concentration (MIC) of compound A alone, MIC_{ab} is the MIC of compound A in combination with compound B, MIC_b is the MIC of compound B alone, and MIC_{ba} is the MIC of compound B in combination with compound A. FIC_a is the FIC index of compound A, and FIC_b is the FIC index of compound B. Synergy is defined as an FIC index of $\leq$ 0.5. An FIC index between 0.5 and 4 is considered indifferent, while an FIC index greater than 4 is antagonistic.

- **Isobolograms**

To define the type of interactions between compounds and antibiotic combinations, results obtained from the checkerboard method were graphically represented as isobologram. Isobologram curve was created by plotting the minimum inhibitory concentration (MIC) of various combination ratios. A straight line indicates an additive effect, a concave curve suggests synergy, and a convex curve represents an antagonistic effect.

3.32. Live/Dead bacteria staining

Overnight cultures of *V. cholerae* strains were diluted in LB broth and incubated at 37 °C for 4 h with either sodium butyrate alone, antibiotics alone, or a combination of both. Following incubation, bacteria were collected and centrifuged. They were then resuspended in PBS to obtain an optical density at 600 nm (OD_{600}) of 0.5. The samples were stained using the LIVE/DEAD BacLight Bacterial Viability Kit (Invitrogen, CA, USA) according to the manufacturer's instructions. Green fluorescently labelled bacteria were live, and red fluorescently labelled bacteria were dead.

3.33. Cytoplasmic content leakage

Release of 260/280nm absorbing materials: - Integrity of the cell membrane of *V. cholerae* was assessed by measuring the release of cellular constituents at wavelengths of 260 nm and 280 nm. In this experiment, 10 ml of cell cultures were incubated at 37 °C with agitation for 24 h, either in the presence of sodium butyrate only, antibiotics only, or a combination of both. Following incubation, samples were centrifuged at 5000 × *g* for 10 min, and the absorbance of the supernatants was measured at 260 nm and 280 nm using a NanoQuant Plate (Tecan Infinite™, model number M200 PRO, Morrisville, NC, USA). The results were further analyzed using agarose gel electrophoresis.

- **Release of nucleic acids: -** Bacteria from the logarithmic growth phase were collected and centrifuged at 10,000 × *g* for 10 min. They were then washed once with 10 mM PBS (pH 7.2) and resuspended to an optical density (OD_{600}) of 0.6. 1 ml of these suspensions was treated either with SB only, antibiotics only, or a combination of both at 37 °C for 2 h and then centrifuged at 10,000 × *g* for 5 min. Supernatants were then analyzed using agarose gel electrophoresis. Ethanol precipitation was performed to isolate the released nucleic acids. The resulting precipitated pellets were dissolved in 10 µl of Tris-EDTA (TE) buffer, which contains 10 mM Tris-HCl at pH 7.5. Subsequently, 10 µl of each sample was mixed with 2 µl of 6× gel loading dye (New England Biolabs, Ipswich, MA, USA). Nucleic acid leakage was visualized using a Bio-Rad

ChemiDoc XRS+ system after electrophoresis in a 0.8% agarose gel containing ethidium bromide. The gel was run with 1× TAE buffer, which consists of 40 mM Tris base, 0.5 mM EDTA (pH 8.0), and 20 mM glacial acetic acid, at a voltage of 100 V for 40-45 min. A 100 bp DNA ladder (from UBPBio, Lucerna-Chem AG, Luzern, Switzerland) was used as a molecular weight size marker.

3.34. Cell membrane disruption

Bacterial cell membrane disruption was evaluated by measuring the release of alkaline phosphatase using a commercial kit (Solaibao, Beijing, China) and, β-galactosidase release was determined through the hydrolysis of 2-nitrophenyl β-D-galactopyranoside and assessed using a colorimetric assay at 405 nm (Y. Liu et al., 2017). ATP levels were determined using a commercial kit (Solaibao, Beijing, China).

3.35. Scanning Electron Microscope

Scanning electron microscopy (SEM) was used to examine the morphological changes in *V. cholerae* upon challenge with SB alone, antibiotics alone, or a combination of both agents. Briefly, bacterial cells were treated with the test agents and incubated for 1 h. They were then washed three times with PBS (pH 7.4) and centrifuged at 6,000 rpm. The obtained pellet was suspended in PBS, and a thin smear was prepared on a glass slide. The slide was then fixed in glutaraldehyde (2.5 g/100 ml) for 2 h. Following fixation, a dehydration step was conducted using increasing concentrations of ethanol, ranging from 50% to 100%. The cells were then dried using liquid CO_2. After drying, the cells were coated with gold using a sputter coater, and the samples were observed under a scanning electron microscope (SEM) (Hitachi-S4300, Japan).

3.36. Membrane Depolarization Assay

To demonstrate membrane depolarization, bacterial cells were grown, treated with test agents, and then washed twice with PBS. Next, 1 µl of $DiBAC_4$ (Bis-(1,3-Dibutylbarbituric Acid Trimethine Oxonol)) staining solution (1 mg/ml, Molecular

Probes, Eugene, OR, USA) was added to the samples. After incubating for 15 min at room temperature, the samples were washed twice with PBS. Then, for fixation, 100 µl of 4% formalin was applied for 15 min. After that, the cells were washed twice with PBS and then re-suspended in 20 µl of 50% glycerol. Confocal microscopy was carried out using an Olympus 300 confocal laser scanning microscope (Olympus, Hachioji, Tokyo, Japan) equipped with a UPIanSApo 63X oil immersion lens. For the observation of $DiBAC_4$ (green), the argon laser was utilized with an excitation wavelength of 488 nm and an emission wavelength of 515 nm.

3.37. EtBr Efflux Assay and intracellular accumulation of antibiotics

The inhibitory effect of the test agents on the activity of efflux pumps was assessed using an EtBr efflux assay. Cells were co-incubated with 5×10^{-6} M EtBr and a sub-minimal inhibitory concentration (sub-MIC) of the test agents, or a known efflux pump inhibitor, CCCP (100×10^{-6} M), at 37 °C until an optical density (OD_{600}) of 0.5 was reached. Next, the cells were centrifuged at 5000 × *g* for 10 min at 4 °C, and the resulting pellets were collected and resuspended in fresh Mueller Hinton Broth (MHB). The efflux of EtBr from the cells was then monitored using an excitation wavelength of 530 nm and an emission wavelength of 600 nm over 60 min.

Accumulated tetracycline levels were measured as described previously (Oh & Jeon et al., 2015). In brief, *V. cholerae* were grown overnight until they reached the late log phase in MHB, in the presence of inhibitors. 1 ml sample was then centrifuged, washed with 100 mM Tris buffer (pH 8), and resuspended in 1 ml of the same buffer. The bacteria were subsequently cultured in the presence of tetracycline (100 µg/ml) for 15 min. After this incubation, 1 ml of 5 M HCl was added, and the cells were boiled for 10 min. This procedure quantitatively converted tetracycline into anhydrous tetracycline. The cooled sample was centrifuged to remove cell debris, and the anhydrous tetracycline present in the supernatant was measured using excitation and emission wavelengths of 400 nm and 520 nm, respectively. The concentration of anhydrous tetracycline in these samples was determined using a standard curve ranging from 0 to 100 mg/l of tetracycline (Oh & Jeon et al., 2015; Andrea et al., 2004).

3.38. Resistance development studies

Due to the sensitivity of *V. cholerae* isolate, C6709 to tetracycline, it was employed further in the resistance development studies. C6709, after culture at 37 °C for 24 h was diluted in 1:100 MHB media supplement with 0.25 × MIC of tetracycline or tetracycline plus 0.25 × MIC of SB (4.4 mg/mL) which was then cultured again at 37 °C for 24 h. Then, the cultures were diluted in 1:100 MHB, and cultured to an OD_{600} of 0.5 while determining the MIC by two-fold serial dilutions in 96-well microtiter plates. Furthermore, the cultures were again diluted in 1:100 MHB media containing 0.25 × MIC of drugs for a total of 30 passages containing C6709 inducing tetracycline-resistant strains along with the calculation of the fold increase in subsequent tetracycline MIC relative to initial MIC (Maisuria et al.,2019).

3.39. MTT Assay

HT-29 cells were cultured in 96-well plates at a density of 1×10^4 cells per well. After the cells reached confluency, they were treated with different doses of inhibitors. The cells were then incubated in an incubator containing 5% CO_2 at 37 °C for 24 h. Cellular viability was assessed using the Colorimetric Cell Viability Kit IV (MTT) (Promokine, Heidelberg, Germany). 20 µl of the reagent was added and incubated at 37 °C for 4 h. Purple crystal formazan was then solubilized by adding 300 µl of DMSO. Optical density (OD) was measured at 570 nm, and % of cell viability was calculated and presented graphically.

3.40. LDH Cytotoxicity Assay

The effect of different inhibitors on the cytotoxicity of the HT-29 cell line was assessed using a lactate dehydrogenase (LDH) release assay, following the manufacturer's protocol (LDH cytotoxicity detection kit, TaKaRa Biosciences). Briefly, HT-29 cells were grown in 6-well cell culture plates till 80% confluency. The cells were then co-incubated with different concentrations of inhibitors for 12 h at 37 °C in a humidified cell culture incubator. Cell culture supernatants were analyzed for the release of lactate dehydrogenase (LDH). The percent cytotoxicity was calculated using the formula: Cytotoxicity (%) = [{(EX - LC) / (HC - LC)} - BC] × 100, where: EX =

Experimental value, LC = Low control (spontaneous LDH release from untreated normal HT-29 cells), HC = High control (maximum releasable LDH in HT-29 cells when treated with 1% Triton X-100), BC = Background control (LDH activity in the assay medium). Treatment with 1% (v/v) Triton X-100 represented maximum LDH release, which corresponds to 100% cytotoxicity.

3.41. Rabbit ileal loop assay for fluid accumulation and bacterial recovery

Rabbit ileal loop experiments were conducted using New Zealand white rabbits weighing between 1.5 and 2 kg, following previously established protocols (Koley et al., 1999). Before surgery, the rabbits were starved for 48 h and provided water as needed. Animals were anesthetized with an intramuscular injection of xylazine (5 mg/kg of body weight) and ketamine (35 mg/kg of body weight). A surgical incision was made in the abdominal wall, and the ileum was carefully cleaned and ligated into separate loops of about 10 cm. Each loop was injected with 1×10^9 CFU per ml of *V. cholerae* N16961, with or without drugs. A loop injected only with PBS served as the negative control loop. After 18 h, the animals were euthanized, and the loops were removed. The length of each loop and the volume of the accumulated fluid were recorded. The accumulated fluid per unit area (F/A) was expressed as the loop fluid volume (ml)/length (cm) ratio. Additionally, collected fluid was used to estimate the production of CT in the intestine. A representative image of rabbit ileal loop injected with *V. cholerae* is shown in ***Fig 3.10.***

Fig 3.10. Rabbit ileal loops (1,2,3) injected with *V. cholerae* [Source: (Atif AB et al.,2014)].

3.42. In vivo intestinal epithelium adhesion assay

In vivo adhesion of *V. cholerae* to the rabbit intestinal mucosa was also evaluated. The ileal loop sections were recovered 18 h after the rabbit ileal loop experiment and analyzed to estimate the number of bacteria adhered to the intestinal mucosa, following the previously described protocol (Alam et al., 1997). Briefly, the fluid in the loops was taken out as outlined above. Each intestine was then excised, opened with a longitudinal incision, and washed three times with PBS to remove any nonadherent or loosely attached bacteria. After washing, the opened intestine was stretched on a wooden sheet with the luminal surface facing upward. Several circular pieces of mucosa, each measuring 7 mm in diameter, were punched out. Each of these intestinal punches was then homogenized in 0.25 ml of Krebs/Ringer/Tris (KRT) buffer at a pH of 7.5. To determine the viable cells of *V. cholerae*, 0.1 ml of the homogenate was serially diluted in PBS, and 0.1 ml aliquots of these dilutions were plated in LA plates containing antibiotics to enumerate viable *V. cholerae* cells. The adhesive ability of *V. cholerae* (adherence index) was expressed as the average number of adhered bacterial cells per punched mucosal surface.

3.43. Suckling mice colonization experiment

In vivo infant mouse colonization assay was performed using BALB/c mice ***(Fig 3.11)*** as described previously (Roy et al., 2016). Four to five-day-old suckling BALB/c mice were orogastrically inoculated with 50 µl of bacterial suspension containing 1×10^5 CFU of *V. cholerae* cells, with or without drugs. Mice were maintained at 30 °C and were sacrificed after 18 h. The entire intestine was then removed and homogenized in PBS. Serial dilutions of the homogenates were plated on LA plates containing antibiotics to enumerate viable *V. cholerae* cells, which were expressed as CFU per mouse intestine. The colonization experiment was performed three times independently in three days with at least four mice in each group, and the combined data for the three experiments was used for statistical analysis.

Fig 3.11. 4 to 5 days old infant mice

3.44. Infant mouse survival challenge assay

The cholera survival protocol was modified from Duan and March (Duan et al., 2010; Rollenhagen et al., 2006). Four-day-old suckling mice were separated from their mother and kept in an incubator at 30 °C for 2 h to allow them to digest the milk in their stomach. Mice were then orally inoculated with 50 µl of LB containing 5×10^7 CFU of *V. cholerae* cells, with or without drugs, before being returned to their dam. Mice were monitored for 48 h for survival and were sacrificed at the end of the study.

3.45. Histopathological studies

Histological analysis was done by collecting tissue samples (1 cm in length) from rabbit ileal loop assays. They were fixed in 10% neutral buffered formalin. Further, the samples were embedded in paraffin. 3-4 µm thin sections were cut in a microtomy rotor (Leica, Germany) and were stained with hematoxylin and eosin and examined under a compound light microscope. Photographs were taken under different magnifications with a Carl Zeiss PrimoStar microscope (Oberkochen, Germany), equipped with a digital imaging system.

3.46. Animal ethics

All animal care and experimental procedures in the study were conducted in accordance with the Animal Ethics Committee for the Purpose of Control and Supervision of Experiments on Animals (CPCSEA). The protocol was also approved by the Institutional Animal Ethics Committee of the National Institute of Cholera and Enteric Diseases (registration no: 68/GO/ReBi/S/99/CPCSEA).

3.47. Statistical Analysis

Statistical analyses were carried out by the GraphPad Prism 9.0 software, and all data are denoted as mean ± standard deviation (SD) unless otherwise specified. The results were analyzed using appropriate statistical tests as indicated in figure legends. Most of the experiments were repeated four to six times. Mean of three biological replicates are represented.

Chapter 4

Results

Screening of potential inhibitors against Vibrio Cholerae growth, motility, adhesion, virulence, and toxin production

Results

4.1. Inhibitor study to assess the virulence of V. cholerae

Antimicrobial agents are generally used to combat *V. cholerae* infections; however, they have minimal impact on the expression of bacterial virulence factors. Several epidemic strains of *V. cholerae* have developed multidrug resistance (MDR) through mechanisms such as horizontal gene transfer and the accumulation of beneficial mutations. Traditional antimicrobials are usually either bacteriostatic or bactericidal, which may contribute to the emergence of MDR strains (Das et al., 2020; Verma et al., 2019). Therefore, there is an urgent need for effective therapies against enteric bacterial infections that do not promote resistance.

One of the most promising strategies being increasingly explored is the targeting of bacterial virulence factors or disrupting the interaction between the host and pathogen, rather than killing the bacteria responsible for infection (Roca et al., 2015). For example, S-CMC has been found to inhibit the adherence of pneumococci to host cells (Sumitomo et al., 2012). Researchers screened a library of 50,000 compounds and identified a small molecule called 4-[N-(1,8-naphthalimide)]-n-butyric acid, commonly referred to as virstatin. This compound can prevent the expression of two key virulence factors in *Vibrio cholerae*: cholera toxin and the toxin-coregulated pilus (Rasko and Sperandio, 2010). In addition to synthetic chemical molecules, natural compounds such as ginger (Zingiber officinale) and capsaicin, the active component of chili peppers from Capsicum genus, have demonstrated promising anti-virulence activity (Ahmad et al., 2015; Jensen et al., 2003). To reduce bacterial virulence during pathogenesis, we have selected various bioactive compounds and evaluated their effects on different virulence attributes, including growth, motility, adhesion, cholera toxin (CT) production, and biofilm formation in *Vibrio cholerae*. After a thorough literature study, the following inhibitors are used, melibiose, glucose, ribose, arabinose as sugars; totarol, geraniol, camphor, eugenol as terpenes; quercetin, allylanisole, ethyl gallate, basil oil, catechin hydrate as polyphenols; ursolic acid, betulinic acid as triterpenoid; Sodium Butyrate, NH125, cyclic-di-GMP as small molecule.

4.2. Effect of the inhibitors on the growth of V. cholerae

Our initial goal is to determine whether the inhibitors have any growth-inhibitory properties. First, we assessed the effect of various sugars at a 0.5% (w/v) concentration to see if they exhibit any growth-inhibitory functions. The sugars we examined, Melibiose, Glucose, Ribose, and Arabinose, showed no significant effect on the growth of *V. cholerae* as compared to the untreated control (***Fig4.2A***). Next, we investigated the effect of phytochemicals on the growth of *V. cholerae*. The phytochemicals used in this study belonged to various classes, including terpenes (Totarol, Geraniol, Camphor, and Eugenol), triterpenoids (Ursolic acid and Betulinic acid), and polyphenols (Quercetin, Allylanisole, Ethyl gallate, Basil oil, and Catechin hydrate). Growth study of *V. cholerae* in the presence of terpenes revealed that, among all the compounds tested, only geraniol (at 125 µg/ml) in the supplemented culture media demonstrated growth inhibition compared to the control; the other compounds did not inhibit the growth of *V. cholerae* (***Fig.4.2B***). In the case of polyphenols, addition of quercetin (25 µg/ml) and allylanisole (125 µg/ml) to the culture media inhibited the growth of *V. cholerae* compared to the untreated control (***Fig.4.2C***). In contrast, addition of other compounds did not show any inhibition of growth (***Fig.4.2C***). Additionally, both compounds from the triterpenoid class, ursolic acid and betulinic acid (25 µg/ml), demonstrated significant growth inhibition compared to the untreated control (***Fig.4.2D***). We also investigated the effects of three small molecules, Sodium Butyrate (SB), NH125, and cyclic-di-GMP (c-di-GMP), on the growth of *V. cholerae*. Out of these, only NH125 at a concentration of 20 µg/ml demonstrated growth inhibition when compared to the untreated control (***Fig.4.2E***). In contrast, the other two small molecules, Sodium Butyrate (40 mM) and c-di-GMP (200 µg/ml), did not exhibit any growth inhibition (***Fig.4.2E***).

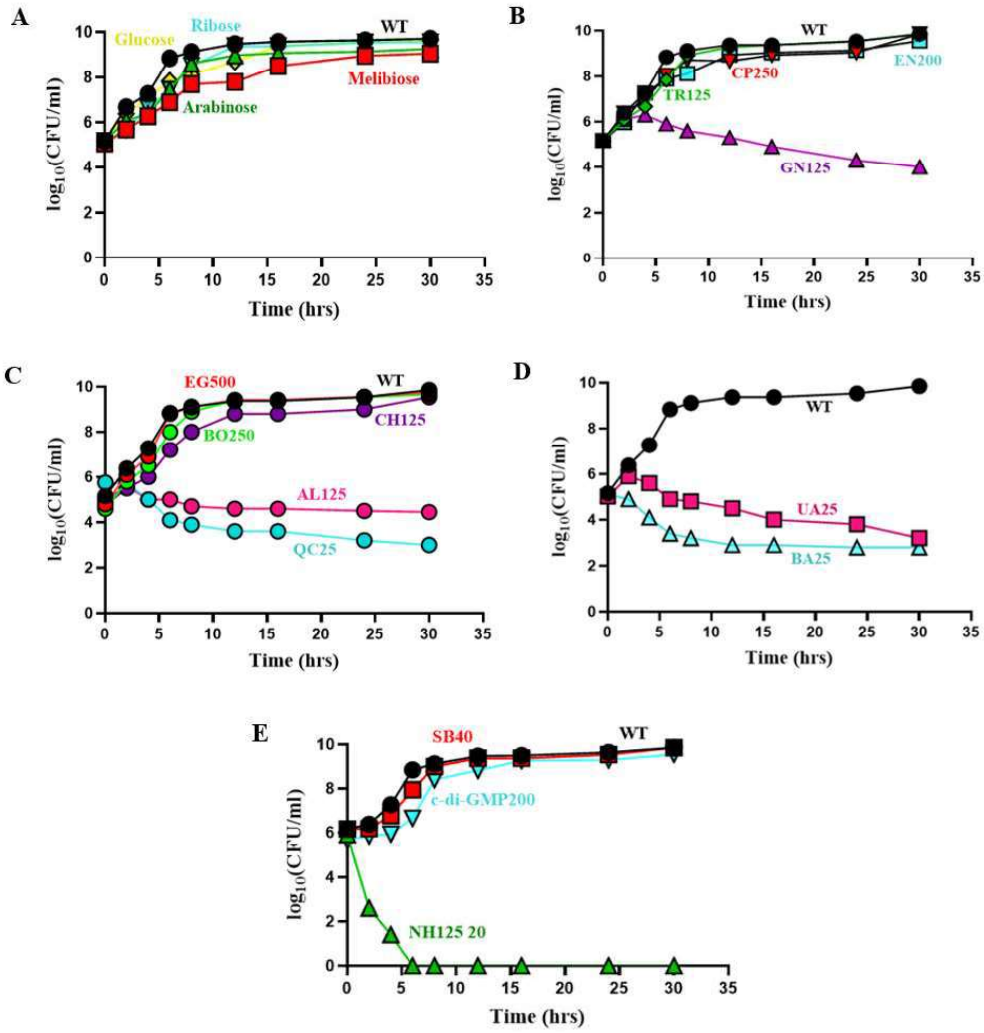

Fig. 4.2. *V. cholerae* growth assay. Wild type *V. cholerae* N16961 was given as an initial inoculum of 5×10^5 CFU/ml in the Luria-Bertani broth medium along with different inhibitors. The viable bacterial counts in CFU/ml were detected by plate count method taking culture samples from different time points and represented graphically. **(A) Sugars** used Glucose, Ribose, Arabinose and Melibiose **(B) Terpenes** used Totarol (TR), Geraniol (GN), Camphor (CP) and Eugenol (EN). **(C) Polyphenols** used Quercetin (QC), Allylanisole (AL), Ethyl Gallate (EG), Basil oil (BO) and Catechin Hydrate (CH) **(D) Triterpenoids** used Ursolic acid (UA) and Betulinic acid (BA). **(E) Small molecules** used Sodium Butyrate (SB), NH125 and cyclic-di-GMP (c-di-GMP).

4.3. Effect of the inhibitors on mucin penetrating ability of V. cholerae

Vibrio cholerae is transmitted in humans via the fecal-oral route. Upon reaching the small intestine, the bacteria must traverse the thick mucus layer to colonize the underlying enterocytes effectively. In this study, we evaluated the ability of *V. cholerae* to penetrate mucin columns composed of porcine mucin in the presence of various

compounds. Both melibiose and glucose treatment did not affect the mucin-penetrating ability of *V. cholerae*. In contrast, treatment with ribose and arabinose at a concentration of 0.5% (w/v) significantly reduced the mucin-penetrating ability by 2.5-fold and 2.6-fold compared to the untreated control respectively (***Fig.4.3A***). We then examined the effect of terpenes on the mucin penetration of *V. cholerae* to determine if they possess any motility inhibitory function. The results indicate that geraniol at a concentration of 31.25 µg/ml and camphor at 250 µg/ml have minimal effects (***Fig.4.3B***). In contrast, treatment with eugenol at 200 µg/ml and totarol at 125 µg/ml caused a reduction in mucin penetration by 2.2-fold and 2-fold, compared to the untreated control respectively (***Fig.4.3B***). Regarding polyphenols, quercetin at 6.25 µg/ml and basil oil at 250 µg/ml reduced mucin penetration by 3.2-fold and 2-fold, compared to the untreated control respectively (***Fig.4.3C***). However, allylanisole, ethyl gallate, and catechin hydrate did not exhibit any significant effects (***Fig.4.3C***). Moreover, both compounds from the triterpenoid class, ursolic acid and betulinic acid (5 µg/ml), demonstrated a reduction in the mucin-penetrating ability of *V. cholerae* by 2.6-fold and 3-fold, compared to the untreated control respectively (***Fig.4.3D***). Among the small molecules tested in this study, none exhibited any inhibitory function on mucin penetration (***Fig.4.3E***).

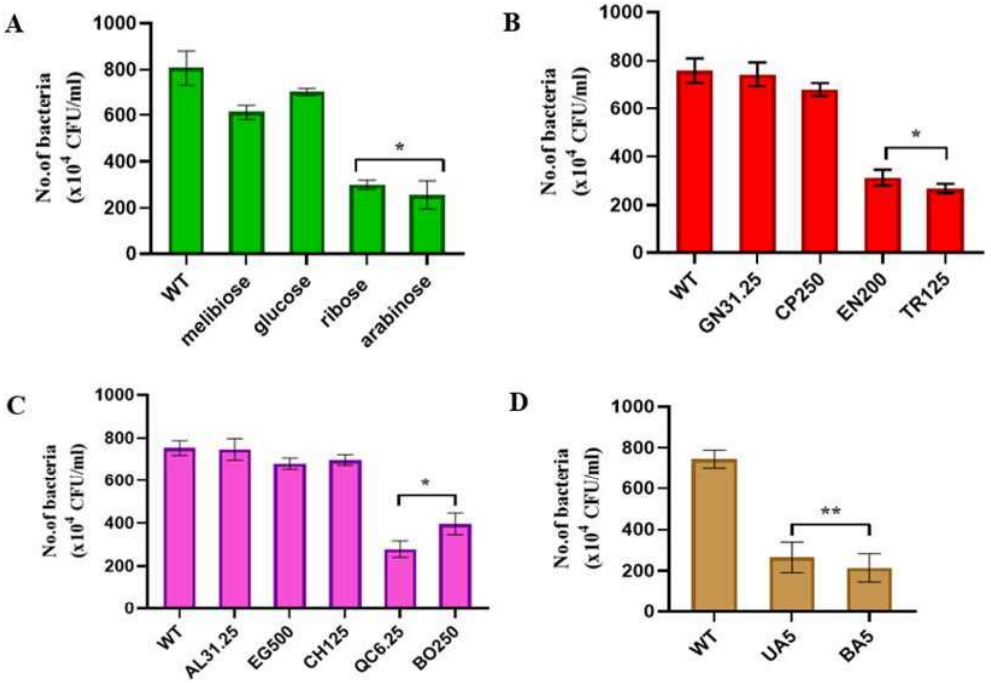

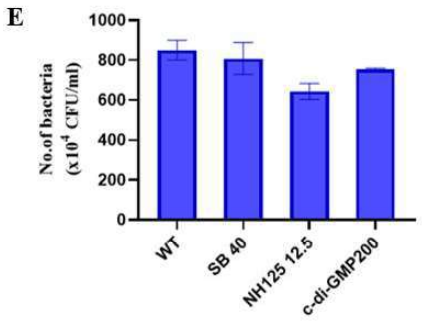

Fig.4.3. *In vitro* mucin penetration assay. Wild type *V. cholerae* N16961 was grown in LB broth till mid-log phase. 100µl of 5×10^8 CFU/ml bacterial culture was loaded on top of the 1.5% 1ml mucin column with or without the inhibitors. Bacterial samples of 100µl were collected from the bottom of the column after 1 h incubation at 37 °C. The samples were serially diluted and plated on LB agar supplemented with proper antibiotics and the bacterial numbers were counted and graphically represented. **(A)** Effect of **Sugars (B)** Effect of **Terpenes (C)** Effect of **Polyphenols (D)** Effect of **Triterpenoids** and **(E)** Effect of **Small molecules**. Each of the experiments was repeated three times (n=3) and the data were expressed as Mean ± SD; * for P <0.05, ** for P <0.01.

4.4. Effect of the inhibitors on the adhesion of V. cholerae to intestinal cells

Host pathogen interaction is dependent on cholera toxin production and TCP expression. We studied the ability of *V. cholerae* to adhere to the mucin-secreting colon-carcinoma cell line HT-29 in the presence of various inhibitors. Bacterial culture treated with 0.5% (w/v) melibiose showed minimal defects in adherence to HT-29 cells. In contrast, *V. cholerae* treated with 0.5% (w/v) glucose, ribose, and arabinose exhibited significant adherence defects, with reductions of 2.6-fold, 2.5-fold, and 2-fold, compared to the untreated control respectively (***Fig.4.4A***). All terpenes used in this study, totarol, geraniol, camphor, and eugenol, had no significant effect on the adhesion of *V. cholerae* (***Fig.4.4B***). Treatment with the triterpenoids ursolic acid and betulinic acid at a concentration of 5 µg/ml resulted in a 2-fold and 8-fold reduction in the adherence efficiency of *V. cholerae*, compared to the untreated control (***Fig.4.4C***). Among all the polyphenols evaluated in this study, quercetin at a concentration of 6.25 µg/ml demonstrated the most significant effect, reducing the adherence of *V. cholerae* by over 7-fold compared to the untreated control, while, the other compounds tested exhibited minimal to no inhibition (***Fig.4.4D***). Finally, small molecule Sodium butyrate at 40mM supplemented bacterial culture reduced adherence of *V. cholerae* by 8-fold, NH125 at 12.5 µg/ml by 1.6-fold, while c-di-GMP showed no inhibition (***Fig.4.4E***).

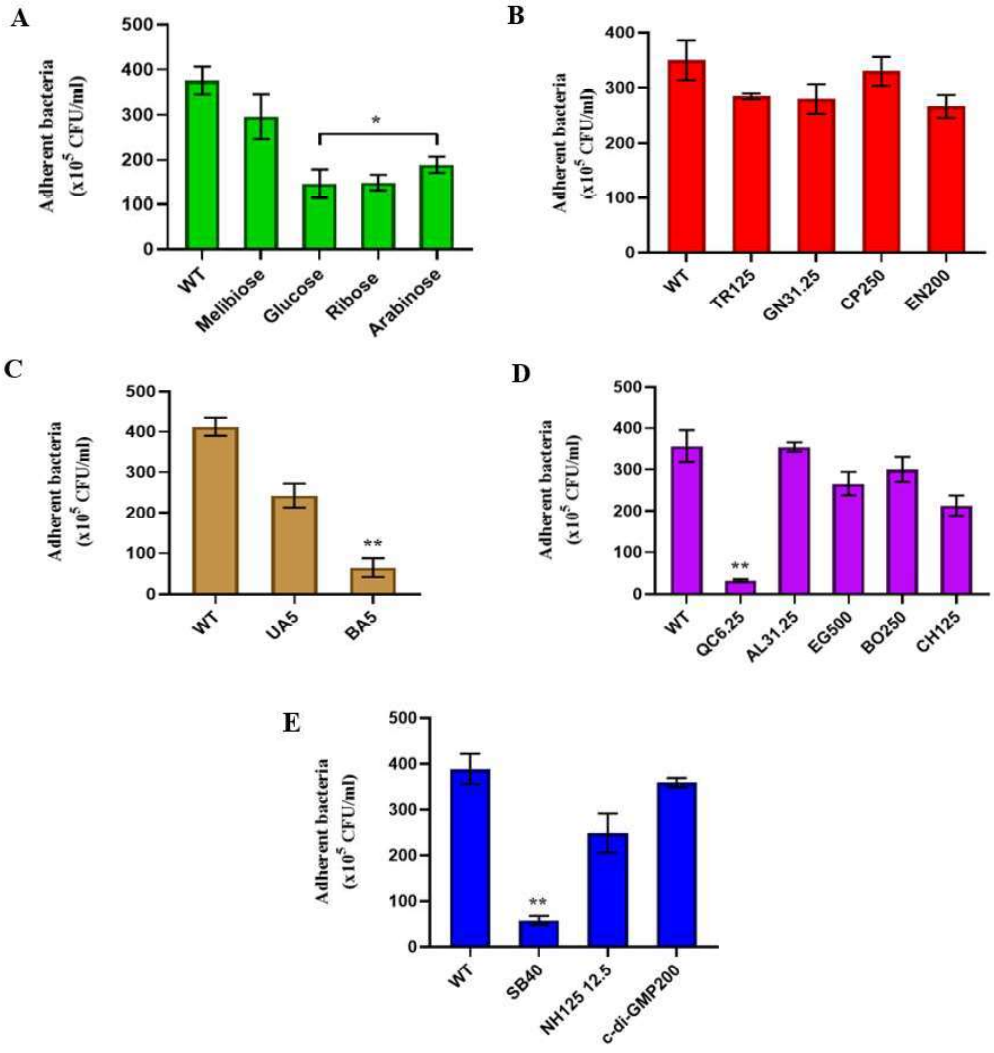

Fig.4.4. Adhesion assay of *V. cholerae* with HT-29 cell line in presence or absence of different inhibitors. *V. cholerae* was grown to mid-log phase and optical density were adjusted to 1. HT-29 cells were grown in 12-well cell culture plate to 80% confluency. The cells were then infected at 100 MOI of bacteria supplemented with or without the inhibitors. After incubation at humidified 37 °C incubator for 1 h, cell culture plate was washed with PBS to remove unbound bacteria, and then bound bacteria were collected and enumerated by plating on streptomycin supplemented LB agar. **(A)** Effect of **Sugars (B)** Effect of **Terpenes (C)** Effect of **Triterpenoids (D)** Effect of **Polyphenols** and **(E)** Effect of **Small molecules**. Each of the experiments was repeated three times (n=3) and the data were expressed as Mean ± SD; * for P <0.05, ** for P <0.01

4.5. Effect of the inhibitors on in vitro Cholera Toxin (CT) production

We then analyzed the production of cholera toxin (CT) by *V. cholerae* using a CT-ELISA in the presence of various inhibitors. Treatment with melibiose and arabinose resulted in a 2-fold and 4-fold reduction in CT production, respectively, compared to the untreated control at a concentration of 0.5% (w/v). In contrast, bacterial cultures treated with glucose and ribose showed no significant difference in CT production compared to the untreated control **(*Fig.4.5A*)**. Among the terpenes studied, totarol (125 µg/ml), geraniol (31.25 µg/ml), and eugenol (200 µg/ml) significantly reduced the production of cholera toxin (CT) by 4-fold, 10-fold, and 2-fold, respectively, compared to the untreated control **(*Fig.4.5B*)**. In contrast, camphor did not show any inhibition of CT production **(*Fig.4.5B*)**. Treatment with triterpenoids ursolic acid and betulinic acid do not have any role in *V. cholerae* CT inhibition **(*Fig.4.5C*)**. Among the polyphenols, allylanisole (31.25 µg/ml) and ethyl gallate (500 µg/ml) significantly reduced the CT production by 10-fold and 2.5-fold compared to the untreated control, whereas, quercetin, basil oil, and catechin hydrate showed no inhibition **(*Fig.4.5D*)**. Finally, small molecule Sodium butyrate at 40mM supplemented bacterial culture reduced CT of *V. cholerae* by 10-fold, NH125 at 12.5 µg/ml by 2.6-fold, while c-di-GMP showed no such inhibition **(*Fig.4.5E*)**.

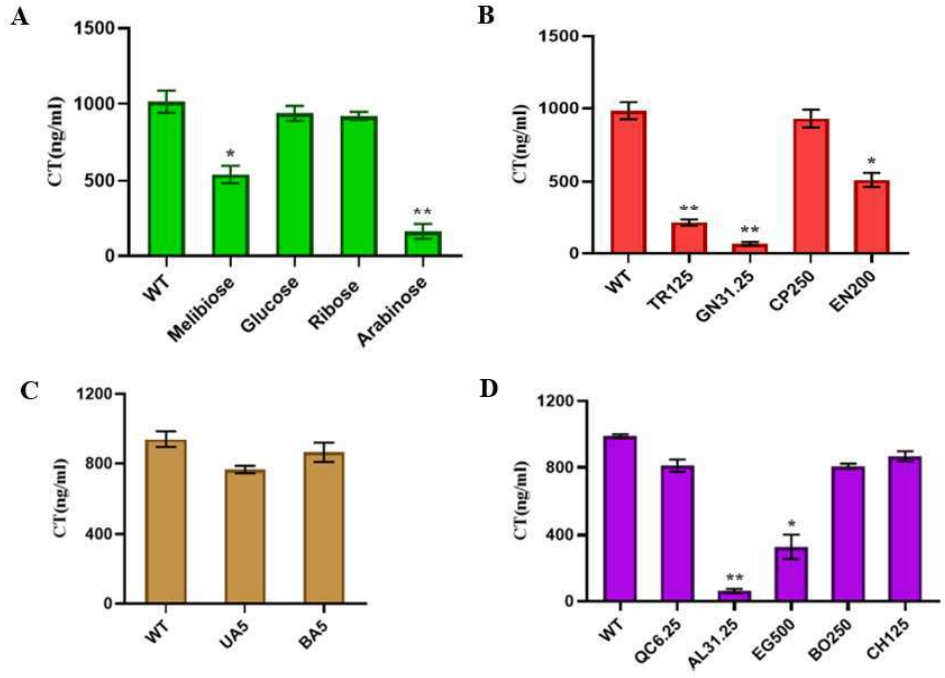

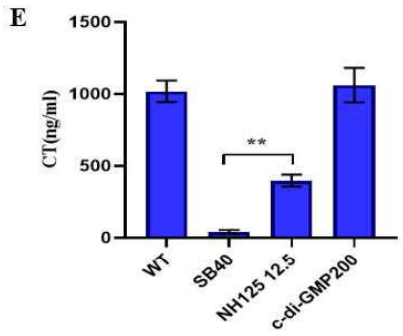

Fig. 4.5. *In vitro* CT production assay in the presence or absence of different inhibitors. Log phase cultures of wild type *V. cholerae* were inoculated (1:100) in AKI media with or without inhibitors and grown statically at 37 °C for 18 h. Culture supernatant was collected, Cholera Toxin (CT) was measured by ELISA and represented graphically. **(A)** Effect of **Sugars (B)** Effect of **Terpenes (C)** Effect of **Triterpenoid (D)** Effect of **Polyphenols (E)** Effect of **Small molecules**. Each of the experiments was repeated three times (n=3) and the data were expressed as Mean ± SD; * for P <0.05, ** for P <0.01

4.6. Effect of the inhibitors on biofilm formation by V. cholerae.

Next, we tested the effect of various inhibitors on biofilm formation by *Vibrio cholerae*. Our results showed that among the sugars, melibiose and arabinose successfully inhibited biofilm formation, whereas the other sugars, glucose and ribose, had no effect (***Fig.4.6A***). Treatment with the terpene camphor at concentration of 250 µg/ml completely inhibited the formation of biofilm in *V. cholerae* compared to the untreated control (***Fig.4.6B***). In contrast, the other terpenes tested, totarol, geraniol, and eugenol, did not have a significant effect on biofilm formation (***Fig.4.6B***). Treatment with ursolic acid at a concentration of 5 µg/ml inhibited biofilm formation in *V. cholerae*, whereas betulinic acid showed no such effect (***Fig.4.6C***). Among the polyphenols, quercetin, allylanisole, and ethyl gallate did not exhibit any inhibition. In contrast, basil oil at 250 µg/ml and catechin hydrate at 125 µg/ml significantly inhibited biofilm formation (***Fig.4.6D***). Finally, biofilm formation was evaluated in the presence of small molecules. c-di-GMP at 200 µg/ml significantly inhibited biofilm formation; however, strikingly, SB at 40 mM increased biofilm formation in *V. cholerae* (***Fig.4.6E***). Treatment with NH125 showed no effect on biofilm formation (***Fig.4.6E***).

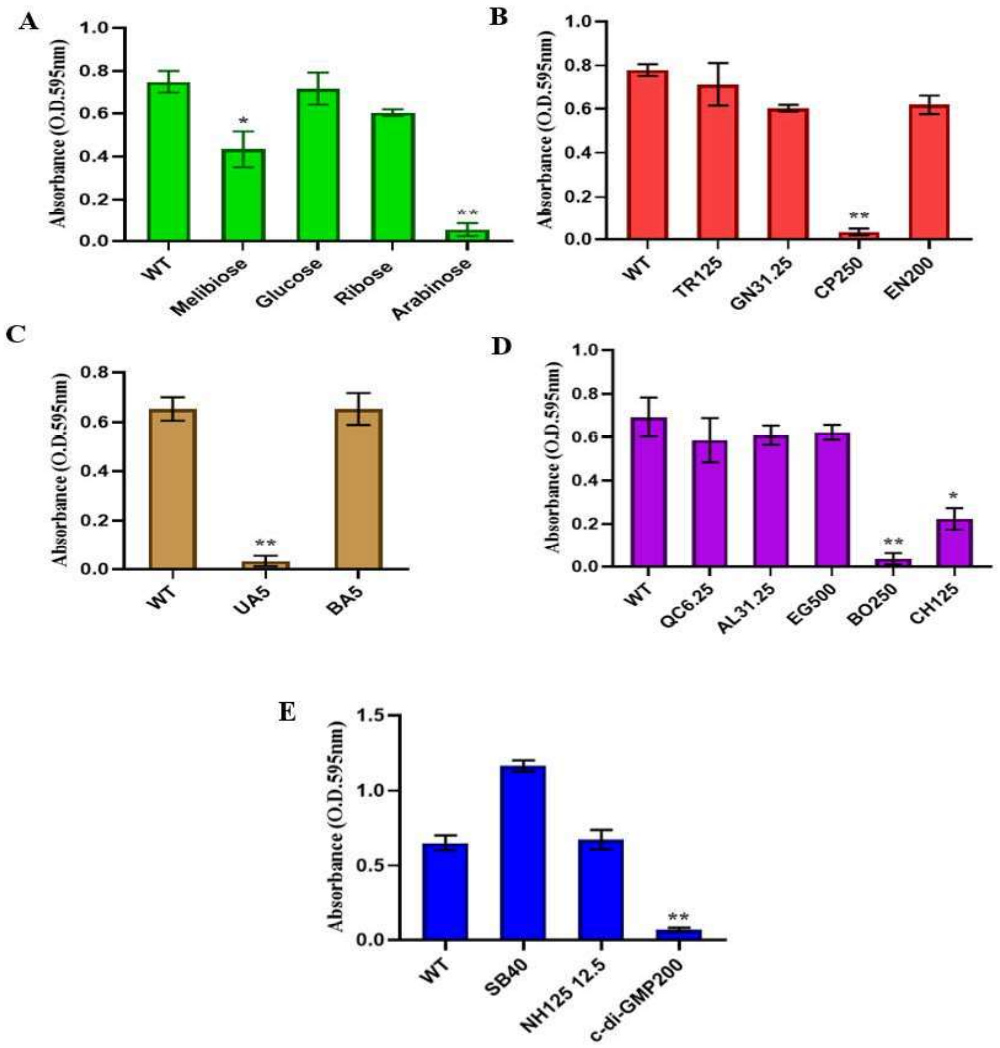

Fig.4.6. Biofilm formation in the presence or absence of different inhibitors. *V. cholerae* was grown in Luria Bertani broth in the presence or absence of different inhibitors. The formation of biofilm was quantified by Crystal Violet staining and represented graphically after measuring the optical density at 595nm. **(A)** Effect of **Sugars (B)** Effect of **Terpenes (C)** Effect of **Triterpenoid (D)** Effect of **Polyphenols (E)** Effect of **Small molecules**. Each of the experiments was repeated three times (n=3) and the data were expressed as Mean ± SD; * for P <0.05, ** for P <0.01

Based on this broad spectrum of activities of several inhibitors, the small molecule Sodium Butyrate (SB) appears to be a potent anti-virulent agent that needs further investigation. Detailed mechanism of inhibition in the presence of SB is further investigated.

Chapter 5

Results

Elucidation of possible mode of action of the potential inhibitor

Results

We have already screened and identified the small molecule Sodium Butyrate, which has shown anti-virulence activities against *V. cholerae*. Our next goal is to investigate the underlying mechanisms of inhibition caused by Sodium Butyrate in both *in vitro* and *in vivo* conditions.

5.1. Molecular docking shows stable binding of Sodium Butyrate (SB) with ToxT.

The clinical symptoms of cholera are primarily caused by two key virulence factors: cholera toxin (CT) and toxin-coregulated pilus (TCP). CT, which belongs to the A-B_5 family of toxins. It is directly responsible for causing profuse watery diarrhea in cholera patients, while TCP is essential for the colonization of the intestine. The coordinated expression of these virulence genes is regulated by a master regulator, ToxT, and given its pivotal role, numerous studies have been focused on its regulation, leading to the characterization of multiple mechanisms that contribute to its stringent regulation. ToxT is a member of the AraC/XylS family of transcriptional activators, consisting of two main domains: N-terminal domain associated with effector binding and potential ToxT monomer association, and a C-terminal DNA-binding domain that shares homology with AraC/XylS. Transcription of *toxT* is regulated by two membrane-localized complexes, ToxRS and TcpPH. Additionally, TcpPH is activated by two activators, AphA and AphB, which respond to factors such as cell density, anaerobiosis, and other environmental conditions.

Targeting the transcriptional activator ToxT in *V. cholerae* offers significant advantages for developing new antimicrobial drugs that focus on virulence factors instead of inhibiting bacterial growth. The activator protein ToxT was molecularly docked with sodium butyrate to explore if any interaction exists between them. The 3D image of the receptor (ToxT) and ligand (sodium butyrate) after optimal docking as visualized is represented (***Fig.5.1A*** **and** ***Fig.5.1B***). The possible amino acid residues located in the binding pocket of ToxT (PDB ID: 3GBG) include Ile226, Tyr26,

Asn28, Asp29, Ser223, Ser227, Asn60, Thr85, Gln8, Lys31, and Lys230. The results revealed a stable interaction between ToxT protein and SB with a binding energy of -7.68 Kcal mol^{-1}. These interactions included two salt bridges with Lys31 and Lys230, as well as a single hydrogen bond with Lys31. Other residues involved in interactions with SB are summarised in ***Fig.5.1C***. Altogether, these data suggest that SB may interact with ToxT and therefore, used for subsequent in vitro and in vivo experiments to test their efficacy against the virulence attributes of *V. cholerae*.

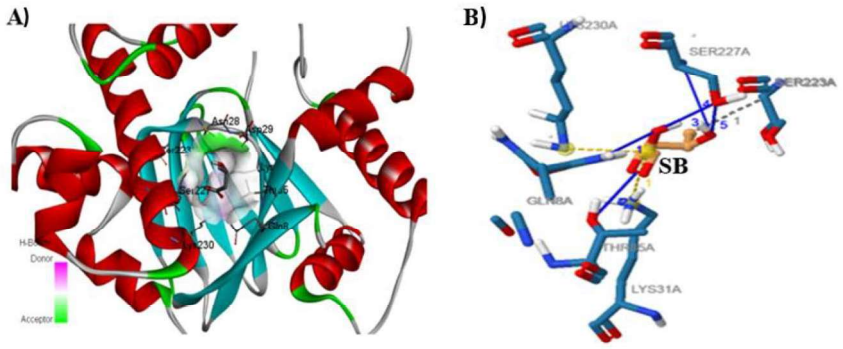

C)

RECEPTOR	LIGAND	BINDING ENERGY (Kcal/mol)	AMINO ACIDS INVOLVED IN INTERACTION	PDB ID
ToxT	Sodium butyrate(SB)	-7.68	GLN8, THR85, SER227, SER223, LYS31, LYS230	3GBG

Fig 5.1. Binding of SB with ToxT in silico. Residues interacting with ligand (SB) and receptor (ToxT) are represented in **A)** 3D conformation, **B)** 2D conformation, and **C)** Table showing the probable interacting residues and the binding energy.

5.2. Viability of bacterial strains and cytotoxicity in HT-29 cells in presence of SB.

Effect of sodium butyrate on the viability was examined on a standard *V. cholerae* (El Tor strain) and two clinical isolates (El Tor variant). The MICs of SB against strains N16961, Micro 78, BCH13298 were found to be 80mM and MBCs were found to be 160mM respectively ***(Fig.5.2A)***. The effect of SB on *V. cholerae* growth was investigated by counting the live cells on the plates in a time-dependent manner. The growth rate of N16961 ***(Fig.5.2B)***, BCH13298***(Fig.5.2C)*** and Micro78***(Fig.5.2D)*** were measured in LB medium along with exogenously added different doses of SB.

Result indicated that there was a complete inhibition of *V. cholerae* growth at 2xMIC (160 mM). No bacteria were recovered after 12 h in N16961 at 2xMIC. The bactericidal activity of SB was much more potent in strains BCH13298 and Micro78 as no bacteria were recovered after 6 h in BCH13298 and after 8 h in Micro78 at 2xMIC. At 1xMIC (80mM), the growth pattern of all the three strains were almost similar with the viable count reduced to 65% 2 h post-initial inoculum. Within the initial 8 h, viability of the bacteria was further reduced to 20% and from 8 to 30 h, there was a bacteriostatic effect on the remaining viable bacteria. At sub-MICs (10, 20 and 40 mM) there was no significant difference in growth rate as compared to the untreated control. Additionally, we tested whether SB exhibits antibacterial activities against *E. coli* strains. The results, as shown in **Fig.5.2E** and **Fig.5.2F**, indicate that the antibacterial effect of SB on *E. coli* B2 and *E. coli* IDH15978 was not as pronounced as that observed for *V. cholerae* strains. Even at the highest concentration of SB tested (=160 mM), viable colonies of *E. coli* strains could still be detected after 30 h, emphasizing *V. cholerae*-specific bactericidal activity of SB. The sub-MICs of SB were used in all subsequent *in vitro* experiments. *In vivo* experiments were performed at both sub-MICs and MIC of SB to compare the effect with the different groups.

A)

	Bacteria	MIC (mM)	MBC (mM)
V. cholerae	N16961	80	160
	BCH13298	80	160
	Micro78	80	160
E. coli	B2	–	–
	IDH15978	–	–

Note: "–" indicates that MIC/MBC was not obtained within the range of concentration (upto 160 mM) of SB tested

B)

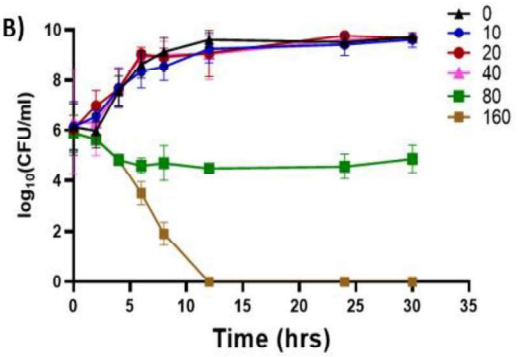

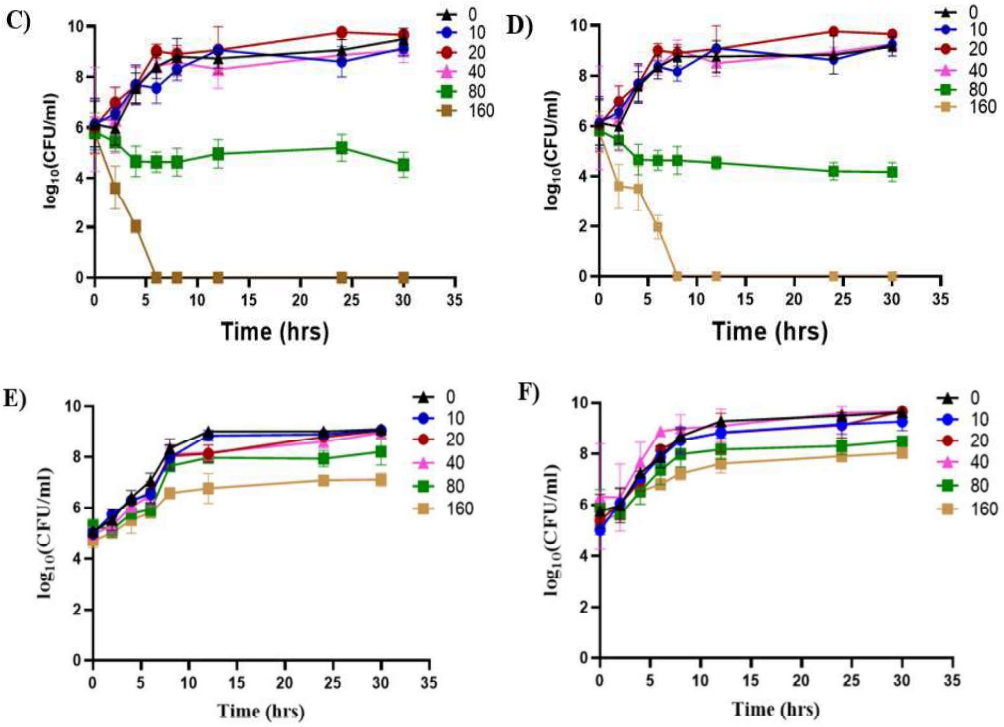

Fig 5.2. Susceptibility testing and effect of SB on *V. cholerae* growth at MIC and sub-MICs. A) Determination of MIC and MBC of SB against bacterial strains. Bacterial strains were grown in LB broth along with SB at MBC (160 mM); MIC (80 mM); 1/2th MIC (40 mM); 1/4th MIC (20 mM); 1/8th MIC (10mM); and SB (0 mM) for the indicated time periods (2, 4, 6, 8, 12, 24 and 30 h). Viable bacterial counts in CFU per ml detected by the plate count method were represented graphically for **B)** multidrug-resistant strain *V. cholerae* N16961, **C)** multidrug-resistant strain *V. cholerae* BCH13298, and **D)** multidrug-resistant strain *V. cholerae* Micro78, **E)** multidrug-resistant *E. coli* B2, and **F)** multidrug-resistant *E. coli* IDH15978

Toxicity of SB in mammalian cell lines was also evaluated. MTT assay revealed that no significant cytotoxicity was observed when HT-29 cells were incubated with varying doses of SB (5-160mM) *(Fig.5.3A)*. In addition to this, LDH cytotoxicity assay was also performed to determine the cytotoxic effect of SB on HT-29 cell line. Different doses of SB were used to treat HT-29 cells and after 12 h the supernatants were collected and assessed for the release of LDH. HT-29 cell treatment with triton X-100 showed maximum membrane damage hence considered to possess 100% cytotoxicity. The experimental result obtained here showed that SB exerts 9%, 4% and <1% cytotoxicity at 160mM, 80 mM and 40 mM concentration respectively, compared to the triton X-100 treated cells *(Fig.5.3B)*. The above

results led to the conclusion that SB at concentrations below 160 mM is safe and does not cause human epithelial cell damage.

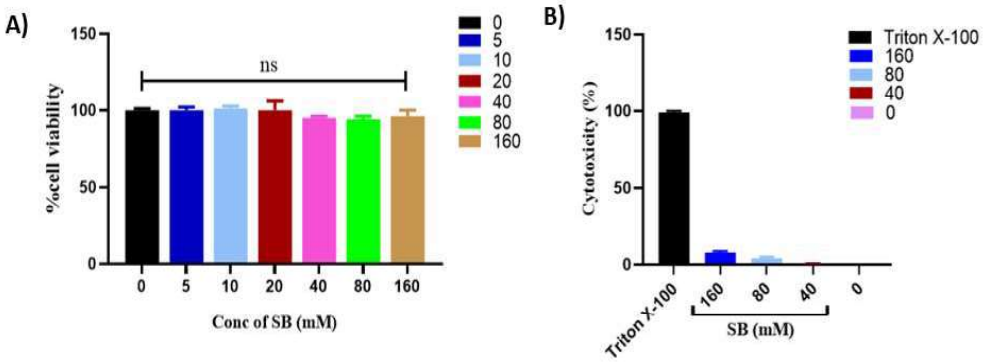

Fig 5.3. Cytotoxic activity of SB in the HT-29 cell line. A) HT-29 cells were treated with or without SB (5-160mM) for 24 h. MTT assay was performed to measure the % viability level. One-way ANOVA was performed, and the significance was calculated as ns=nonsignificant **B)** Cytotoxic effect of SB at different concentrations was measured by LDH release assay and graphically represented as percent cytotoxicity taking Triton X-100 treated cell LDH release as a positive control.

5.3. Inhibition of Cholera toxin production.

Host pathogen interaction is dependent on cholera toxin production and TCP expression. To begin with, El Tor *V. cholerae* strain N16961 and two multidrug resistant El tor variant strains Micro78 and BCH13298 were used for the study to check the effect of sodium butyrate (SB) on cholera toxin production (CT) ***(Fig.5.4A)***. We explored the classical GM1-CT ELISA assay to detect the level of CT secreted in the supernatant of the bacterial culture grown in presence or absence of SB. The sub-MIC concentrations of SB that had no adverse effect on viability of the bacteria was found to have significant effect on CT production. There was almost 10-fold, 6-fold and 5-fold reduction in cholera toxin (CT) production at 20 mM (1/4thMIC) for N16961, BCH13298 and Micro 78 ***(Fig.5.4)*** respectively. Similarly, at 40 mM (1/2thMIC) SB there was 20-fold, 25-fold and 14-fold reduction in CT in N16961, BCH13298 and Micro 78 ***(Fig.5.4)*** as compared to the SB-free culture. The results obtained from this assay showed that although sodium butyrate (SB) had no effect on bacterial growth, but it demonstrated significant activity in reduction of CT production.

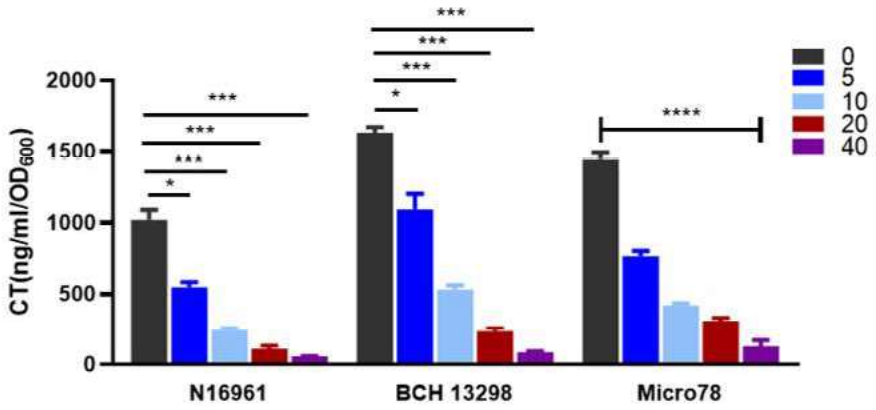

Fig 5.4. Dose-dependent inhibitory effects of Sodium butyrate (SB) on cholera toxin (CT) production in different *Vibrio cholerae* O1 El Tor strains. *In vitro* CT production from different O1 El Tor strains were measured by ELISA from the samples grown in AKI media (pH=7.5, 37 °C, static condition for 18 h) with or without SB respectively. The amount of CT produced is graphically represented. All data are represented as mean ± S.E.M. ($n = 3$). One-way ANOVA was performed. Significance levels were denoted as ∗for $P < 0.05$, ∗∗∗ for $P < 0.001$, ∗∗∗∗for $P < 0.0001$.

5.4. Effect of SB on virulence-related gene expression.

To understand the underlying mechanism behind CT reduction, we further checked the transcript levels of virulence genes. The inhibitory effect of SB on CT production was analysed using El Tor strain N16961 by assessing *ctxA*, *ctxB* gene transcripts and other virulence genes by qRT-PCR ***(Fig.5.5A)***. There was almost 4.3-fold and 3.8-fold reduction in *ctxA* and in *ctxB* transcripts respectively. In addition to this, the influence of SB on transcription of *toxS, toxR, tcpH, tcpP, tcpA, toxT* genes were also analysed. Along with *ctxAB* transcripts there was significant reduction of 9-fold in *tcpA* transcripts. However, there was no effect of SB on the transcription of *toxS, toxR, tcpH, tcpP and toxT*. The results obtained from this assay indicated a significant inhibitory effect of SB on the transcription of *ctxAB* and *tcpA* genes, however, no difference in the transcript level of *toxT* gene was observed in the presence of SB.

To rule out the possible mechanism that the reduced transcription of *ctxAB* and *tcpA* genes depend on the post-transcriptional or translational regulation of *toxT*, the levels of ToxT and TcpA proteins were measured. Western blot assay was performed on total protein extracts obtained from the treated and untreated samples ***(Fig.5.5B)***. The results demonstrated that SB had no relevant effect on the protein levels of ToxT.

Moreover, the reduction in TcpA protein level in presence of SB was consistent with the corresponding transcriptional profile. These observations are noteworthy in indicating that inhibition of SB is related to virulence cascade but not with ToxT production.

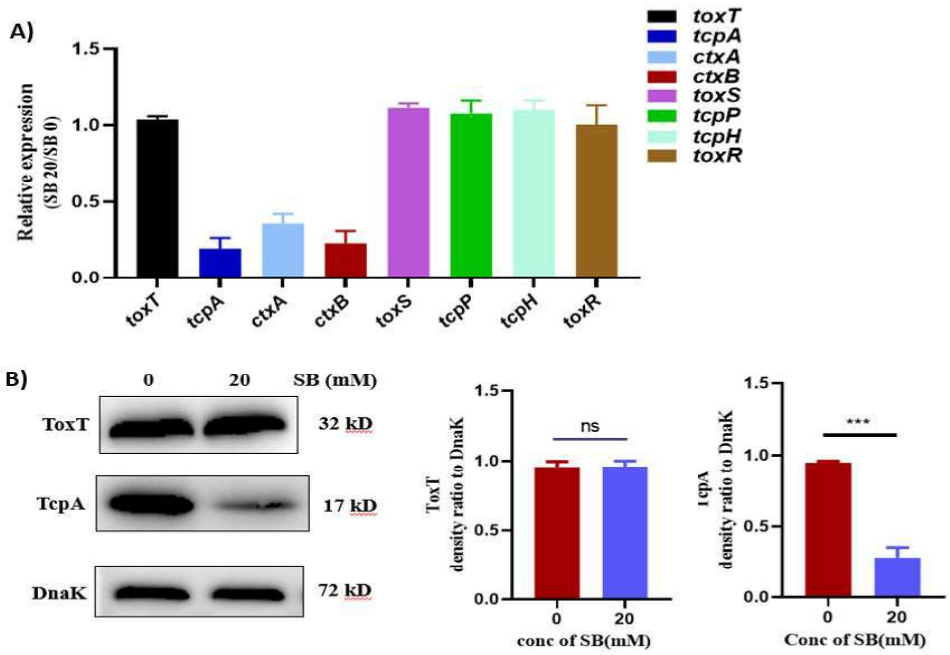

Fig 5.5. Effect of Sodium butyrate (SB) on virulence attributes of *Vibrio cholerae* O1 El Tor strain N16961. *Vibrio cholerae* N16961 was cultured under virulence inducing conditions (AKI media [pH 7.5], 37 °C, static condition for 18 h) in the presence or absence of 20mM SB. **(A)** Transcript levels of *ctxA*, *ctxB*, *toxS*, *toxR*, *tcpH*, *tcpP*, *tcpA*, *toxT* virulence genes were analyzed by real-time PCR and normalized using *recA* gene as the internal control and graphically represented. Values represent the number of times the genes are expressed compared to the untreated cells. One-way ANOVA was performed. **(B)** Expression of major virulence proteins ToxT and TcpA was determined by western blotting followed by densitometric analysis which is graphically represented. *Students t-test* was performed. All data are represented as mean ± S.E.M. (n = 3). Significance levels were denoted as n.s for non-significant, *** for $P < 0.001$.

5.5. SB binds to the ToxT protein and affects its interaction with the promoter

Results from the qRT-PCR and western blot analyses demonstrated a stable production of the ToxT protein regardless of the presence or absence of SB. Since ToxT is the direct transcriptional activator of the *tcpA* and *ctxAB* genes, it is possible that this compound influences the transcriptional activity of ToxT, which could lead to reduction in the activation of the *tcpA* and *ctxAB* genes. The probable explanation for the decrease in *tcpA* and *ctxAB* levels mediated by SB may be due to the ability of SB to interact with and inactivate the ToxT protein. We conducted a fluorescence quenching experiment to directly assess the binding of SB to ToxT ***(Fig.5.6)***. Our results indicate that SB does interact with ToxT protein, with a quenching constant (K_{sv}) of 6.04±0.04 × 10^2 M^{-1} and a dissociation constant (K_D) of 2.6±0.03 mM, which supports our previous *in silico* predictions.

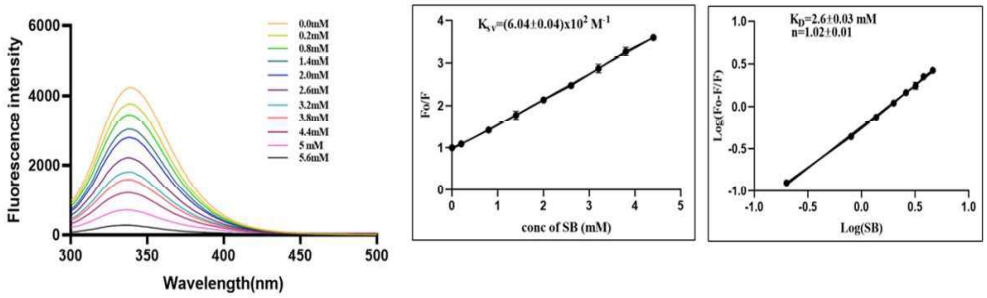

Fig 5.6. Fluorescence quenching spectra of ToxT in the presence of SB. A concentration of 0.1μM ToxT protein was excited at 280 nm, and fluorescence quenching was recorded in the presence of different concentrations of SB (0.2 to 5.6 mM). Stern-Volmer plots of decrease in fluorescence of ToxT in the presence of SB was used to determine the quenching rate constant, *Ksv* (calculated from the slope of line). Logarithmic plots of relative fluorescence quenching of ToxT against logarithmic concentrations of SB was used to determine K_D (calculated from the intersection of the line with the y-axis) and the number of binding sites, n (calculated from the slope of the line). Error bars indicate standard deviations calculated from three individual experiments.

Next, we examined whether SB could inhibit the binding of ToxT to its DNA binding site, which is located upstream of the *tcpA* gene. We conducted an electrophoretic mobility shift assay (EMSA). The results of the EMSA demonstrated that ToxT binds to the P_{tcpA} region in a concentration-dependent manner ***(Fig.5.7B)***. This interaction between ToxT and P_{tcpA} is specific, as CytR (another protein) was unable to interact with P_{tcpA} ***(Fig.5.7A)***. Additionally, a 70-fold molar excess of nonspecific

competitor DNA did not affect the ToxT-P_{tcpA} binding. In contrast, a 70-fold molar excess of specific competitor DNA completely inhibited the binding, indicating the specificity of the ToxT-P_{tcpA} interaction ***(Fig.5.7A)***. Next, we examined the effect of SB on ToxT-P_{tcpA} binding. Addition of 20 mM of SB prevented ToxT from binding to DNA ***(Fig.5.7B)***, and the interaction was completely inhibited at 40 mM of SB ***(Fig5.7D)***. Based on the concentration of ToxT needed to bind 50% of the P_{tcpA}, the dissociation constant (K_d) for ToxT without SB was 0.6 µM, while with 20 mM SB, it increased to 1.4 µM ***(Fig.5.7C)***. This rise in the Kd value in the presence of SB further confirms that SB significantly affects the equilibrium between DNA-bound ToxT and free DNA ***(Fig.5.7C)***. Another butyrate derivative, tributyrate (TB), was tested, and it showed no inhibition of ToxT-DNA binding, as illustrated in Figure ***(Fig.5.7E)***. We also explored the alternative hypothesis that SB could interact with DNA and inhibit DNA-protein binding. As demonstrated in Figure ***(Fig.5.7F)***, no inhibition of DNA binding activity was observed under these experimental conditions (when SB was incubated with DNA first, instead of ToxT). This indicates that SB specifically binds to ToxT and not to DNA.

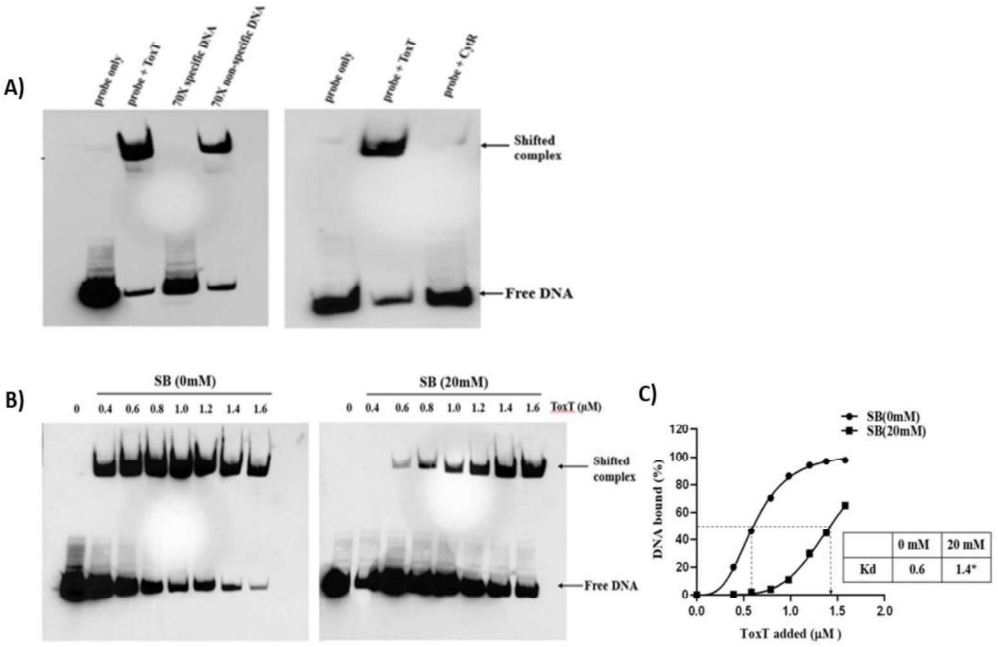

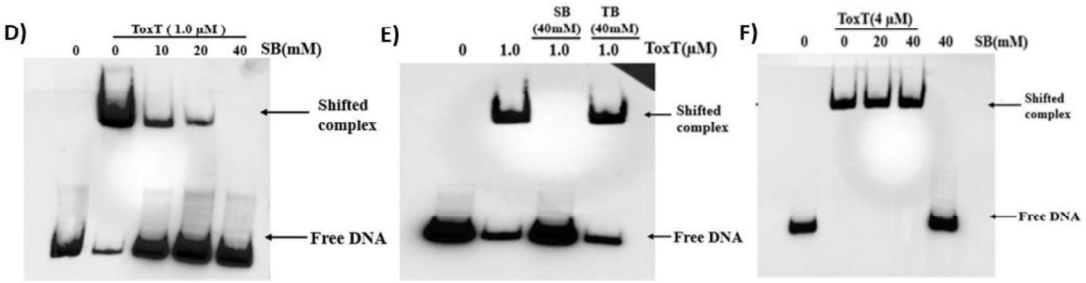

Fig.5.7. SB interacts with and inactivates ToxT protein. A) ToxT binds specifically to P_{tcpA}. ToxT was incubated with 1nM of biotin-labeled P_{tcpA} in the reaction buffer in the presence or absence of either 70x specific or non-specific competitors. 1nM of biotin-labeled P_{tcpA} was incubated with ToxT or CytR in the reaction buffer. **B)** For EMSA, a 150 bp P_{tcpA} DNA fragment was biotin-labeled and then used as a DNA probe. Purified ToxT protein was added to the probe (1nM) in the presence or absence of SB (20mM). **C)** Relative affinities of ToxT protein in the presence or absence of SB were compared using the data from panel B. The percentage of bound DNA was calculated and plotted against the concentration of ToxT added. K_d is shown in the inset. A significant difference between the best-fit values indicated by an asterisk ($*P < 0.05$). **D)** EMSA was performed as described for panel B, except that ToxT was mixed with increasing amounts of SB. EMSAs presented are representative of three independent experiments. **E)** ToxT interacts with SB but not with TB. ToxT (1.0 μM) was incubated with 40mM Sodium Butyrate (SB) or 40mM Tributyrate (TB) followed by the addition of P_{tcpA}. **F)** SB binds with ToxT but not with DNA. Biotin labeled P_{tcpA} DNA (0.5nM) was incubated with SB (20 an 40mM) followed by ToxT protein (4 μM) addition. EMSAs presented are representative of three independent experiments

Results from the electrophoretic mobility shift assays (EMSAs) indicated that SB interferes with the DNA binding ability of ToxT *in vitro*. To further investigate this effect under physiological conditions, we conducted a chromatin immunoprecipitation (ChIP) assay to determine whether SB impacts ToxT-DNA binding in the presence of other transcription factors. As anticipated, ToxT occupancy at the *tcpA* (P_{tcpA}) and *ctxAB* (P_{ctxAB}) promoter regions was significantly reduced in SB-treated *V. cholerae* cells compared to untreated cells. This finding suggests that SB strongly interferes with the binding of ToxT to both the P_{tcpA} and P_{ctxAB} sites ***(Fig.5.8)***. In addition, we evaluated whether the interaction of ToxT with the promoter DNAs of the *acfA* (P_{acfA}), *aldA* (P_{aldA}), *acfD* (P_{acfD}), *tagA* (P_{tagA}), and *tcpI* (P_{tcpI}) genes, which are regulated by ToxT and encode accessory virulence factors, was influenced by the addition of SB. Our results showed that ToxT occupancy at each of these promoters was reduced in *V. cholerae* cells treated with SB compared to untreated cells ***(Fig.5.8)***. Overall, these

findings indicate that SB significantly inhibits the binding of ToxT to its various downstream promoter DNAs.

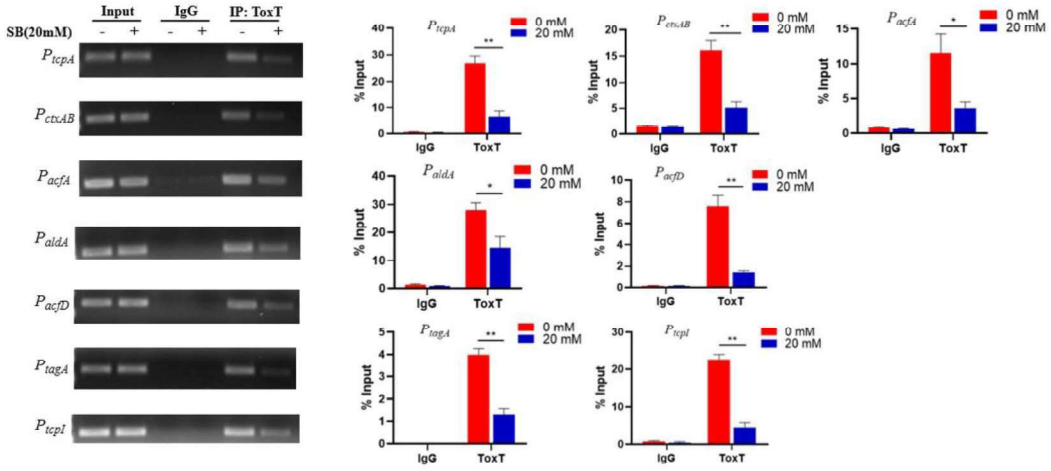

Fig.5.8. Interaction between ToxT and promoter DNAs at the cellular level in the presence or absence of SB (20 mM) was analyzed by ChIP. Expression of promoter DNAs was checked and compared to input in real-time PCR assay and agarose gel electrophoresis. Two-way ANOVA was performed. The data are expressed as mean ± S.D ($n=3$). IP, Immunoprecipitation; significance levels were denoted as ∗for $P < 0.05$, ∗∗for $P < 0.01$.

5.6. SB triggers global changes in the transcriptome of V. cholerae.

We investigated the global effects of SB on the transcriptional profile of *V. cholerae* using an RNA-seq approach. Our analysis revealed that SB induced significant changes in gene expression: 53 genes were upregulated, while 95 genes were downregulated compared to the untreated condition ***(Fig.5.9)***. Notably, genes involved in pathogenesis, metabolism, and regulatory factors related to transcription and translation were primarily downregulated, whereas biofilm-related genes showed increased expression ***(Fig.5.9A-C)***. Twelve differentially expressed genes were randomly selected for quantitative reverse transcription polymerase chain reaction (qRT-PCR) to validate the RNA sequencing (RNA-seq) data. Our results showed that the expression trends of the twelve genes were consistent between RNA-seq and qRT-PCR data, suggesting that RNA-seq was reliable in identifying transcriptional changes ***(Fig.5.9D)***.

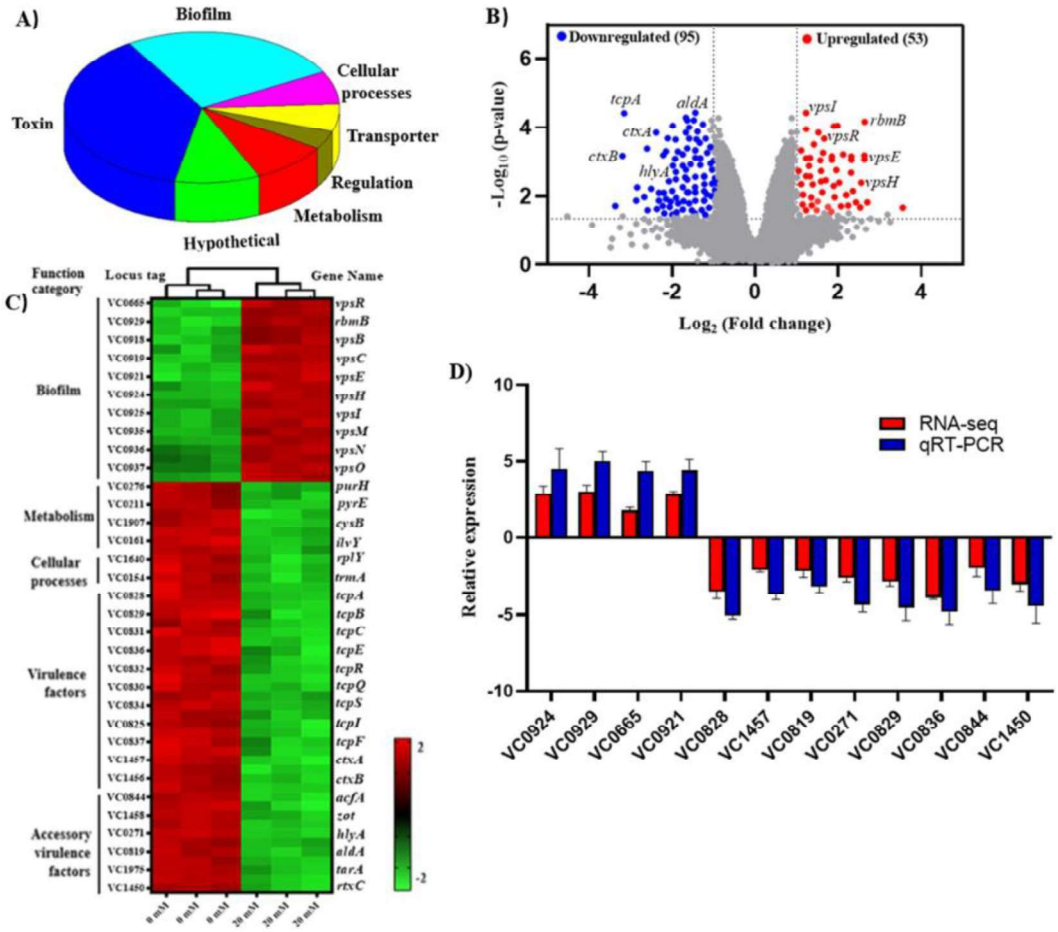

Fig.5.9. Global transcriptional responses to SB. **A)** Genes whose expression is dysregulated in SB-treated cells (20mM) relative to the untreated cells, as identified by RNA-seq analysis. The genes in each functional category are shown as percentages of the total genes dysregulated. **B)** Volcano plot of differentially expressed genes of N16961 cells in the presence or absence of SB treatment. The log_2fold change difference is represented on the X-axis and -log_{10} (*p-value*) is on the Y-axis. Red and blue dots show upregulated and downregulated genes. **C)** Heatmap of differentially expressed genes of N16961 cells in the presence or absence of 20mM of SB. *Z-score* indicates whether the genes were upregulated (red) or downregulated (green). Columns represent independent RNA samples. **D)** RNA-seq results validation by qRT-PCR. Data are presented as mean ± SD ($n = 3$).

5.7. Adhesion to intestinal epithelial cells is affected by Sodium butyrate (SB).

Adhesion of *V. cholerae* to epithelial cells is facilitated by TcpA, an important colonization factor that plays a key role in forming microcolonies and adhering to epithelial cells. The ability of *V. cholerae* to adhere to intestinal epithelial cells was evaluated using the HT-29 cell line and further confirmed through *in vivo* animal models. Since SB decreased TcpA levels, we first examined its effect on the ability of *V.*

cholerae to adhere to intestinal epithelial cells, specifically intestinal cells ***(Fig.5.10A)***. Results from the cell adherence assays showed that the adherence of *V. cholerae* to HT-29 cells was significantly reduced in the presence of SB compared to the untreated condition ***(Fig.5.10A)***. Additionally, an *in vivo* adherence study conducted in rabbit ileal loops demonstrated a significant reduction in bacterial adhesion (adherence index) in SB-treated loops compared to untreated loops ***(Fig.5.10B)***. The effect of sodium butyrate (SB) on the colonization ability of *V. cholerae* in suckling mice was evaluated. In mice treated with SB (administered orogastrically at concentrations of 40 and 80 mM), intestinal colonization of *V. cholerae* was significantly reduced by at least two orders of magnitude compared to the untreated group ***(Fig.5.10C)***. However, the administration of another butyrate derivative, Tributyrate, to suckling mice did not reduce intestinal colonization of N16961 compared to untreated mice ***(Fig.5.10C)***.

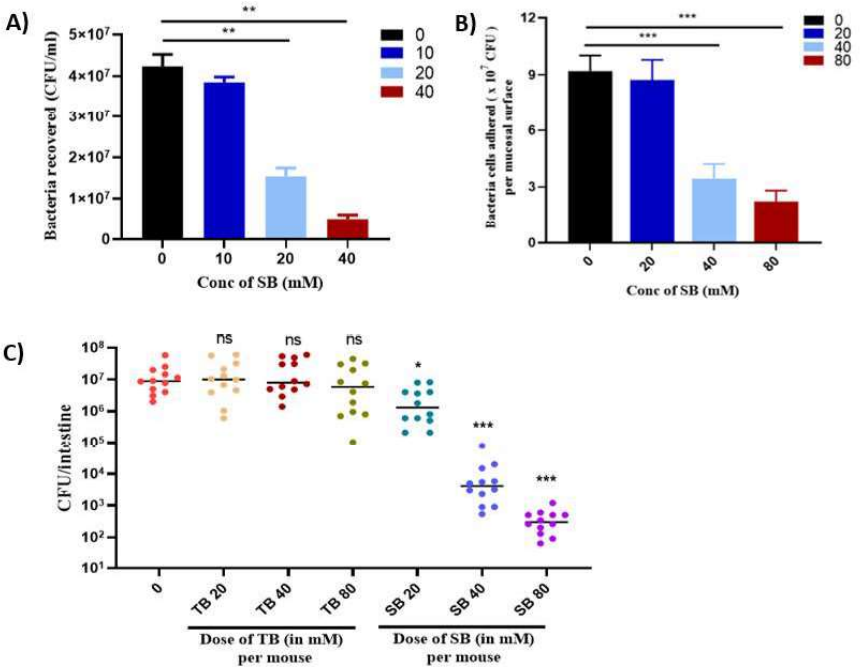

Fig.5.10. Influence of Sodium butyrate (SB) on the adhesion of *V. cholerae* to the epithelial cells. A) Adherence of *V. cholerae* to HT-29 cell line performed at different concentrations of SB (0-40 mM). One-way ANOVA was performed. Significance levels were denoted as ∗∗for $P < 0.01$. **B)** The rabbit ileal loop was injected with 1×10^9 CFU/ml *V. cholerae* N16961 with or without SB. After 18 h, the animals were euthanized, the loops were removed and adherence index of N16961 were estimated in the presence or absence of SB. Adherence index is denoted by the average number of adhered bacterial cells per punched mucosal surface where each punch was 38.5 mm^2 (7 mm diameter). **C)** Effect of drugs on bacterial colonization in 4 to 5-day-old suckling BALB/c mice (*n=12* per group). The mice were orogastrically challenged with 10^5 CFU of *V. cholerae* strain N16961 with or without drugs [TB or SB (20, 40, and 80 mM)] and kept at 30 ºC for 18 h. Bacterial colonization was estimated as CFU/intestine and graphically represented. Each circle represents an individual mouse. Horizontal lines

are medians. Significance was determined by Mann–Whitney U test (*n=12* per group). Significance levels (compared to controls challenged without any drug) were denoted as ns=nonsignificant, ∗ for $P < 0.05$, ∗∗∗ for $P < 0.001$.

5.8. SB displays a substantial reduction in virulence attributes of *V. cholerae* in animal models.

The results described so far show that SB has a strong negative impact on ToxT activity *in vitro*, as evidenced by both gene expression (CT and TcpA production) and DNA binding experiments (EMSA). Next step is to determine whether administering SB in animal models for cholera will reduce the production of virulence factors. We assessed the effects of SB on fluid accumulation (FA) and CT production by N16961 using the rabbit ileal loop model ***(Fig.5.11A-C)***. The fluid accumulation (FA) ratio in treatment loops using SB at concentrations of 40 mM and 80 mM showed a more than 20-fold reduction in fluid accumulation compared to the loop that did not receive SB ***(Fig.5.11B)***. At these two higher concentrations (40 mM and 80 mM), the level of CT was significantly decreased by over 10-fold compared to the loop without SB ***(Fig.5.11C)***. Additionally, the expression of virulence genes, specifically *ctxAB* and *tcpA*, was downregulated in *V. cholerae* cells collected from the SB-treated loop fluid compared to those from the untreated loop ***(Fig.5.11D)***.

Next, we examined the histological changes associated with *V. cholerae* infection. H&E staining revealed that the infected loop exhibited necrotic changes in the mucosa, submucosa, and lamina propria, along with deformed villi and hemorrhage at the muscularis mucosa site. Notably, treatment with SB effectively prevented the tissue damage induced by *V. cholerae* infection ***(Fig.5.11E)***. Additionally, the loops treated with SB showed a significant reduction in the concentration of inflammatory cytokines (IL-6, IL-8, IL-1β, TNF-α) compared to the loops that did not receive SB treatment ***(Fig.5.11F)***.

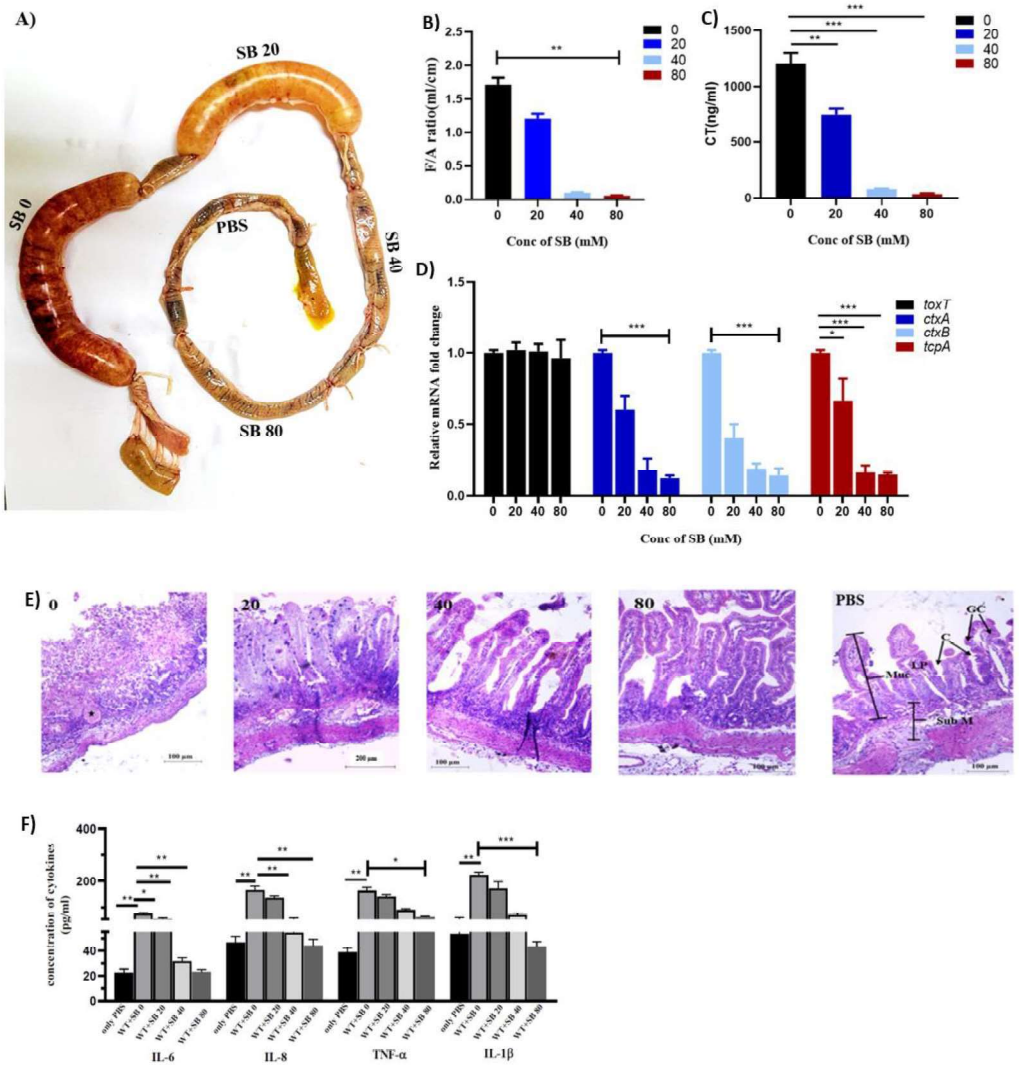

Fig.5.11. Efficacy of SB in an in vivo rabbit ileal loop model infected with N16961. Each loop was injected with 1 × 10^9 CFU/ml *V. cholerae* N16961 with or without SB and loop injected only with PBS served as negative control loop. After 18 h, animals were euthanized, and the loops were removed. **A)** Representative image of recovered rabbit intestine segment with infected loop at 18 h after infection. **B)** Fluid accumulation per unit area (F/A) ratio of each loop was evaluated and graphically represented as mean ± S.E.M. (*n = 3*). **C)** The accumulated fluid samples from SB treated and untreated ileal loops were used to measure CT production by ELISA. **D)** Relative expression of major virulence genes *ctxA*, *ctxB*, *tcpA*, *toxT* were analyzed by real-time PCR. Normalization was done using *recA* gene as the internal control. One-way ANOVA was performed. All data are represented as mean ± S.E.M. (*n = 3*). Significance levels were denoted as ∗for $P < 0.05$, ∗∗for $P < 0.01$, ∗∗∗ for $P < 0.001$. **E)** Representative H&E staining section of rabbit intestinal tissues. SB treatment prevented mucosal damage, disruption of villus structure, and necrotic changes induced by N16961 infection. GC, Goblet Cells; C, Crypts; LP, Lamina Propria; Muc, Mucosa; SubM, Submucosa; *, indicating the site of haemorrhage. **F)** ELISA results for IL-6, IL-8, IL-1β, and TNF-α cytokine expression in each of the ileal loops in the presence or absence of SB.

We also examined the virulence of *V. cholerae* in the presence of TB ***(Fig.5.12A-C)***. As expected, there was no reduction in fluid accumulation or CT levels in the ileal loop treated with TB compared to the untreated loop (***(Fig.5.12B&C)***. The expression profile of virulence genes in *V. cholerae* cells from the TB-treated loop was nearly identical to that of the untreated loop ***(Fig.5.12D)***.

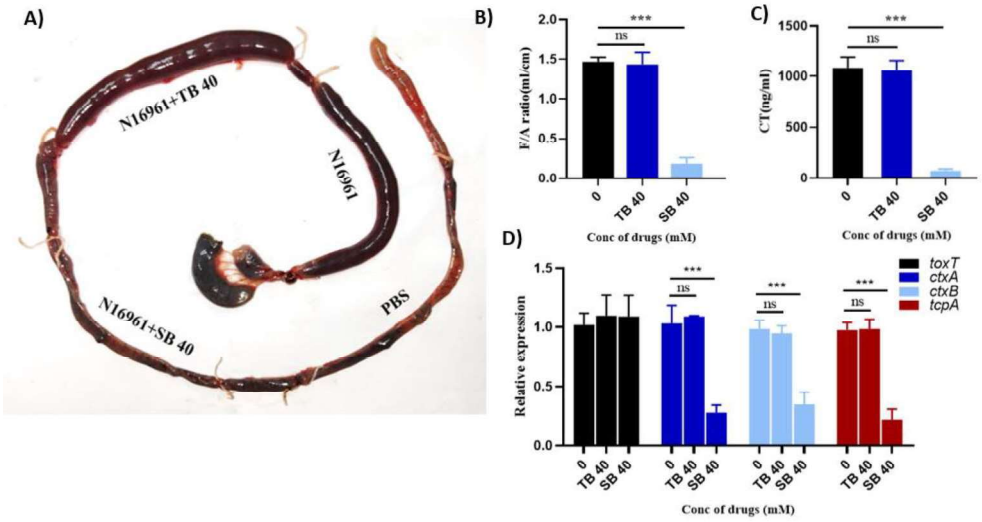

Fig.5.12. Efficacy of drugs against the virulence factors in rabbit ileal loop. The rabbit ileal loop was injected with 1×10^9 CFU/ml *V. cholerae* N16961 with or without drugs [TB or SB (40 mM)]. After 18 h, the animals were euthanized, and the loops were removed. **A)** Image of the recovered rabbit intestine segment presented here is representative of three independent experiments. **B)** The loop length and the amount of fluid accumulated in each loop were measured, and the amount of fluid (ml) per unit length (cm) of the loop was determined in the presence or absence of drugs [TB or SB (40 mM)]. **C)** CT ELISA of rabbit ileal loop fluid produced in the presence and absence of drugs [TB or SB (40 mM)]. **D)** Relative expression of major virulence genes *ctxA*, *ctxB*, *tcpA*, *toxT* were analyzed by real-time PCR. Significance was calculated by one-way ANOVA. Significance levels were denoted as ∗for $P < 0.05$, ∗∗for $P < 0.01$, ∗∗∗ for $P < 0.001$.

Chapter 6

Results

Investigate the effect of potential inhibitor in combination with known drugs in vitro and in vivo models

Results

Our findings revealed that small molecule sodium butyrate is a strong anti-virulence agent against *V. cholerae*. Based on our findings, our next objective is to investigate the synergistic effects of sodium butyrate in combination with various conventional antibiotics, to evaluate the combinatorial efficacy *in vitro* and *in vivo* conditions.

6.1. Sodium butyrate and tetracycline combination exhibit synergistic antibacterial effects on multidrug-resistant V. cholerae

We evaluated the antibacterial activity of eight antibiotics against eight strains of *V. cholerae*, both individually and in combination with sodium butyrate (SB). According to the results of the microdilution test, the bacterial strains used in this study were all multidrug-resistant (MDR) strains ***(Table 6.1A)***. As shown in ***Table 6.1B***, the MICs of SB against the strains were ≥8.8 mg/ml and MBCs were ≥17.6 mg/ml, indicating that SB alone did not exhibit significant antibacterial activity against *V. cholerae* strains. Therefore, we evaluated the synergistic effect of SB and antibiotics by determining the FIC index ***(Table 6.1C)***. The results showed that out of all the antibiotics, SB can act as a synergistic antibacterial agent with tetracycline against multidrug-resistant *V. cholerae* strains ***(Table 6.1C)***, with FIC index values ranging from 0.09375 to 0.5, respectively.

	IDH1986	IDH07976	IDH14062	IDH13966	V32	V24	V100	Micro78
Streptomycin	64 (R)	64 (R)	32 (S)	128 (R)	8 (S)	8 (S)	16 (S)	64 (R)
Ampicillin	32 (R)	32 (R)	32 (R)	32 (R)	8 (S)	32 (R)	32 (R)	32 (R)
Azithromycin	64 (R)	64 (R)	64 (R)	8 (S)	64 (R)	8 (S)	8 (S)	64 (R)
Chloramphenicol	32 (R)	32 (R)	32 (R)	8 (S)	4 (S)	4 (S)	64 (R)	32 (R)
Tetracycline	16 (R)	16 (R)	8 (I)	8 (I)	2 (S)	4 (S)	8 (I)	16 (R)
Ciprofloxacin	4 (R)	4 (R)	2 (I)	4 (R)	8 (R)	1 (S)	1 (S)	4 (R)
Gentamicin	1 (S)	1 (S)	2 (S)	8 (I)	8 (I)	16 (R)	2 (S)	1 (S)

Table 6.1A. MICs of different antibiotics against V. cholerae strains (µg/ml).

Strains	MIC	MBC
IDH1986	8.8	17.6
IDH07976	8.8	17.6
IDH14062	8.8	17.6
IDH13966	8.8	17.6
V32	17.6	35.2
V24	17.6	35.2
V100	17.6	35.2
Micro78	8.8	17.6

Table 6.1B. MICs and MBCs of SB against eight strains of V. cholerae (mg/ml).

	IDH1986	IDH07976	IDH14062	IDH13966	V32	V24	V100	Micro78
Streptomycin	1	0.5625	0.75	0.625	0.5625	1	0.53125	0.625
Ampicillin	0.625	1	1	0.5625	0.75	0.75	0.5625	1
Azithromycin	0.75	0.625	0.5625	0.75	1	0.53125	0.53125	0.75
Chloramphenicol	0.5625	1	0.75	0.75	0.625	1	1	1
Tetracycline	0.09375	0.375	0.5	0.1875	0.5	0.375	0.5	0.75
Ciprofloxacin	1	0.5625	0.75	1	0.625	1	1	0.75
Gentamicin	0.5625	1	0.625	0.75	0.5625	1	0.5625	1

Table 6.1C. FICs of SB combined with different antibiotics against *V. cholerae*

Of all the strains, *V. cholerae* IDH1986 (tetracycline-resistant strain), V24 (tetracycline-susceptible strain), and IDH13966 (tetracycline-intermediate strain) were selected for further study. In *V. cholerae* IDH1986, the MIC of tetracycline was reduced from 16 µg/ml to 0.5 µg/ml when used in combination with 1.1 mg/ml of SB, with a further decrease to 0.063 µg/ml observed in combination with 4.4 mg/ml of SB ***(Fig.6.1A)***. Furthermore, combination of SB and Tet also exhibited a strong synergistic antimicrobial effect on the other *V. cholerae* strains, with results showing that the Tet MIC was reduced from 8 µg/ml to 0.5 µg/ml when used in combination with 1.1 mg/ml of SB for strain IDH13966 ***(Fig.6.1B)***, and the Tet MIC reduction from 4 µg/ml to 1µg/ml when used in combination with 2.2 mg/ml of SB for strain V24 ***(Fig.6.1C)***. Moreover, the Tet MIC of strain IDH13966 was significantly decreased to 0.063 µg/ml when used in combination with 4.4 mg/ml of SB ***(Fig.6.1B)*** and for strain V24, the Tet MIC was reduced to 0.063 µg/ml when used in combination with 8.8 mg/ml of SB ***(Fig.6.1C)***, suggesting that SB exhibited a dose-dependent enhancement effect on the

ability of Tet to kill multidrug-resistant *V. cholerae* strains. Isobologram curves established from the results of the checkerboard assays confirmed the synergistic antimicrobial effect of Tet combined with SB against strain IDH1986, V24 and IDH13966 *(Fig.6.1D-F)*. The concave isobole (represented by the solid lines) indicates the confirmation of antimicrobial synergy observed against *V. cholerae* strains. Since SB FIC index with Tet was FICI=0.09375 for IDH1986 (tetracycline-resistant strain), FICI=0.375 for V24 (tetracycline-susceptible strain) and FICI=0.1875 for IDH13966 (tetracycline-intermediate strain), it indicated that the synergistic effect of SB with tetracycline existed in *V. cholerae* strains no matter it is tetracycline resistant or not.

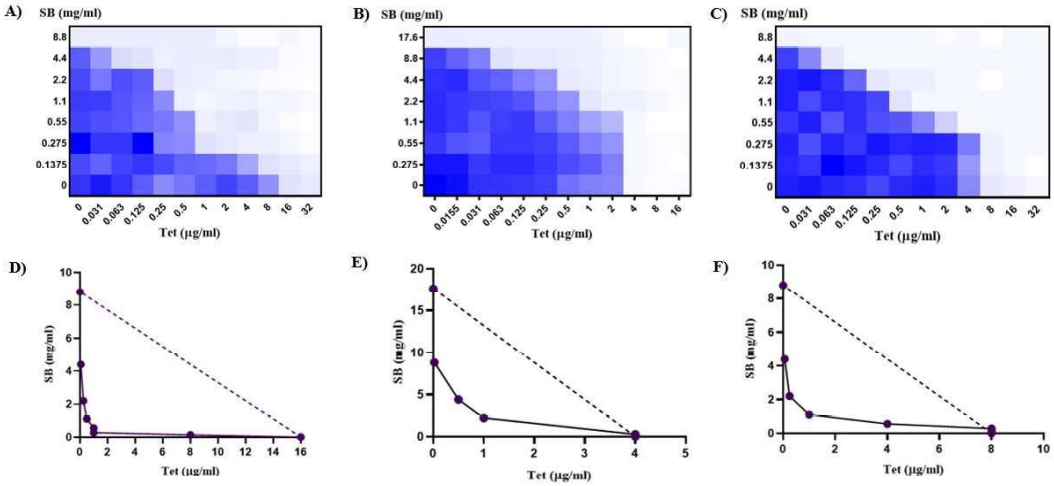

Fig.6.1. SB in combination with Tetracycline exhibits synergistic antimicrobial effects against MDR *V. cholerae* strains. A) Checkerboard assays of SB in combination with tetracycline against *V. cholerae* IDH1986, FICI=0.09375; **B)** Checkerboard assays of SB in combination with tetracycline against *V. cholerae* strain V24, FICI=0.375; **C)** Checkerboard assays of SB in combination with tetracycline against *V. cholerae* strain IDH13966, FICI=0.1875; **D)** Isobologram of the synergistic interaction for the combination of SB with Tet against strain *V. cholerae* IDH1986; **E)** Isobologram of the synergistic interaction for the combination of SB with Tet against strain *V. cholerae* V24; **F)** Isobologram of the synergistic interaction for the combination of SB with Tet against strain *V. cholerae* IDH13966.

A critical consideration for combinational therapy in clinical settings is the potential for increased toxicity when antibiotics are used together with adjuvants. Thus, the cytotoxicity of tetracycline, alone and in combination with SB, was evaluated in the mammalian HT-29 cell line. Results from the MTT assay indicated that the combination of SB and tetracycline did not result in significant cytotoxic effects on HT-29 cells, suggesting that the co-administration is likely safe in this *in vitro* model cytotoxicity of tetracycline, alone and in combination with SB, was evaluated in the

mammalian HT-29 cell line. Results from the MTT assay indicated that the combination of SB and tetracycline did not result in significant cytotoxic effects on HT-29 cells, suggesting that the co-administration is likely safe in this *in vitro* model ***(Fig.6.2)***.

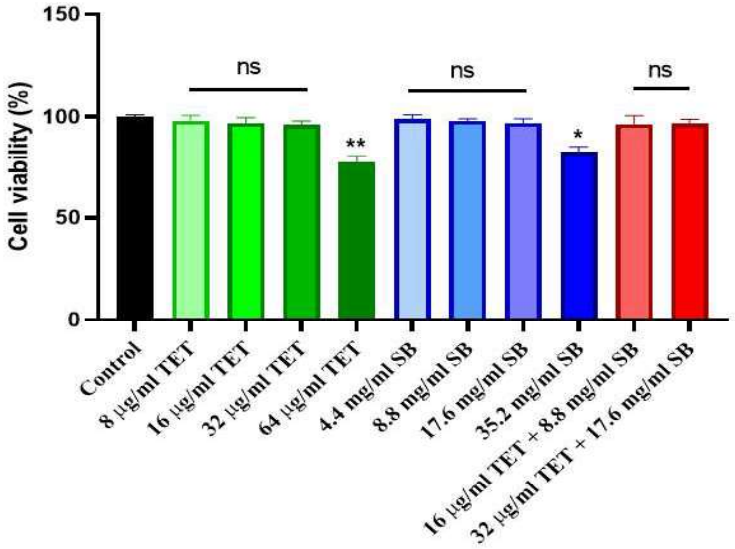

Fig.6.2. Cytotoxicity of tetracycline in combination with SB against HT-29 cell line. Data are presented as mean ± SD, and the significances were determined by nonparametric one-way ANOVA (*p<0.05, **p<0.01), ns=non-significance.

6.2. SB enhances tetracycline efficacy and minimizes the emergence of resistance

To further investigate the synergistic bactericidal effect of SB and Tet combination, time-dependent killing assays were conducted on *V. cholerae* strains. In this experiment, we found that growth of *V. cholerae* strain IDH1986 was not inhibited by treatment with 2.2 mg/ml SB alone; treatment with 4 µg/ml of Tet alone caused only a slight reduction in bacterial population size ***(Fig.6.3A)***. However, on combined treatment with 2.2 mg/ml SB and 4 µg/ml Tet, the tetracycline-resistant strain IDH1986 was completely eradicated within 6 h ***(Fig.6.3A)***. In the tetracycline-intermediate strain IDH13966, treatment with 2.2 mg/ml SB alone and treatment with 4 µg/ml Tet alone showed no significant change in bacterial population ***(Fig.6.3B)***, while, combined treatment with 2.2 mg/ml SB and 4 µg/ml Tet, resulted in complete eradication of strain IDH13966 within 12 h of treatment ***(Fig.6.3B)***. Similarly, for tetracycline-

susceptible strain V24, treatment with 4.4 mg/ml SB alone and treatment with 2 µg/ml Tet alone could not kill the strain, while combined treatment with 4.4 mg/ml SB and 2 µg/ml Tet resulted in complete eradication of strain V24 within 18 h of treatment *(Fig.6.3C)*. These results suggested that SB significantly enhanced the bactericidal effect of Tet on *V. cholerae* strains.

To get better understanding of SB on the development of tetracycline resistance, we performed serial passages of C6709 with sub-MIC (0.25 × MIC) of tetracycline in the presence and absence of SB (4.4 mg/ml) during 30 d. Interestingly, we failed to obtain the resistant mutants in the combination group *(Fig.6.3D)*. In contrast, the tetracycline alone group produces high-resistant strains with 32-fold increase of MIC. These results suggested that the combination of tetracycline and SB could effectively minimize the *de novo* emergence of tetracycline resistance.

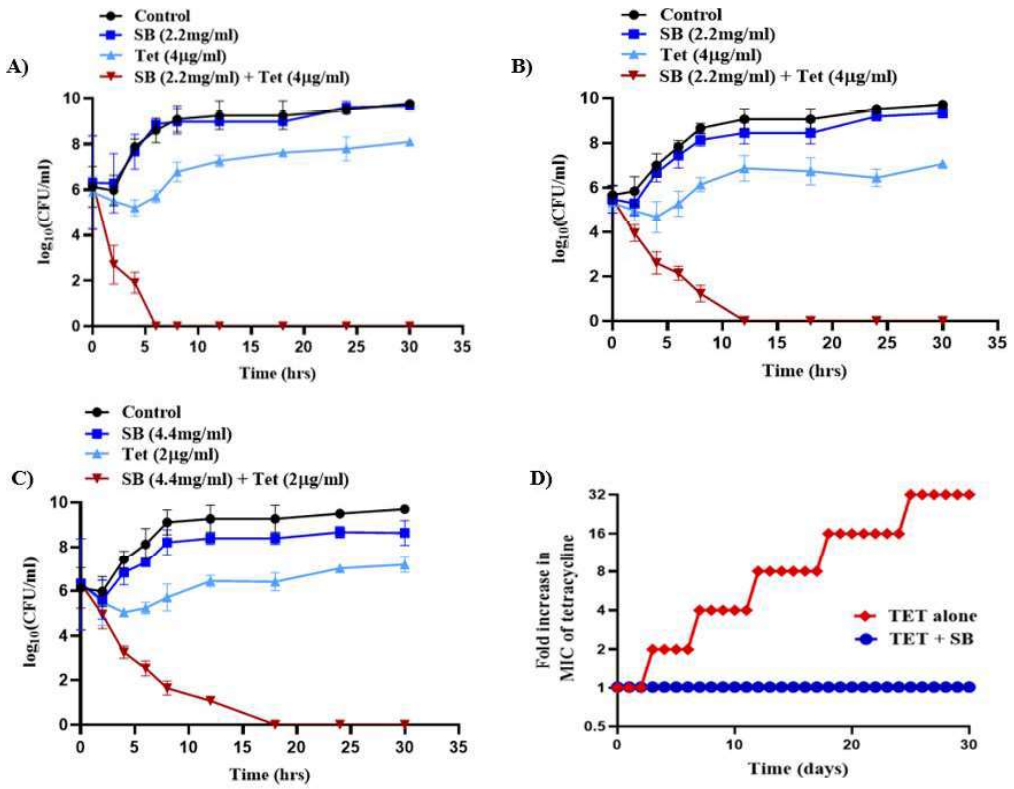

Fig.6.3. Time-dependent killing of MDR *V. cholerae* strains by combining SB with Tet. *V. cholerae* strains were grown in LB along with SB, Tet, combination of SB and Tet for the indicated time periods (2, 4, 6, 8, 12, 18, 24, and 30 hrs). Viable bacterial counts in CFU per ml detected by the plate count method were represented graphically for **A)** SB (2.2 mg/ml), Tet (4µg/ml), combination of SB and Tet (2.2 mg/ml + 4 µg/ml) were selected as treatment concentrations for strain IDH1986; **B)** SB (2.2 mg/ml), Tet (4 µg/ml), combination of SB and

Tet (2.2 mg/ml + 4µg/ml) were selected as treatment concentrations for strain IDH13966; **C)** SB (4.4 mg/ml), Tet (2 µg/ml), combination of SB and Tet (4.4 mg/ml + 2 µg/ml) were selected as treatment concentrations for strain V24. **D)** The addition of SB (4.4 mg/ml) prevents the evolution of tetracycline resistance to *V. cholerae* C6709 *in vitro*.

A synergistic bactericidal effect of SB and tetracycline combination on *V. cholerae* strains was also illustrated by LIVE/DEAD staining ***(Fig.6.3)***. Treatment with SB (2.2 mg/ml) or Tet (4 µg/ml) alone did not significantly reduce bacterial viability in the *V. cholerae* IDH1986, with death rates similar to the control; however combined treatment with 2.2 mg/ml SB and 4 µg/ml Tet resulted in death of 89.46% of bacterial population (dead/live ratio, 8) ***(Fig.6.3A)***. Similarly, for the other two strains, IDH13966 and V24, neither SB alone (2.2 mg/ml for Tet-intermediate strain and 4.4 mg/ml for Tet-susceptible strain) nor tetracycline alone (4 µg/ml for the Tet-intermediate strain and 2 µg/ml for the Tet-susceptible strain) was effective in killing the bacteria, with death rates comparable to the control group. In contrast, the combined treatment led to the death of 89% of the bacterial population (dead/ratio, 8) in the Tet-intermediate strain IDH13966 ***(Fig.6.3B)***, and death of 97.73% of bacterial population (dead/ratio, 9.6) in the Tet-susceptible strain V24 ***(Fig.6.3C)***.

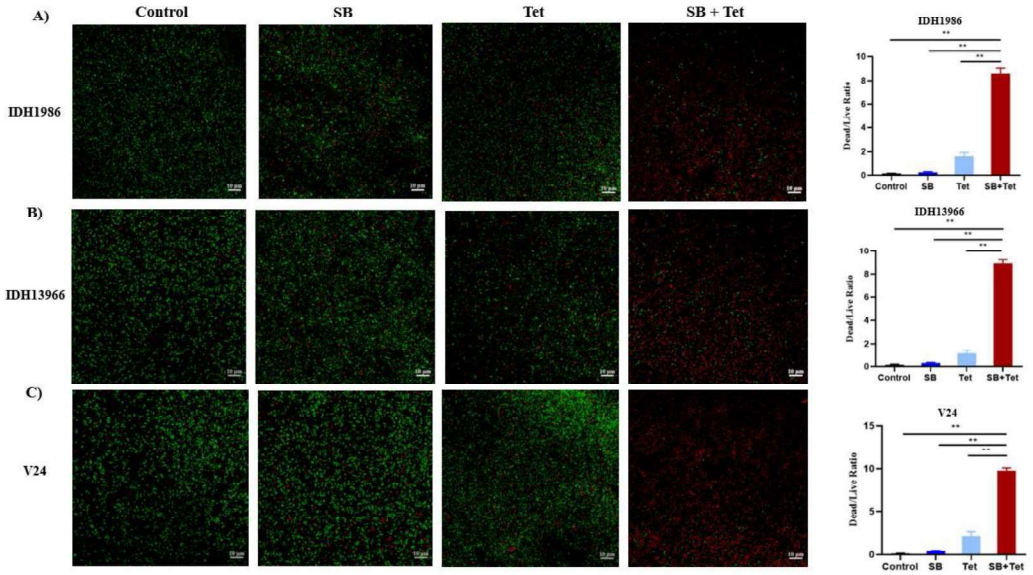

Fig.6.3. LIVE/DEAD staining to depict synergistic bactericidal effect of SB and Tet combination on multidrug-resistant *V. cholerae* strains IDH1986, IDH13966, and V24. A) Strain IDH1986 was treated with SB (2.2 mg/ml), Tet (4 µg/ml), combination of SB and Tet (2.2mg/ml + 4 µg/ml) followed by the graphical representation of LIVE/DEAD ratio; **B)** Strain IDH13966 was treated with SB (2.2 mg/ml), Tet (4µg/ml), combination of SB and Tet (2.2mg/ml+4µg/ml) followed by the graphical representation of LIVE/DEAD ratio; **C)** Strain V24 was treated with SB (4.4 mg/ml), Tet (2µg/ml), combination of SB and Tet (4.4mg/ml +

2µg/ml) followed by the graphical representation of LIVE/DEAD ratio. All data are presented as mean ± SD and data were analyzed using one-way ANOVA and Tukey test (**p<0.01)

6.3. SB-Tet combination induces cytoplasmic content leakage.

Membrane leakage assays were also carried out to assess the integrity of the cell membrane of *V. cholerae* ***(Fig.6.4)***. Firstly, we determined the leakage of nucleic acids by measuring the O.D. of the culture supernatant. The data indicated that SB-Tet combination significantly increased $O.D_{260}$ by 2-fold compared to untreated or individual treatment ***(Fig.6.4A)***. This was further confirmed when the nucleic acid release was visualized by agarose gel electrophoresis, which revealed a markedly higher release of nucleic acids in the SB-Tet combination group, clearly distinguishable from the minimal release observed with individual SB or Tet treatments ***(Fig.6.4B)***.

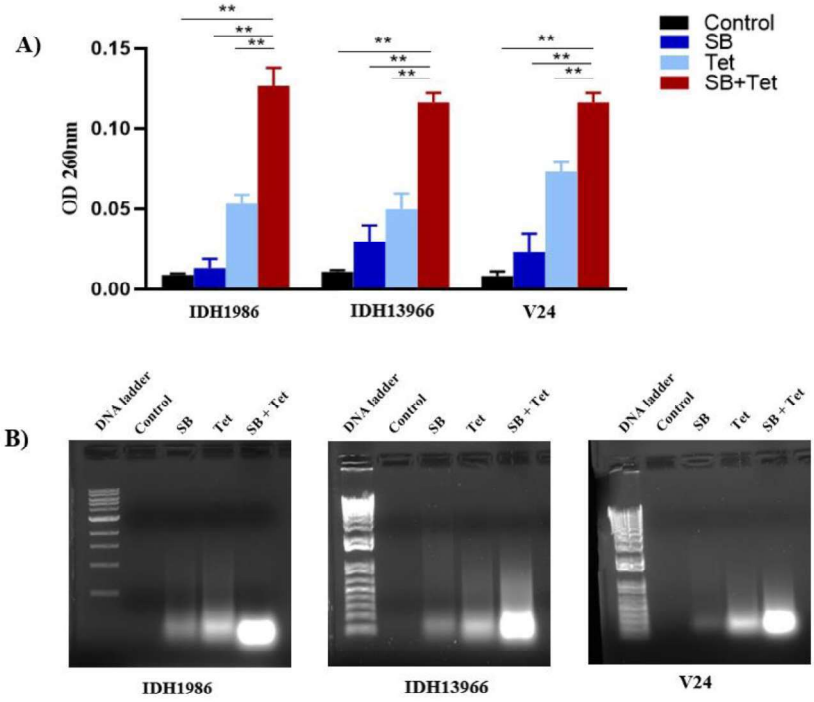

Fig.6.4. The SB-Tet combination leads to the cytoplasmic content leakage. A) Spectrofluorometric measurement of change in release of cytoplasmic content in *V. cholerae* strain IDH1986 in the presence of SB (2.2mg/ml), Tet (4µg/ml), combination of SB and Tet (2.2 mg/ml+4µg/ml); in *V. cholerae* strain IDH13966 in the presence of SB (2.2mg/ml), Tet (4µg/ml), combination of SB and Tet (2.2 mg/ml + 4 µg/ml); in *V. cholerae* strain V24 in the presence of SB (4.4mg/ml), Tet (2µg/ml), combination of SB and Tet (4.4 mg/ml+2µg/ml). **B)** Agarose gel (0.8%, w/v) electrophoresis and ethidium bromide staining of the released nucleic acid from *V. cholerae* strains IDH1986 [SB (2.2mg/ml), Tet (4µg/ml), combination of SB and Tet (2.2 mg/ml+4µg/ml)]; IDH13966 [SB (2.2mg/ml), Tet(4µg/ml), combination of SB and Tet (2.2 mg/ml+4µg/ml)] and; V24 [SB (4.4mg/ml), Tet (2µg/ml), combination of SB and Tet (4.4mg/ml+2µg/ml)]. 1 kb ladder was used as a reference. All data are presented as

mean ± SD, and the significances were determined by nonparametric one-way ANOVA (**p<0.01)

6.4. SB-Tet combination treatment causes profound morphological changes and increases membrane permeability.

For a better understanding of the effect of SB-Tet combination treatment, we used SEM to investigate the morphology of the cells after treatment with SB, Tet and the combination of both ***(Fig.6.5)***. No morphological changes were observed when *V. cholerae* IDH1986 was treated with 2.2 mg/ml SB; while treatment with 4 µg/ml Tet led to minor morphological changes where bacterial cells were shortened ***(Fig.6.5A)***. Interestingly, when treated with 2.2 mg/ml SB and 4 µg/ml Tet combination, bacteria were lysed and deformed with disrupted membranes ***(Fig.6.5A)***.

Furthermore, the levels of both β-galactosidase and alkaline phosphatase were significantly elevated in the SB-Tet combination treatment compared to treatment with SB or Tet alone ***(Fig.6.5B and Fig.6.5C)***. This disruption was further illustrated using a PI uptake assay. The SB-Tet combination also generated a significant increase in fluorescence intensity due to PI uptake ***(Fig.6.5D)***. Next, we evaluated the ATP level in *V. cholerae* IDH1986 treated with SB, Tet, and their combination. As shown in **Fig.6.5E**, the combined use of tetracycline and SB significantly reduced the intracellular ATP level compared to that of monotreatment with tetracycline or SB, suggesting that SB had a synergistic effect with tetracycline in inhibiting ATP synthesis. Together, these data indicate that combination therapy produces profound ultrastructural changes leading to increased permeability and cell membrane damage.

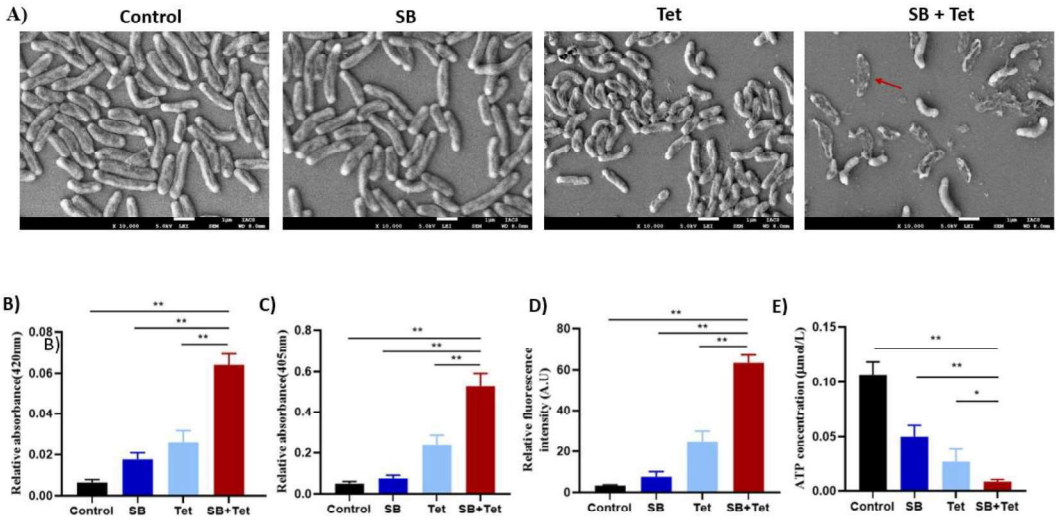

Fig.6.5. Combination of SB and Tet damages the bacterial cell envelope and enhances the membrane permeability. A) SEM analysis representing morphological changes of tetracycline-resistant strain *V. cholerae* strain IDH1986 after treatment with [SB (2.2mg/ml), Tet (4 µg/ml), combination of SB and Tet (2.2 mg/ml+4µg/ml)]. The red arrow indicates the cell damage; **B)** Integrity of the membrane determined by β-galactosidase [SB(2.2mg/ml), Tet(4µg/ml), combination of SB and Tet (2.2 mg/ml+4µg/ml)]; **C)**Integrity of the membrane determined by alkaline phosphatase [SB (2.2mg/ml), Tet (4µg/ml), combination of SB and Tet (2.2 mg/ml+4µg/ml)] **D)** Integrity of the membrane determined by propidium iodide [SB (2.2mg/ml), Tet (4µg/ml), combination of SB and Tet (2.2 mg/ml+4µg/ml)] and, **E)** Integrity of the membrane determined by ATP production [SB (2.2mg/ml), Tet (4µg/ml), combination of SB and Tet (2.2 mg/ml+4µg/ml)]. All data are presented as mean ± SD, and the significances were determined by nonparametric one-way ANOVA (*p<0.05, **p<0.01).

6.5. SB-Tet combination disrupts bacterial membrane potential.

Proton motive force (PMF; ΔP) is an electrochemical gradient of protons generated by the electron transport chain in bacteria, which acts by extruding protons out of the cells. PMF, which is necessary for ATP synthesis and transport of various solutes, is the sum of two parameters: the electric or membrane potential (Δψ) and the transmembrane proton gradient (ΔpH). To further investigate the nature of damage inflicted by SB and Tet combination on bacterial cell membrane, the membrane potential of *V. cholerae* IDH1986 was determined using green fluorescent dye $DiBAC_4$. This label can enter depolarized cells where it binds to intracellular proteins or membranes and exhibits enhanced fluorescence. As evidenced in **Fig.6.6**, no change in membrane potential was observed when the cells were treated only with Tet; while SB-treated cells exhibited a slight change in membrane potential (Fig.7.6). Remarkably, the

combination of SB and Tet led to a significant decrease in membrane potential as evidenced by increase in fluorescence intensity *(Fig.6.6)*.

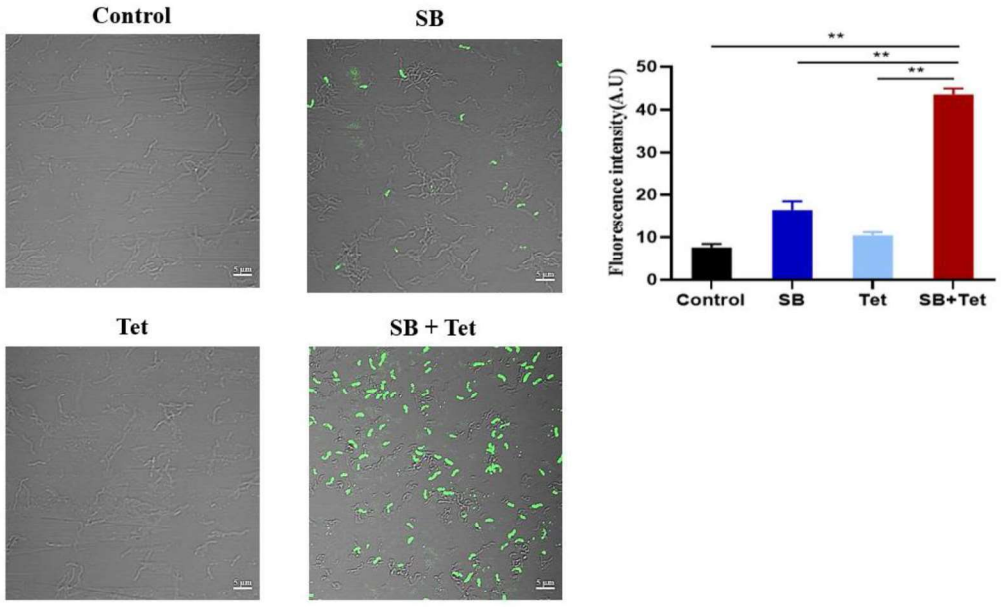

Fig.6.6.SB-Tet combination dissipates bacterial membrane potential. Bacterial membrane potential of tetracycline-resistant *V. cholerae* IDH1986 in the presence of SB (2.2mg/ml), Tet (4 µg/ml), combination of SB and Tet (2.2mg/ml+4µg/ml) was determined by using $DiBAC_4$ and the fluorescence intensity of $DiBAC_4$ is represented graphically. All data are presented as mean ± SD, and the significances were determined by nonparametric one-way ANOVA (**p<0.01).

6.6. SB-Tet combination suppresses efflux activity and promotes intracellular accumulation of tetracycline.

Since PMF is required for driving efflux activities, the effect of the combination of SB and Tet on the efflux activities was determined using the EtBr efflux assay. EtBr is a substrate for many efflux pumps and is widely used to monitor the inhibition of drug efflux in bacteria. The fluorescence signal of EtBr is higher after its intercalation into bacterial DNA; thus, an increase in the fluorescence signal indicates its intracellular accumulation, reflecting impaired efflux activity. The accumulation of EtBr in bacterial cells increased in a dose-dependent manner after adding SB, with values comparable to those of the positive control, CCCP, which is an established PMF modulator *(Fig.6.7)*. The fluorescence intensity of cells treated with SB increased significantly, indicating the accumulation of EtBr in the cells due to the inhibition of efflux pumps. Markedly, the combination of SB and Tet inhibited the efflux pumps' activity more

significantly than the positive control CCCP *(Fig.6.7)*, confirming that SB and Tet act synergistically in inhibiting EtBr efflux.

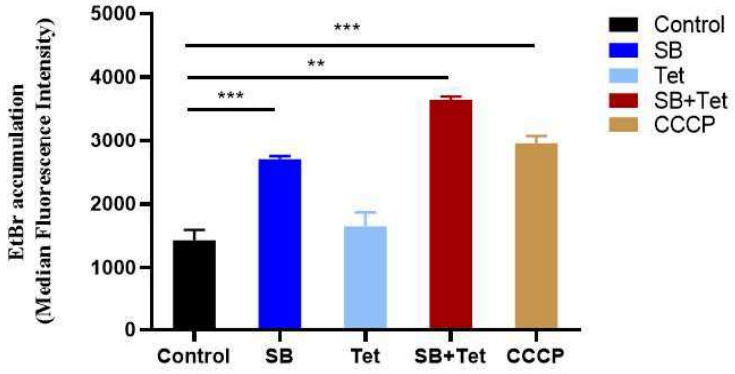

Fig.6.7. Combination of SB and Tet inhibits efflux pumps activity. Accumulation of ethidium bromide (EtBr) was used to assess the activity of efflux pumps induced by SB (2.2mg/ml), Tet (4 µg/ml), combination of SB and Tet (2.2mg/ml + 4µg/ml). All data are presented as mean ± SD, and the significances were determined by nonparametric one-way ANOVA (**p<0.01, ***p<0.001)

The ability of tetracyclines to inhibit bacterial protein synthesis is essential for their antibacterial activity; therefore, it is important to ensure sufficient drug accumulation within bacterial cells. The high susceptibility of *V. cholerae* IDH1986 to tetracycline in the presence of SB may be due to its increased intracellular concentration. To verify this possibility, the level of tetracycline in the cells of IDH1986 was determined using the tetracycline accumulation assays. As shown in **Fig.6.8**, the presence of SB led to an increase in intracellular tetracycline levels in *V. cholerae* IDH1986 in a concentration-dependent manner.

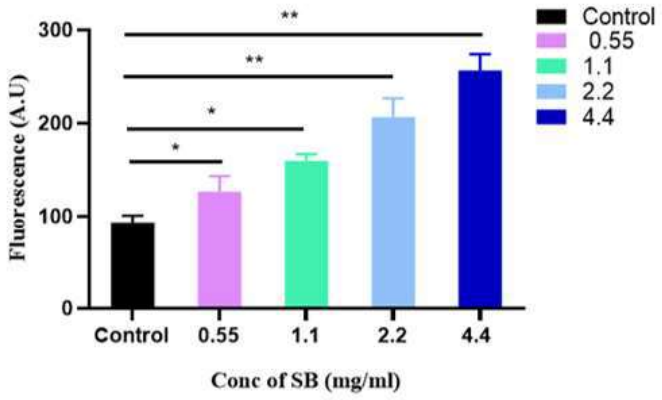

Fig.6.8. Combination of SB and Tet increases the intracellular accumulation of Tetracycline. Increased intracellular accumulation of tetracycline in *V. cholerae* strain IDH1986 caused by SB in a dose-dependent manner. All data are presented as mean ± SD, and the significances were determined by nonparametric one-way ANOVA (*p<0.05, **p<0.01).

6.7. Combination of SB and Tet showed potent anti-virulence activity.

The secretory diarrhoea caused by *V. cholerae* is attributed to two major virulence factors, Cholera enterotoxin (CT) and adhesion factor (TcpA), which facilitate infection in the host. Since our previous study has already shown that SB possesses strong anti-CT and anti-TcpA activity, we aimed to test the anti-virulence activity of SB against *V. cholerae* strain IDH1986 and whether combining SB with Tet enhances its anti-virulence effect. Firstly, we explored the classical GM1-CT ELISA for detecting the secreted CT level in the supernatant of bacterial cultures grown in the presence of SB (0.55 mg/ml), Tet (0.125 µg/ml) or a combination of SB (0.55 mg/ml) and Tet (0.125 µg/ml). As shown in **Fig.6.9A**, no change in CT production was observed in cells treated with 0.125 µg/ml of Tet; treatment with 0.55 mg/ml of SB resulted in 2-fold reduction in CT production compared to untreated control; while combining SB (0.55 mg/ml) with Tet (0.125 µg/ml) resulted in ≥ 5-fold reduction in CT production compared to the untreated control or single treatment. Next, we determined whether the combination of SB and Tet can affect the adhering ability of *V. cholerae* IDH1986 to HT-29 cell line. In the presence of 0.125 µg/ml of Tet there was no significant change in the adhesion of *V. cholerae* to HT-29; in the presence of 2.2 mg/ml of SB the adhering ability was reduced by 2-fold; while combining SB (2.2 mg/ml) with Tet (0.125 µg/ml) resulted in ≥ 4-fold reduction in adhering ability of *V. cholerae* to HT-29 compared to the untreated control or single treatment ***(Fig.6.9B)***. The adhering ability of *V. cholerae* to HT-29 cells under different treatment conditions was also confirmed by using GFP-labelled *V. cholerae*. The fluorescent microscopic images of GFP-labelled *V. cholerae* bound to HT-29 cells also revealed a similar pattern of change where the combination of SB and Tet affected the adhering ability of *V. cholerae* to HT-29 to a greater extent than untreated control or single treatment ***(Fig.6.9C)***. Since the adhesion of *V. cholerae* to HT-29 cells is highly dependent on TcpA, IDH1986 cultures grown under different treatment conditions were also analyzed for TcpA expression by immunoblot. As shown in **Fig.6.9D**, it is evident that the expression levels of TcpA in cells treated with 0.125 µg/ml of Tet was almost similar to untreated control; in the presence of 2.2 mg/ml of SB the TcpA levels was decreased by 2-fold; while combining SB (2.2 mg/ml) with Tet (0.125 µg/ml) resulted in ≥4-fold decrease in TcpA levels compared to untreated control or single treatment.

To understand the underlying mechanism behind the reduced production of CT and TcpA, qRT-PCR was used to measure the expression levels of cholera toxin-encoding *ctxAB* and pilus-encoding *tcpA* genes in *V. cholerae* IDH1986. The expression of *ctxAB* and *tcpA* in cells treated with 0.125 µg/ml of Tet was similar to untreated control; in the presence of 2.2 mg/ml of SB the expression of *ctxAB* and *tcpA* was downregulated by 2.5-fold; while in cells treated with both SB (2.2 mg/ml) and Tet (0.125 µg/ml), the expression of *ctxAB* and *tcpA* was significantly downregulated by ≥5-fold compared to the untreated control or single treatment ***(Fig.6.9E)***.

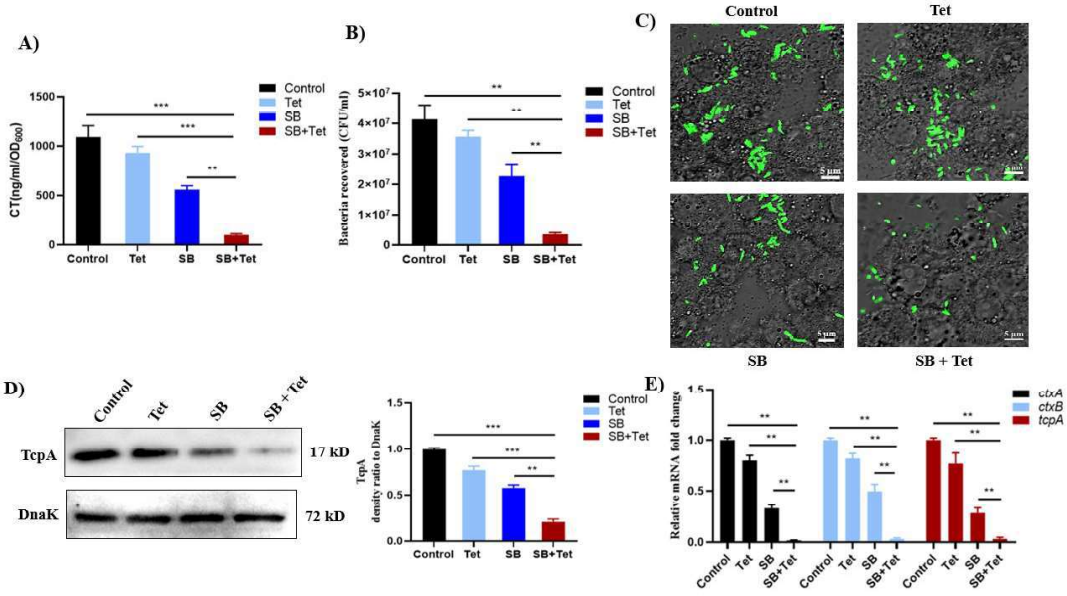

Fig.6.9. Inhibitory effects of SB-Tet combination on the virulence attributes of *V. cholerae* IDH1986. A) ELISA measured CT expression levels in *V. cholerae* IDH1986 from the samples grown in AKI media with SB (0.55mg/ml), Tet (0.125µg/ml), or combination of SB and Tet (0.55mg/ml+0.125µg/ml). One-way ANOVA was performed. **B)** *V. cholerae* IDH1986 was grown to mid-log phase, and optical density was adjusted to 1. HT-29 cells were grown in 12-well cell-culture plate to 70% confluency. The cells were then infected at 100 MOI. After incubation at humidified 37 °C incubator for 1h, the cell-culture plate was washed with PBS to remove unbound bacteria, and bound bacteria were collected and enumerated by plating on streptomycin-supplemented LA plates. Graphical representation of *V. cholerae* IDH1986 bound to HT-29 cells in the presence of SB (2.2mg/ml), Tet (0.125µg/ml) or combination of SB and Tet (2.2mg/ml and 0.125µg/ml) **C)** Fluorescent microscopy images of bound bacteria with HT-29 cells. **D)** Expression of major adhesion protein TcpA of *V. cholerae* IDH1986 measured by western blot of cells grown in the presence of SB (2.2 mg/ml), Tet (0.125µg/ml) or combination of SB and Tet (2.2 mg/ml+0.125µg/ml). DnaK was used as a loading control. Densitometric analyses are graphically represented. Student's *t-test* was performed. All data are expressed as mean ± S.D from three biological replicates. Significance levels were denoted as ∗for $P < 0.05$, ∗∗∗ for $P < 0.001$, ∗∗∗∗for $P < 0.0001$. **E)** Relative expression of major virulence genes *ctxA, ctxB* and *tcpA* was analyzed by real-time PCR. Significance was calculated by one-way ANOVA. Significance levels were denoted as ∗∗$p<0.01$, ∗∗∗$p<0.001$

6.8. SB-Tet combination synergistically reduces virulence in animal models of cholera

Given that the combination of SB and Tet displayed excellent synergistic bactericidal and anti-virulence activity against *V. cholerae in vitro*, we reasoned that SB would be effective in reducing tetracycline resistance *in vivo* and thereby restore its clinical efficacy. Firstly, we determined the combinatorial effect of SB and Tet on intestinal colonization of *V. cholerae* IDH1986 in suckling mouse model. In suckling mice colonization experiment in which mice were infected with 1×10^5 CFU of tetracycline resistant IDH1986, treatment with 8 µg/ml of Tet showed no change on the intestinal colonization of *V. cholerae*; intestinal colonization in SB-treated mice (4.4 mg/ml) was reduced by two orders of magnitude; whereas in mice treated with both SB and Tet (4.4mg/ml and 8µg/ml) the intestinal colonization was reduced by four orders of magnitude compared to the untreated mice ***(Fig.6.10A)***. Next, we checked if the combination of SB and Tet could protect suckling mice infected with IDH1986 strain. For this purpose, the mice were challenged with 5×10^7 CFU of the tetracycline-resistant IDH1986 and oral administration of the drugs. Mortality monitored for 48 hours showed that 90% of mice infected with IDH1986 strain succumbed within 22 h postinfection ***(Fig.6.10B)***. Treatment with 4.4 mg/ml of SB could effectively protect 40% of infected mice, while treatment with 8µg/ml of Tet could protect 15% of infected mice ***(Fig6.10B)***. However, the combination of 4.4 mg/ml SB and 8µg/ml Tet could effectively rescue 50% of infected mice within 48 h postinfection ***(Fig.6.10B)***.

The effects of SB-Tet combination on fluid accumulation (FA) and CT production by *V. cholerae* IDH1986 were also assessed in the rabbit ileal loop model ***(Fig.6.10C-E)***. FA (fluid accumulation) ratio of Tet treatment loop (8µg/ml) is almost similar to untreated loop; FA (fluid accumulation) ratio of SB treatment showed 7-fold reduction in fluid accumulation compared to the untreated loop; while combination of SB (4.4 mg/ml) and Tet (8µg/ml) showed 15-fold reduction in fluid accumulation compared to the untreated loop ***(Fig.6.10D)***. Similarly, the CT level was reduced by 4-fold in SB treated loop (4.4 mg/ml) compared to the untreated loop, while the CT level was markedly reduced by 12-fold in the loop that received combination of SB (4.4 mg/ml) and Tet (8µg/ml) compared to the untreated loop ***(Fig.6.10E).***

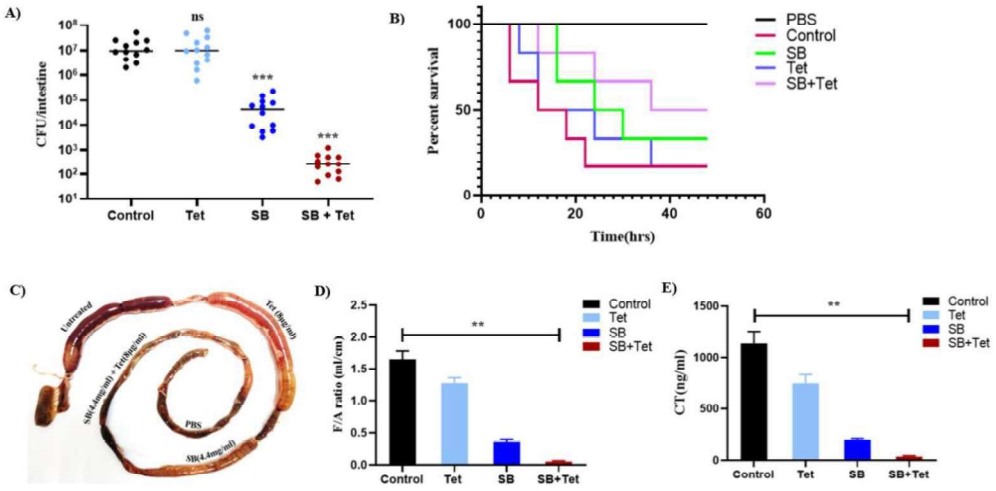

Fig.6.10. The efficacy of SB-Tet in animal models of cholera. A) Effect of drugs on bacterial colonization in 4 to 5-day-old suckling BALB/c mice (*n=12* per group). The mice were orogastrically challenged with 1×10^5 CFU of *V. cholerae* strain IDH1986 with or without drugs [SB (4.4mg/ml), Tet (8µg/ml), and combination of SB and Tet (4.4mg/ml+8µg/ml)] and kept at 30 ºC for 18 h. Bacterial colonization was estimated as CFU/intestine and graphically represented. Each circle represents an individual mouse. Horizontal lines are medians. Significance was determined by *Mann–Whitney U test* (*n=12* per group). Significance levels (compared to controls challenged without any drug) were denoted as ns=nonsignificant, *** for $P < 0.001$. **B)** The mice were orogastrically challenged with 5×10^7 CFU of *V. cholerae* strain IDH1986 with or without drugs [SB (4.4mg/ml), Tet (8µg/ml), and combination of SB and Tet (4.4mg/ml+8µg/ml)] and the survival rate was measured after 48 h. **C)** Each loop was injected with 1×10^9 CFU per ml *V. cholerae* IDH1986 with or without drug [SB (4.4mg/ml), Tet (8µg/ml), and combination of SB and Tet (4.4mg/ml+8µg/ml)] and loop injected only with PBS served as negative control loop. After 18 h, the animals were euthanized, and the loops were removed. Representative image of recovered rabbit intestine segment with infected loop at 18 h after infection. **D)** Fluid accumulation per unit area (F/A) ratio of each loop was evaluated and graphically represented as mean ± S.D. (*n = 3*). **C)** The accumulated fluid samples from the ileal loops were used to measure the CT production by ELISA.

Chapter 7

Discussion

Discussion

Cholera has long been one of the harmful diseases, with outbreaks documented since 1817 (Pollitzer et al., 1954). In 1849, Sir John Snow linked cholera to contaminated water, shaping our understanding of its transmission. The disease persists in environmental sources between outbreaks but has declined globally due to increased awareness, hygiene, and access to safe water. According to WHO, cholera affects 1 to 4 million people annually, causing 21,000 to 143,000 deaths(Ganesan et al., 2019), though cases dropped by 60% in 2018 (WHO, 2019). Treatment primarily involves electrolyte replacement, and antibiotics are used in some cases.

The inappropriate and excessive use of antibiotics led to the emergence of multidrug-resistant (MDR) epidemic bacterial strains. Antibiotic-resistant *V. cholerae* is increasingly prevalent worldwide (Verma et al., 2019) An extensive review by Kitaoka et al. (2011) highlighted major drug-resistant *V. cholerae* strains reported in various countries. This resistance primarily arises from the frequent acquisition of extrachromosomal mobile genetic elements through horizontal gene transfer from other bacterial species (Das et al., 2020; Narendrakumar et al., 2019; Verma et al., 2019).

Traditional antimicrobials, which are often bacteriostatic or bactericidal, can further induce the development of MDR strains. Increasing antibiotic resistance poses a significant global public health challenge, contributing to rising healthcare costs. Therefore, there is an urgent need for novel treatment strategies that effectively target pathogenic bacteria without disrupting the normal gut microbiota. There are also vaccines against *V. cholerae* but efficacy of vaccines is not 100% (Sen Gupta et al., 2016). Promising alternative approaches include bioactive compounds, small molecules, and plant or herbal extracts, specifically targeting bacterial virulence factors, offering a potential solution to combat antibiotic resistance.

Anti-virulence drugs are gaining recognition as an innovative approach in combating infectious diseases by employing strategies distinct from traditional antibiotics. Instead of directly killing pathogens, these drugs neutralize them by targeting their virulence factors, allowing the immune system to effectively eliminate infection (Roca et al., 2015). This approach mitigates several drawbacks of antibiotics, as it reduces

selective pressure for resistance and minimizes the elimination of beneficial gut microbiota. Previous studies have identified various small molecules, such as toxtazin B, unsaturated fatty acids, and ribavirin that inhibit virulence gene regulatory cascades (Anthouard et al., 2013; Mandal et al., 2016; Withey et al., 2015). Additionally, several herbal products and bioactive compounds have demonstrated potent anti-virulence activity. For example, 6-gingerol prevents cholera toxin (CT) from binding to GM1 receptors (Saha et al., 2013), while zinc oxide nanoparticles disrupt the toxin's secondary structure (Sarwar et al., 2017). Other inhibitors, including carbohydrate-based compounds (Kumar et al., 2018) and fucosylated molecules (Wands et al., 2018), interfere with cholera toxin activity. Furthermore, probiotic treatments using *Bdellovibrio bacteriovorus* and *Micavibrio aeruginosavorus* have shown promise in reducing the spread of antibiotic resistance in *V. cholerae*, offering a novel and sustainable therapeutic strategy against bacterial infections (Dashiff et al., 2011).

In this study, we screened various compounds, including sugar molecules, phytochemicals, and small molecules (S. Wang et al., 2015), for their effects on the growth, motility, adhesion, and cholera toxin (CT) production of *V. cholerae*. These molecules were selected based on a comprehensive literature review. Among them, the short-chain fatty acid sodium butyrate, a microbial metabolite produced through the fermentation of dietary fibers in the colonic lumen, demonstrated significant inhibition of *V. cholerae* virulence both *in vitro* and *in vivo*. We conducted a detailed investigation for sodium butyrate's effect on various virulence factors involved in *V. cholerae* pathogenesis. Other inhibitory compounds such as ribose, arabinose, eugenol, totarol, quercetin, basil oil decreased the mucin penetrating ability of *V. cholerae*. Ursolic acid and betulinic acid reduced adhesion efficiency, while totarol, geraniol, and eugenol notably suppressed cholera toxin (CT) production. Additionally, melibiose, arabinose, and ursolic acid effectively inhibited biofilm formation. These findings suggest that these inhibitory molecules may interfere with *V. cholerae* adhesion, motility, and toxin production, thereby reducing its overall pathogenicity. Based on their therapeutic potential, these compounds could serve as dietary additives to mitigate the risk of *V. cholerae* infection. Further studies are needed to optimize their use, either individually or in combination, at minimal effective doses to combat *V. cholerae* pathogenesis.

Sodium butyrate is a short-chain fatty acid produced through the fermentation of dietary fibers in the colonic lumen. It exhibits potent anti-microbial and anti-virulence activity against a range of pathogenic bacteria, including *Salmonella typhimurium, Clostridium perfringens, Escherichia coli, Staphylococcus pseudointermedius, Acinetobacter baumannii, Vibrio campbellii,* and *Vibrio parahaemolyticus* (Defoirdt et al., 2018; Kennedy et al., 2019; Namkung et al., 2011; W. Zhu et al., 2022). Studies have demonstrated that sodium butyrate possesses antibacterial, anti-inflammatory, and antioxidant properties (Zhang et al., 2021). Additionally, it plays important role in modulating host immunity and impairs the colonization ability of various enteric pathogens in intestinal epithelial cells (Zhang et al., 2021) ***(Fig.7.1).*** Notably, in colorectal cells, butyrate treatment has been shown to induce the production of antimicrobial peptide cathelicidin (Du et al., 2021), further contributing to its protective effects.

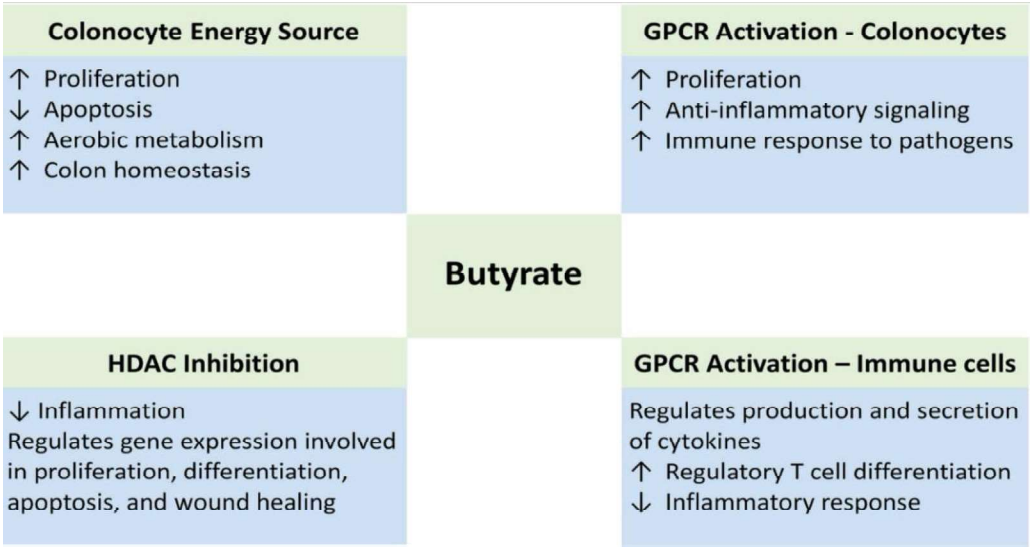

Fig.7.1. Summary of butyrate mechanisms of action. Butyrate plays an important role in maintaining intestinal homeostasis through different mechanisms: as an energy source for colonocytes, via HDAC inhibition, and GPR activation in colonocytes and immune cells [Source: (Hodgkinson et al., 2023)].

Despite extensive research on sodium butyrate in recent years, its anti-virulence effects against *V. cholerae* have not yet been reported. In this study, we investigated the effect of sodium butyrate on the virulence factors of *V. cholerae*, with a particular focus on cholera toxin (CT) and the adhesion factor TcpA. We assessed its anti-virulence activity both *in vitro* and *in vivo* using suckling mice and rabbit ileal loop models.

Our findings demonstrate that sodium butyrate significantly reduced the expression of CT and TcpA under both conditions. Furthermore, we explored the potential molecular mechanisms underlying sodium butyrate-mediated inhibition of virulence gene expression in *V. cholerae*.

In this present study, we examined the sub-inhibitory concentrations of SB on *V. cholerae* to access its wide range of biological functions under pathogenic conditions. According to our experimental findings, SB at sub-MICs strongly suppressed the virulence attributes without significantly attenuating the growth of *V. cholerae*. So, we performed all the experiments at sub-MICs (1/2 MIC and lower) to study the inhibitory role of SB against *V. cholerae*. Additionally, it was also ensured that at a specific optical density (O.D) both SB-treated and SB-untreated *V. cholerae* cultures possess equal number of viable bacteria thereby ruling out the possibility of growth-reducing effects of SB on bacteria. *V. cholerae* is transmitted to humans through the ingestion of contaminated food and water. Upon entering the host, it survives the acidic environment of the stomach and colonizes the small intestine, where it penetrates the mucous barrier and adheres to the microvilli of epithelial cells. Following adhesion, the bacteria release cholera toxin (CT), the primary factor responsible for clinical manifestations of cholera. Based on this pathogenic mechanism, our study focused on investigating the anti-CT and anti-TcpA effects of sodium butyrate.

This study demonstrated that sodium butyrate impaired the adherence of *V. cholerae* to epithelial cells and inhibited the expression of cholera toxin (CT). We also evaluated the effect of SB on two multidrug-resistant clinical isolates of *V. cholerae*. Notably, SB effectively suppressed CT production in both isolates. Our findings are in accordance with previous studies showing that various bioactive phytochemicals, such as capsaicin and anethole (Erfanimanesh et al., 2018; Zahid et al., 2015) exert anti-virulence effects against *V. cholerae* by inhibiting cholera toxin production. Additionally, unsaturated fatty acids (UFAs) present in bile and several conjugated UFA derivatives have been identified as potent repressors of CT expression in *V. cholerae* (Plecha & Withey, 2015; Withey et al., 2015)

Based on our initial findings on CT production and adhesion, we further focussed the effect of SB at the gene level and extended our study to uncover its precise mechanism of action. In the canonical *V. cholerae* virulence regulation model, gene

expression follows a three-tiered cascade. First, AphA and AphB activate TcpPH, which, in synergy with ToxRS, induces the transcription of the master regulator *toxT*. ToxT then activates the expression of key virulence factors: *tcp* (toxin co-regulated pilus, responsible for adhesion) and *ctx* (cholera toxin gene, encoding major toxin proteins like CtxA/B (Matson et al., 2007) ***(Fig.7.2).*** These genes serve as prime targets for novel inhibitors because they play critical role in bacterial virulence.

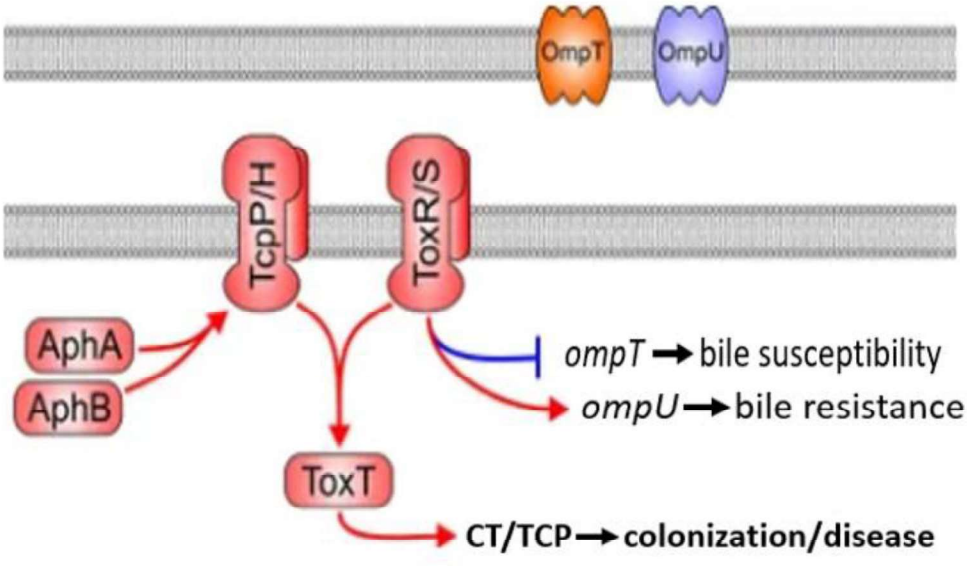

Fig.7.2. The *Vibrio cholerae* ToxR virulence regulon. In response to low cell density and low oxygen tension, the AphA and AphB transcription factors bind to the promoter and activate transcription of the tcpPH operon. TcpP/H and ToxR/S then bind to the toxT promoter to induce its transcription. ToxT then activates the transcription of multiple virulence genes including the genes encoding for production of cholera toxin (CT) and the toxin co-regulated pilus (TCP). ToxR/S, independently of TcpP/H, also modulates transcription of outer membrane porins OmpU and OmpT [Source: (Bina et al., 2023)].

Quantitative RT-PCR analysis revealed significant downregulation of *ctxAB* and *tcpA* transcripts in the presence of SB, while the transcript levels of *toxRS, tcpPH*, and the master regulator *toxT* remain unaffected. To validate these findings, we further examined ToxT and TcpA protein expression levels. The unchanged ToxT levels at both RNA and protein levels suggest that SB-mediated inhibition occurs either post-translationally or during promoter binding. Notably, previous studies on small molecules such as virstatin and bile salts against *V. cholerae* have reported similar effects

(Hung et al., 2005; Plecha & Withey, 2015). These findings indicate that the reduction in CT and TcpA production may result from SB-induced dysregulation of ToxT binding to its target promoters. This hypothesis was strongly supported by two key protein-DNA interaction assays, ChIP and EMSA, which demonstrated that SB binds to ToxT and restricts its interaction with the *tcpA* promoter. To assess the specificity of SB, we tested another butyrate derivative, tributyrate (TB), but observed no interaction between TB and ToxT, reinforcing the unique specificity of SB. To further elucidate the molecular mechanism, we performed docking analysis to investigate the interaction between ToxT (target) and SB (ligand). Our results identified two critical residues, Lys31 and Lys230, forming conventional hydrogen bonds with the carboxyl group of SB. Previous studies on the crystal structure of ToxT co-purified with UFA (cis-palmitoleate) have shown that lysine-carboxylate interactions play a crucial role in stabilizing the bound conformation of ToxT (Lowden et al., 2010). Consistently, our docking analysis revealed a low binding energy (-7.68 kcal/mol), indicating a highly favourable ligand-target interaction. Altogether, these data suggest that SB interacts with ToxT in a way that locks it into a "closed" conformation, thereby preventing DNA binding. These findings align with previous reports showing that unsaturated fatty acids inhibit ToxT binding to promoter elements (Cruite et al., 2019; Woodbrey et al., 2017).

Our RNA-seq data further supports the observations that SB attenuates *ctx* and *tcp* gene expression in a ToxT-dependent manner. Interestingly, we also observed an increase in the expression of biofilm-related genes. While this may seem contradictory, similar patterns have been reported in previous studies, where anti-virulence agents downregulate *tcp* and *ctx* expression while simultaneously upregulating biofilm-associated genes (Perez-Soto et al., 2017; B. X. Wang et al., 2023). Additionally, SB significantly reduced the expression of accessory virulence genes critical for *V. cholerae* pathogenesis, including *hlyA* (hemolysin), *acfA* (accessory colonization factor), and *zot* (zonula occludens toxin). This broad dysregulation of virulence factors, particularly *ctx* and *tcp*, suggests a potential reduction in *V. cholerae* pathogenicity. These findings suggest that targeting ToxT emerges as a highly promising strategy for anti-virulence dependent intervention.

The demand for alternative therapeutics with minimal side effects for treating *V. cholerae* infections remains high. A group of researchers identified sulfonamides, a

widely used class of bacteriostatic agents, that inhibit cell growth by interfering with folic acid biosynthesis (Ovung et al., 2021). These compounds exhibit broad-spectrum activity against both Gram-negative and Gram-positive bacteria, as well as certain protozoa (Ovung et al., 2021). In *V. cholerae*, sulfonamides demonstrate both antibacterial and anti-virulence properties by inhibiting the metalloenzyme carbonic anhydrase. This inhibition reduces bicarbonate production, which in turn affects ToxT activity, the master regulator of virulence factors (Gheibzadeh et al., 2024; Nocentini et al., 2023; Supuran, 2011).

However, a major limitation of sulfonamides is their non-selective inhibition of human carbonic anhydrase isoforms, which can lead to serious side effects. These include metabolic acidosis, kidney stones, and in rare cases, severe conditions such as Stevens-Johnson syndrome (SJS) and toxic epidermal necrolysis (Ferraroni et al., 2017).

In contrast, sodium butyrate has been extensively reported to exert beneficial effects on the host by maintaining intestinal homeostasis through the modulation of gene expression and signaling pathways (Hodgkinson et al., 2023; Recharla et al., 2023). It supports normal intestinal function by serving as an energy source for colonocytes, promoting their proliferation, and enhancing gut motility and blood flow, all of which are essential for digestion (Hodgkinson et al., 2023). Additionally, butyrate has been shown to alleviate obesity-related complications by strengthening the intestinal barrier through tight junction regulation, thereby reducing inflammation and improving metabolic health (Fang et al., 2019; Zhou et al., 2017).

Beyond its role in gut health, butyrate also exhibits antibacterial activity against various Gram-positive and Gram-negative bacteria, including *Acinetobacter baumannii*, *Bacillus anthracis, Bacillus subtilis, and Staphylococcus epidermidis* (Du et al., 2021). Our study demonstrated that SB exerts anti-virulence activity against *V. cholerae* by directly binding to ToxT and inhibiting its function, leading to the downregulation of genes in the *tcp* and *ctxAB* operons.

Despite its numerous benefits, SB is not without potential drawbacks. Some studies have reported a paradoxical effect of butyrate on glucose and lipid metabolism. While butyrate has been shown to alleviate diet-induced obesity in mice (Hong et al., 2016), other reports suggest that short-chain fatty acids (SCFAs), including butyrate,

may contribute to obesity in humans by promoting lipid biosynthesis from acetyl-CoA, fatty acids, and ketone bodies (Birt et al., 2013; H. Liu et al., 2018). Additionally, butyrate can influence appetite and eating behaviour by stimulating the vagus nerve and the hypothalamus, as it can cross the blood-brain barrier (Gagliano et al., 2014; van de Wouw et al., 2017).

Overall, these findings highlight the therapeutic potential of SB in treating *V. cholerae* infections due to its antibacterial and anti-virulence properties. However, it's possible metabolic effects require further investigation to optimize its application in targeted therapeutics.

The rationale for using sodium butyrate as a therapeutic arises from its endogenous production through fermentation, where it plays a crucial role in modulating the gut microbiota by supplying energy to intestinal cells, inhibiting harmful bacteria, and regulating immune-related genes. As a U.S. Food and Drug Administration-approved compound (Butyric acid – 21CFR182.60), butyrate has been used to treat autoimmune disorders, cancer, and neurological diseases (X. Chen et al., 2017; Kim et al., 2020; F. Wang et al., 2020).

Butyrate is well-documented to promote intestinal epithelial barrier function and modulate the host mucosal immune system (Jiminez et al., 2017). Notably, butyrate enhances mucosal barrier integrity and stimulates the secretion of antimicrobial peptides (AMPs), thereby limiting pathogen proliferation (Chen et al., 2020).

In our study, sodium butyrate treatment significantly reduced *V. cholerae* colonization in suckling mice. Since colonization in mammalian hosts relies heavily on TCP expression, specifically its major subunit, TcpA, mutants lacking *tcpA* are significantly less competitive than wild-type strains (Chiang et al., 1998; Merrell et al., 2002). Our findings revealed a substantial reduction in *tcpA* levels in the presence of sodium butyrate, which likely accounts for the observed decrease in *V. cholerae* colonization. This result corroborates with a previous report where butyrate administration affected the colonizing ability of *Salmonella* (Chu et al., 2020; Onrust et al., 2020).

Moreover, SB also suppressed cholera toxin (CT) production and prevented fluid accumulation in the rabbit ileal loop. In contrast, another butyrate derivative, tributyrate (TB), was ineffective in reducing *V. cholerae* virulence in animal models. In

accordance, our *in vitro* studies demonstrated SB-mediated inhibition of ToxT activity, while TB showed no such effect. Therefore, we hypothesize that SB attenuates *V. cholerae* virulence *in vivo* by specifically targeting ToxT.

These findings strongly suggest that SB effectively reduces *V. cholerae* virulence, potentially mitigating disease severity and duration. Altogether, these suggest that sodium butyrate is able to abrogate *V. cholerae* colonization in the small intestinal mucosa. Therefore, dietary supplementation of SB during *V. cholerae* infection, particularly in nutritionally deprived environments, could help reduce bacterial colonization and toxin production without causing adverse effects on the host. There are several reports regarding *in vitro* inhibition of ToxT activity by unsaturated fatty acids and bile, but there is still a scarcity of validation *in vivo* models.

While our study demonstrates the protective effects of sodium butyrate against *V. cholerae*, it is important to acknowledge certain limitations that needs further investigation. Firstly, our molecular docking analysis predicted the binding site of SB on ToxT. However, a more detailed structural analysis is necessary to precisely determine the binding position and its impact on DNA-binding ability of ToxT. Secondly, although our results indicate a downregulation of virulence genes, they do not fully explain the observed increase in biofilm-associated genes. Further research is needed to elucidate the molecular pathways linking these differential gene expression patterns. Thirdly, while our *in vivo* studies in suckling mice and rabbit ileal loop models provided valuable insights, these models have inherent limitations. Suckling mice lack a fully developed immune system and do not exhibit severe diarrhea, making it difficult to assess host factors involved in the secretory response. On the other hand, the rabbit ileal loop model involves a closed intestinal loop, which bypasses the natural infection route and key physiological processes such as peristalsis. To confirm our findings, future research should employ improved mammalian models that better mimic human *V. cholerae* infections.

In conclusion, this study reports that SB inhibits ToxT activity, in *V. cholerae*. This is the first report of direct binding of SCFA, butyrate, to a virulence regulator in *V. cholerae*. Mitigation of *V. cholerae* virulence without reducing bacterial burden may also reduce the development of antibiotic resistance. Furthermore, the homology of ToxT with other virulence regulators in different pathogenic bacteria could facilitate

the development of broad-spectrum anti-virulent agents (Midgett et al., 2021; Trirocco et al., 2023). Such therapeutics would offer a new option to treat MDR bacterial infections *(Fig.7.3)*.

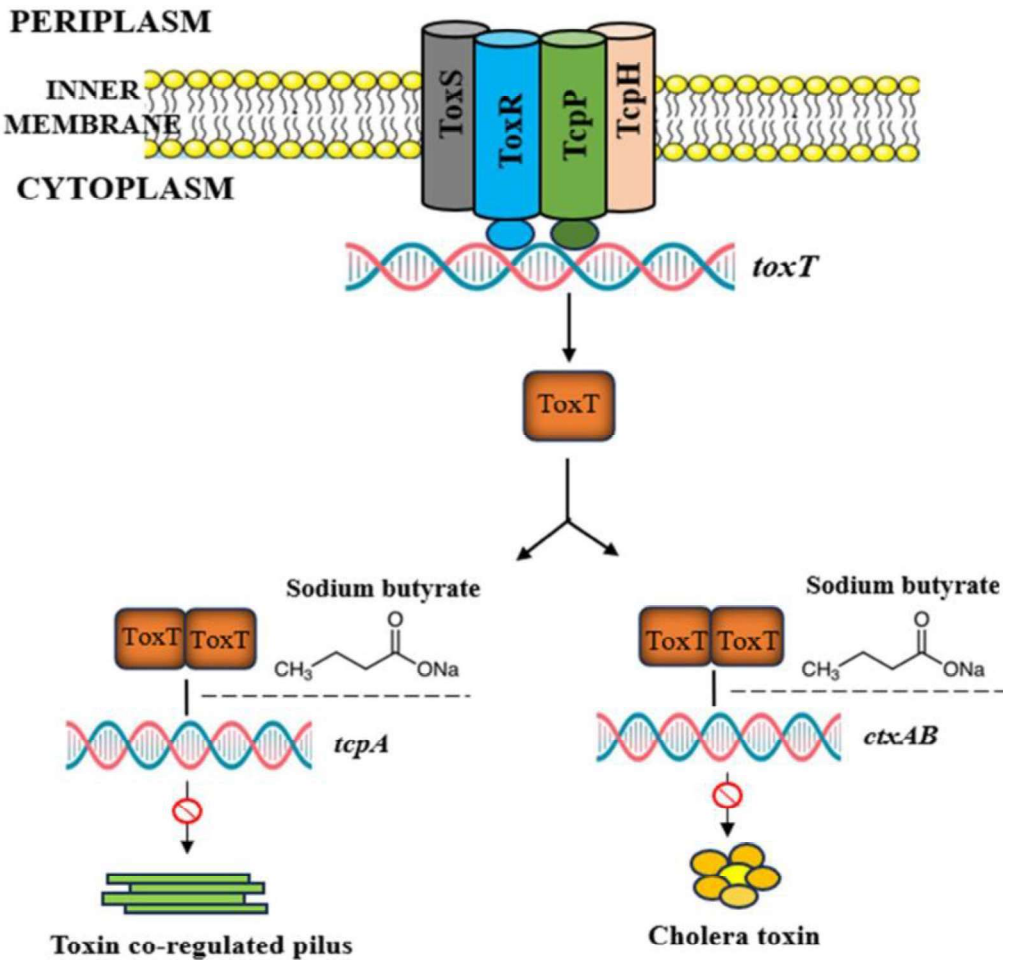

Fig.7.3. Model showing the inhibition of virulence cascade in *V. cholerae* by SB. The virulence cascade in *V. cholerae* is tightly regulated. TcpPH forms an inner membrane complex with ToxR and ToxS to activate the transcription of *toxT*. ToxT activates the transcription of *tcpA-F*, which encodes the toxin coregulated pilus, and *ctxAB*, which encodes the cholera toxin subunits. Based on our experiments, we propose that SB inhibits the binding of ToxT protein to the promoter region of *tcpA /ctxAB* and eventually inhibits cholera toxin and *tcpA* production.

As antibiotic resistance continues to rise, combating this problem demands both the development of new antimicrobial agents and preserving the efficacy of existing antibiotics (Melander et al., 2017) ***(Fig.7.4).*** One promising and increasingly recognized strategy involves the identification of novel adjuvants that can restore antibiotic activity and improve clinical outcomes for patients with infectious diseases. Moreover, repurposing non-antibiotic drugs as adjuvants offers time and cost-effectiveness compared to *de novo* development (Melander et al., 2017).

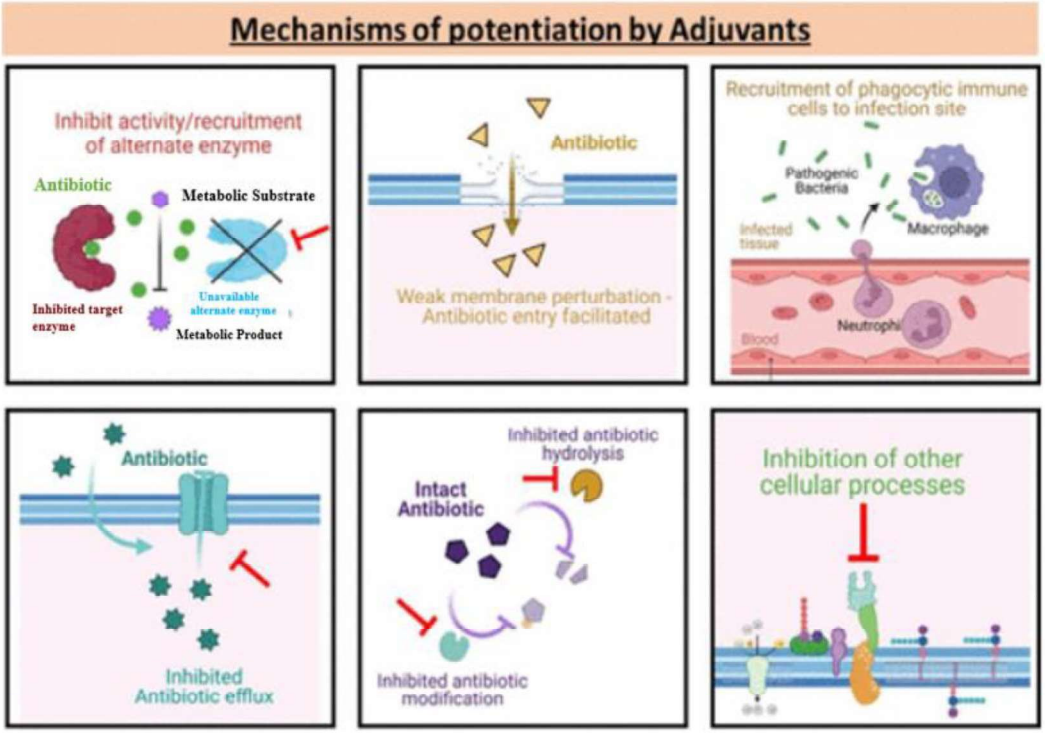

Fig.7.4. Mechanisms by which different types of adjuvants can potentiate antibiotics [Source: (Dhanda et al., 2023)].

In particular, the inhibitors of β-lactamases such as clavulanic acid have been widely used in clinics for decades, effectively enhancing the antibacterial activity of penicillin and cephalosporin antibiotics (Cole et al., 1977). Recently, the combination of statins and penicillin was reportedly more effective in controlling methicillin-resistant *S. aureus* than penicillin monotherapy, as statins can help penicillin penetrate cells to disable PBP2a oligomerization by disrupting the structure of the bacterial membrane (García-Fernández et al., 2017). Additionally, the antiprotozoal drug pentamidine, which functions as a membrane disruptor, can potentiate the activity of hydrophobic antibiotics and help overcome acquired resistance to colistin (Stokes et al.,

2017). These existing examples encourage us to investigate the potential adjuvant activity of sodium butyrate to enhance the antibacterial activity of antibiotics via different mechanisms. Sodium butyrate exhibits antibacterial, anti-inflammatory, and antioxidant properties, while also playing a crucial role in modulating host immunity and inhibiting the colonization of enteric pathogens in intestinal epithelial cells (Zimmerman et al., 2012). Moreover, we have demonstrated that SB exhibits potent anti-virulence activity against *V. cholerae* infections (Kundu et al., 2025). Although multiple functions of SB in various aspects have been documented, at present, there is currently limited information about the synergistic antibacterial activity between SB and other compounds, except that cyclic AMP synergizes with butyrate in promoting β-defensin 9 expression in chickens leading to enhanced immune response against bacterial infections (Sunkara et al., 2014). In this study, we investigated the synergistic potential of SB in combination with conventional antibiotics and found that SB selectively enhanced the antibacterial activity of tetracycline against *V. cholerae.*

Infections caused by this bacterium remain a challenging public health problem due to the emergence of widespread drug-resistant strains (Boucher et al., 2009). As one of the "big four" classes of antibiotics, tetracyclines have been used for the treatment of infections caused by a variety of pathogens, including Gram-positive and Gram-negative bacteria (Grossman, 2016; Nguyen et al., 2014; Thaker et al., 2010). However, the increased resistance to these antibiotics together with their toxicity has limited the use of these groups of antibiotics in the clinic (Grossman, 2016; Nguyen et al., 2014; Thaker et al., 2010). Currently, tetracyclines are mainly used as anti-staphylococcal agents, particularly for treating skin and skin structure infections (Gelmetti et al., 2008; Ruhe et al., 2005). In this study, we demonstrated that SB effectively potentiates the activity of tetracycline against *V. cholerae*. This was established through multiple evaluation assays, including a checkerboard assay whose primary screening identified that SB had a synergistic activity with tetracycline against *V. cholerae*, along with the utilization of time-kill kinetics assay that provided significant evidence regarding the synergistic effect of SB combination with tetracycline. It was also confirmed that SB in combination with Tetracycline resulted in collapsed and visibly lysed/destroyed bacteria, indicative of disrupted bacterial cell membrane integrity.

In bacteria, the electron transport chains generate an electrochemical gradient of protons across the cell membrane, known as the proton motive force (PMF), by

actively translocating protons (Farha et al., 2013). It was found that the PMF is essential for the production of ATP via the FoF_1-ATPase complex, and its dissipation effectively halts ATP production (Farha et al., 2013). Consistent with this, the addition of SB to tetracycline inhibits the function of PMF, resulting in a marked decrease in intracellular ATP levels. Hence, we hypothesize that the mechanism underlying the observed bacterial inhibition may involve the collapse of the PMF, which is critical for maintaining vital cellular processes such as ATP generation (Paul et al., 2008). Considering that ATP acts as the primary energy source for almost all biological processes, ATP could be regarded as the metabolic reporter (Lopatkin et al., 2019). Thus, the reduction in intracellular levels of ATP induced by SB and Tet combination could cause perturbations to bacterial metabolic homeostasis or even death. We further ascertained the inhibitory effect of SB and tetracycline on bacterial efflux pumps by the EtBr efflux pump accumulation assay. The results observed in this study suggested that the activity of the efflux pump was significantly inhibited by the addition of SB in both single or combination treatments. Prior studies have shown that drugs such as metformin, and loperamide reduced the functions of PMF-driven efflux pumps in resistant bacteria (Ejim et al., 2011; Y. Liu et al., 2020). Therefore, the observed efflux pump inhibition is particularly noteworthy, as it may enhance intracellular drug accumulation and restore the efficacy of antimicrobials against resistant strains.

An intriguing phenomenon was the potentiation of SB only on tetracyclines against *V. cholerae* but not on other antibiotics (ciprofloxacin, streptomycin, ampicillin, azithromycin, chloramphenicol, gentamicin). Antibiotic efflux pumps widely distributed in various bacterial species are membrane transport proteins that can be specific for a single substrate (for example, TetA in *E. coli* selectively excludes tetracycline) or capable of pumping out a wide range of structurally diverse substrates (for example, NorA can extrude several distinct classes of antibiotics) (Sharma et al., 2019). The latest tally shows that a total of 36 distinct tetracycline-specific efflux pumps has been characterized in Gram-negative and Gram-positive bacteria (Chopra et al., 2001). The most common tetracycline-specific efflux pumps are members of the major facilitator superfamily (MFS) of transporters (Schnappinger et al., 1996; Grossman et al., 2016). In *V. cholerae*, tetracycline-specific pumps called TetA and TetG have been described (Das et al, 2019; Samal et al., 2025). In this study, the potentiation of SB only on tetracyclines may be due to its inhibition of an efflux pump such as

TetA, TetG, or other unknown transporters. However, whether the selectively enhanced antibacterial effects of SB on tetracyclines are related to its specific efflux pump inhibition activity remains to be further clarified.

Survival stress experienced by pathogens plays a critical role in driving phenotypic switching from wild type to tolerant or resistant forms (Dawan et al., 2020). Therefore, evaluating whether repeated exposure to a test compound can induce tolerance or resistance is essential. Although it is currently not feasible to assess this directly in human infections, we addressed this by serially passaging *V. cholerae* in the presence of the test compounds over an extended period in tube cultures. The results indicated that, unlike tetracycline alone, the SB-Tet combination did not induce resistance in *V. cholerae*, suggesting that this combination may effectively reduce the risk of *de novo* emergence of tetracycline resistance. However, these preliminary findings should be confirmed with a broader range of clinical isolates, concentrations, and exposure durations to draw more definitive conclusions.

In our previous study, we demonstrated the anti-virulence properties of SB against *V. cholerae*, showing that it effectively reduced the expression of key virulence factors such as cholera toxin (CT) and toxin-coregulated pilus A (TcpA) (Kundu et al., 2025). Notably, in the present study, the combination treatment resulted in a more substantial reduction in virulence gene expression compared to SB monotherapy. Confocal microscopy confirmed that the SB-Tet combination significantly decreased the adhesion of GFP-expressing *V. cholerae* to HT-29 cells. This effect is likely attributable to the downregulation of TcpA, a major adhesion factor in *V. cholerae*. Additionally, CT, a well-characterized toxin that initiates pathogenesis by binding to GM1 ganglioside receptors on the intestinal epithelium, ultimately leading to disruption of cellular function and excessive fluid and electrolyte loss, was also markedly reduced under the combination treatment compared to either agent alone. These findings suggest that the combinatorial approach exerts a synergistic effect, resulting in more effective suppression of virulence gene expression than monotherapies. Interestingly, previous studies have shown that methyl gallate, when combined with tylosin, synergistically inhibits the adhesion of *Salmonella* Typhimurium to Caco-2 epithelial cells (Mechesso et al., 2019), underscoring the potential of phytochemical-antibiotic combinations in anti-virulence strategies. Similarly, another study found that the combination of chlorhexidine and azithromycin significantly reduced bacterial adherence to colonic

epithelial cells and downregulated NF-κB expression (Samgane et al., 2024). However, further investigation is required to elucidate the precise molecular mechanisms underlying the potent anti-virulence activity observed with the SB-Tet combination against *V. cholerae*.

Curtailing the proliferation and virulence of *V. cholerae* reduces its ability to colonize and infect the host. To evaluate the efficacy of our drug combination under *in vivo* conditions, we employed two animal models, suckling mice and the rabbit ileal loop. In suckling mice, the combination of drugs delayed the death of mice and increased the survival rate by 40%. In addition, drug combination also led to decreased bacterial colonization in suckling mice compared to those that received individual drugs. Since our *in vitro* findings have already demonstrated that the combination exhibits both anti-bacterial and anti-virulence effects, we hypothesize that the observed delay in mortality may be attributed to the synergistic action of these effects. In the rabbit ileal loop model, the combination therapy significantly reduced cholera toxin (CT) production and fluid accumulation compared to monotherapies. Similarly, previous *in vivo* studies have shown that combining quorum-sensing inhibitors or extracellular polymeric substance repressors with conventional antibiotics enhanced antipseudomonal efficacy(Mitra et al., 2024). Altogether, these findings suggest that SB-Tet combination in animal models can reduce the duration and severity of the disease.

One of the major limitations of tetracycline in clinical use is its potential hepatotoxicity and the risk of exacerbating preexisting renal impairment(Andrade et al., 2011). Therefore, strategies that enhance the efficacy of tetracycline could enable the use of lower therapeutic doses, thereby minimizing its toxic side effects. In our study, the SB-Tet combination demonstrated no significant cytotoxicity when tested in HT-29 human intestinal epithelial cell line, suggesting that this approach may offer a safer alternative for clinical application.

The primary limitation of the present study is the evaluation of the synergistic antimicrobial activity of the SB and tetracycline combination on only a small number of multidrug-resistant *V. cholerae* strains. To enhance the reliability of the results, further investigations involving a larger and more diverse set of bacterial strains are needed. Moreover, clinical trials are essential to confirm the efficacy and safety of this drug combination in practical, real-world applications.

In conclusion, this study demonstrated that the combination of SB and tetracycline effectively eliminates multidrug-resistant *V. cholerae* strains. It is highly probable that this combination could also be effective against other Gram-negative bacterial pathogens. Overall, this strategy highlights the potential of SB as a promising adjuvant to the currently limited use of tetracycline in treating *V. cholerae* infections, eventually aiding clinical translation. These findings hold significant clinical relevance and need further investigation to enhance their clinical application potential ***(Fig.7.5).***

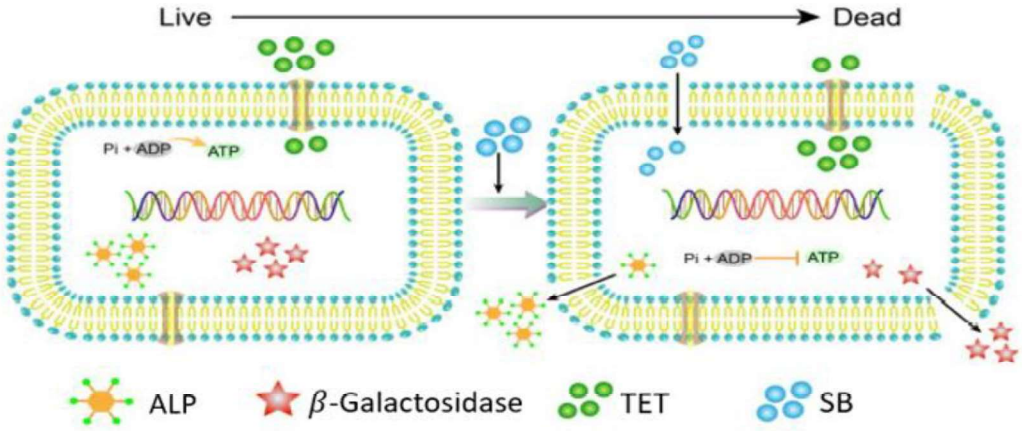

Fig.7.5. A model of sodium butyrate and tetracycline combination therapy on *V. cholerae* cells

Chapter 8

Conclusion

Conclusion

This thesis deals with anti-virulence activity of sodium butyrate against multidrug-resistant *V. cholerae* strains, focusing on inhibition of virulence without affecting bacterial viability. The conclusion of the thesis is as follows:

- We screened several bioactive compounds for anti-virulence activity and found that arabinose, eugenol, quercetin, allylanisole, and sodium butyrate significantly inhibited cholera toxin production, adhesion, motility, and biofilm formation. Sodium butyrate at 20 mM (2.2 mg/ml) was chosen for subsequent analyses owing to its significant anti-virulence potential.

- We found that sodium butyrate significantly reduced the expression of cholera toxin (CT) and TcpA in *V. cholerae* at both RNA and protein levels, without affecting ToxT production. qRT-PCR confirmed decreased *ctxAB* and *tcpA* transcripts, while *toxT* and its upstream regulators (*tcpP*, *tcpH*, *toxR*, *toxS*) remained unchanged.

- Molecular docking identified sodium butyrate as a potential inhibitor that binds at the interface of N-terminal regulatory/dimerization domain and C-terminal DNA binding domain of ToxT, interacting with key residues Lys31 and Lys230. These interactions suggest SB may disrupt ToxT function by interfering with domain interaction or dimerization.

- Two major protein-DNA binding assays confirmed the interaction between SB and ToxT, demonstrating that SB interferes with the binding of ToxT to its target promoter DNAs.

- RNA-seq analysis further confirmed the inhibitory effect of SB on *V. cholerae* virulence genes, including *ctx, tcp, zot,* and *hlyA*. The 2- to 4-fold downregulation of these genes also contributes to the reduction of pathogenicity of the bacteria.

- Inhibition of *V. cholerae* virulence factors by SB were further confirmed by reduced pathogenicity in two animal models: suckling mice and the rabbit ileal loop assay. In suckling mice, decreased levels of the colonization factor TcpA in the presence of SB likely contributed to reduced bacterial colonization. Similarly, reduced cholera toxin production was correlated with a 10-fold decrease in fluid accumulation in the rabbit ileal loop, indicating attenuated enterotoxic effects by SB.

- In addition to exploring anti-virulence strategies, we also investigated combination therapy approaches, wherein the efficacy of existing antibiotics was restored through the use of novel adjuvants.

- In our study, we found that sodium butyrate selectively enhanced the antibacterial activity of tetracycline against *V. cholerae* leading to bacterial lysis, indicating a disruption of bacterial cell membrane integrity.

- Combination of sodium butyrate and tetracycline disrupted the proton motive force (PMF), resulting in decreased intracellular ATP levels and subsequent loss of bacterial viability. Additionally, the SB-tetracycline combination inhibited efflux pump activity, leading to increased intracellular accumulation of tetracycline.

- SB-tetracycline combination also suppressed the expression of virulence factors, cholera toxin (CT) and toxin-coregulated pilus A (TcpA), more effectively than either treatment alone.

- SB-tetracycline combination also delayed mortality in suckling mice and increased survival by 40 %. In the rabbit ileal loop model, the combination therapy more effectively reduced cholera toxin (CT) production and fluid accumulation compared to monotherapy.

- In summary, the SB-tetracycline combination effectively reduces the growth of multidrug-resistant *V. cholerae* strains and presents a promising strategy to overcome the current limitations of tetracycline in treating *V. cholerae* infections. Future studies may explore its broader applicability against other Gram-negative pathogens.

Chapter 9

References

References

Abuaita, B. H., & Withey, J. H. (2009). Bicarbonate induces Vibrio cholerae virulence gene expression by enhancing ToxT activity. *Infection and Immunity, 77(9)*, 4111–4120. https://doi.org/10.1128/IAI.00409-09

Alam, M., Miyoshi, S., Sonoda, Y., Chowdhury, M. A. R., Tomochika, K., & Shinoda, S. (1997). Role of a protease in the adherence and enterotoxicity of Vibrio mimicus. *World Journal of Microbiology and Biotechnology, 13(1),* 37–41. https://doi.org/10.1007/BF02770805

Almagro-Moreno, S., Pruss, K., & Taylor, R. K. (2015). Intestinal Colonization Dynamics of Vibrio cholerae. *PLoS pathogens*, *11*(5), e1004787. https://doi.org/10.1371/journal.ppat.1004787

Alm, E. J., Huang, K. H., Price, M. N., Koche, R. P., Keller, K., Dubchak, I. L., & Arkin, A. P. (2005). The MicrobesOnline Web site for comparative genomics. *Genome research*, *15*(7), 1015–1022. https://doi.org/10.1101/gr.3844805

Al-Mekhlafi H. M. (2018). Yemen in a Time of Cholera: Current Situation and Challenges. *The American journal of tropical medicine and hygiene*, *98*(6), 1558–1562. https://doi.org/10.4269/ajtmh.17-0811

Alm, R. A., & Manning, P. A. (1990). Biotype-specific probe for Vibrio cholerae serogroup O1. *Journal of clinical microbiology*, *28*(4), 823–824. https://doi.org/10.1128/jcm.28.4.823-824.1990

Aminov R. I. (2010). A brief history of the antibiotic era: lessons learned and challenges for the future. *Frontiers in microbiology*, *1*, 134. https://doi.org/10.3389/fmicb.2010.00134

Aminzare, M., Hashemi, M., Abbasi, Z., Mohseni, M., & Amiri, E. (2018). Vibriosis phytotherapy: A review on the most important world medicinal plants effective on Vibrio spp. *Journal of Applied Pharmaceutical Science, 8(1)*, 170–177. https://doi.org/10.7324/JAPS.2018.8126

Andrade, R. J., & Tulkens, P. M. (2011). Hepatic safety of antibiotics used in primary care. *Journal of Antimicrobial Chemotherapy, 66(7),* 1431–1446. https://doi.org/10.1093/jac/dkr159

Anthouard, R., & DiRita, V. J. (2013). Small-molecule inhibitors of toxT expression in Vibrio cholerae. *mBio*, *4*(4), e00403-13. https://doi.org/10.1128/mBio.00403-13

Antonova, E. S., Bernardy, E. E., & Hammer, B. K. (2012). Natural competence in Vibrio cholerae is controlled by a nucleoside scavenging response that requires CytR-dependent anti-activation. *Molecular Microbiology, 86(5),* 1215–1231. https://doi.org/10.1111/mmi.12054

Baker-Austin, C., Oliver, J.D., Alam, M. *et al. Vibrio* spp. infections. *Nature Reviews Disease Primers* ***4***, 1–19 (2018). https://doi.org/10.1038/s41572-018-0005-8

Banerjee, R., Das, B., Balakrish Nair, G., & Basak, S. (2014). Dynamics in genome evolution of Vibrio cholerae. *Infection, genetics and evolution: journal of molecular epidemiology and evolutionary genetics in infectious diseases*, *23*, 32–41. https://doi.org/10.1016/j.meegid.2014.01.006

Baudry, B., Fasano, A., Ketley, J., & Kaper, J. B. (1992). Cloning of a gene (zot) encoding a new toxin produced by Vibrio cholerae. *Infection and immunity*, *60*(2), 428–434. https://doi.org/10.1128/iai.60.2.428-434.1992

Bauer, A. W., Kirby, W. M., Sherris, J. C., & Turck, M. (1966). Antibiotic susceptibility testing by a standardized single disk method. *American journal of clinical pathology*, *45*(4), 493–496. https://academic.oup.com/ajcp/article-abstract/45/4_ts/493/4821085

Bear, C. E., Li, C. H., Kartner, N., Bridges, R. J., Jensen, T. J., Ramjeesingh, M., & Riordan, J. R. (1992). Purification and functional reconstitution of the cystic fibrosis transmembrane conductance regulator (CFTR). *Cell*, *68*(4), 809–818. https://doi.org/10.1016/0092-8674(92)90155-6

Beck, N. A., Krukonis, E. S., & DiRita, V. J. (2004). TcpH influences virulence gene expression in Vibrio cholerae by inhibiting degradation of the transcription activator TcpP. *Journal of bacteriology*, *186*(24), 8309–8316. https://doi.org/10.1128/JB.186.24.8309-8316.2004

Behari, J., Stagon, L., & Calderwood, S. B. (2001). pepA, a gene mediating pH regulation of virulence genes in Vibrio cholerae. *Journal of bacteriology*, *183*(1), 178–188. https://doi.org/10.1128/JB.183.1.178-188.2001

Bina XR and Bina JE (2023) Vibrio cholerae RND efflux systems: mediators of stress responses, colonization and pathogenesis. *Frontiers in Cellular and Infection Microbiology* 13:1203487. https://doi.org/10.3389/fcimb.2023.1203487

Birt, D. F., Boylston, T., Hendrich, S., Jane, J. L., Hollis, J., Li, L., McClelland, J., Moore, S., Phillips, G. J., Rowling, M., Schalinske, K., Scott, M. P., &Whitley, E. M. (2013). Resistant starch: promise for improving human health. *Advances in nutrition (Bethesda, Md.)*, *4*(6), 587-601. https://doi.org/10.3945/an.113.004325

Bogard, R. W., Davies, B. W., & Mekalanos, J. J. (2012). MetR-regulated Vibrio cholerae metabolism is required for virulence. *mBio*, *3*(5), e00236-12. https://doi.org/10.1128/mBio.00236-12

Bollenbach T. (2015). Antimicrobial interactions: mechanisms and implications for drug discovery and resistance evolution. *Current opinion in microbiology*, *27*, 1–9. https://doi.org/10.1016/j.mib.2015.05.008

Boucher, H. W., Talbot, G. H., Bradley, J. S., Edwards, J. E., Gilbert, D., Rice, L. B., Scheld, M., Spellberg, B., & Bartlett, J. (2009). Bad bugs, no drugs: no ESKAPE! An update from the Infectious Diseases Society of America. *Clinical infectious diseases: an official publication of the Infectious Diseases Society of America*, *48*(1), 1–12. https://doi.org/10.1086/595011

Boucher Y. (2016). Sustained Local Diversity of Vibrio cholerae O1 Biotypes in a Previously Cholera-Free Country. *mBio*, *7*(3), e00570-16. https://doi.org/10.1128/mBio.00570-16

Boyd, E. F., Moyer, K. E., Shi, L., & Waldor, M. K. (2000). Infectious CTXPhi and the vibrio pathogenicity island prophage in Vibrio mimicus: evidence for recent

horizontal transfer between V. mimicus and V. cholerae. *Infection and immunity*, *68*(3), 1507–1513. https://doi.org/10.1128/IAI.68.3.1507-1513.2000

Burt S. (2004). Essential oils: their antibacterial properties and potential applications in foods--a review. *International journal of food microbiology*, *94*(3), 223–253. https://doi.org/10.1016/j.ijfoodmicro.2004.03.022

Butler, S. M., & Camilli, A. (2005). Going against the grain: chemotaxis and infection in Vibrio cholerae. *Nature reviews. Microbiology*, *3*(8), 611–620. https://doi.org/10.1038/nrmicro1207

Cash, R. A., Music, S. I., Libonati, J. P., Snyder, M. J., Wenzel, R. P., & Hornick, R. B. (1974). Response of man to infection with Vibrio cholerae. I. Clinical, serologic, and bacteriologic responses to a known inoculum. *The Journal of infectious diseases*, *129*(1), 45–52. https://doi.org/10.1093/infdis/129.1.45

Cassel, D., & Pfeuffer, T. (1978). Mechanism of cholera toxin action: covalent modification of the guanyl nucleotide-binding protein of the adenylate cyclase system. *Proceedings of the National Academy of Sciences of the United States of America*, *75*(6), 2669–2673. https://doi.org/10.1073/pnas.75.6.2669

Chac, D., Dunmire, C. N., Singh, J., & Weil, A. A. (2021). Update on Environmental and Host Factors Impacting the Risk of Vibrio cholerae Infection. *ACS Infectious Diseases, 7(5),* 1010–1019. https://doi.org/10.1021/acsinfecdis.0c00914

Chakraborty, S., Mukhopadhyay, A. K., Bhadra, R. K., Ghosh, A. N., Mitra, R., Shimada, T., Yamasaki, S., Faruque, S. M., Takeda, Y., Colwell, R. R., & Nair, G. B. (2000). Virulence genes in environmental strains of Vibrio cholerae. *Applied and environmental microbiology*, *66*(9), 4022–4028. https://doi.org/10.1128/AEM.66.9.4022-4028.2000

Champion, G. A., Neely, M. N., Brennan, M. A., & DiRita, V. J. (1997). A branch in the ToxR regulatory cascade of Vibrio cholerae revealed by characterization of toxT mutant strains. *Molecular microbiology*, *23*(2), 323–331. https://doi.org/10.1046/j.1365-2958.1997.2191585.x

Chang, YW., Kjær, A., Ortega, D. *et al.* Architecture of the *Vibrio cholerae* toxin-coregulated pilus machine revealed by electron cryotomography. *Nature Microbiology, 2,* 16269 (2017). https://doi.org/10.1038/nmicrobiol.2016.269

Chatterjee, A., Dutta, P. K., & Chowdhury, R. (2007). Effect of fatty acids and cholesterol present in bile on expression of virulence factors and motility of Vibrio cholerae. *Infection and Immunity, 75(4),* 1946–1953. https://doi.org/10.1128/IAI.01435-06

Chatterjee, S. N., & Chaudhuri, K. (2003). Lipopolysaccharides of Vibrio cholerae. I. Physical and chemical characterization. *Biochimica et biophysica acta*, *1639*(2), 65–79. https://doi.org/10.1016/j.bbadis.2003.08.004

Chen, J., & Vitetta, L. (2020). The Role of Butyrate in Attenuating Pathobiont-Induced Hyperinflammation. *Immune network*, *20*(2), e15. https://doi.org/10.4110/in.2020.20.e15

Chen, X., Su, W., Wan, T., Yu, J., Zhu, W., Tang, F., Liu, G., Olsen, N., Liang, D., & Zheng, S. G. (2017). Sodium butyrate regulates Th17/Treg cell balance to ameliorate uveitis via the Nrf2/HO-1 pathway. *Biochemical pharmacology*, *142*, 111–119. https://doi.org/10.1016/j.bcp.2017.06.136

Chiang, S. L., & Mekalanos, J. J. (1998). Use of signature-tagged transposon mutagenesis to identify Vibrio cholerae genes critical for colonization. *Molecular Microbiology, 27(4)*, 797–805. https://doi.org/10.1046/j.1365-2958.1998.00726.x

Chopra, I., & Roberts, M. (2001). Tetracycline Antibiotics: Mode of Action, Applications, Molecular Biology, and Epidemiology of Bacterial Resistance. *Microbiology and Molecular Biology Reviews, 65(2),* 232–260. https://doi.org/10.1128/mmbr.65.2.232-260.2001

Chourashi, R., Mondal, M., Sinha, R., Debnath, A., Das, S., Koley, H., & Chatterjee, N. S. (2016). Role of a sensor histidine kinase ChiS of Vibrio cholerae in pathogenesis. *International Journal of Medical Microbiology, 306(8),* 657–665. https://doi.org/10.1016/j.ijmm.2016.09.003

Chiang, S. L., & Mekalanos, J. J. (1999). rfb mutations in Vibrio cholerae do not affect surface production of toxin-coregulated pili but still inhibit intestinal colonization. *Infection and immunity*, *67*(2), 976–980. https://doi.org/10.1128/IAI.67.2.976-980.1999

Chu, B., Zhu, Y., Su, J., Xia, B., Zou, Y., Nie, J., Zhang, W., & Wang, J. (2020). Butyrate-mediated autophagy inhibition limits cytosolic Salmonella Infantis replication in the colon of pigs treated with a mixture of Lactobacillus and Bacillus. *Veterinary research*, *51*(1), 99. https://doi.org/10.1186/s13567-020-00823-8

Colwell R. R. (2002). A voyage of discovery: cholera, climate and complexity. *Environmental microbiology*, *4*(2), 67–69. https://doi.org/10.1046/j.1462-2920.2002.00270.x

Cruite, J. T., Kovacikova, G., Clark, K. A., Woodbrey, A. K., Skorupski, K., & Kull, F. J. (2019). Structural basis for virulence regulation in Vibrio cholerae by unsaturated fatty acid components of bile. *Communications Biology, 2(1).* https://doi.org/10.1038/s42003-019-0686-x

Czerkinsky, C., Russell, M. W., Lycke, N., Lindblad, M., & Holmgren, J. (1989). Oral administration of a streptococcal antigen coupled to cholera toxin B subunit evokes strong antibody responses in salivary glands and extramucosal tissues. *Infection and immunity, 57(4),* 1072–1077. https://doi.org/10.1128/iai.57.4.1072-1077.1989

Dalsgaard, A., Forslund, A., Tam, N. V., Vinh, D. X., & Cam, P. D. (1999). Cholera in Vietnam: changes in genotypes and emergence of class I integrons containing aminoglycoside resistance gene cassettes in vibrio cholerae O1 strains isolated from 1979 to 1996. *Journal of clinical microbiology*, *37*(3), 734–741. https://doi.org/10.1128/JCM.37.3.734-741.1999

Das, B., Bischerour, J., & Barre, F. X. (2011). Molecular mechanism of acquisition of the cholera toxin genes. *The Indian journal of medical research*, *133*(2), 195–200

Das, B., Verma, J., Kumar, P., Ghosh, A., & Ramamurthy, T. (2020). Antibiotic resistance in Vibrio cholerae: Understanding the ecology of resistance genes and mechanisms. *Vaccine*, *38 Suppl 1*, A83–A92. https://doi.org/10.1016/j.vaccine.2019.06.031

Dashiff, A., Junka, R. A., Libera, M., & Kadouri, D. E. (2011). Predation of human pathogens by the predatory bacteria Micavibrio aeruginosavorus and

Bdellovibrio bacteriovorus. *Journal of Applied Microbiology, 110(2),* 431–444. https://doi.org/10.1111/j.1365-2672.2010.04900.x

Davis, B. M., Kimsey, H. H., Chang, W., & Waldor, M. K. (1999). The Vibrio cholerae O139 Calcutta bacteriophage CTXphi is infectious and encodes a novel repressor. *Journal of bacteriology*, *181*(21), 6779–6787. https://doi.org/10.1128/JB.181.21.6779-6787.1999

Davis, B. M., & Waldor, M. K. (2003). Filamentous phages linked to virulence of Vibrio cholerae. *Current opinion in microbiology*, *6*(1), 35–42. https://doi.org/10.1016/s1369-5274(02)00005-x

Dawan, J., Wei, S., & Ahn, J. (2020). Role of antibiotic stress in phenotypic switching to persister cells of antibiotic-resistant Staphylococcus aureus. *Annals of Microbiology, 70(1).* https://doi.org/10.1186/s13213-020-01552-1

De, K., Ramamurthy, T., Faruque, S. M., Yamasaki, S., Takeda, Y., Nair, G. B., & Nandy, R. K. (2004). Molecular characterisation of rough strains of Vibrio cholerae isolated from diarrhoeal cases in India and their comparison to smooth strains. *FEMS Microbiology Letters, 232(1),* 23–30. https://doi.org/10.1016/S0378-1097(04)00013-8

Defoirdt, T., Mai Anh, N. T., & De Schryver, P. (2018). Virulence-inhibitory activity of the degradation product 3-hydroxybutyrate explains the protective effect of poly-β-hydroxybutyrate against the major aquaculture pathogen Vibrio campbellii. *Scientific Reports, 8(1).* https://doi.org/10.1038/s41598-018-25385-w

Dehbanipour, R., & Ghalavand, Z. (2022). Anti-virulence therapeutic strategies against bacterial infections: recent advances. *Germs*, *12*(2), 262–275. https://doi.org/10.18683/germs.2022.1328

Di Pierro, M., Lu, R., Uzzau, S., Wang, W., Margaretten, K., Pazzani, C., Maimone, F., & Fasano, A. (2001). Zonula occludens toxin structure-function analysis: Identification of the fragment biologically active on tight junctions and of the zonulin receptor binding domain. *Journal of Biological Chemistry, 276(22),* 19160–19165. https://doi.org/10.1074/jbc.M009674200

DiRita V. J. (1992). Co-ordinate expression of virulence genes by ToxR in Vibrio cholerae.*Molecular microbiology*, *6*(4),451–458.https://doi.org/10.1111/j.1365-2958.1992.tb01489.x

Dirk Schnappinger · Wolfgang Hillen. (1996). Tetracyclines: antibiotic action, uptake, and resistance mechanisms. *Archives of Microbiology* 165, 359–369 (1996). https://doi.org/10.1007/s002030050339

D'Mello-Guyett, L., Gallandat, K., Van den Bergh, R., Taylor, D., Bulit, G., Legros, D., Maes, P., Checchi, F., & Cumming, O. (2020). Prevention and control of cholera with household and community water, sanitation and hygiene (WASH) interventions: A scoping review of current international guidelines. *PloS one*, *15*(1), e0226549. https://doi.org/10.1371/journal.pone.0226549

Du, K., Bereswill, S., & Heimesaat, M. M. (2021). A literature survey on antimicrobial and immune-modulatory effects of butyrate revealing non-antibiotic approaches to tackle bacterial infections. *European Journal of Microbiology and Immunology, 11(1)*, 1–9. https://doi.org/10.1556/1886.2021.00001

Duan, F., & March, J. C. (2010). Engineered bacterial communication prevents Vibrio cholerae virulence in an infant mouse model. *Proceedings of the National Academy of Sciences of the United States of America*, *107*(25), 11260–11264. https://doi.org/10.1073/pnas.1001294107

Echazarreta MA and Klose KE (2019) *Vibrio* Flagellar Synthesis. *Frontiers in Cellular and Infection Microbiology*. 9:131. https://doi.org/10.3389/fcimb.2019.00131

Ejim, L., Farha, M. A., Falconer, S. B., Wildenhain, J., Coombes, B. K., Tyers, M., Brown, E. D., & Wright, G. D. (2011). Combinations of antibiotics and nonantibiotic drugs enhance antimicrobial efficacy. *Nature Chemical Biology, 7(6),* 348–350. https://doi.org/10.1038/nchembio.559

Erfanimanesh, S., Eslami, G., Taherpour, A., & Hashemi, A. (2019). Capsaicin inhibitory effects on *Vibrio cholerae* toxin genes expression. *Avicenna journal of phytomedicine*, *9*(3), 187–194.

Erken, M., Lutz, C., & McDougald, D. (2015). Interactions of Vibrio spp. with Zooplankton. *Microbiology Spectrum, 3(3).* https://doi.org/10.1128/microbiolspec.ve-0003-2014

Fang, W., Xue, H., Chen, X., Chen, K., & Ling, W. (2019). Supplementation with sodium butyrate modulates the composition of the gut microbiota and ameliorates high-fat diet-induced obesity in mice. *Journal of Nutrition, 149(5),* 747–754. https://doi.org/10.1093/jn/nxy324

Farha, M. A., Verschoor, C. P., Bowdish, D., & Brown, E. D. (2013). Collapsing the proton motive force to identify synergistic combinations against staphylococcus aureus. *Chemistry and Biology, 20(9),* 1168–1178. https://doi.org/10.1016/j.chembiol.2013.07.006

Farmer, J. J. (2006). The Family Vibrionaceae. The Prokaryotes (pp. 495–507). Springer New York. https://doi.org/10.1007/0-387-30746-x_17

Faruque, S. M., & Mekalanos, J. J. (2003). Pathogenicity islands and phages in Vibrio cholerae evolution. *Trends in microbiology*, *11*(11), 505–510. https://doi.org/10.1016/j.tim.2003.09.003

Fasano, A., Baudry, B., Pumplin, D. W., Wasserman, S. S., Tall, B. D., Ketley, J. M., & Kaper, J. B. (1991). Vibrio cholerae produces a second enterotoxin, which affects intestinal tight junctions. *Proceedings of the National Academy of Sciences of the United States of America*, *88*(12), 5242–5246. https://doi.org/10.1073/pnas.88.12.5242

Ferraroni, M., Cornelio, B., Sapi, J., Supuran, C. T., & Scozzafava, A. (2018). Sulfonamide carbonic anhydrase inhibitors: Zinc coordination and tail effects influence inhibitory efficacy and selectivity for different isoforms. *Inorganica Chimica Acta, 470,* 128–132. https://doi.org/10.1016/j.ica.2017.03.038

Field M. (2003). Intestinal ion transport and the pathophysiology of diarrhea. *The Journal of clinical investigation*, *111*(7), 931–943. https://doi.org/10.1172/JCI18326

Finkelstein, R. A., & LoSpalluto, J. J. (1969). Pathogenesis of experimental cholera. Preparation and isolation of choleragen and choleragenoid. *The Journal of experimental medicine*, *130*(1), 185–202. https://doi.org/10.1084/jem.130.1.185

Gagliano, H., Delgado-Morales, R., Sanz-Garcia, A., & Armario, A. (2014). High doses of the histone deacetylase inhibitor sodium butyrate trigger a stress-like response. *Neuropharmacology*, *79*, 75–82. https://doi.org/10.1016/j.neuropharm.2013.10.031

García-Fernández, E., Koch, G., Wagner, R. M., Fekete, A., Stengel, S. T., Schneider, J., Mielich-Süss, B., Geibel, S., Markert, S. M., Stigloher, C., & Lopez, D. (2017). Membrane Microdomain Disassembly Inhibits MRSA Antibiotic Resistance. *Cell, 171(6),* 1354-1367.e20. https://doi.org/10.1016/j.cell.2017.10.012

Garrity, G. M., Bell, J. A., & Lilburn, T. G. (2005). *Bergey's Manual of Systematic Bacteriology* (2nd ed., Vol. 2, Part B: The Gammaproteobacteria, Springer.

Gelmetti C. (2008). Local antibiotics in dermatology. *Dermatologic therapy*, *21*(3), 187–195. https://doi.org/10.1111/j.1529-8019.2008.00190.x

Gheibzadeh, M. S., Capasso, C., Supuran, C. T., & Zolfaghari Emameh, R. (2024). Antibacterial carbonic anhydrase inhibitors targeting Vibrio cholerae enzymes. *Expert Opinion on Therapeutic Targets* (Vol. 28, Issue 7, pp. 623–635). Taylor and Francis Ltd. https://doi.org/10.1080/14728222.2024.2369622

Goss, T. J., Morgan, S. J., French, E. L., & Krukonis, E. S. (2013). ToxR recognizes a direct repeat element in the toxT, ompU, ompT, and ctxA promoters of Vibrio cholerae to regulate transcription. *Infection and immunity*, *81*(3), 884–895. https://doi.org/10.1128/IAI.00889-12

Grossman T. H. (2016). Tetracycline Antibiotics and Resistance. *Cold Spring Harbor perspectives in medicine*, *6*(4), a025387. https://doi.org/10.1101/cshperspect.a025387

Gupta, S., & Chowdhury, R. (1997). Bile affects production of virulence factors and motility of Vibrio cholerae. *Infection and immunity*, *65*(3), 1131–1134. https://doi.org/10.1128/IAI.65.3.1131-1134.1997

Gupta, S. S., Bharati, K., Sur, D., Khera, A., Ganguly, N. K., & Nair, G. B. (2016). Why is the oral cholera vaccine not considered an option for prevention of

cholera in India? Analysis of possible reasons. *The Indian journal of medical research*, *143*(5), 545–551. https://doi.org/10.4103/0971-5916.187102

Hall, R. H., Losonsky, G., Silveira, A. P., Taylor, R. K., Mekalanos, J. J., Witham, N. D., & Levine, M. M. (1991). Immunogenicity of Vibrio cholerae O1 toxin-coregulated pili in experimental and clinical cholera. *Infection and immunity*, *59*(7), 2508–2512. https://doi.org/10.1128/iai.59.7.2508-2512.1991

Heidelberg, J. F., Eisen, J. A., Nelson, W. C., Clayton, R. A., Gwinn, M. L., Dodson, R. J., Haft, D. H., Hickey, E. K., Peterson, J. D., Umayam, L., Gill, S. R., Nelson, K. E., Read, T. D., Tettelin, H., Richardson, D., Ermolaeva, M. D., Vamathevan, J., Bass, S., Qin, H., Dragoi, I., … Fraser, C. M. (2000). DNA sequence of both chromosomes of the cholera pathogen Vibrio cholerae. *Nature*, *406*(6795), 477–483. https://doi.org/10.1038/35020000

Hellman, L. M., & Fried, M. G. (2007). Electrophoretic mobility shift assay (EMSA) for detecting protein-nucleic acid interactions. *Nature protocols*, *2*(8), 1849–1861. https://doi.org/10.1038/nprot.2007.249

Higgins, D. A., Pomianek, M. E., Kraml, C. M., Taylor, R. K., Semmelhack, M. F., & Bassler, B. L. (2007). The major Vibrio cholerae autoinducer and its role in virulence factor production. *Nature, 450(7171),* 883–886. https://doi.org/10.1038/nature06284

Hodgkinson, K., El Abbar, F., Dobranowski, P., Manoogian, J., Butcher, J., Figeys, D., Mack, D., & Stintzi, A. (2023). Butyrate's role in human health and the current progress towards its clinical application to treat gastrointestinal disease. *Clinical nutrition (Edinburgh, Scotland)*, *42*(2), 61–75. https://doi.org/10.1016/j.clnu.2022.10.024

Hong, J., Jia, Y., Pan, S., Jia, L., Li, H., Han, Z., Cai, D., & Zhao, R. (2016). Butyrate alleviates high fat diet-induced obesity through activation of adiponectin-mediated pathway and stimulation of mitochondrial function in the skeletal muscle of mice. *Oncotarget*, *7*(35), 56071–56082. https://doi.org/10.18632/oncotarget.11267

Hsiao, A., & Zhu, J. (2020). Pathogenicity and virulence regulation of *Vibrio cholerae* at the interface of host-gut microbiome interactions. *Virulence*, *11*(1), 1582–1599. https://doi.org/10.1080/21505594.2020.1845039

Hulbert, R. R., & Taylor, R. K. (2002). Mechanism of ToxT-dependent transcriptional activation at the Vibrio cholerae tcpA promoter. *Journal of Bacteriology, 184(20)*, 5533–5544. https://doi.org/10.1128/JB.184.20.5533-5544.2002

Hung, D. T., Shakhnovich, E. A., Pierson, E., & Mekalanos, J. J. (2005). Small-molecule inhibitor of Vibrio cholerae virulence and intestinal colonization. *Science, 310(5748)*, 670–674. https://doi.org/10.1126/science.1116739

Huq, A., Sack, R. B., Nizam, A., Longini, I. M., Nair, G. B., Ali, A., Morris, J. G., Khan, M. N. H., Siddique, A. K., Yunus, M., Albert, M. J., Sack, D. A., & Colwell, R. R. (2005). Critical factors influencing the occurrence of Vibrio cholerae in the environment of Bangladesh. *Applied and Environmental Microbiology, 71(8)*, 4645–4654. https://doi.org/10.1128/AEM.71.8.4645-4654.2005

Huq, A., Small, E. B., West, P. A., Huq, M. I., Rahman, R., & Colwell, R. R. (1983). Ecological relationships between Vibrio cholerae and planktonic crustacean copepods. *Applied and environmental microbiology*, *45*(1), 275–283. https://doi.org/10.1128/aem.45.1.275-283.1983

Jiminez, J. A., Uwiera, T. C., Abbott, D. W., Uwiera, R. R. E., & Inglis, G. D. (2017). Butyrate Supplementation at High Concentrations Alters Enteric Bacterial Communities and Reduces Intestinal Inflammation in Mice Infected with *Citrobacter rodentium*. *mSphere*, *2*(4), e00243-17. https://doi.org/10.1128/mSphere.00243-17

Johnson, S. B., Park, H. S., Gross, C. P., & Yu, J. B. (2018). Use of alternative medicine for cancer and its impact on survival. *Journal of the National Cancer Institute, 110(1),* 121–124. https://doi.org/10.1093/jnci/djx145

Kaper, J. B., Morris, J. G., Jr, & Levine, M. M. (1995). Cholera. *Clinical microbiology reviews*, *8*(1), 48–86. https://doi.org/10.1128/CMR.8.1.48

Kathryn L Cottingham, D. A. C. and R. K. T. (2003). Environmental microbe and human pathogen: the ecology and microbiology of Vibrio cholerae.

Kennedy, G. M., Min, M. Y., Fitzgerald, J. F., Nguyen, M. T., Schultz, S. L., Crum, M. T., Starke, J. A., Butkus, M. A., Bowman, D. D., & Labare, M. P. (2019).

Inactivation of the bacterial pathogens Staphylococcus pseudintermedius and Acinetobacter baumannii by butanoic acid. *Journal of Applied Microbiology, 126(3)*, 752–763. https://doi.org/10.1111/jam.14180

Kim, S. Y., Chae, C. W., Lee, H. J., Jung, Y. H., Choi, G. E., Kim, J. S., Lim, J. R., Lee, J. E., Cho, J. H., Park, H., Park, C., & Han, H. J. (2020). Sodium butyrate inhibits high cholesterol-induced neuronal amyloidogenesis by modulating NRF2 stabilization-mediated ROS levels: involvement of NOX2 and SOD1. *Cell death & disease*, *11*(6), 469. https://doi.org/10.1038/s41419-020-2663-1

Kitaoka, M., Miyata, S. T., Unterweger, D., & Pukatzki, S. (2011). Antibiotic resistance mechanisms of Vibrio cholerae. *Journal of medical microbiology*, *60*(Pt 4), 397–407. https://doi.org/10.1099/jmm.0.023051-0

Klose, K. E., & Mekalanos, J. J. (1998). Distinct roles of an alternative sigma factor during both free-swimming and colonizing phases of the Vibrio cholerae pathogenic cycle. *Molecular microbiology*, *28*(3), 501–520. https://doi.org/10.1046/j.1365-2958.1998.00809.x.

Koley, H., Mitra, R., Basu, A., Mukhopadhyay, A. K., Saha, P. K., Ramakrishna, B. S., Krishnan, S., Takeda, Y., & Nair, G. B. (1999). Response of wild-type mutants of Vibrio cholerae O1 possessing different combinations of virulence genes in the ligated rabbit ileal loop and in Ussing chambers: evidence for the presence of additional secretogen. *Journal of medical microbiology*, *48*(1), 51–57. https://doi.org/10.1099/00222615-48-1-51

Krukonis, E. S., Yu, R. R., & Dirita, V. J. (2000). The Vibrio cholerae ToxR/TcpP/ToxT virulence cascade: distinct roles for two membrane-localized transcriptional activators on a single promoter. *Molecular microbiology*, *38*(1), 67–84. https://doi.org/10.1046/j.1365-2958.2000.02111.x

Kumar, V., & Turnbull, W. B. (2018). Carbohydrate inhibitors of cholera toxin. *Beilstein journal of organic chemistry*, *14*, 484–498. https://doi.org/10.3762/bjoc.14.34

Kundu, S., Das, S., Maitra, P., Halder, P., Koley, H., Mukhopadhyay, A. K., Miyoshi, S.-i, Dutta, S., Chatterjee, N. S., & Bhattacharya, S. (2025). Sodium butyrate inhibits the expression of virulence factors in *Vibrio cholerae* by targeting ToxT protein. *mSphere*, e0082424. https://doi.org/10.1128/msphere.00824-24

Langeveld, W. T., Veldhuizen, E. J., & Burt, S. A. (2014). Synergy between essential oil components and antibiotics: a review. *Critical reviews in microbiology*, *40*(1), 76–94. https://doi.org/10.3109/1040841X.2013.763219

Ling, H., Boodhoo, A., Hazes, B., Cummings, M. D., Armstrong, G. D., Brunton, J. L., & Read, R. J. (1998). Structure of the shiga-like toxin I B-pentamer complexed with an analogue of its receptor Gb3. *Biochemistry*, *37*(7), 1777–1788. https://doi.org/10.1021/bi971806n

Lloyd, C. J., Guo, S., Kinrade, B., Zahiri, H., Eves, R., Ali, S. K., Yildiz, F., Voets, I. K., Davies, P. L., & Klose, K. E. (2023). A peptide-binding domain shared with an Antarctic bacterium facilitates *Vibrio cholerae* human cell binding and intestinal colonization. *Proceedings of the National Academy of Sciences of the United States of America*, *120*(39), e2308238120. https://doi.org/10.1073/pnas.2308238120

Lipp, E. K., Huq, A., & Colwell, R. R. (2002). Effects of global climate on infectious disease: the cholera model. *Clinical microbiology reviews*, *15*(4), 757–770. https://doi.org/10.1128/CMR.15.4.757-770.2002

Lippi, D., & Gotuzzo, E. (2014). The greatest steps towards the discovery of Vibrio cholerae. *Clinical microbiology and infection: the official publication of the European Society of Clinical Microbiology and Infectious Diseases*, *20*(3), 191–195. https://doi.org/10.1111/1469-0691.12390

Liu, H., Wang, J., He, T., Becker, S., Zhang, G., Li, D., & Ma, X. (2018). Butyrate: A Double-Edged Sword for Health? *Advances in nutrition (Bethesda, Md.)*, *9*(1), 21–29. https://doi.org/10.1093/advances/nmx009

Liu, Y., Ding, S., Dietrich, R., Märtlbauer, E., & Zhu, K. (2017). A Biosurfactant-Inspired Heptapeptide with Improved Specificity to Kill MRSA. *Angewandte Chemie, 129(6),* 1508–1512. https://doi.org/10.1002/ange.201609277

Liu, Y., Jia, Y., Yang, K., Li, R., Xiao, X., Zhu, K., & Wang, Z. (2020). Metformin Restores Tetracyclines Susceptibility against Multidrug Resistant Bacteria. *Advanced science (Weinheim, Baden-Wurttemberg, Germany)*, *7*(12), 1902227. https://doi.org/10.1002/advs.201902227

Liu, Y., Xu, T., Wang, Q., Huang, J., Zhu, Y., Liu, X., Liu, R., Yang, B., & Zhou, K. (2022). Vibrio cholerae senses human enteric α-defensin 5 through a CarSR two-component system to promote bacterial pathogenicity. *Communications biology*, *5*(1), 559. https://doi.org/10.1038/s42003-022-03525-3

Liu, Z., Miyashiro, T., Tsou, A., Hsiao, A., Goulian, M., & Zhu, J. (2008). Mucosal penetration primes Vibrio cholerae for host colonization by repressing quorum sensing. *Proceedings of the National Academy of Sciences of the United States of America*, *105*(28), 9769–9774. https://doi.org/10.1073/pnas.0802241105

Liu, Z., Stirling, F. R., & Zhu, J. (2007). Temporal quorum-sensing induction regulates Vibrio cholerae biofilm architecture. *Infection and Immunity, 75(1),* 122–126. https://doi.org/10.1128/IAI.01190-06

Livak, K. J., & Schmittgen, T. D. (2001). Analysis of relative gene expression data using real-time quantitative PCR and the 2(-Delta Delta C(T)) Method. *Methods (San Diego, Calif.)*, *25*(4), 402–408. https://doi.org/10.1006/meth.2001.1262

Lo Scrudato, M., & Blokesch, M. (2012). The regulatory network of natural competence and transformation of Vibrio cholerae. *PLoS genetics*, *8*(6), e1002778. https://doi.org/10.1371/journal.pgen.1002778

Lo Scrudato, M., & Blokesch, M. (2013). A transcriptional regulator linking quorum sensing and chitin induction to render Vibrio cholerae naturally transformable. *Nucleic acids research*, *41*(6), 3644–3658. https://doi.org/10.1093/nar/gkt041

Lobitz, B., Beck, L., Huq, A., Wood, B., Fuchs, G., Faruque, A. S., & Colwell, R. (2000). Climate and infectious disease: use of remote sensing for detection of Vibrio cholerae by indirect measurement. *Proceedings of the National Academy of Sciences of the United States of America*, *97*(4), 1438–1443. https://doi.org/10.1073/pnas.97.4.1438

Lopatkin, A. J., Stokes, J. M., Zheng, E. J., Yang, J. H., Takahashi, M. K., You, L., & Collins, J. J. (2019). Bacterial metabolic state more accurately predicts antibiotic lethality than growth rate. *Nature microbiology*, *4*(12), 2109–2117. https://doi.org/10.1038/s41564-019-0536-0

Lowden, M. J., Skorupski, K., Pellegrini, M., Chiorazzo, M. G., Taylor, R. K., & Kull, F. J. (2010). Structure of Vibrio cholerae ToxT reveals a mechanism for fatty acid regulation of virulence genes. *Proceedings of the National Academy of Sciences of the United States of America*, *107*(7), 2860–2865. https://doi.org/10.1073/pnas.0915021107

LOWRY, O. H., ROSEBROUGH, N. J., FARR, A. L., & RANDALL, R. J. (1951). Protein measurement with the Folin phenol reagent. *The Journal of biological chemistry*, *193*(1), 265–275.https://doi.org/10.1016/s0021-9258(19)52451-6

Lutz, C., Erken, M., Noorian, P., Sun, S., & McDougald, D. (2013). Environmental reservoirs and mechanisms of persistence of Vibrio cholerae. *Frontiers in microbiology*, *4*, 375. https://doi.org/10.3389/fmicb.2013.00375

Maisuria, V. B., Okshevsky, M., Déziel, E., & Tufenkji, N. (2019). Proanthocyanidin Interferes with Intrinsic Antibiotic Resistance Mechanisms of Gram-Negative Bacteria. *Advanced science (Weinheim, Baden-Wurttemberg, Germany)*, *6*(15), 1802333. https://doi.org/10.1002/advs.201802333

Mandal, R. S., Ta, A., Sinha, R., Theeya, N., Ghosh, A., Tasneem, M., Bhunia, A., Koley, H., & Das, S. (2016). Ribavirin suppresses bacterial virulence by targeting LysR-Type transcriptional regulators. *Scientific Reports, 6.* 39454.https://doi.org/10.1038/srep39454

Manneh-Roussel, J., Haycocks, J. R. J., Magán, A., Perez-Soto, N., Voelz, K., Camilli, A., Krachler, A. M., & Grainger, D. C. (2018). cAMP Receptor Protein Controls Vibrio cholerae Gene Expression in Response to Host Colonization. *mBio*, *9*(4), e00966-18. https://doi.org/10.1128/mBio.00966-18

Martínez-Govea, A., Ambrosio, J., Gutiérrez-Cogco, L., & Flisser, A. (2001). Identification and strain differentiation of Vibrio cholerae by using polyclonal

antibodies against outer membrane proteins. *Clinical and diagnostic laboratory immunology*, *8*(4), 768–771. https://doi.org/10.1128/CDLI.8.4.768-771.2001

Matson, J. S., Withey, J. H., & DiRita, V. J. (2007). Regulatory networks controlling Vibrio cholerae virulence gene expression. *Infection and immunity*, *75*(12), 5542–5549. https://doi.org/10.1128/IAI.01094-07

McCarter L. L. (2004). Dual flagellar systems enable motility under different circumstances. *Journal of molecular microbiology and biotechnology*, *7*(1-2), 18–29. https://doi.org/10.1159/000077866

Mechesso, A. F., Yixian, Q., & Park, S. C. (2019). Methyl gallate and tylosin synergistically reduce the membrane integrity and intracellular survival of Salmonella Typhimurium. *PloS one*, *14*(9), e0221386. https://doi.org/10.1371/journal.pone.0221386

Meibom, K. L., Li, X. B., Nielsen, A. T., Wu, C. Y., Roseman, S., & Schoolnik, G. K. (2004). The Vibrio cholerae chitin utilization program. *Proceedings of the National Academy of Sciences of the United States of America*, *101*(8), 2524–2529. https://doi.org/10.1073/pnas.0308707101

Mekalanos, J. J., Swartz, D. J., Pearson, G. D., Harford, N., Groyne, F., & de Wilde, M. (1983). Cholera toxin genes: nucleotide sequence, deletion analysis and vaccine development. *Nature*, *306*(5943), 551–557. https://doi.org/10.1038/306551a0

Melander, R. J., & Melander, C. (2017). The Challenge of Overcoming Antibiotic Resistance: An Adjuvant Approach? *ACS infectious diseases*, *3*(8), 559–563. https://doi.org/10.1021/acsinfecdis.7b00071

Merrell, D. S., Hava, D. L., & Camilli, A. (2002). Identification of novel factors involved in colonization and acid tolerance of Vibrio cholerae. *Molecular microbiology*, *43*(6), 1471–1491. https://doi.org/10.1046/j.1365-2958.2002.02857.x

Meyer, T. S., & Lamberts, B. L. (1965). Use of coomassie brilliant blue R250 for the electrophoresis of microgram quantities of parotid saliva proteins on acrylamide-gel strips. *Biochimica et biophysica acta*, *107*(1), 144–145. https://doi.org/10.1016/0304-4165(65)90403-4

Midgett, C. R., Talbot, K. M., Day, J. L., Munson, G. P., & Kull, F. J. (2021). Structure of the master regulator Rns reveals an inhibitor of enterotoxigenic Escherichia coli virulence regulons. *Scientific reports*, *11*(1), 15663. https://doi.org/10.1038/s41598-021-95123-2

Mitra A. (2024). Combatting biofilm-mediated infections in clinical settings by targeting quorum sensing. *Cell surface (Amsterdam, Netherlands)*, *12*, 100133. https://doi.org/10.1016/j.tcsw.2024.100133

Momba, M. and Azab El-Liethy, M. 2017. Vibrio cholerae and Cholera biotypes. In: J.B. Rose and B. Jiménez-Cisneros, (eds) Global Water Pathogens Project. http://www.waterpathogens.org (A. Pruden, N. Ashbolt and J.Miller (eds) Part 3 Bacteria) http://www.waterpathogens.org/book/Vibrio

Mondal, M., Nag, D., Koley, H., Saha, D. R., & Chatterjee, N. S. (2014). The Vibrio cholerae extracellular chitinase ChiA2 is important for survival and pathogenesis in the host intestine. *PloS one*, *9*(9), e103119. https://doi.org/10.1371/journal.pone.0103119

Morgan, S. J., Felek, S., Gadwal, S., Koropatkin, N. M., Perry, J. W., Bryson, A. B., & Krukonis, E. S. (2011). The two faces of ToxR: activator of ompU, co-regulator of toxT in Vibrio cholerae. *Molecular microbiology*, *81*(1), 113–128. https://doi.org/10.1111/j.1365-2958.2011.07681.x

Muanprasat, C., & Chatsudthipong, V. (2013). Cholera: pathophysiology and emerging therapeutic targets. *Future medicinal chemistry*, *5*(7), 781–798. https://doi.org/10.4155/fmc.13.42

Munguia, J., & Nizet, V. (2017). Pharmacological Targeting of the Host-Pathogen Interaction: Alternatives to Classical Antibiotics to Combat Drug-Resistant Superbugs. *Trends in pharmacological sciences*, *38*(5), 473–488. https://doi.org/10.1016/j.tips.2017.02.003

Namkung, H., Yu, H., Gong, J., & Leeson, S. (2011). Antimicrobial activity of butyrate glycerides toward salmonella typhimurium and clostridium perfringens. *Poultry Science, 90(10),* 2217–2222. https://doi.org/10.3382/ps.2011-01498

Narendrakumar, L., Gupta, S. S., Johnson, J. B., Ramamurthy, T., & Thomas, S. (2019). Molecular Adaptations and Antibiotic Resistance in *Vibrio cholerae*: A Communal Challenge. *Microbial drug resistance (Larchmont, N.Y.)*, *25*(7), 1012–1022. https://doi.org/10.1089/mdr.2018.0354

Nelson, E. J., Harris, J. B., Morris, J. G., Jr, Calderwood, S. B., & Camilli, A. (2009). Cholera transmission: the host, pathogen and bacteriophage dynamic. *Nature reviews. Microbiology*, *7*(10), 693–702. https://doi.org/10.1038/nrmicro2204

Ng, W. L., Perez, L. J., Wei, Y., Kraml, C., Semmelhack, M. F., & Bassler, B. L. (2011). Signal production and detection specificity in Vibrio CqsA/CqsS quorum-sensing systems. *Molecular microbiology*, *79*(6), 1407–1417. https://doi.org/10.1111/j.1365-2958.2011.07548.x

Nguyen, F., Starosta, A. L., Arenz, S., Sohmen, D., Dönhöfer, A., & Wilson, D. N. (2014). Tetracycline antibiotics and resistance mechanisms. *Biological chemistry*, *395*(5), 559–575. https://doi.org/10.1515/hsz-2013-0292

Njoroge, J. W., Nguyen, Y., Curtis, M. M., Moreira, C. G., & Sperandio, V. (2012). Virulence meets metabolism: Cra and KdpE gene regulation in enterohemorrhagic Escherichia coli. *mBio*, *3*(5), e00280-12. https://doi.org/10.1128/mBio.00280-12

Nocentini, A., Capasso, C., & Supuran, C. T. (2023). Carbonic Anhydrase Inhibitors as Novel Antibacterials in the Era of Antibiotic Resistance: Where Are We Now? *Antibiotics (Basel, Switzerland)*, *12*(1), 142. https://doi.org/10.3390/antibiotics12010142

Odumosu, O., Nicholas, D., Yano, H., & Langridge, W. (2010). AB toxins: a paradigm switch from deadly to desirable. *Toxins*, *2*(7), 1612–1645. https://doi.org/10.3390/toxins2071612

Oh, E., & Jeon, B. (2015). Synergistic anti-Campylobacter jejuni activity of fluoroquinolone and macrolide antibiotics with phenolic compounds. *Frontiers in microbiology*, *6*, 1129. https://doi.org/10.3389/fmicb.2015.01129

Oki, H., Kawahara, K., Iimori, M., Imoto, Y., Nishiumi, H., Maruno, T., Uchiyama, S., Muroga, Y., Yoshida, A., Yoshida, T., Ohkubo, T., Matsuda, S., Iida, T., &

Nakamura, S. (2022). Structural basis for the toxin-coregulated pilus-dependent secretion of *Vibrio cholerae* colonization factor. *Science advances*, *8*(41), eabo3013. https://doi.org/10.1126/sciadv.abo3013

Onrust, L., Baeyen, S., Haesebrouck, F., Ducatelle, R., & Van Immerseel, F. (2020). Effect of in feed administration of different butyrate formulations on Salmonella Enteritidis colonization and cecal microbiota in broilers. *Veterinary research*, *51*(1), 56. https://doi.org/10.1186/s13567-020-00780-2

Ovung, A., & Bhattacharyya, J. (2021). Sulfonamide drugs: structure, antibacterial property, toxicity, and biophysical interactions. *Biophysical reviews*, *13*(2), 259–272. https://doi.org/10.1007/s12551-021-00795-9

Pant, A., Bag, S., Saha, B., Verma, J., Kumar, P., Banerjee, S., Kumar, B., Kumar, Y., Desigamani, A., Maiti, S., Maiti, T. K., Banerjee, S. K., Bhadra, R. K., Koley, H., Dutta, S., Nair, G. B., Ramamurthy, T., & Das, B. (2020). Molecular insights into the genome dynamics and interactions between core and acquired genomes of *Vibrio cholerae*. *Proceedings of the National Academy of Sciences of the United States of America*, *117*(38), 23762–23773. https://doi.org/10.1073/pnas.2006283117

Patra, T., Koley, H., Ramamurthy, T., Ghose, A. C., & Nandy, R. K. (2012). The Entner-Doudoroff pathway is obligatory for gluconate utilization and contributes to the pathogenicity of Vibrio cholerae. *Journal of bacteriology*, *194*(13), 3377–3385. https://doi.org/10.1128/JB.06379-11

Paul, K., Erhardt, M., Hirano, T., Blair, D. F., & Hughes, K. T. (2008). Energy source of flagellar type III secretion. *Nature, 451(7177),* 489–492. https://doi.org/10.1038/nature06497

Perez-Soto, N., Moule, L., Crisan, D. N., Insua, I., Taylor-Smith, L. M., Voelz, K., Fernandez-Trillo, F., & Krachler, A. M. (2017). Engineering microbial physiology with synthetic polymers: cationic polymers induce biofilm formation in *Vibrio cholerae* and downregulate the expression of virulence genes. *Chemical science*, *8*(8), 5291–5298. https://doi.org/10.1039/c7sc00615b

Plecha, S. C., & Withey, J. H. (2015). Mechanism for inhibition of Vibrio cholerae ToxT activity by the unsaturated fatty acid components of bile. *Journal of bacteriology*, *197*(10), 1716–1725. https://doi.org/10.1128/JB.02409-14

Podobnik, M., Savory, P., Rojko, N., Kisovec, M., Wood, N., Hambley, R., Pugh, J., Wallace, E. J., McNeill, L., Bruce, M., Liko, I., Allison, T. M., Mehmood, S., Yilmaz, N., Kobayashi, T., Gilbert, R. J., Robinson, C. V., Jayasinghe, L., & Anderluh, G. (2016). Crystal structure of an invertebrate cytolysin pore reveals unique properties and mechanism of assembly. *Nature communications*, *7*, 11598. https://doi.org/10.1038/ncomms11598

Pollitzer R. (1954). Cholera studies. 1. History of the disease. *Bulletin of the World Health Organization*, *10*(3), 421–461.

Prince, A., Roy, S., & McDonald, D. (2022). Exploration of the Antimicrobial Synergy between Selected Natural Substances on Streptococcus mutans to Identify Candidates for the Control of Dental Caries. *Microbiology spectrum*, *10*(3), e0235721. https://doi.org/10.1128/spectrum.02357-21

Rahaman, M. H., Islam, T., Colwell, R. R., & Alam, M. (2015). Molecular tools in understanding the evolution of Vibrio cholerae. *Frontiers in microbiology*, *6*, 1040. https://doi.org/10.3389/fmicb.2015.01040

Ramamurthy, T., Nandy, R. K., Mukhopadhyay, A. K., Dutta, S., Mutreja, A., Okamoto, K., Miyoshi, S. I., Nair, G. B., & Ghosh, A. (2020). Virulence Regulation and Innate Host Response in the Pathogenicity of *Vibrio cholerae*. *Frontiers in cellular and infection microbiology*, *10*, 572096. https://doi.org/10.3389/fcimb.2020.572096

Rasko, D. A., & Sperandio, V. (2010). Anti-virulence strategies to combat bacteria-mediated disease. *Nature reviews. Drug discovery*, *9*(2), 117–128. https://doi.org/10.1038/nrd3013

RAYMOND, S., & WEINTRAUB, L. (1959). Acrylamide gel as a supporting medium for zone electrophoresis. *Science (New York, N.Y.)*, *130*(3377), 711. https://doi.org/10.1126/science.130.3377.711

Reading, C., & Cole, M. (1977). Clavulanic acid: a beta-lactamase-inhiting beta-lactam from Streptomyces clavuligerus. *Antimicrobial agents and chemotherapy*, *11*(5), 852–857. https://doi.org/10.1128/AAC.11.5.852

Recharla, N., Geesala, R., & Shi, X. Z. (2023). Gut Microbial Metabolite Butyrate and Its Therapeutic Role in Inflammatory Bowel Disease: A Literature Review. *Nutrients*, *15*(10), 2275. https://doi.org/10.3390/nu15102275

Ruhe, J. J., Monson, T., Bradsher, R. W., & Menon, A. (2005). Use of long-acting tetracyclines for methicillin-resistant Staphylococcus aureus infections: case series and review of the literature. *Clinical infectious diseases: an official publication of the Infectious Diseases Society of America*, *40*(10), 1429–1434. https://doi.org/10.1086/429628

Richard, A. L., Withey, J. H., Beyhan, S., Yildiz, F., & DiRita, V. J. (2010). The Vibrio cholerae virulence regulatory cascade controls glucose uptake through activation of TarA, a small regulatory RNA. *Molecular microbiology*, *78*(5), 1171–1181. https://doi.org/10.1111/j.1365-2958.2010.07397.x

Roca, I., Akova, M., Baquero, F., Carlet, J., Cavaleri, M., Coenen, S., Cohen, J., Findlay, D., Gyssens, I., Heuer, O. E., Kahlmeter, G., Kruse, H., Laxminarayan, R., Liébana, E., López-Cerero, L., MacGowan, A., Martins, M., Rodríguez-Baño, J., Rolain, J. M., Segovia, C., … Vila, J. (2015). The global threat of antimicrobial resistance: science for intervention. *New microbes and new infections*, *6*, 22–29. https://doi.org/10.1016/j.nmni.2015.02.007

Rollenhagen, J. E., Kalsy, A., Cerda, F., John, M., Harris, J. B., Larocque, R. C., Qadri, F., Calderwood, S. B., Taylor, R. K., & Ryan, E. T. (2006). Transcutaneous immunization with toxin-coregulated pilin A induces protective immunity against Vibrio cholerae O1 El Tor challenge in mice. *Infection and immunity*, *74*(10), 5834–5839. https://doi.org/10.1128/IAI.00438-06

Roy, S., Patra, T., Golder, T., Chatterjee, S., Koley, H., & Nandy, R. K. (2016). Characterization of the gluconate utilization system of Vibrio cholerae with special reference to virulence modulation. *Pathogens and disease*, *74*(8), 1-10. https://doi.org/10.1093/femspd/ftw085

Saha, P., Das, B., & Chaudhuri, K. (2013). Role of 6-gingerol in reduction of cholera toxin activity in vitro and in vivo. *Antimicrobial agents and chemotherapy*, *57*(9), 4373–4380. https://doi.org/10.1128/AAC.00122-13

Samal, D., Turuk, J., Nayak, S. R., Pany, S., Pal, B. B., & Pati, S. (2025). Genomic insights into the dynamic antibiotic resistance landscape of Vibrio cholerae during the Cholera outbreak 2022 in Odisha, India. *Scientific reports*, *15*(1), 1503. https://doi.org/10.1038/s41598-024-81596-4

Samgane, G., Karaçam, S., & Tunçer Çağlayan, S. (2024). Unveiling the synergistic potency of chlorhexidine and azithromycin in combined action. *Naunyn-Schmiedeberg's archives of pharmacology*, *397*(8), 5975–5987. https://doi.org/10.1007/s00210-024-03010-0

Sarwar, S., Ali, A., Pal, M., & Chakrabarti, P. (2017). Zinc oxide nanoparticles provide anti-cholera activity by disrupting the interaction of cholera toxin with the human GM1 receptor. *The Journal of biological chemistry*, *292*(44), 18303–18311. https://doi.org/10.1074/jbc.M117.793240

Shakhnovich, E. A., Hung, D. T., Pierson, E., Lee, K., & Mekalanos, J. J. (2007). Virstatin inhibits dimerization of the transcriptional activator ToxT. *Proceedings of the National Academy of Sciences of the United States of America*, *104*(7), 2372–2377. https://doi.org/10.1073/pnas.0611643104

Sharma, A., Gupta, V. K., & Pathania, R. (2019). Efflux pump inhibitors for bacterial pathogens: From bench to bedside. *The Indian journal of medical research*, *149*(2), 129–145. https://doi.org/10.4103/ijmr.IJMR_2079_17

Shimada, T., Arakawa, E., Itoh, K., Okitsu, T., Matsushima, A., Asai, Y., Yamai, S., Nakazato, T., Balakrish Nair, G., John Albert, M., & Takeda, Y. (1994). Extended Serotyping Scheme for Vibrio cholerae. *Current Microbiology 28,* 175–178. https://doi.org/10.1007/BF01571061

Skorupski, K., & Taylor, R. K. (1997). Control of the ToxR virulence regulon in Vibrio cholerae by environmental stimuli. *Molecular microbiology*, *25*(6), 1003–1009. https://doi.org/10.1046/j.1365-2958.1997.5481909.x

Spangler B. D. (1992). Structure and function of cholera toxin and the related Escherichia coli heat-labile enterotoxin. *Microbiological reviews*, *56*(4), 622–647. https://doi.org/10.1128/mr.56.4.622-647.1992

Stokes, J. M., MacNair, C. R., Ilyas, B., French, S., Côté, J. P., Bouwman, C., Farha, M. A., Sieron, A. O., Whitfield, C., Coombes, B. K., & Brown, E. D. (2017). Pentamidine sensitizes Gram-negative pathogens to antibiotics and overcomes acquired colistin resistance. *Nature microbiology*, *2*, 17028. https://doi.org/10.1038/nmicrobiol.2017.28

Sudano Roccaro, A., Blanco, A. R., Giuliano, F., Rusciano, D., & Enea, V. (2004). Epigallocatechin-gallate enhances the activity of tetracycline in staphylococci by inhibiting its efflux from bacterial cells. *Antimicrobial agents and chemotherapy*, *48*(6), 1968–1973. https://doi.org/10.1128/AAC.48.6.1968-1973.2004

Sunkara, L. T., Zeng, X., Curtis, A. R., & Zhang, G. (2014). Cyclic AMP synergizes with butyrate in promoting β-defensin 9 expression in chickens. *Molecular immunology*, *57*(2), 171–180. https://doi.org/10.1016/j.molimm.2013.09.003

Supuran C. T. (2011). Bacterial carbonic anhydrases as drug targets: toward novel antibiotics? *Frontiers in pharmacology*, *2*, 34. https://doi.org/10.3389/fphar.2011.00034

Syed, K. A., Beyhan, S., Correa, N., Queen, J., Liu, J., Peng, F., Satchell, K. J., Yildiz, F., & Klose, K. E. (2009). The Vibrio cholerae flagellar regulatory hierarchy controls expression of virulence factors. *Journal of bacteriology*, *191*(21), 6555–6570. https://doi.org/10.1128/JB.00949-09

Syed, K.A., Klose, K.E. (2011). *Vibrio cholerae* Flagellar Synthesis and Virulence. In: Ramamurthy, T., Bhattacharya, S. (eds) Epidemiological and Molecular Aspects on Cholera. *Infectious Disease. Springer, New York, NY.* https://doi.org/10.1007/978-1-60327-265-0_11

Tamma, P. D., Cosgrove, S. E., & Maragakis, L. L. (2012). Combination therapy for treatment of infections with gram-negative bacteria. *Clinical microbiology reviews*, *25*(3), 450–470. https://doi.org/10.1128/CMR.05041-11

Tamplin, M. L., Gauzens, A. L., Huq, A., Sack, D. A., & Colwell, R. R. (1990). Attachment of Vibrio cholerae serogroup O1 to zooplankton and phytoplankton of Bangladesh waters. *Applied and environmental microbiology*, *56*(6), 1977–1980. https://doi.org/10.1128/aem.56.6.1977-1980.1990

Taylor, R. K., Miller, V. L., Furlong, D. B., & Mekalanos, J. J. (1987). Use of phoA gene fusions to identify a pilus colonization factor coordinately regulated with cholera toxin. *Proceedings of the National Academy of Sciences of the United States of America*, *84*(9), 2833–2837. https://doi.org/10.1073/pnas.84.9.2833

Taylor, D. L., Kahawita, T. M., Cairncross, S., & Ensink, J. H. (2015). The Impact of Water, Sanitation and Hygiene Interventions to Control Cholera: A Systematic Review. *PloS one*, *10*(8), e0135676. https://doi.org/10.1371/journal.pone.0135676

Thaker, M., Spanogiannopoulos, P., & Wright, G. D. (2010). The tetracycline resistome. *Cellular and molecular life sciences: CMLS*, *67*(3), 419–431. https://doi.org/10.1007/s00018-009-0172-6

Towbin, H., Staehelin, T., & Gordon, J. (1979). Electrophoretic transfer of proteins from polyacrylamide gels to nitrocellulose sheets: procedure and some applications. *Proceedings of the National Academy of Sciences of the United States of America*, *76*(9), 4350–4354. https://doi.org/10.1073/pnas.76.9.4350

Trirocco, R., Pasqua, M., Tramonti, A., Grossi, M., Colonna, B., Paiardini, A., & Prosseda, G. (2023). Fatty Acids Abolish *Shigella* Virulence by Inhibiting Its Master Regulator, VirF. *Microbiology spectrum*, *11*(3), e0077823. https://doi.org/10.1128/spectrum.00778-23

Trucksis, M., Michalski, J., Deng, Y. K., & Kaper, J. B. (1998). The Vibrio cholerae genome contains two unique circular chromosomes. *Proceedings of the National Academy of Sciences of the United States of America*, *95*(24), 14464–14469. https://doi.org/10.1073/pnas.95.24.14464

Tükenmez, H., Sarkar, S., Anoosheh, S., Kruchanova, A., Edström, I., Harrison, G. A., Stallings, C. L., Almqvist, F., & Larsson, C. (2021). Mycobacterium tuberculosis Rv3160c is a TetR-like transcriptional repressor that regulates expression of

the putative oxygenase Rv3161c. *Scientific reports*, *11*(1), 1523. https://doi.org/10.1038/s41598-021-81104-y

Turner, J. W., Good, B., Cole, D., & Lipp, E. K. (2009). Plankton composition and environmental factors contribute to Vibrio seasonality. *The ISME journal*, *3*(9), 1082–1092. https://doi.org/10.1038/ismej.2009.50

Turner, J. W., Malayil, L., Guadagnoli, D., Cole, D., & Lipp, E. K. (2014). Detection of Vibrio parahaemolyticus, Vibrio vulnificus and Vibrio cholerae with respect to seasonal fluctuations in temperature and plankton abundance. *Environmental microbiology*, *16*(4), 1019–1028. https://doi.org/10.1111/1462-2920.12246

Vale, F. F., Lehours, P., & Yamaoka, Y. (2022). Editorial: The Role of Mobile Genetic Elements in Bacterial Evolution and Their Adaptability. *Frontiers in microbiology*, *13*, 849667. https://doi.org/10.3389/fmicb.2022.849667

Valiente, E., Davies, C., Mills, D. C., Getino, M., Ritchie, J. M., & Wren, B. W. (2018). Vibrio cholerae accessory colonisation factor AcfC: a chemotactic protein with a role in hyperinfectivity. *Scientific reports*, *8*(1), 8390. https://doi.org/10.1038/s41598-018-26570-7

van de Wouw, M., Schellekens, H., Dinan, T. G., & Cryan, J. F. (2017). Microbiota-Gut-Brain Axis: Modulator of Host Metabolism and Appetite. *The Journal of nutrition*, *147*(5), 727–745. https://doi.org/10.3945/jn.116.240481

Vercruysse, M., Köhrer, C., Davies, B. W., Arnold, M. F., Mekalanos, J. J., RajBhandary, U. L., & Walker, G. C. (2014). The highly conserved bacterial RNase YbeY is essential in Vibrio cholerae, playing a critical role in virulence, stress regulation, and RNA processing. *PLoS pathogens*, *10*(6), e1004175. https://doi.org/10.1371/journal.ppat.1004175

Verma, J., Bag, S., Saha, B., Kumar, P., Ghosh, T. S., Dayal, M., Senapati, T., Mehra, S., Dey, P., Desigamani, A., Kumar, D., Rana, P., Kumar, B., Maiti, T. K., Sharma, N. C., Bhadra, R. K., Mutreja, A., Nair, G. B., Ramamurthy, T., & Das, B. (2019). Genomic plasticity associated with antimicrobial resistance in *Vibrio cholerae*. *Proceedings of the National Academy of Sciences of the United States of America*, *116*(13), 6226–6231. https://doi.org/10.1073/pnas.1900141116

Vezzulli, L., Pruzzo, C., Huq, A., & Colwell, R. R. (2010). Environmental reservoirs of Vibrio cholerae and their role in cholera. *Environmental microbiology reports*, *2*(1), 27–33. https://doi.org/10.1111/j.1758-2229.2009.00128.x

Villeneuve, S., Souchon, H., Riottot, M. M., Mazie, J. C., Lei, P., Glaudemans, C. P., Kovác, P., Fournier, J. M., & Alzari, P. M. (2000). Crystal structure of an anti-carbohydrate antibody directed against Vibrio cholerae O1 in complex with antigen: molecular basis for serotype specificity. *Proceedings of the National Academy of Sciences of the United States of America*, *97*(15), 8433–8438. https://doi.org/10.1073/pnas.060022997

Waldor, M. K., & Mekalanos, J. J. (1996). Lysogenic conversion by a filamentous phage encoding cholera toxin. *Science (New York, N.Y.)*, *272*(5270), 1910–1914. https://doi.org/10.1126/science.272.5270.1910

Wands, A. M., Cervin, J., Huang, H., Zhang, Y., Youn, G., Brautigam, C. A., Matson Dzebo, M., Björklund, P., Wallenius, V., Bright, D. K., Bennett, C. S., Wittung-Stafshede, P., Sampson, N. S., Yrlid, U., & Kohler, J. J. (2018). Fucosylated Molecules Competitively Interfere with Cholera Toxin Binding to Host Cells. *ACS infectious diseases*, *4*(5), 758–770. https://doi.org/10.1021/acsinfecdis.7b00085

Wang, B. X., Takagi, J., McShane, A., Park, J. H., Aoki, K., Griffin, C., Teschler, J., Kitts, G., Minzer, G., Tiemeyer, M., Hevey, R., Yildiz, F., & Ribbeck, K. (2023). Host-derived O-glycans inhibit toxigenic conversion by a virulence-encoding phage in Vibrio cholerae. *The EMBO journal*, *42*(3), e111562. https://doi.org/10.15252/embj.2022111562

Wang, F., Wu, H., Fan, M., Yu, R., Zhang, Y., Liu, J., Zhou, X., Cai, Y., Huang, S., Hu, Z., & Jin, X. (2020). Sodium butyrate inhibits migration and induces AMPK-mTOR pathway-dependent autophagy and ROS-mediated apoptosis via the miR-139-5p/Bmi-1 axis in human bladder cancer cells. *FASEB journal: official publication of the Federation of American Societies for Experimental Biology*, *34*(3), 4266–4282. https://doi.org/10.1096/fj.201902626R

Wang, N., Luo, J., Deng, F., Huang, Y., & Zhou, H. (2022). Antibiotic Combination Therapy: A Strategy to Overcome Bacterial Resistance to Aminoglycoside Antibiotics. *Frontiers in pharmacology*, *13*, 839808. https://doi.org/10.3389/fphar.2022.839808

Wang, S., Wang, J., Mou, H., Luo, B., & Jiang, X. (2015). Inhibition of adhesion of intestinal pathogens (Escherichia coli, Vibrio cholerae, Campylobacter jejuni, and Salmonella Typhimurium) by common oligosaccharides. *Foodborne pathogens and disease*, *12*(4), 360–365. https://doi.org/10.1089/fpd.2014.1835

Waters, C. M., Lu, W., Rabinowitz, J. D., & Bassler, B. L. (2008). Quorum sensing controls biofilm formation in Vibrio cholerae through modulation of cyclic di-GMP levels and repression of vpsT. *Journal of bacteriology*, *190*(7), 2527–2536. https://doi.org/10.1128/JB.01756-07

Watnick, P. I., Fullner, K. J., & Kolter, R. (1999). A role for the mannose-sensitive hemagglutinin in biofilm formation by Vibrio cholerae El Tor. *Journal of bacteriology*, *181*(11), 3606–3609. https://doi.org/10.1128/JB.181.11.3606-3609.1999

Wei, Y., Ng, W. L., Cong, J., & Bassler, B. L. (2012). Ligand and antagonist driven regulation of the Vibrio cholerae quorum-sensing receptor CqsS. *Molecular microbiology*, *83*(6), 1095–1108. https://doi.org/10.1111/j.1365-2958.2012.07992.x

Withey, J. H., & DiRita, V. J. (2005). Activation of both acfA and acfD transcription by Vibrio cholerae ToxT requires binding to two centrally located DNA sites in an inverted repeat conformation. *Molecular microbiology*, *56*(4), 1062–1077. https://doi.org/10.1111/j.1365-2958.2005.04589.x

Withey, J. H., & DiRita, V. J. (2006). The toxbox: Specific DNA sequence requirements for activation of Vibrio cholerae virulence genes by ToxT. *Molecular Microbiology, 59(6),* 1779–1789. https://doi.org/10.1111/j.1365-2958.2006.05053.x

Withey, J. H., Nag, D., Plecha, S. C., Sinha, R., & Koley, H. (2015). Conjugated Linoleic Acid Reduces Cholera Toxin Production In Vitro and In Vivo by Inhibiting Vibrio cholerae ToxT Activity. *Antimicrobial agents and chemotherapy*, *59*(12), 7471–7476. https://doi.org/10.1128/AAC.01029-15

Wolska, K. I., Grześ, K., & Kurek, A. (2012). Synergy between novel antimicrobials and conventional antibiotics or bacteriocins. *Polish journal of microbiology*, *61*(2), 95–104.

Wood, T. I., Griffith, K. L., Fawcett, W. P., Jair, K. W., Schneider, T. D., & Wolf, R. E., Jr (1999). Interdependence of the position and orientation of SoxS binding sites in the transcriptional activation of the class I subset of Escherichia coli superoxide-inducible promoters. *Molecular microbiology*, *34*(3), 414–430. https://doi.org/10.1046/j.1365-2958.1999.01598.x

Woodbrey, A. K., Onyango, E. O., Pellegrini, M., Kovacikova, G., Taylor, R. K., Gribble, G. W., & Kull, F. J. (2017). A new class of inhibitors of the AraC family virulence regulator Vibrio cholerae ToxT. *Scientific reports*, *7*, 45011. https://doi.org/10.1038/srep45011

Yamamoto, S., Okujo, N., Fujita, Y., Saito, M., Yoshida, T., & Shinoda, S. (1993). Structures of two polyamine-containing catecholate siderophores from Vibrio fluvialis. *Journal of biochemistry*, *113*(5), 538–544. https://doi.org/10.1093/oxfordjournals.jbchem.a124079

Yan, J., Liu, Q., Xue, X., Li, J., Li, Y., Su, Y., & Cao, B. (2023). The Response Regulator VC1795 of *Vibrio* Pathogenicity Island-2 Contributes to Intestinal Colonization by *Vibrio cholerae*. *International journal of molecular sciences*, *24*(17), 13523. https://doi.org/10.3390/ijms241713523

Yildiz, F. H., & Visick, K. L. (2009). Vibrio biofilms: so much the same yet so different. *Trends in microbiology*, *17*(3), 109–118. https://doi.org/10.1016/j.tim.2008.12.004

Zahid, M. S., Awasthi, S. P., Asakura, M., Chatterjee, S., Hinenoya, A., Faruque, S. M., & Yamasaki, S. (2015). Suppression of Virulence of Toxigenic Vibrio cholerae by Anethole through the Cyclic AMP (cAMP)-cAMP Receptor Protein Signaling System. *PloS one*, *10*(9), e0137529. https://doi.org/10.1371/journal.pone.0137529

Zhang, L., Liu, C., Jiang, Q., & Yin, Y. (2021). Butyrate in Energy Metabolism: There Is Still More to Learn. *Trends in endocrinology and metabolism: TEM*, *32*(3), 159–169. https://doi.org/10.1016/j.tem.2020.12.003

Zhou, D., Pan, Q., Xin, F. Z., Zhang, R. N., He, C. X., Chen, G. Y., Liu, C., Chen, Y. W., & Fan, J. G. (2017). Sodium butyrate attenuates high-fat diet-induced steatohepatitis in mice by improving gut microbiota and gastrointestinal barrier. *World journal of gastroenterology*, *23*(1), 60–75. https://doi.org/10.3748/wjg.v23.i1.60

Zhu, J., & Mekalanos, J. J. (2003). Quorum sensing-dependent biofilms enhance colonization in Vibrio cholerae. *Developmental cell*, *5*(4), 647–656. https://doi.org/10.1016/s1534-5807(03)00295-8

Zhu, W., Gao, J., Liu, H., Liu, J., Jin, T., Qin, N., Ren, X., & xia, X. (2022). Antibiofilm effect of sodium butyrate against Vibrio parahaemolyticus. *Food Control, 131*. https://doi.org/10.1016/j.foodcont.2021.108422

Zimmerman, M. A., Singh, N., Martin, P. M., Thangaraju, M., Ganapathy, V., Waller, J. L., Shi, H., Robertson, K. D., Munn, D. H., & Liu, K. (2012). Butyrate suppresses colonic inflammation through HDAC1-dependent Fas upregulation and Fas-mediated apoptosis of T cells. *American journal of physiology. Gastrointestinal and liver physiology*, *302*(12), G1405–G1415. https://doi.org/10.1152/ajpgi.00543.2011

Chapter 10

Appendix

Appendix

Table 10.1. Bacterial strains and plasmid strains used in this study.

Strain	Relevant genotype and/or phenotype	Source/ Reference
V. cholerae N16961	O1 El Tor	Lab stock
V. cholerae IDH1986	O1 El Tor	Lab stock
V. cholerae IDH07976	O1 El Tor	Lab stock
V. cholerae IDH14062	O1 El Tor	Lab stock
V. cholerae IDH13966	O1 El Tor	Lab stock
V. cholerae V32	O1 El Tor	Lab stock
V. cholerae V24	O1 El Tor	Lab stock
V. cholerae V100	O1 El Tor	Lab stock
V. cholerae Micro78	O1 El Tor	Lab stock
C6709	O1 El Tor	Lab stock
E. coli B2	Not available	Lab stock
E. coli IDH15978	Not available	Lab stock

Table 10.2. Different media used in this study.

Media	Constituents	pH
Luria Broth (LB)	1 % Bactopeptone (Difco, USA), 0.5 % Yeast Extract (Difco, USA), and 0.5 - 1.0 % NaCl dissolved in distilled water followed by sterilization at 15 psi for 15 min.	7.2
Luria Agar or LA (for plate)	LB containing 1.5 % Bactoagar (Difco, USA), sterilization was done at 15 psi for 15 min.	7.2
M9 minimal (M9M) medium	5× M9M salts [(Difco, USA), 56.4 g dissolved in distilled water followed by sterilization at 10 lb for 10 min] as a stock, from 5× stock solution 1× complete M9M medium was prepared by using sterile distilled water followed by addition of filter sterilized 2 mM $MgSO_4$, 0.4 % glucose or 0.5% Na-DL-Lactate, 0.1 mM $CaCl_2$. To prepare M9M agar, 1.5% agar was added in 1× M9M complete medium followed by sterilization at 10 psi for 10 min.	7.4

Table 10.3. Different buffers and solutions used in this study.

For isolation of plasmid DNA from bacterial cells	
Cell Resuspension Solution (CRS)	50 mM Tris-HCl (pH 7.5), 10 mM EDTA, 100 µg/ml RNase A
Cell Lysis Solution (CLS)	0.2 M NaOH, 1% SDS
Neutralization Solution (NS)	1.32 M Potassium Acetate (pH 4.8)
Column Wash Solution (CWS)	80 mM Potassium acetate, 8.3 mM Tris – HCl (pH 7.5), 40 µM EDTA, 55% 95% Ethanol
For agarose gel electrophoresis of DNA	
50× TAE	242 g Tris base in double-distilled H2O, 57.1 ml Glacial acetic acid, 100 ml 0.5 M EDTA solution (pH 8.0). Adjust final volume to 1 L. [Molarity in 1× TAE – EDTA disodium salt, 1 mM; Tris, 40 mM; Glacial acetic acid, 20 mM]
10× DNA gel loading dye	0.25 % (w/v) Bromophenol blue, 0.25 % (w/v) Xylene cyanol, 50 mM EDTA, 50 % (v/v) glycerol, 10% SDS in distilled water.
Gel staining solution	Ethidium bromide stock solution (10 mg/ml) in distilled water. The final working solution was of 0.5 µg/ml concentration, which was used for staining DNA fragments.
For transformation of *E. coli* cells with plasmid DNA	
Transformation buffer	10 mM Tris-HCl, 100 mM $CaCl_2.2H_2O$ (pH 7.6); sterilized at 15 lb for 15 min
For electroporation of *V. cholerae* cells with plasmid DNA	
Electroporation buffer	272 mM sucrose, 1 mM HEPES (pH 8.0), 10% Glycerol in Milli-Q water; sterilized at 15 psi for 15 min

Table 10.3. Different buffers and solutions used in this study (contd.).

For Selection of recombinants	
Isopropyl-D-thiogalactopyranoside (IPTG) stock solution	0.1 M IPTG prepared in sterile distilled water and stored at -20°C.
5-Bromo-4-chloro-3-D-galactoside (X-gal) stock solution	40 mg/ml X-gal dissolved) in N, N'- dimethyl formamide (DMF) and stored at -20°C in a dark container.

LA plate with antibiotics/IPTG/X-Gal

1.5% of LA plate was incubated at 37 °C for 30 min, and 100 µl of 100 mM IPTG and 20 µl of 40 mg/ml X-Gal were spread on the LA plate. The plate was incubated for 30 min at 37 °C.

L-arabinose solution	20 % (w/v) L-arabinose in water and filter sterilized, stored at -20°C.

For SDS-PAGE	
Solution A	29.2% Acrylamide, 0.8% Bis-acrylamide dissolved in Elix water. The solution was stored in light resistant container.
Solution B	1.5 M Tris HCl (pH 8.8), 0.4% SDS
Solution C	0.5 M Tris HCl (pH 6.8), 0.4% SDS
Gel Running buffer	0.025 M Tris base, 0.192 M Glycine, 0.1% SDS dissolved in Elix Water. pH 8.3
5×Gel loading Dye	100 mM Tris-HCl pH 6.8, 4% (w/v) SDS, 0.2% (w/v) Bromophenol blue, 20% (v/v) Glycerol, 200 mM β-mercaptoethanol.
Staining Solution	0.25 % (w/v) Coomassie Blue (R-250) was dissolved in a solution of 50 % methanol (v/v), 40 % water and 10 % acetic acid (v/v) and the solution was filtered through Whatman filter paper (No. 1).
Destaining Solution	40% methanol (v/v), 10% acetic acid (v/v) and 50 % (v/v) water

Table 10.3. Different buffers and solutions used in this study (contd.).

For Western blotting	
Transfer Buffer	25 mM Tris, 192 mM glycine, 0.05% Glycine, 20 % (v/v) methanol.
Washing Buffer (TBS and TBST buffer)	Solution TBS was prepared by adding 10 mM Tris and 150 mM NaCl and adjusting pH to 7.4. To this solution 0.1 % (v/v) Tween 20 was added to get the TBS-T solution.
Blocking Buffer	5 % (w/v) BSA dissolved in TBST buffer.
Bicarbonate buffer	168 mg $NaHCO_3$, 4.06 mg $MgCl_2$ for 20 ml, pH adjusted to 9.8 with NaOH
Ponceau S	1 % (w/v) Ponceau S in 7 % (v/v) acetic acid.
For AKI medium preparation	
3% $NaHCO_3$	3% (w/v) $NaHCO_3$ in distilled water and filter sterilized.
For ELISA	
1× PBS buffer	137 mM NaCl, 2.7 mM KCl, 10 mM Na_2HPO_4, 2 mM KH_2PO_4 (pH 7.4).
PBS Tween-20 (PBS-T) solution	0.05 % (v/v) Tween-20 in 1X PBS.
For isolation of cytoplasmic fraction of recombinant proteins from the inclusion bodies	
Cell Resuspension Buffer (CRB)	50 mM Tris-HCl, 50 mM NaCl, 0.5 mM EDTA (3.72 mg / 20 ml), 1 mM TCEP (make 1 M TCEP stock and store at -80°C.), 5% Glycerol, add protease inhibitor cocktail or 1 mM PMSF (final concentration), pH 8.0
Inclusion Wash Buffer (IWB)	50 mM Tris-HCl, 50 mM NaCl, 0.5 mM EDTA (3.72 mg / 20 ml), 1 mM TCEP (make 1 M TCEP stock and store at -80°C.), 5% Glycerol, 0.125 M NDSB-201 (make 1.5 M NDSB stock solution and store at -80°C), pH 8.0
Denaturation Buffer (DB)	50 mM Tris-HCl, 0.2 M NaCl, 20 mM EDTA, 8 M Urea, pH 8.0

Table 10.3. Different buffers and solutions used in this study (contd.).

For isolation of cytoplasmic fraction of recombinant proteins from the inclusion bodies (contd.)	
Cell lysis buffer	50 mM Potassium phosphate buffer pH 7.8 [prepare the potassium phosphate buffer by mixing 0.3 ml KH_2PO_4 and 4.7 ml K_2HPO_4 from their respective 1 M stock], 400 mM NaCl, 100 mM KCl, 10% Glycerol, 0.5% Triton X-100, 10 mM Imidazole
Sonication buffer	20 mM Tris-HCl pH 7.4, 5 mM PMSF, 1 mM DTT, 20% v/v Glycerol
Binding buffer (buffer A)	25 mM Tris, 100 mM NaCl, 0.1% Triton X-100, and 7 M urea at pH 7.5
Washing buffer	25 mM Tris, 100 mM NaCl, 0.1% Triton X-100, and 7 M urea at pH 7.5, 10 mM Imidazole
Elution buffer	25 mM Tris, 100 mM NaCl, 0.1% Triton X-100, and 7 M urea at pH 7.5, 250 mM Imidazole
For maintenance of tissue culture cells	
Dulbecco's Modified Eagle's Medium (DMEM) Complete media	13.5 g/l DMEM, 3.7 g/l Sodium Bicarbonate, 100 ml FBS, 10 ml Antibiotics (Penicillin-Streptomycin), 10 ml Non-Essential Amino Acid, volume adjusted to 1 l with MilliQ water, pH 7.4
Dulbecco's Modified Eagle's Medium (DMEM) Incomplete media	13.5 g/l DMEM, 3.7 g/l Sodium Bicarbonate, 5 ml FBS, 10 ml Non-Essential Amino Acid, volume adjusted to 1 l with MilliQ water, pH 7.4
For Purification of DNA from Agarose gel	
Membrane Wash Solution (MWS)	10 mM Potassium acetate (pH 5.0), 80% 95% Ethanol, 16.7 µM EDTA (pH 8.0)
Membrane Binding Solution (MBS)	4.5 M Guanidine Isothiocyanate, 0.5 M Potassium acetate (pH 5.0)

Table 10.3. Different buffers and solutions used in this study (contd.).

Protein-DNA Binding Experiments (Chromatin Immunoprecipitation)	
lysis buffer	10 mM Tris-HCl, pH 8.0; 50 mM NaCl, containing 20 ng/µl RNase A and 10^5 kU of ready lyse lysozyme
IP buffer	200 mM Tris HCl, pH 7.5; 600 mM NaCl; 4% Triton X-100, protease inhibitor cocktail or 1 mM PMSF (final concentration)
Wash buffer	500 mM NaCl lysis buffer
LiCl immune complex buffer	20 mM Tris–HCl (pH 8.0), 0.25 M LiCl, 1 mM EDTA, 0.5% (wt/vol) NP-40, 0.5% (wt/vol) DOC, and 1% (wt/vol) PMSF
TE buffer	10 mM Tris–HCl, pH 8.0, 1 mM EDTA
Protein-DNA Binding Experiments (Electrophoretic mobility shift assay)	
Binding buffer	10 mM Tris-HCl (pH 7.5), 100 mM KCl, 1 mM EDTA, 1 mM dithiothreitol, 200 µg of bovine serum albumin per ml, and 10% glycerol.

Table 10.4.1 List of Primers used in quantitative real-time PCR experiment.

Primers	Sequence (5' – 3')	Gene Locus
CtxA RT FP	CCTAACAAATCCCGTCTGAGTT	VC1457
CtxA RT RP	GTCTTATGCCAAGAGGACAGAG	
ToxR RT FP	GACGAATAAATCGGCTCCAAAC	VC0984
ToxR RT RP	AGGGTGGTTATTCGGCATATT	
ToxS RT FP	GTTGTGCATCCATCTTGAACAG	VC0983
ToxS RT RP	GGTTACGCCAGTCGAGTTT	
TcpH RT FP	CATTGCCAGATCCTAGCTCTC	VC0827
TcpH RT RP	CAACCTTTGCCGAGTTGATAAAT	
TcpP RT FP	CAGCTCTGAAAGTCTAACTCAGG	VC0826
TcpP RT RP	GACTACAGTCAGCTTCATCAACA	
ToxT RT FP	TTACTGATGATCTTGATGCTATGGA	VC0838
ToxT RT RP	ATTCTCTAAACTTTACTCCTCGAGAC	
CtxB RT FP	TGTGCAGAATACCACAACAC	VC1456
CtxB RT RP	TGTGAATCTATATGTTGACTACCT	
TcpA RT FP	CGAAACTCTGCAGCGAATAAAG	VC0828
TcpA RT RP	CGTTTCGAAATCACCAAGATCAG	
RecA RT FP	GTCGCAAGCAATGCGTAAAC	VC0543
RecA RT RP	CCAAACGAACAGAAGCGTAGA	
VpsH RT FP	GCTACGTTAGCCCGCTATTT	VC0924
VpsH RT RP	CGTGTCTCAATCACCTGTCTATC	
RbmB RT FP	ATCCTGTGTACCGTGCATTT	VC0929
RbmB RT RP	TCGATACCACCAGGCTCTAT	
VpsR RT FP	CGAAAGTGGTACTGGGAAAGA	VC0665
VpsR RT RP	TTCTGACATAGCTCGGCAATTA	
VpsE RT FP	CTCCATCCTTTCGCTCTCTTG	VC0921
VpsE RT RP	TTTAGGCCGCTGAGGTAAAC	
AldA RT FP	CAGAGCCGAAACCATTAACAAC	VC0819
AldA RT RP	CTCAAACCTGCAGAACAAACC	
HlyA RT FP	CACATCACCCAGTAGCAAGT	VC0271
HlyA RT RP	GCTGATTTACAGCGAAGAGAAAG	
TcpB RT FP	CCTGATCGTGTCGGGTATTT	VC0829
TcpB RT RP	CCAACGCCAGAGTTCTATCTT	
TcpE RT FP	CTCATCTATGATCACGCCTAGC	VC0836
TcpE RT RP	CTCACAGGAAGTACAGACTCAAA	
AcfA RT FP	TGTGTATGTGTCACACCAACTT	VC0844
AcfA RT RP	CACGAATGGAGCTCTGAGATTG	
RtxC RT FP	TGATCTTCGTCGTCGTGTATTT	VC1450
RtxC RT RP	CACTGCACCTTTCGGATACA	

Table 10.4.2 List of Primers used in EMSA.

Primer	Sequence (5' – 3')	Amplicon length (bp)
EMSA TcpA FP	ATTCTCTATGTGAATGTTGCA	150 bp
EMSA TcpA RP	GTCCTTTTTTAAAGAAAAAGAAA	
Non-specific DNA FP	ATTGCTGAGCTAAAGGGGCTGG	150 bp
Non-specific DNA RP	TGGTATTGCAGGTAGCTAGGGT	

Table 10.4.3 List of Primers used in ChIP.

Primer	Sequence (5' – 3')	Amplicon length (bp)
ChIP Ctx FP	TTTTACTATTTTTTCCTGATTT	150 bp
ChIP Ctx RP	AATGGTATATTACGAGGGAAAC	
ChIP TcpA FP	ATTCTCTATGTGAATGTTGCA	150 bp
ChIP TcpA RP	GTCCTTTTTTAAAGAAAAAGAAA	
ChIP TcpI FP	ATAATTAGTTAAAAATGAAATT	150 bp
ChIP TcpI RP	TTGGTTACATTATCTTTCCTGT	
ChIP AcfA FP	ATTTTTACCTGTGTTTCACAT	150 bp
ChIP AcfA RP	AAACAAGAATTAATTATCCTT	
ChIP AcfD FP	ATTTTTACCTGTGTTTCACAT	150 bp
ChIP AcfD RP	AAACAAGAATTAATTATCCTT	
ChIP TagA FP	CAAAATCGTATTGAAATTTCAA	150 bp
ChIP TagA RP	ATCTTACCACCACTAACTCCTC	
ChIP AldA FP	AACTACAAAAAAATTACGTAAT	150 bp
ChIP AldA RP	TCGATGGAAAAAACTACCTTTT	

Cloning vectors used in this study

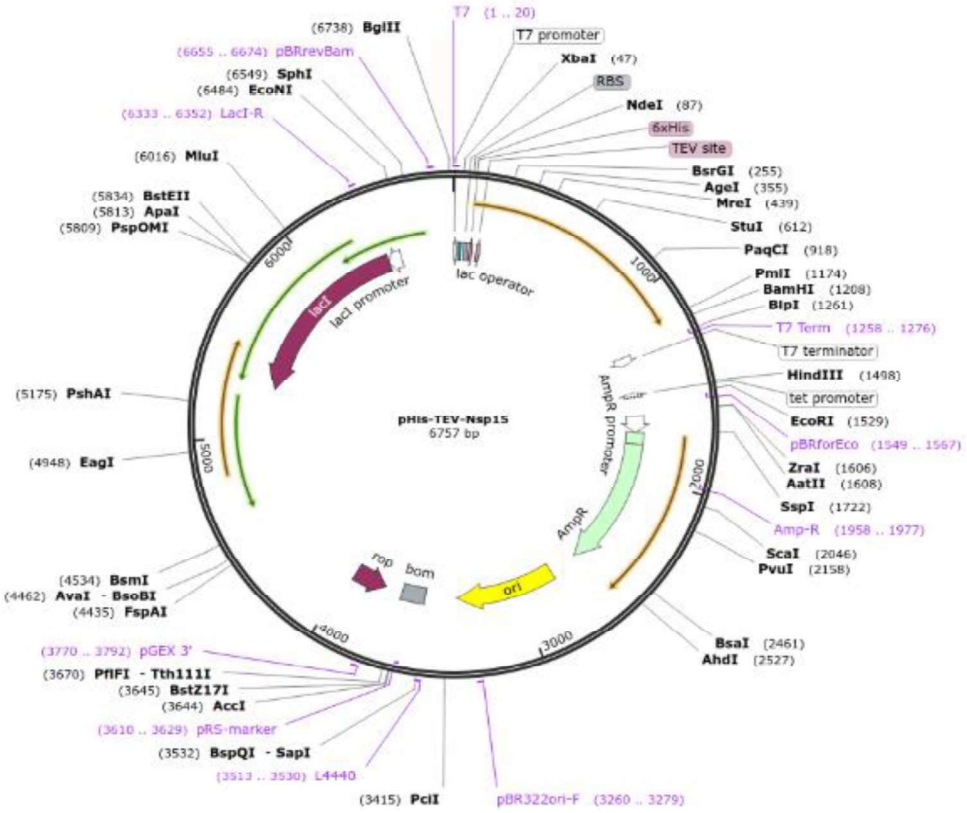

Fig.10.4. Vector map of pHis-TEV (Addgene). This vector is used for recombinant protein expression.

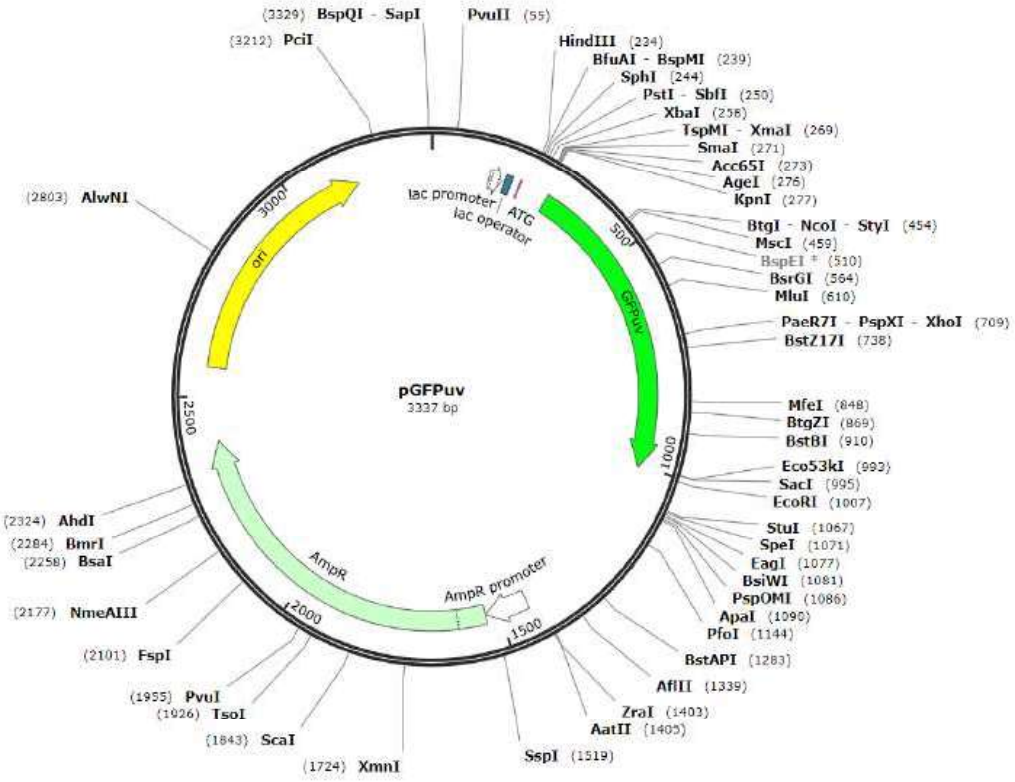

Fig.10.5. Vector map of pGFPuv (Snapgene). This vector is used for expressing GFP in bacteria

Chapter 11

Publications & Conferences

Journal articles published

- **Kundu S, Das S, Maitra P, Halder P, Koley H, Mukhopadhyay A. K, Miyoshi S, Dutta S, Chatterjee N. S, & Bhattacharya S**. Sodium butyrate inhibits the expression of virulence factors in Vibrio cholerae by targeting ToxT protein. *MSphere*. Mar **2025**.https://doi.org/10.1128/msphere.00824-24

- **Das S, Chourashi R, Mukherjee P, Kundu S, Koley H, Dutta M, Mukhopadhyay AK, Okamoto K, Chatterjee NS.** Carvacrol abrogates pathogenesis in *Vibrio cholerae*. *Journal of Applied Microbiology*. Jan **2021**. doi: 10.1111/jam.15022.

Conferences attended

- Presented a poster on "*Potential use of small molecule Sodium 3-Hydroxy Butyrate(3HB) as an anti-virulence agent against Streptomycin resistance Vibrio cholerae*" in the 16th Asian conference on Diarrhoeal disease and Nutrition (ASCODD 2022) held at the Western Kolkata Rajarhat, India during *11-13 November,* ***2020,*** organized by ICMR-National Institute of Cholera and Enteric Diseases, Kolkata, India.
- Presented a poster on "*Potential use of small molecule Sodium Butyrate(SB) as an anti-virulence agent against Vibrio cholerae*" at the National Seminar on "Recent Advances in Animal Science" RAASAB-2024 held at and organized by Department of Zoology, Siksha Bhavana (Institute of Science), Visva-Bharati (A Central University) during *7-8 March,* ***2024.***
- Presented a poster on "*Potential use of small molecule Sodium Butyrate(SB) as an anti-virulence agent against Vibrio cholerae*" at the National Conference on Antimicrobial Resistance (AMRC 2024) held at Science City, Kolkata, India during *4-5 April,* ***2024,*** organized jointly by the Institute of Bioresources and Sustainable Development (IBSD), Imphal, and ICMR-National Institute of Cholera and Enteric Diseases, Kolkata, India.

Chapter 12

Addendum

(Responses to Examinar's Comments)

DECLARATION (ADDENDUM)

This Addendum is submitted as a continuation to the original hard-bound thesis titled **"Identification and Understanding the Mode of Actions of Inhibitors against *Vibrio cholerae*"** in accordance with the examiner's recommendations.

I hereby declare that **all corrections, clarifications and revisions** suggested in the adjudication report have been duly incorporated. Texts requiring rewriting, figures needing correction, methodological details, and scientific justifications have been appropriately addressed in the accompanying **Responses to Examiner's Comments**.

This Addendum represents all modifications made prior to the Viva Voce examination, as advised by the examiner.

Date: 08/12/2025
Place: Kolkata

Sushmita Kundu

Signature of the Candidate

(Sushmita Kundu)

Addendum

Comment 1:

Throughout the review of literature all tables and figures were borrowed from publication though with the source and bibliographic references. However, in the PhD thesis some relevant text, tables statement and historical references (Fig 1.4 in particular) should have been in own words.

Response:

The text in Section 1.5 has been revised to ensure original phrasing. Figure legend and accompanying explanation have been rewritten.

Revised Text:

The emergence and diversification of many bacterial pathogens are closely tied to the dynamic nature of their genomes. In *Vibrio cholerae*, evolutionary change is largely shaped by the acquisition of mobile genetic elements (MGEs) that introduce advantageous traits. The species contains several such elements that contribute to its ability to cause disease and persist in the environment (Faruque et al., 2003; Vale et al., 2022). Remarkably, among more than 200 known serogroups, only the O1 and O139 lineages are typically associated with cholera outbreaks. Their major virulence determinants are not intrinsic but are carried on horizontally transferred genetic modules.

The cholera toxin (CT) is encoded by the filamentous bacteriophage CTXΦ (Das et al., 2011). This phage spreads among *V. cholerae* strains using the toxin-coregulated pilus (TCP) as its receptor, and TCP itself is encoded on *Vibrio* pathogenicity island-1 (VPI-1). Other MGEs, including the SXT integrative conjugative element, VPI-2, and the *Vibrio* seventh pandemic islands (VSP-1 and VSP-2), are also strongly associated with pathogenicity (Dalsgaard et al., 2000). The SXT element enables resistance to streptomycin, sulfamethoxazole, and trimethoprim (Dalsgaard et al., 2000). VPI-2, present exclusively in pathogenic isolates, contains genes required for sialic acid uptake and degradation, giving toxigenic strains a growth advantage in the host intestine.

VSP-1 encodes the regulator VspR, which is controlled by a ToxT-dependent small RNA (Faruque et al., 2003). VspR influences several VSP-1-associated genes, including *dncV*, which produces a unique cyclic AMP-GMP signalling molecule. This messenger enhances intestinal colonization and suppresses chemotaxis, a trait linked with hyperinfectivity (Dalsgaard et al., 2000). The biological role of VSP-2 remains uncertain. Importantly, all four pathogenicity islands, VPI-1, VPI-2, VSP-1, and VSP-2, are capable of excision and circularization, potentially enabling their transfer to non-pathogenic strains (Banerjee et al., 2014).

Additionally, some environmental, non-O1/non-O139 isolates contain virulence-associated genes, suggesting they may act as reservoirs for pathogenic determinants. The ability of *V. cholerae* to become naturally competent on chitin and the identification of hybrid strains carrying combinations of virulence-associated MGEs indicate that chitinous surfaces of copepods may serve as hotspots for DNA exchange, facilitating the emergence of new pathogenic variants (Dalsgaard et al., 2000; Vale et al., 2022) **(*Fig.1.4*).**

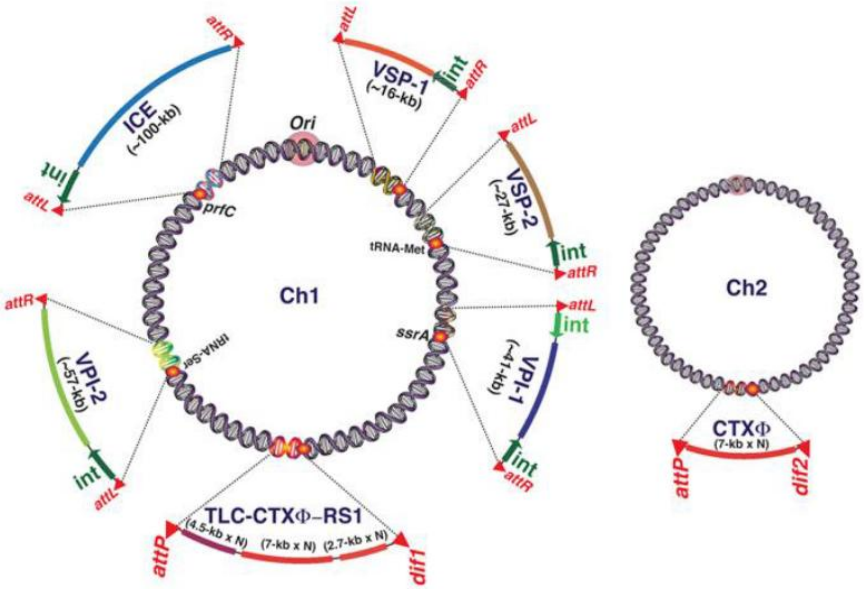

Fig.1.4. Genomic distribution of mobile elements in clinical *V. cholerae* isolates. The figure illustrates the arrangement of genomic islands (GIs), prophages, and the integrative conjugative element (ICE) within the *V. cholerae* genome. Except for prophages, these elements are associated with mobility-related features such as integrases and repeat sequences. VPI-1: *Vibrio* pathogenicity island-1; VPI-2: *Vibrio* pathogenicity island-2; VSP-1: *Vibrio* seventh pandemic island-1; VSP-2: *Vibrio* seventh pandemic island-2; int: integrase

Comment 2:

Pg l: Please recheck the figure 1: Robert Koch photo?

Response:

The previously inserted photograph in Figure 1 was incorrect. The image has now been replaced with the correct and verified photograph of Robert Koch. The updated figure has been checked for authenticity and proper citation. The revised Figure 1 is now included in the addendum.

Revised Figure:

Robert Koch

Comment 3:

Pg 53: Section 3.2: The vendor name repetitions could have been avoided. And same purchased items could be clubbed together.

Response:

The repeated mention of vendor names has been corrected, and compounds purchased from the same supplier have been grouped together for clarity. The revised text is provided in the addendum.

Revised Text:

For the inhibitor study, the following bioactive compounds were used: Sodium butyrate, cyclic-di-GMP, quercetin, allylanisole, geraniol, ethyl gallate, camphor, basil oil, catechin hydrate, rosmarinic acid, melibiose, ribose, 1,2-deoxywithastramonolide,

eugenol, and xylose (all from Sigma-Aldrich, Saint Louis, Missouri, USA); NH125 (Calbiochem, San Diego, California, USA); and totarol (Cayman Chemicals, Ann Arbor, Michigan, USA) (Table 3.1). Stock solutions and working dilutions were prepared in DNase/RNase-free water or in dimethyl sulfoxide (DMSO), followed by 0.2 µm filtration. The additives were incorporated into LB or AKI medium at the required concentrations, while medium lacking additives served as the control

Comment 4:

Pg 64: Fig 3.3: Please check whether PCR cycle is correct and standard?

Response:

The qPCR cycling conditions shown in Figure 3.3 have been rechecked and confirmed to follow the standard SYBR Green-based qPCR protocol used on 7500 Real-Time PCR detection system (Applied Biosystems, Foster City, California). The figure accurately represents the denaturation, annealing/extension, and melt curve conditions routinely used for quantitative PCR, and thus the figure is correct.

Comment 5:

Pg 66: Fig 3.4 Why ladder is without MW marking?

Response:

The DNA ladder used in Figure 3.4 did not originally display molecular weight (MW) markings in the image. The figure has now been corrected by adding the corresponding MW labels for the DNA ladder bands. The revised figure is included in the addendum.

Revised Figure:

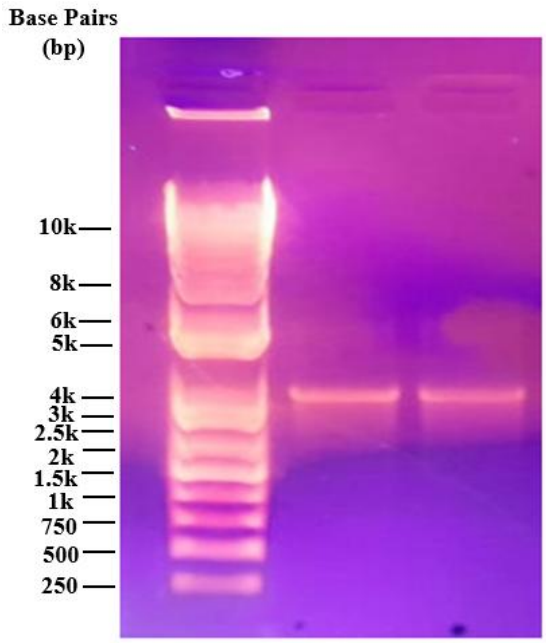

Fig.3.4. Agarose Gel of Extracted Plasmid DNA

Comment 6:

Pg 67: what percentage PA Gels were used? All percentages used?

Response:

The percentage of polyacrylamide gels used in this study has been specified. All SDS-PAGE analyses were performed using a 12.5% separating gel with a 4% stacking gel. The revised information is now included in addendum

Revised Text:

Protein samples were analysed using SDS-PAGE (Raymond et al., 1959). Prior to loading, samples were heated with loading dye at 100 °C for 5 min. Electrophoresis was performed at 80-120 V at room temperature using an Atto gel running system (Atto, Japan). The composition of the running buffer is provided in the appendix.

For all protein analyses in this study, a 12.5% separating gel with a 4% stacking gel was used.

The full compositions of gels ranging from 5% to 20% are shown in Table 3.5 for reference.

Comment 7:

Explain why protein was estimated using that particular equation?

Revised Text:

The concentration of the protein sample was measured using the modified Lowry method (Lowry et al., 1951). Three reagents were used for this estimation:

Reagent A: 2% Na_2CO_3 in 0.1 M NaOH containing 0.16% Na-K tartrate and 0.1% SDS

Reagent B: 4% $CuSO_4 \cdot 5H_2O$

Reagent C: Prepared by mixing Reagent A and Reagent B in a 100:1 ratio (10 ml + 100 µl)

A total of 200 µl of protein sample was incubated with 600 µl of Reagent C at room temperature for 15 min, followed by addition of 1 N Folin-Ciocalteu's reagent and incubation at 37 °C for 30 min. The absorbance (OD) was measured at 660 nm.

The equation used for estimating protein concentration,
concentration = OD_{660} / 0.0026, was derived from the slope of the BSA standard curve prepared under identical assay conditions.
Because the relationship between absorbance and BSA concentration was linear, the slope (0.0026) represents the change in OD per µg/µl of protein. Dividing the sample OD by this slope provides an accurate estimation of protein concentration based on the assay calibration.

Comment 8:

Page 70: Ladder does not have MW marks

Response:

Thank you for pointing this out. The figure has now been updated to include the molecular weight (MW) markers in the ladder for clarity and accurate interpretation. The revised version has been incorporated into the addendum.

Revised Figure:

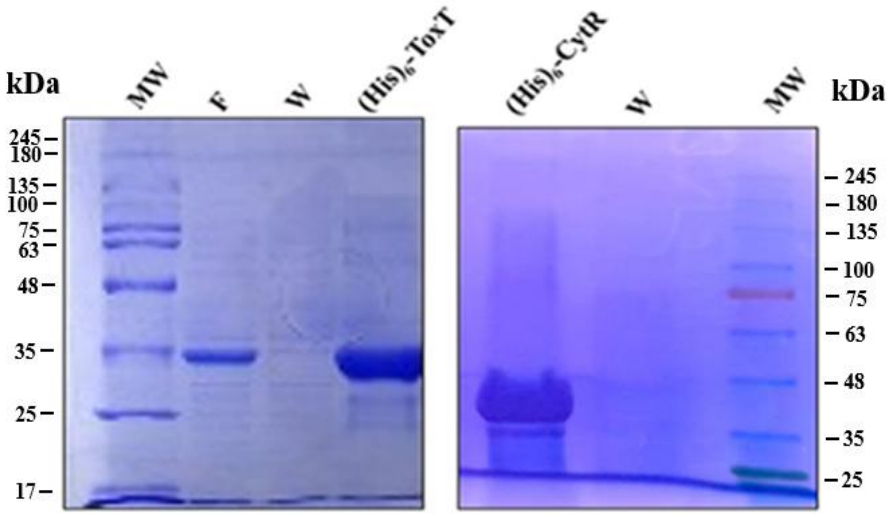

Fig.3.6. Coomassie blue staining of the purification of $(His)_6$-ToxT/$(His)_6$-CytR fusion protein using nickel chelated affinity chromatography. Mw, molecular weight marker; F, flow-through fraction; W, washed fraction

Comment 9:

Any time line of the Sodium Butyrate (SB) dose kinetics to prove the concept? Pharmacokinetics is
important in these research designs.

Response:

In the present study we did not perform a detailed pharmacokinetic or time-course analysis of sodium butyrate. Our experiments were designed as *in vitro* proof-of-concept assays, in which *V. cholerae* cultures were exposed to fixed concentrations of SB

for a defined incubation period. The SB doses used (20-80mM) were chosen based on previously published *in vitro* studies and on concentrations reported to be achievable in the intestinal lumen, and were first confirmed not to affect bacterial viability under our experimental conditions.

We acknowledge that a full description of SB dose- and time-dependent kinetics *in vivo* is beyond the scope of this thesis and represents an important limitation of the current work. Future studies, including animal or clinical pharmacokinetic analyses, will be required to correlate the effective *in vitro* concentrations with physiologically relevant exposure profiles.

Comment 10:

Any flow diagram or graphics abstract would have better

Response:

A graphical abstract summarizing the overall study design and major objectives has now been incorporated into the addendum. The graphical abstract provides a visual overview of the screening of potential inhibitors, elucidation of their mode of action, and evaluation in combination with known drugs in both *in vitro* and *in vivo* models. The new figure is included in the revised version of the addendum.

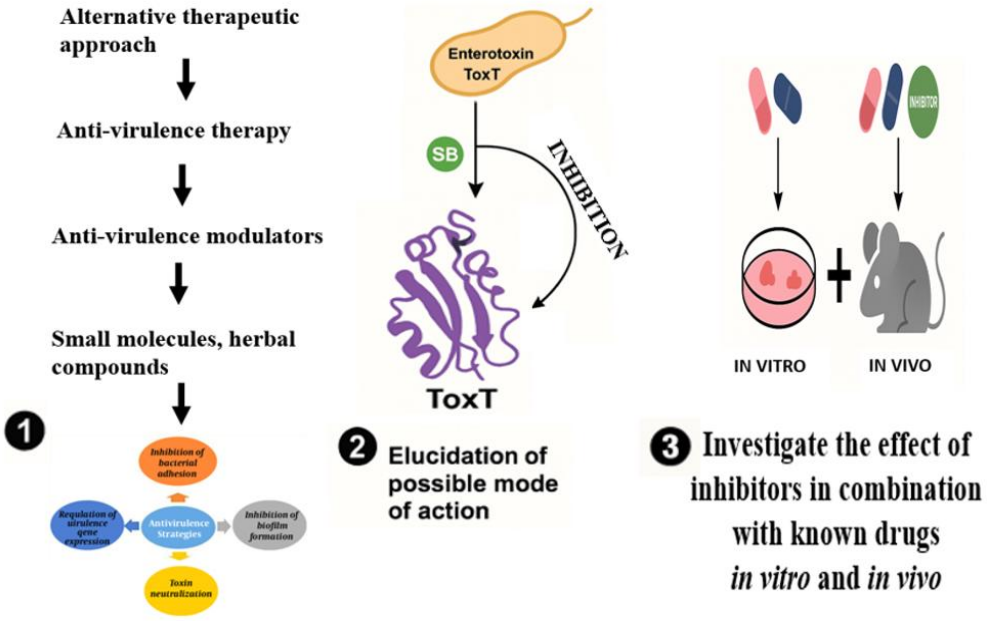

Comment 11:

Results: Where is Fig 4.1? I believe it is numbered according to the paragraph sub section.

Response:

Thank you for the comment. The subsection 4.1 does not contain any figure; therefore, Fig. 4.1 is not applicable in this section. The figure numbering starts from the next subsection where the first figure appears. All figure numbers have been assigned according to the paragraph subsection structure, and the numbering has been verified to be correct as per the thesis format.

Comment 12:

From Fig 4.3-4.6 the axis values are different for different graphs of inhibitors? Is it done resolutely?

Response:

Thank you for the comment. Yes, the axis values from Fig. 4.3 to Fig. 4.6 differ intentionally. Each inhibitor exhibited a distinct range of responses, and the axis limits were adjusted accordingly to accurately represent the data distribution and highlight the variations observed for each compound. This approach ensures clarity and prevents misinterpretation that may arise from forcing all graphs into a uniform axis range. However, the comparative trends remain clearly visible across the figures.

Comment 13:

A little more discussion justifying the selection of SB as the potential inhibitor would have been required.

Response:

Thank you for the comment.

Sodium butyrate (SB) was selected as the potential inhibitor based on multiple converging lines of evidence. During the initial *in vitro* screening, SB consistently

demonstrated comparatively higher inhibitory activity than several other tested compounds, indicating a strong primary response. In addition to suppressing overall bacterial growth at relevant concentrations, SB markedly reduced key virulence-associated factors, including adhesion factors such as TCP and the production of cholera toxin. These observations indicate that SB is not acting solely as a general growth inhibitor but may specifically interfere with pathways involved in virulence regulation.

Furthermore, existing literature reports that short-chain fatty acids, including butyrate, can influence bacterial gene expression, membrane integrity, and stress-response systems. Such previously documented modulatory effects align with the inhibitory patterns observed in our assays, providing a biological rationale for its targeted impact on *Vibrio cholerae*. Taken together, its reproducible screening performance, its multilevel impact on virulence determinants, and its biologically plausible mechanism of action collectively justified prioritizing SB for detailed mechanistic and functional investigation in this study.

Comment 14:

Page 117: Fig 6.4: DNA ladders are same for all three electrophoresis?

Response:

Thank you for the comment. The DNA ladders appear similar across the three electrophoresis images because the same standard molecular weight marker was used in each run. However, each gel was run separately with its own ladder lane. The gels have been rechecked, and the images have now been clearly presented to avoid any confusion regarding the ladder lanes.

Comment 15:

The plan of thesis should have been mention at the beginning or in introduction.

Response:

Thank you for the comment. Although the thesis does not contain a separate Introduction chapter, a brief roadmap has now been added at the beginning of the thesis, before the Review of Literature section. This roadmap outlines the overall structure, including

the Review of Literature, Objectives, Materials and Methods, Results sections, discussions, and conclusion to provide readers with a clear overview of the organization and flow of the work.

Thesis Roadmap:

This thesis is organized to provide a logical flow of the research work. It begins with the Review of Literature, which summarizes the current understanding and background relevant to the study. This is followed by the Objectives, outlining the specific aims of the research. The Materials and Methods section then describes the experimental approaches and techniques used to address these objectives. The Results section presents the findings of the study in a structured and coherent manner. This is followed by the Discussion, where the results are interpreted in the context of existing literature. Finally, the Conclusion summarizes the major outcomes of the study and highlights its overall significance. Together, these sections offer a comprehensive overview of the research carried out in this thesis.

Comment 16:

None of the diagram is original and hand written. It does not confer a strong message for a PhD thesis where author should show some copy-edited concepts and figures from literature justifying own finding.

Response:

Thank you for the comment. The diagrams in the Review of Literature section are original and were created by me. They have been refined to clearly represent the concepts and to appropriately support the findings in the thesis.

Revised Figures:

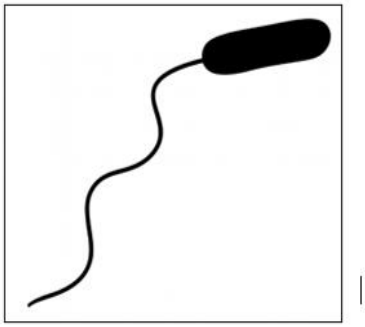

Fig.1.1. ***V. cholerae*** **displaying a single polar flagellum**

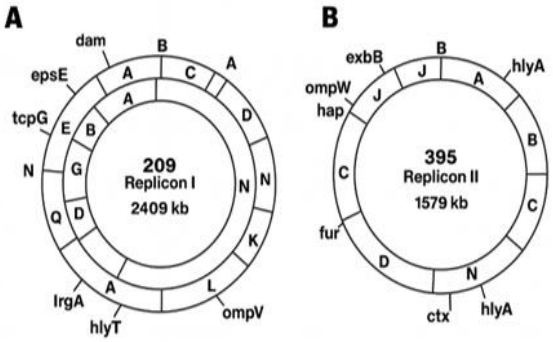

Fig.1.3. Genomic layout of ***V. cholerae*** **showing its large and small chromosomes.**

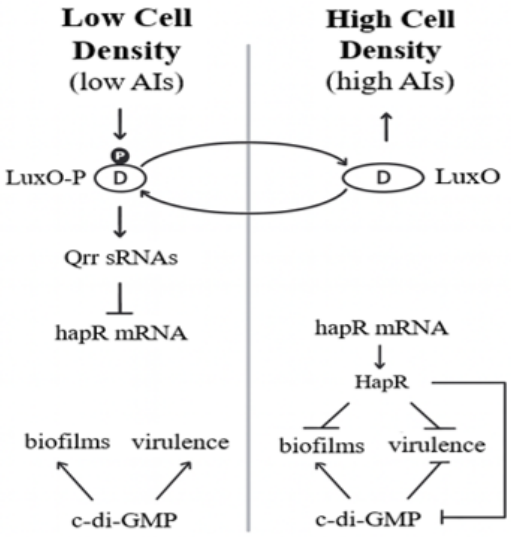

Fig.1.12. Simplified model illustrating how quorum sensing and c-di-GMP interact to regulate gene expression in ***V. cholerae*****.** At low AI levels (left), phosphorylated LuxO activates production of Qrr sRNAs, which inhibit HapR translation. At high AI levels (right), LuxO is dephosphorylated, qrr expression ceases, and HapR is produced. HapR suppresses both biofilm formation and virulence gene expression. Similarly, c-di-GMP downregulates virulence genes, but unlike HapR, it promotes biofilm formation. HapR inhibits biofilm development directly (through regulation of *vpsT*) and indirectly by lowering c-di-GMP levels.

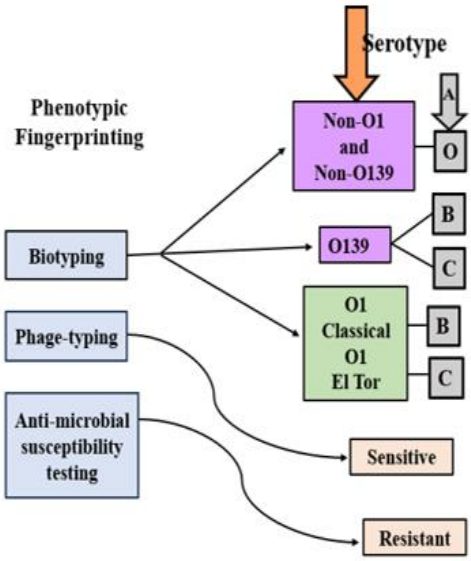

Fig.1.5. Schematic representation of *V. cholerae* classification

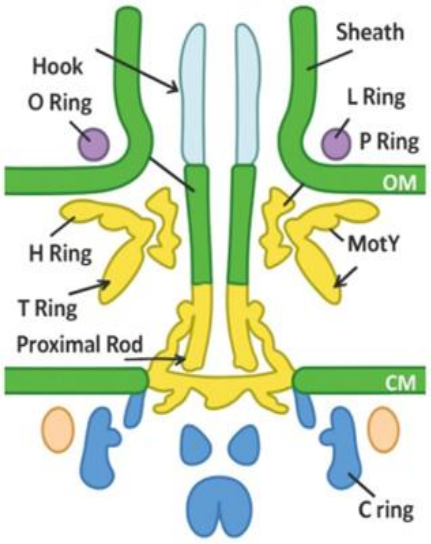

Fig.1.11. Schematic representation of the sheathed flagellar complex in *Vibrio cholerae*

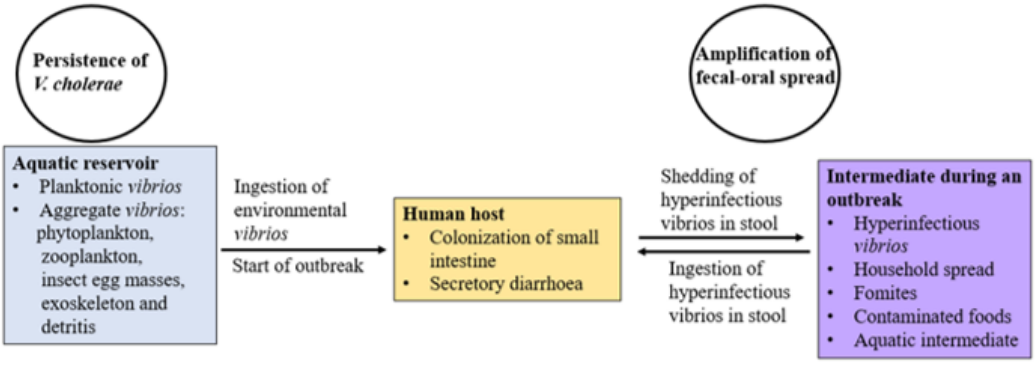

Fig.1.14. Life cycle of pathogenic *V. cholerae*. Toxigenic strains persist in aquatic habitats together with non-toxigenic strains, supported by biofilm formation on biotic surfaces and the utilization of chitin as nutrient sources. After ingestion through contaminated food or water, toxigenic bacteria colonize the small intestine, proliferate, produce cholera toxin, and are excreted in diarrheal fluids. These shed cells enter a transient hyper-infectious state, enhancing transmission and facilitating further spread during outbreaks.

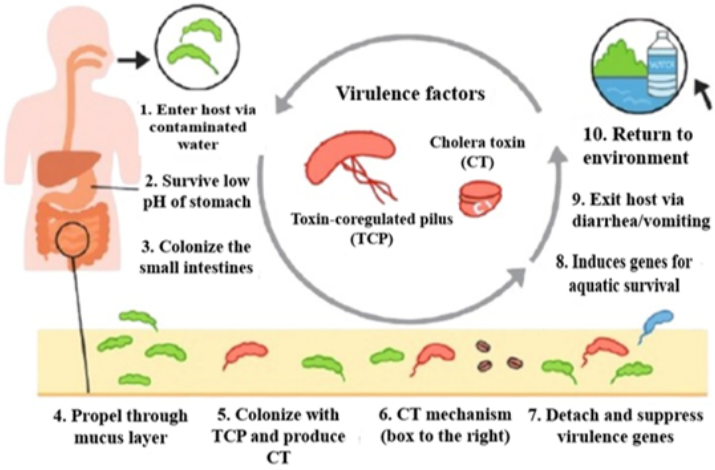

Fig.1.16. Life cycle and pathogenesis of *V. cholerae*. *V. cholerae*, a human-restricted, waterborne pathogen, enters the host via contaminated water. After surviving the acidic stomach, the bacteria reach the small intestine, where they penetrate the mucus layer using their single polar flagellum. In response to host cues, they activate virulence factors including the toxin-coregulated pilus (TCP) and cholera toxin (CT). TCP promotes epithelial colonization, while CT binds GM1 receptors, is internalized, and elevates intracellular cAMP levels, driving electrolyte and water loss that results in profuse watery diarrhea. As colonization progresses, microcolonies and biofilm matrix components form. At high cell density, quorum sensing downregulates virulence genes, and the bacteria detach, move into the intestinal lumen, and activate genes needed for survival in the external environment. *V. cholerae* is then shed in diarrheal fluid, returning to aquatic settings where it can contaminate water sources and infect new hosts.

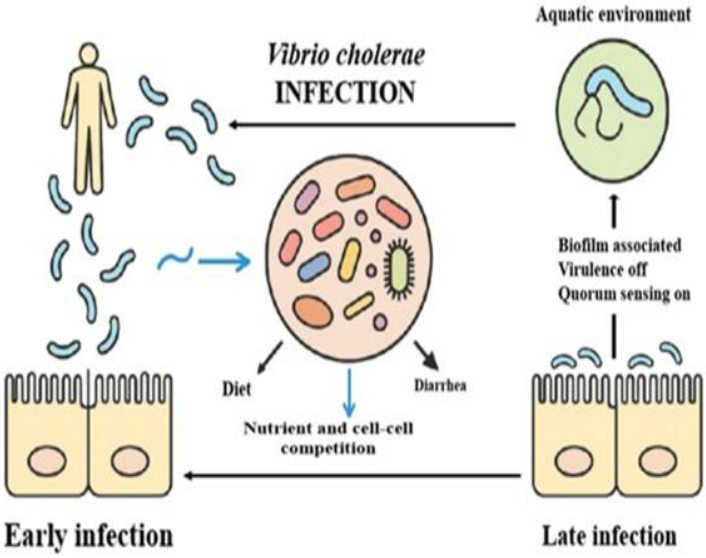

Fig.1.20. Interaction between the gut microbiome and environmental signals during the *V. cholerae* life cycle. An individual's microbiome, shaped by diet, microbial exposures, and past gut disturbances such as diarrhea, malnutrition, or inflammation, modulates the chemical cues that *V. cholerae* relies on to coordinate gene expression during early and late stages of infection

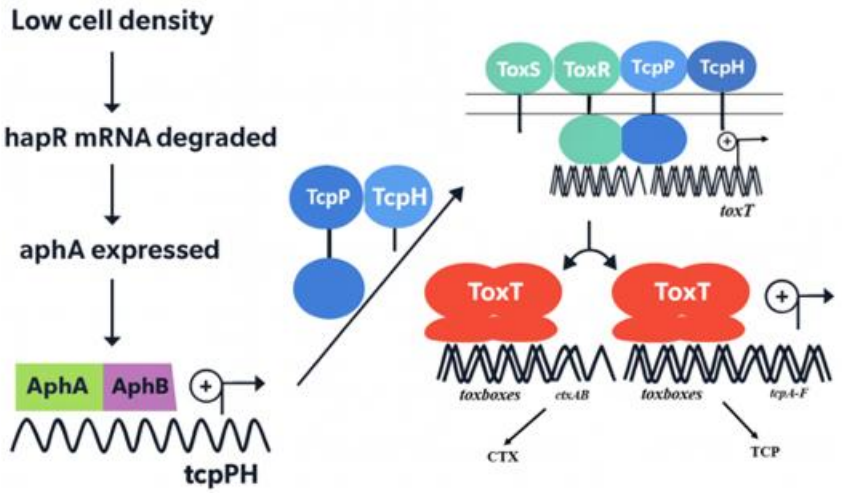

Fig.1.21. Schematic of the ToxR regulon highlighting the components that control production of the key virulence factors CT and TCP

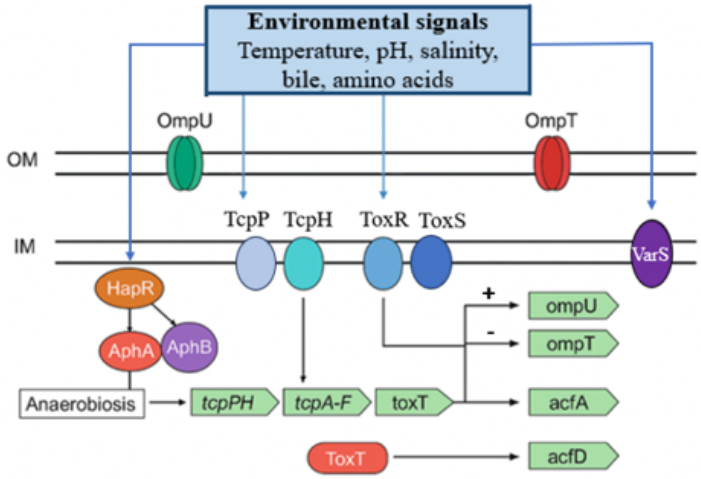

Fig.1.22. Regulatory model of ToxT-dependent virulence gene expression in *V. cholerae*. TcpP/TcpH and ToxR/ToxS act together to activate *toxT* transcription, with ToxS and TcpH serving as required accessory proteins. ToxT then induces transcription of the *tcp* operon. The regulators AphA and AphB activate the *tcpPH* operon in response to environmental cues. Coordinated regulation by ToxRS, TcpPH, and ToxT controls *tcp* expression, with AphB linked to enhanced *tcpPH* expression under anaerobic conditions. ToxR independently activates *ompU* and represses *ompT*, indicated by (+) and (–).

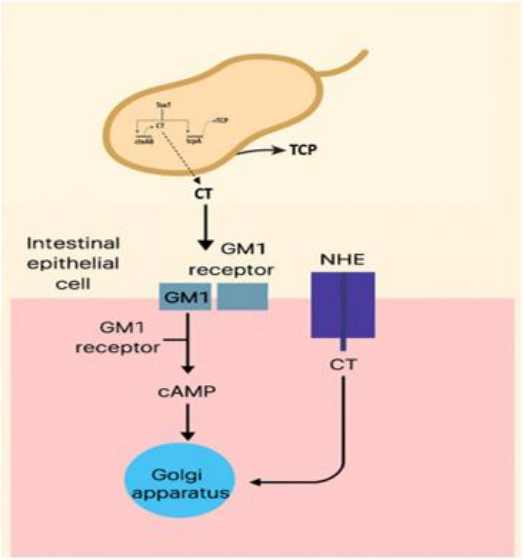

Fig.1.24. Simplified mechanism of cholera toxin (CT) action. *ToxT*-regulated genes in *V. cholerae* direct the production of cholera toxin (CT) and the toxin-coregulated pilus (TCP). Secreted CT binds to the GM1 receptor on the intestinal epithelial cell surface, leading to internalization and activation of cAMP signalling. Elevated cAMP influences intracellular trafficking, including the Golgi apparatus, and disrupts ion transport by inhibiting the Na^+-H^+ exchanger (NHE), contributing to fluid loss characteristic of cholera.

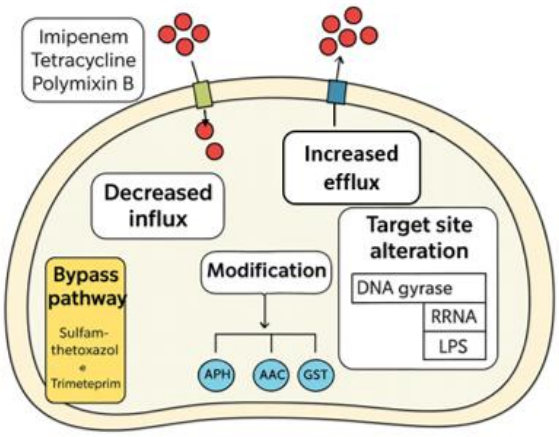

Fig.1.29. Mechanisms underlying antibiotic resistance in *V. cholerae*. *V. cholerae* acquires antimicrobial resistance either through mutations in its own genome or by obtaining resistance genes from other bacteria. These traits can reduce membrane permeability, inactivate or modify antibiotics, alter drug targets, introduce bypass metabolic pathways, or expel antimicrobial agents via efflux pumps

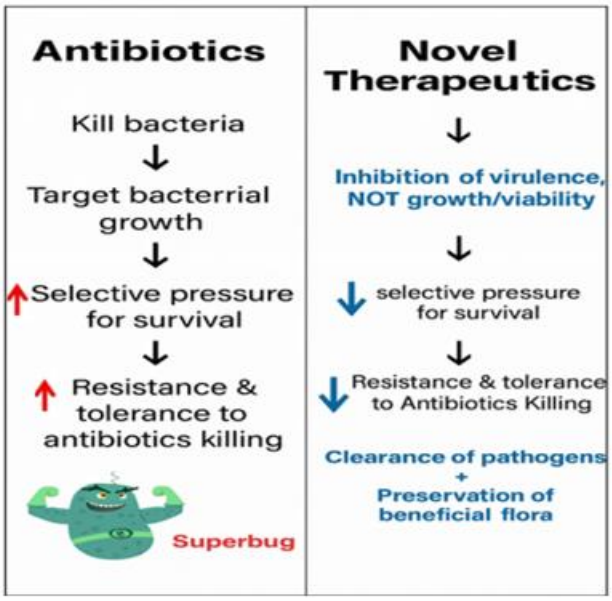

Fig.1.30. Overview comparing antibacterial and anti-virulence strategies

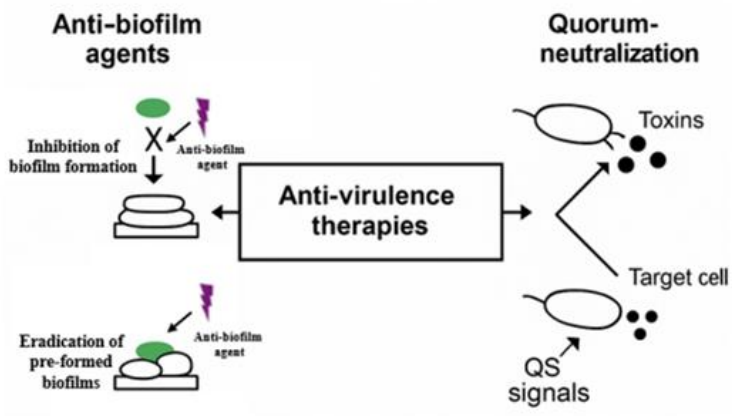

Fig.1.31. Overview of anti-virulence therapeutic strategies. Anti-virulence approaches target pathogenic mechanisms rather than bacterial viability. Anti-biofilm agents can block biofilm formation or disrupt established biofilms, while quorum-neutralizing strategies interfere with QS signalling, preventing toxin production and reducing damage to host cells.

AMERICAN SOCIETY FOR MICROBIOLOGY | mSphere

| Microbial Pathogenesis | Research Article

Sodium butyrate inhibits the expression of virulence factors in *Vibrio cholerae* by targeting ToxT protein

Sushmita Kundu,[1] Suman Das,[1] Priyanka Maitra,[1] Prolay Halder,[2] Hemanta Koley,[2] Asish K. Mukhopadhyay,[2] Shin-ichi Miyoshi,[3] Shanta Dutta,[2] Nabendu Sekhar Chatterjee,[1] Sushmita Bhattacharya[1]

AUTHOR AFFILIATIONS See affiliation list on p. 17.

ABSTRACT Cholera, a diarrheal disease caused by the gram-negative bacterium *Vibrio cholerae*, remains a global health threat in developing countries due to its high transmissibility and increased antibiotic resistance. There is a pressing need for alternative strategies, with an emphasis on anti-virulent approaches to alter the outcome of bacterial infections, given the increase in antimicrobial-resistant strains. *V. cholerae* causes cholera by secreting virulence factors in the intestinal epithelial cells. These virulence factors facilitate bacterial colonization and cholera toxin production during infection. Here, we demonstrate that sodium butyrate (SB), a small molecule, had no effect on bacterial viability but was effective in suppressing the virulence attributes of *V. cholerae*. The production of cholera toxin (CT) was significantly reduced in a standard *V. cholerae* El Tor strain and two clinical isolates when grown in the presence of SB. Analysis of mRNA and protein levels further revealed that SB reduced the expression of the ToxT-dependent virulence genes like *tcpA* and *ctxAB*. DNA-protein interaction assays, conducted at cellular (ChIP) and *in vitro* conditions (EMSA), indicated that SB weakens the binding between ToxT and its downstream promoter DNA, likely by blocking DNA binding. Furthermore, the anti-virulence efficacy of SB was confirmed in animal models. These findings suggest that SB could be developed as an anti-virulence agent against *V. cholerae,* serving as a potential alternative to conventional antibiotics or as an adjunctive therapy to combat cholera.

IMPORTANCE The world has been facing an upsurge in cholera cases since 2021, a similar trend continuing into 2022, with over 29 countries reporting cholera outbreaks (World Health Organization, 16 December 2022, Disease Outbreak News, Cholera—global situation). Treatment of cholera involves oral rehydration therapy coupled with antibiotics to reduce the duration of the illness. However, in recent years, indiscriminate use of antibiotics has contributed to the emergence of antibiotic-resistant strains. In this study, we have addressed the problem of antibiotic resistance by targeting virulence factors. Screening various compounds using *in silico* methods led to the identification of a small molecule, SB, that inhibits the virulence cascade in *V. cholerae*. We demonstrated that (i) SB intervened in ToxT protein-DNA binding and subsequently affected the expression of ToxT-regulated virulence genes (*ctxAB* and *tcpA*) and (ii) SB is a potential therapeutic candidate for the development of a novel antimicrobial agent.

KEYWORDS sodium butyrate (SB), inhibitor, pathogenesis, *Vibrio cholerae*, *ctxAB*, antimicrobial resistance, toxin-coregulated pilus (TcpA)

Cholera is an acute, severely dehydrating diarrheal disease caused by water-borne bacterium *Vibrio cholerae* (1). Since mid-2021, the world has witnessed a drastic upsurge of the ongoing seventh cholera pandemic, characterized by frequent outbreaks along with the increased incidence mortality rate (1.9%) (2). This trend continued into

Editor Alfredo G. Torres, The University of Texas Medical Branch at Galveston, Galveston, Texas, USA

Address correspondence to Sushmita Bhattacharya, durgasushmita@gmail.com.

The authors declare no conflict of interest.

See the funding table on p. 18.

Received 1 October 2024
Accepted 21 March 2025
Published 22 April 2025

2022, and as of February 2023, at least 18 countries continued reporting cholera cases. The mortality linked to these outbreaks was particularly concerning, with many countries reporting higher case fatality ratios (CFR) compared with previous years (2). Although over 200 *V. cholerae* serogroups have been identified, only the O1 (classical and El Tor biotypes) and O139 serogroups of *V. cholerae* have been implicated in epidemic and pandemic cholera (3, 4).

The clinical symptoms of cholera are primarily driven by two essential virulence factors, cholera toxin (CT) and toxin-coregulated pilus (TCP) (5). CT is an A-B_5 family toxin directly responsible for inducing profuse watery cholera diarrhea (6, 7), whereas TCP is required for intestinal colonization (8). Coordinated expression of these virulence genes is directly under the control of the master regulator, ToxT, and given its pivotal role, numerous studies have been focused on its regulation, leading to the characterization of multiple mechanisms that contribute to its stringent regulation. ToxT belongs to the AraC/XylS family of transcriptional activators and consists of two domains: an N-terminal domain that has been linked to effector binding and potential ToxT monomer association, and a C-terminal DNA-binding domain that contains AraC/XylS homology (9). The transcription of *toxT* is regulated by two membrane-localized complexes ToxRS and TcpPH (10). TcpPH is further activated by two activators, AphA and AphB, which respond to cell density, anaerobiosis, and other environmental factors (11, 12).

The primary therapy of cholera is an oral rehydration solution (ORS), which contains different types of salts and glucose, to avoid dehydration (13, 14). Without intervention, the survival rate for cholera can be as low as 50%; however, ORS supplementation reverses the survival rate to more than 99% (15). Antibiotics are a secondary treatment in severe cases to shorten the duration of the illness (16). Although antibiotics can effectively reduce cholera burden, WHO does not recommend this practice due to the risk of developing and spreading drug-resistant bacteria (17–19). There are also vaccines against *V. cholerae,* but their efficacy is not 100% (20). Consequently, there is an unmet need for clinical intervention to control the spread of drug-resistant bacteria through rapid preventive measures.

Anti-virulence drugs are gaining popularity as an alternative approach to combat bacterial infections. Unlike antibiotics, these drugs disarm the pathogen by targeting its virulence factors and further activate the immune system to eradicate the infection (21). This strategy exerts less selective pressure on the emergence of resistant strains and reduces the impact on commensal microbiota. Previous studies identified small molecules such as toxtazin B, unsaturated fatty acids, and ribavirin targeting the virulence gene regulatory cascade (15, 22, 23). Along with small molecules, several herbal products and bioactive compounds are also reported to be potent repressors of the virulence factors, such as anethole (24), capsaicin (25) inhibiting the CT production, zinc oxide nanoparticles disrupting the secondary structure of CT (26), carbohydrate inhibitors (27), and fucosylated molecules (28), interfering with the activity of CT.

Short-chain fatty acids (SCFA), such as butyrate, are microbial metabolites synthesized from the fermentation of dietary fibers in the colonic lumen. Multiple studies have documented the substantial effects of butyrate on host immunity, energy metabolism, and overall health (29). In colorectal cells, butyrate treatment is reported to induce the production of antimicrobial peptide, cathelicidin (30). The anti-microbial and anti-virulence activity of butyrate has been well characterized in a variety of pathogenic bacteria such as *Salmonella* Typhimurium, *Clostridium perfringens* (31), *Staphylococcus pseudointermedius*, *Acinetobacter baumannii* (32), *Vibrio campbellii* (33), and *Vibrio parahaemolyticus* (34). Despite extensive research on butyrate, its antimicrobial activity against *V. cholerae* has not been reported.

In this study, we aimed to screen potential bioactive compounds against *V. cholerae* and understand the mechanism behind antivirulence activities against standard and resistant strains.

RESULTS

In silico screening of bioactive compounds identifies SB as a potential inhibitor

Among different transcriptional activators present in *V. cholerae*, targeting ToxT has frequently been reported to have additional advantages for developing new antimicrobial drugs, aimed at targeting the virulence factor rather than bacterial growth. Hence, to identify potential inhibitors, we have used an *in silico* virtual screening technique, important for the drug discovery process. To focus on potent ToxT inhibitors, several bioactive compounds (Table S1) were docked individually with the binding pocket of ToxT protein (PDB ID: 3GBG). The possible amino acid residues present in the binding pocket of ToxT are Ile226, Tyr26, Asn28, Asp29, Ser223, Ser227, Asn60, Thr85, Gln8, Lys31, and Lys230. Based on the docking pose and possible interaction, the binding energy of the compounds is listed in Table S1. Among the docked ligands, the compound SB showed the highest binding affinity of −7.68 Kcal/mol and stable interaction with ToxT, forming two salt bridges with Lys31 and Lys230 and a single hydrogen bond with Lys31 (Fig. 1A and B). Other residues involved in interactions with SB are summarized in Fig. 1C. Altogether, these data suggest that SB may interact with ToxT and therefore are chosen for subsequent *in vitro* and *in vivo* experiments to test their efficacy against the virulence factors in *V. cholerae*.

The viability of bacterial strains and cytotoxicity in the HT-29 cell line in the presence of SB

To evaluate the antibacterial activity of SB, the MIC and MBC values of SB against bacterial strains were determined (Fig. S1A). The growth rate of the strains in the presence of SB was evaluated in a time-dependent manner (Fig. 2). The results indicated complete bactericidal activity of SB against N16961 at 160 mM (MBC), as no live bacteria could be detected after 12 h (Fig. 2A). Notably, the bactericidal activity of SB (160 mM) observed against the other two strains was more potent than N16961, as no live bacteria could be detected after 6 h in BCH13298 and after 8 h in Micro78 (Fig. 2B and C). At 80 mM (MIC) of SB, the growth pattern of all the bacterial strains was similar,

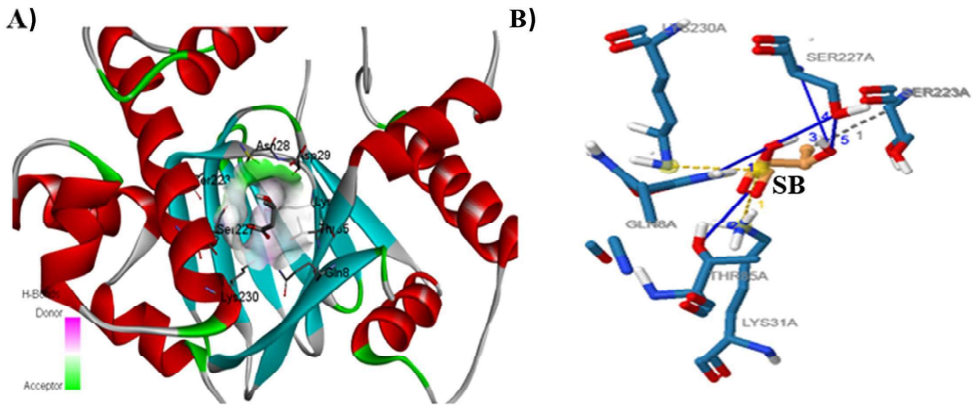

C)

RECEPTOR	LIGAND	BINDING ENERGY (Kcal/mol)	AMINO ACIDS INVOLVED IN INTERACTION	PDB ID
ToxT	Sodium butyrate(SB)	-7.68	GLN8, THR85, SER227, SER223, LYS31, LYS230	3GBG

FIG 1 Binding of SB with ToxT *in silico*. Residues interacting with ligand (SB) and receptor (ToxT) are represented in (A) 3D conformation, (B) 2D conformation, and (C) table showing the probable interacting residues and the binding energy.

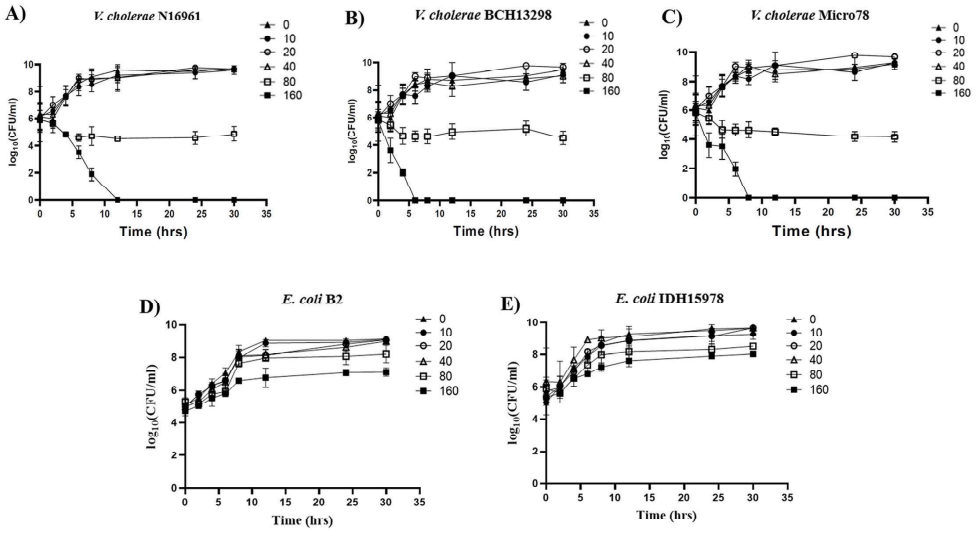

FIG 2 Effect of SB on the bacterial growth at MIC and sub-MICs. El Tor *V. cholerae* strains were grown in LB broth along with SB at MBC (160 mM), SB 160 (■); MIC (80 mM), SB 80 (□); 1/2th MIC (40 mM), SB 40 (Δ), 1/4th MIC (20 mM), SB 20 (○), 1/8th MIC (10 mM), SB 10 (●), and SB 0 (▲) for the indicated periods (2, 4, 6, 8, 12, 24, and 30 h). The viable bacterial counts in CFU per mL detected by the plate count method were represented graphically for (A) multidrug-resistant *V. cholerae* N16961, (B) multidrug-resistant *V. cholerae* BCH13298, (C) multidrug-resistant *V. cholerae* Micro78, (D) multidrug-resistant *E. coli* B2, and (E) multidrug-resistant *E. coli* IDH15978.

with a significant reduction observed in viability count compared with the untreated *V. cholerae* cells (Fig. 2A through C). At 10–40 mM (sub-MICs) of SB, there was no significant difference in growth rate as compared with the untreated cells (Fig. 2A through C). Additionally, we tested whether SB exhibits antibacterial activities against *E. coli* strains. The results, as shown in Fig. 2D and E, indicate that the antibacterial effect of SB on *E. coli* B2 and *E. coli* IDH15978 was not as pronounced as that observed for *V. cholerae* strains. Even at the highest concentration of SB tested (=160 mM), viable colonies of *E. coli* strains could still be detected after 30 h, emphasizing *V. cholerae*-specific bactericidal activity of SB. The sub-MICs of SB were used in all subsequent *in vitro* experiments. *In vivo* experiments were performed at both sub-MICs and MIC of SB to compare the effect with the different groups.

Toxicity of SB in mammalian cell lines was also evaluated. No significant cytotoxicity was observed when HT-29 cells were incubated with varying doses of SB (5–160mM) (Fig. S1B).

SB inhibits CT and TcpA production

The above *in silico* results predict that SB forms stable interaction with ToxT. Given the role of ToxT in regulating *V. cholerae* virulence genes, we sought to investigate whether SB could affect the expression of ToxT-regulated virulence genes. First, we explored the classical GM1-CT ELISA for detecting the secreted CT level in the supernatant of bacterial cultures grown in the presence or absence of sub-MICs of SB (10–40 mM). It was observed that SB significantly inhibited CT production in all three *V. cholerae* strains in a dose-dependent manner (Fig. 3A). Since the expression of CT is coordinately regulated with the expression of TcpA, N16961 cultures grown in the presence of SB were also analyzed for TcpA expression by immunoblot. SB significantly decreased the TcpA levels relative to the untreated cells (Fig. 3B).

To understand the underlying mechanism behind the reduced production of CT and TcpA, qRT-PCR was used to measure the expression levels of cholera toxin-encoding *ctxAB* and pilus-encoding *tcpA* genes in N16961. The expressions of *ctxAB* and *tcpA* were significantly downregulated by SB (more than 3-fold) compared with the untreated cells

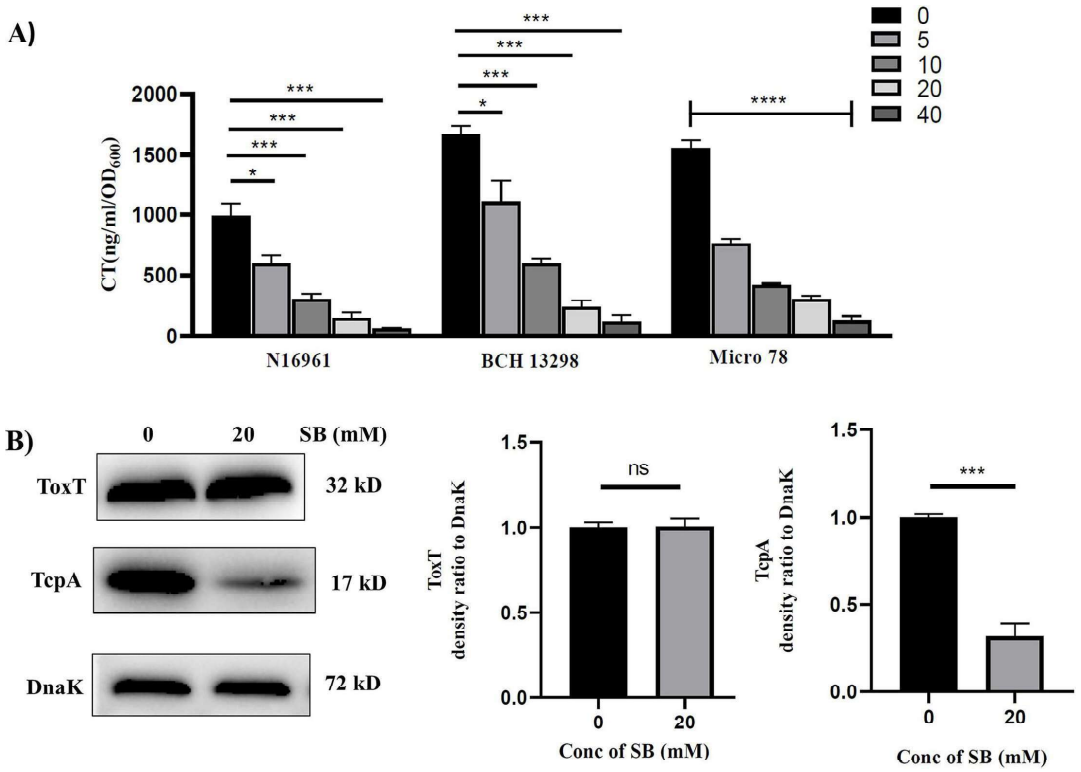

FIG 3 Inhibitory effects of SB on the virulence attributes of *V. cholerae*. (A) CT expression levels in different O1 El Tor strains were measured by ELISA from the samples grown in AKI media with or without SB. One-way ANOVA was performed. (B) Expression of major virulence proteins ToxT and TcpA of *V. cholerae* N16961 measured by western blot of cells grown in the presence or absence of SB (20 mM). DnaK was used as a loading control. Densitometric analyses are graphically represented. Student's *t*-test was performed. All data are expressed as mean ± S.D. from three biological replicates. Significance levels were denoted as * for $P < 0.05$, *** for $P < 0.001$, **** for $P < 0.0001$.

(Fig. S2A). In addition to this, we also determined whether SB affects the expression of genes encoding virulence regulators (i.e., *toxS, toxR, tcpH, tcpP,* and *toxT* genes) in N16961 using qRT-PCR. Notably, SB did not affect the expression of any of these genes compared with the untreated cells (Fig. S2A). To rule out the possibility that the reduced *ctxAB* and *tcpA* transcription depends on the posttranscriptional or translational regulation of *toxT*, the levels of ToxT protein were measured in the presence or absence of SB. As shown in , SB did not affect the cellular levels of the ToxT protein, indicating that SB affects the virulence cascade without affecting ToxT expression.

Adhering ability of *V. cholerae* to intestinal epithelial cells is highly dependent on TcpA. Since SB decreased the TcpA levels, we also examined the effect of SB on the adhering ability of *V. cholerae* to intestinal epithelial cells, HT-29 cells (Fig. S2B). The cell adherence assays revealed that the adhering ability of *V. cholerae* to HT-29 cells was significantly reduced in the presence of SB compared with the untreated condition (Fig. S2B).

SB binds to the ToxT protein and affects its interaction with the target promoter DNAs

ToxT is a direct activator of *tcpA* and *ctxAB* genes. The probable explanation for SB-mediated decrease in *tcpA* and *ctxAB* levels may be that SB can interact with and inactivate ToxT. We, therefore, examined the direct binding of SB to ToxT protein using fluorescence quenching experiment (Fig. 4A). Our results show that SB does interact with ToxT protein (K_{SV}=[6.04 ± 0.04] × 10^2 M^{-1} and K_D = 2.6 ± 0.03 mM), further supporting our *in silico* predictions.

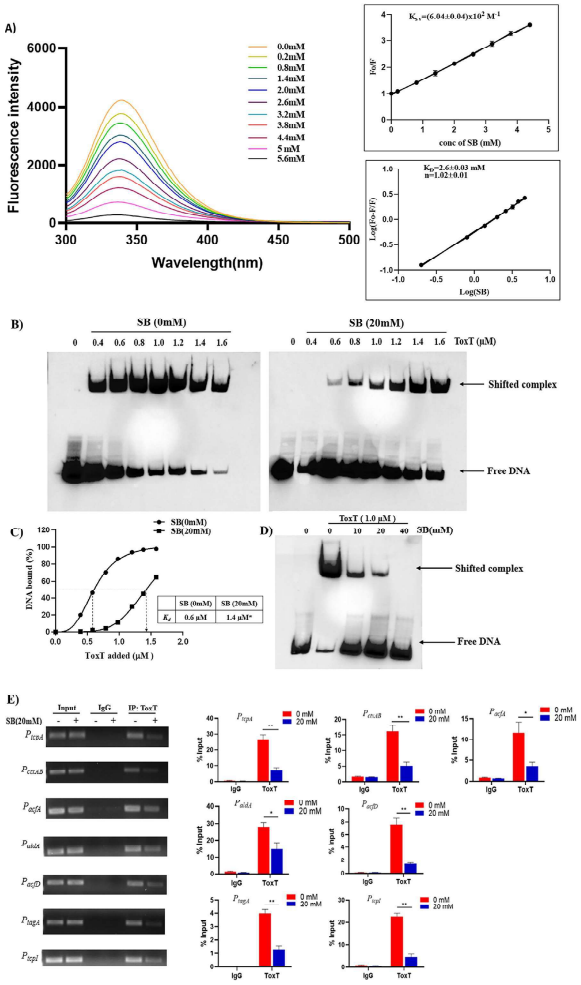

FIG 4 SB interacts with and inactivates the ToxT protein. (A) Fluorescence quenching spectra of ToxT in the presence of SB. A concentration of 0.1 µM ToxT protein was excited at 280 nm, and fluorescence quenching was recorded in the presence of various concentrations of SB (0.2–5.6 mM). Stern-Volmer plots of the decrease in fluorescence of ToxT in the presence of various concentrations of SB were used to determine the quenching rate constant, K_{SV} (calculated from the slope of the line). Logarithmic plots of relative fluorescence quenching of ToxT against logarithmic concentrations of SB were used to determine K_D (calculated from the intersection of the line with the *y*-axis) and the number of binding sites, *n* (calculated from the slope of the line). Error bars indicate standard deviations calculated from three individual experiments. (B) For EMSA, a 150 bp P_{tcpA} DNA fragment was biotin-labeled and then used as a DNA probe. Purified ToxT protein (0.4, 0.6, 0.8, 1.0, 1.2, 1.4, and 1.6 µM) was pre-incubated with SB (20 mM) for 20 min, followed by incubation with the probe (1 nM) for an additional 20 min. (C) The relative affinities of ToxT protein in the presence or absence of SB were compared using the data from panel B. The percentage of bound DNA was calculated and plotted against the concentration of ToxT added. The K_d is shown in the inset. A significant difference between the best-fit values is indicated by an asterisk (*P < 0.05). (D) EMSA was performed as described for panel B, except that ToxT (1.0 µM) was mixed with increasing amounts of SB (10, 20, and 40 mM). The EMSAs presented are representative of three independent experiments. (E) The interaction between ToxT and promoter DNAs at the cellular level in the presence or absence of SB (20 mM) was analyzed by ChIP. Expression of promoter DNAs was checked and compared to input in real-time PCR assay and agarose gel electrophoresis. Two-way ANOVA was performed. The data are expressed as mean ± S.D. (n = 3). IP, Immunoprecipitation; significance levels were denoted as * for P < 0.05 and ** for P < 0.01.

Next, we checked whether SB could prevent the binding of ToxT to its DNA binding site, located upstream of the *tcpA* gene. Hence, we performed an electrophoretic mobility shift assay (EMSA). The EMSA results revealed the binding of ToxT to the P_{tcpA} region in a concentration-dependent manner (Fig. 4B). The interaction between ToxT and P_{tcpA} is specific, as CytR could not interact with the P_{tcpA} (Fig. S3B). Similarly, a 70-fold molar excess of nonspecific competitor DNA did not affect the ToxT-P_{tcpA} binding. In contrast, a 70-fold molar excess of specific competitor DNA completely inhibited the binding, indicating the specificity of the ToxT-P_{tcpA} interaction (Fig. S3B). Next, the effect of SB on ToxT-P_{tcpA} binding was examined. The addition of 20 mM of SB prevented ToxT from binding to DNA (Fig. 4B and D), and the interaction was completely inhibited at 40 mM of SB (Fig. 4D). Based on the concentration of ToxT required to bind 50% of the P_{tcpA}, the K_d for ToxT without SB was 0.6 µM, whereas that with 20 mM SB was 1.4 µM (Fig. 4C). The increase in K_d value in the presence of SB further strengthens the fact that SB significantly affected the equilibrium between DNA-bound ToxT and free DNA (Fig. 4C). Another butyrate derivative, tributyrate (TB), was used, and it showed no inhibition on ToxT-DNA binding (Fig. S3C). We also checked the alternative hypothesis that SB can interact with DNA and inhibit the DNA-protein binding. As shown in Fig. S3D, no inhibition on DNA binding activity was observed under this reaction condition (SB incubated with DNA first instead of ToxT), indicating that SB specifically binds to ToxT but not DNA.

The results obtained from the EMSAs indicated that SB affects the DNA binding ability of ToxT *in vitro*. Similarly, we performed a chromatin immunoprecipitation (ChIP) assay to determine whether SB could affect the ToxT-DNA binding under physiological conditions where ToxT co-exist with other transcriptional factors. As predicted, ToxT occupancy at the *tcpA*(P_{tcpA}) and *ctxAB*(P_{ctxAB}) promoter region was drastically reduced in SB-treated *V. cholerae* cells compared with untreated cells, suggesting a strong interference of SB on the ToxT-P_{tcpA} and ToxT-P_{ctxAB} binding (Fig. 4E). In addition to this, we also assessed whether ToxT interaction with the promoter DNAs of *acfA* (P_{acfA}), *aldA* (P_{aldA}), *acfD* (P_{acfD}), *tagA* (P_{tagA}), and *tcpI* (P_{tcpI}) genes (ToxT-regulated genes that encode accessory virulence factors) was affected by the addition of SB. Our results indicated that ToxT occupancy at each of these promoters was also reduced in SB-treated *V. cholerae* cells compared with the untreated cells (Fig. 4E). Altogether, these data indicate that SB strongly inhibits the binding of ToxT to its various downstream promoter DNAs.

SB triggers global changes in the transcriptome of *V. cholerae*

Next, we determined the global effects of SB on the transcriptional profile of *V. cholerae.* By using an RNA-seq approach, we found out that SB triggered global changes in gene expression, significantly upregulating 53 genes and downregulating 95 genes compared with untreated conditions (Fig. 5A through C). Genes primarily involved in pathogenesis, metabolism, and transcriptional/translational regulatory factors exhibited downregulation while biofilm-related genes showed upregulation (Fig. 5A through C). Twelve differentially expressed genes were randomly selected for qRT-PCR to validate the RNA-seq data. Our results showed that the expression trends of the twelve genes were consistent between RNA-seq and qRT-PCR data, suggesting that RNA-seq was reliable in identifying transcriptional changes (Fig. 5D).

SB displays a substantial reduction in virulence attributes of *V. cholerae* in animal models

The results described so far indicate that SB has a strong negative effect on ToxT activity *in vitro*, as assessed by both gene expression (CT and TcpA production) and DNA binding experiments (EMSA). The next step was to determine whether the administration of SB in animal models for cholera would reduce virulence factor production. First, we assessed the effect of SB on the colonizing ability of *V. cholerae* N16961 in suckling mice. Intestinal colonization of N16961 in SB-treated mice (40 and 80 mM of SB administered orogastrically) was significantly reduced by at least two orders of magnitude compared

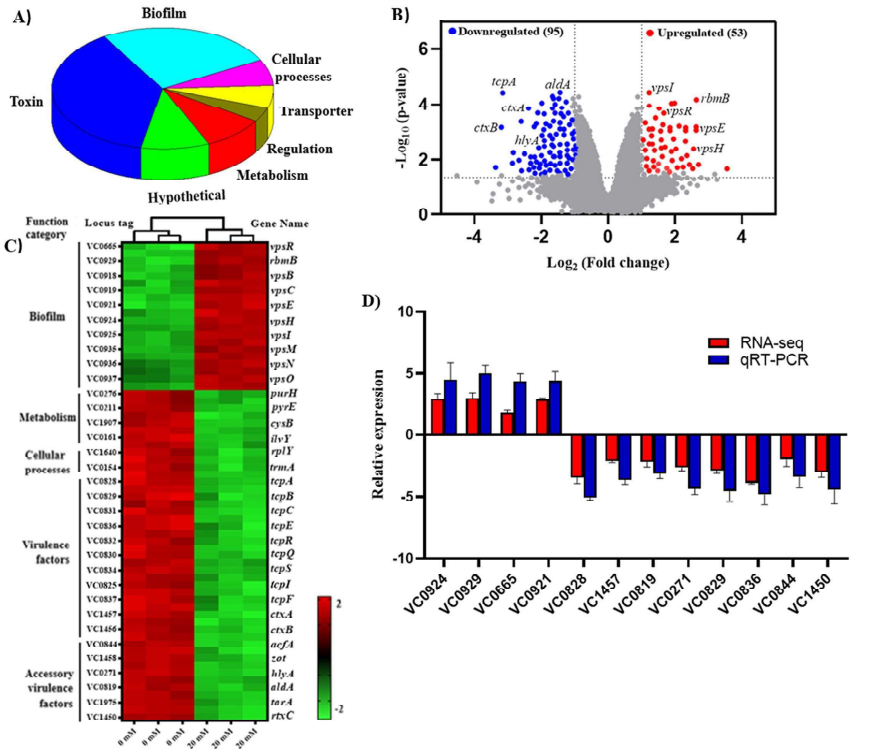

FIG 5 Global transcriptional responses to SB. (A) Genes whose expression is dysregulated in SB-treated cells (20 mM) relative to the untreated cells, as identified by RNA-seq analysis. The genes in each functional category are shown as percentages of the total genes dysregulated. (B) Volcano plot of differentially expressed genes of N16961 cells in the presence or absence of SB treatment. The $\log_2$ fold change difference is represented on the *X*-axis and $-\log_{10}$ (*P*-value) is on the *Y*-axis. Red and blue dots show upregulated and downregulated genes. (C) Heatmap of differentially expressed genes of N16961 cells in the presence or absence of 20 mM of SB. The z-score indicates whether the genes were upregulated (red) or downregulated (green). Columns represent independent RNA samples. (D) RNA-seq results validation by qRT-PCR. Data are presented as mean ± SD ($n = 3$).

with the untreated mice group (Fig. S4A). *In vivo* adherence study performed in rabbit ileal loop also revealed a significant reduction in bacterial adhesion (adherence index) in SB-treated loops compared with the untreated loop (Fig. S4B).

The effects of SB on fluid accumulation (FA) and CT production by N16961 were also assessed in the rabbit ileal loop model (Fig. 6). FA (fluid accumulation) ratio of SB treatment loops (40 and 80 mM) showed more than 20-fold reduction in fluid accumulation compared with the loop without SB (Fig. 6B). At the two highest SB concentrations (40 and 80 mM), the CT level was markedly reduced by more than 10-fold compared with the loop that received no SB (Fig. 6C). The expression of virulence genes (*ctxAB* and *tcpA*) was downregulated in *V. cholerae* cells collected from SB-treated loop fluid compared to the untreated loop (Fig. 6D).

We also checked the *V. cholerae* virulence in the presence of TB. As anticipated, the administration of TB to suckling mice did not reduce intestinal colonization of N16961 compared with untreated mice (Fig. S4A). Similarly, no reduction in fluid accumulation and CT level was observed in the TB-treated ileal loop compared with the untreated loop (Fig. S4D through F). The expression profile of virulence genes of *V. cholerae* cells in the TB-treated loop was almost similar to that of the untreated loop (Fig. S4G).

The histopathological analysis of the infected ileal loop, stained with H&E, showed damage in the mucosa, submucosa, and lamina propria, along with disrupted villi and hemorrhage at the site of the muscularis mucosa. In contrast, the analysis of the ileal loops treated with SB displayed an almost normal microvilli structure. There were no

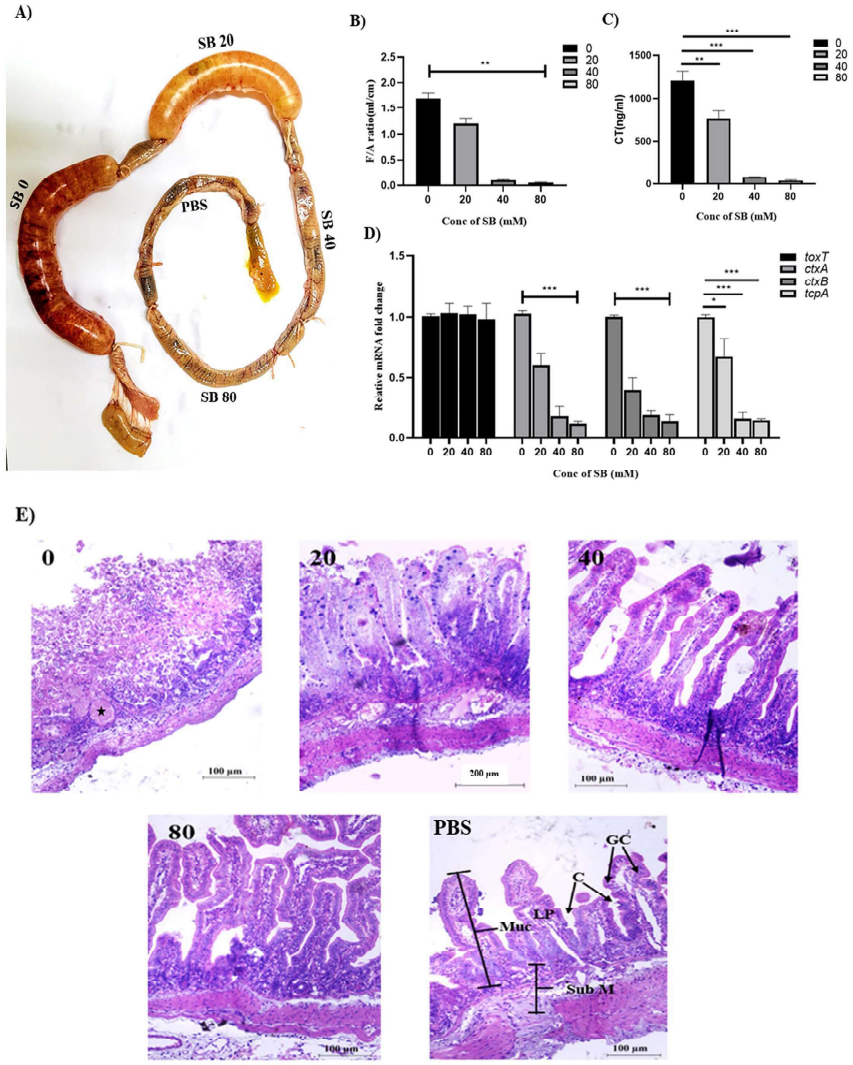

FIG 6 The efficacy of SB in an *in vivo* rabbit ileal loop model infected with N16961. Each loop was infected with 10^9 CFU per mL *V. cholerae* N16961 in the presence or absence of SB (20, 40, and 80 mM). After 18 h, the animals were euthanized, and the loops were removed. (A) The image of the recovered rabbit intestine segment presented here is representative of three independent experiments. (B) The loop length and the amount of fluid accumulated in each loop were measured, and the amount of fluid (mL) per unit length (cm) of the loop was determined. (C) CT ELISA of rabbit ileal loop fluid produced in the presence and absence of SB. (D) Relative expression of major virulence genes *ctxA*, *ctxB*, *tcpA*, and *toxT* was analyzed by real-time PCR. All the data are expressed as mean ± SD from three independent experiments. Significance was calculated by one-way ANOVA. (E) Representative H&E staining section of rabbit intestinal tissues. In the infected loop, the damage was observed in the mucosa, submucosa, and lamina propria, along with disrupted villi and hemorrhage at the site of the muscularis mucosa. The ileal loops treated with SB showed normal microvilli structure with no alterations in the villi or mucosal structure, and no substantial damage was observed either in the submucosa or muscularis mucosa. GC, goblet cells; C, crypts; LP, lamina propria; Muc, mucosa; SubM, submucosa; *, indicating the site of hemorrhage.

significant alterations in the villi and mucosal structure, and no substantial damage was observed either in the submucosa or muscularis mucosa (Fig. 6E). Furthermore, loops that were subjected to SB treatment displayed a significant reduction in concentration of inflammatory cytokines (IL-6, IL-8, IL-1β, and TNF-α) compared with the loop that

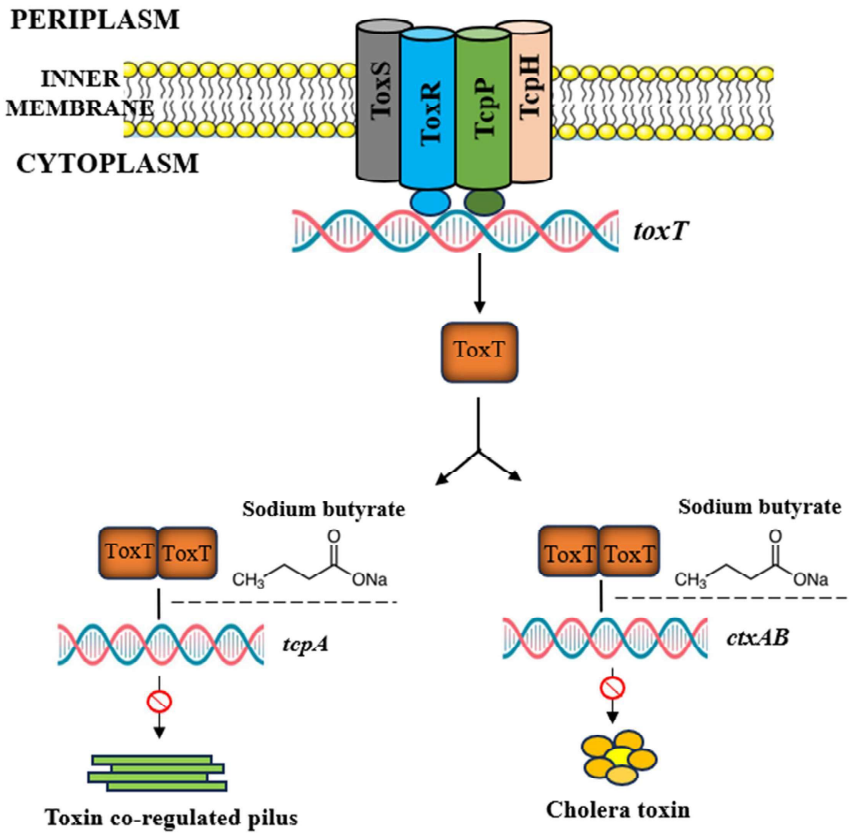

FIG 7 Model showing the inhibition of virulence cascade in *V. cholerae* by SB. The virulence cascade in *V. cholerae* is tightly regulated. TcpPH forms an inner membrane complex with ToxR and ToxS to activate the transcription of *toxT*. ToxT activates the transcription of *tcpA-F*, which encodes the toxin coregulated pilus, and *ctxAB*, which encodes the cholera toxin subunits. Based on our experiments, we propose that SB inhibits the binding of ToxT protein to the promoter region of *tcpA*/*ctxAB* and eventually inhibits cholera toxin and *tcpA* production.

received no SB (Fig. S4C). In summary, SB downregulates the expression of *ctxAB* and *tcpA* genes by inhibiting ToxT activity (Fig. 7).

DISCUSSION

Despite the use of antibiotics and oral rehydration therapy (ORT), *V. cholerae* remains a significant public health concern. This situation has emerged due to the increase of antibiotic-resistant *V. cholerae* strains, found in the majority of cholera cases, causing substantial mortality and morbidity (35). Developing new treatment therapies that target the key virulence factors without affecting the bacterial viability could be useful in managing these antibiotic-resistant strains (36). This study demonstrates that a small molecule, SB, effectively reduces the virulence potential of *V. cholerae in vitro* and *in vivo* conditions, without significantly affecting their viability.

In *V. cholerae*, the ToxR regulon plays a central role in the pathogenesis of the organism by regulating multiple virulence pathways (37). Of all the regulatory factors constituting the ToxR regulon, the ToxT protein directly activates the expression of major virulence factors *tcp* (toxin co-regulated pilus, expressing different adhesion proteins) and *ctx* (cholera toxin gene, expressing major toxin proteins like CtxA/B); therefore, it is considered a key target for the development of novel inhibitors (38). ToxT functions as a dimer with two well-defined functional domains in each monomer, a C-terminal DNA binding domain and an N-terminal regulatory/dimerization domain (39). Therefore, any compound that disrupts DNA binding and/or dimerization of ToxT would be expected

to inhibit its activity. Based on our molecular docking analyses, SB was identified as a potential drug candidate that binds at the interface between the regulatory and DNA-binding domains of ToxT. SB was then experimentally tested to assess its impact on the ToxT-mediated transcription of *tcpA* and *ctxAB* genes. The results of our *in vitro* assays (EMSA and ChIP-qPCR) further confirmed that SB strongly reduced the expression of virulence genes by affecting the DNA binding ability of ToxT. Previous studies have shown a similar mechanism of action where unsaturated fatty acids (UFAs) and their conjugated forms exhibited anti-ToxT activity (22, 40).

Our RNA-seq data also provide evidence that SB attenuates the expression of *ctx* and *tcp* genes in a ToxT-mediated manner; however, an increase in the expression of biofilm genes was observed. This apparently conflicting result is not unprecedented. Previous studies have reported the ability of anti-virulence agents to downregulate the expression of *tcp* and *ctx* genes while simultaneously upregulating the expression of biofilm genes (41, 42). In addition, SB decreased the expression of accessory genes important for pathogenesis such as hemolysin (*hlyA*), accessory colonization factors (*acfA*), and enterotoxins (*zot*). Therefore, dysregulation of these virulence factors, particularly *ctx* and *tcp* genes, may reduce the pathogenicity of *V. cholerae*. Hence, targeting ToxT becomes even more significant in this context.

Prior studies have shown that when the anionic carboxylate of UFAs formed salt bridges with the two specific lysines (i.e., Lys31 and Lys230) of ToxT, the protein was locked in a closed conformation and failed to dimerize and/or bind DNA (39, 43). Likewise, another study highlighted the importance of the carboxyl moiety of synthetic compounds, as it was found to be necessary for binding and inhibition of ToxT (44). In our present study, the docking analysis identified two key residues of ToxT, namely Lys31 (located at the N-terminal end) and Lys230 (situated at the C-terminal end) to be involved in SB-ToxT interaction. These two residues are predicted to form H-bonds and salt bridges with the anionic carboxylate group of SB. The absence of a free carboxyl group in TB may explain the molecule's inability to interact with ToxT. Based on these observations, we speculate that interaction between the carboxyl group of SB and lysines of ToxT may play a crucial role in SB-ToxT stability, resulting in a direct blockage of protein-DNA binding and/or dimerization. Loss of activity triggered by ligand binding (SE-1, decanoic acid) is also well documented in other transcriptional factors such as VirF, Rns (45, 46).

There is a constant demand for alternative medicines that can be an efficient therapeutic to cure *V. cholerae* infections with minimal side effects on the host. A group of researchers identified a class of compounds, sulfonamides, which are widely used as bacteriostatic agents that inhibit cell growth by interfering with folic acid biosynthesis (47). Their spectrum of activity encompasses a wide range of gram-negative, gram-positive bacteria, and some protozoan species (47). In *V. cholerae*, sulfonamides exhibited anti-bacterial and anti-virulence activity by inhibiting metalloenzyme carbonic anhydrase, which reduced bicarbonate production, in turn affecting ToxT activity (major regulator of virulence factors in *V. cholerae*) (48–50). However, the main problem is that sulfonamides are promiscuous inhibitors of most human carbonic anhydrase isoforms, causing serious side effects like metabolic acidosis, kidney stones, and rare but severe conditions like Stevens-Johnson syndrome (SJS), toxic epidermal necrolysis (51). In the case of SB, several reports indicate that it exerts diverse beneficial effects on the host by maintaining intestinal homeostasis through changes in gene expression and signaling pathways (52, 53). It supports normal intestinal function by acting as an energy source for aerobic metabolism and increasing the proliferation of normal colonocytes (54). Butyrate also promotes blood flow and gut motility, which are important for digestion (53). Reports suggest that butyrate can alleviate obesity-related complications by significantly enhancing intestinal epithelial function, primarily by strengthening the gut barrier through tight junction regulation, thereby reducing inflammation and improving metabolic health (55, 56). Butyrate also possesses antibacterial activity against various gram-positive and gram-negative bacteria such as *Acinetobacter baumannii*, *Bacillus*

anthracis, Bacillus subtilis, and *Staphylococcus epidermidis* (30). In our experiment, SB exhibited anti-virulence activity against *V. cholerae* by directly binding to ToxT and inhibiting its activity, which led to the downregulation of genes belonging to *tcp* and *ctxAB* operons. Although there are many benefits associated with SB for gut health, including its anti-bacterial and anti-virulence properties, it is important to acknowledge a few disadvantages associated with its use. First, studies have reported a paradoxical effect of butyrate on glucose and lipid metabolism, particularly in relation to its role in obesity. Although butyrate is reported to alleviate diet-induced obesity in mice (57), on the contrary, in a few studies, butyrate and other SCFAs have been found to contribute to the obese phenotype in humans by increasing lipid biosynthesis from acetyl CoA, FAs, and ketone bodies (58, 59). Second, butyrate may indirectly affect the host's appetite and eating behavior by stimulating the vagus nerve and the hypothalamus, due to its capability to penetrate the blood-brain barrier (60, 61). Altogether, these reports suggest that SB is beneficial for gut health, but there are also a few side effects that may be manageable while developing targeted therapeutics to treat *V. cholerae* infections.

Butyric acid is a SCFA and one of the main metabolites of intestinal microbial fermentation of dietary fiber (62). Compared with other SCFAs, extensive research has been done on butyrate, which highlighted its importance in various pathological processes (63–65). As a U.S. Food and Drug Administration-approved drug (Butyric acid- 21CFR182.60), butyrate has been used in patients suffering from autoimmunity, cancer, and neurological diseases (66–68). Butyrate promotes intestinal epithelial barrier function and regulates the host mucosal immune system (69). Notably, butyrate is reported to limit pathogen proliferation through increasing mucosal barrier and secretion of AMPs (70). In our experiments, SB treatment decreased bacterial colonization in the suckling mice. Our findings are further supported by studies about the inhibitory effect of SB on the colonization of *Salmonella sp* (71, 72). Remarkably, SB treatment also reduced CT production and fluid accumulation in the rabbit ileal loop. However, when another butyrate derivative (TB) was used in animal models, it was ineffective against *V. cholerae* virulence. Since our *in vitro* findings demonstrated that SB inhibits ToxT activity while TB showed no such inhibition, we hypothesize that SB attenuates *V. cholerae* virulence *in vivo* possibly by targeting ToxT-mediated virulence. Altogether, these findings suggest that SB is highly effective against *V. cholerae* virulence, which may reduce the severity and duration of the disease. There are various reports regarding the *in vitro* inhibition of ToxT activity by the inhibitors, but their efficacy *in vivo* conditions remains far from being elucidated (40, 43). Here, we have shown for the first time that SB exhibited strong anti-virulence activity against *V. cholerae in vitro* and *in vivo* conditions.

Although we have demonstrated the protective effects of SB against *V. cholerae*, it is essential to acknowledge that our research currently possesses certain limitations and needs further investigation. First, in our study, a molecular docking experiment predicted the binding site of SB with ToxT. In addition to docking studies, a structural, in-depth analysis is requisite for gaining better insights into the exact binding position of SB and how this interaction affects the DNA binding ability. Second, our results so far do not offer a specific explanation for the increase in biofilm-forming genes. Future work will therefore aim to unravel the pathway(s) that can link the differential changes in virulence gene expression. Third, although we have explored the *in vivo* mechanisms of SB in suckling mice and rabbit ileal loops, these two animal models hold certain limitations. The lack of severe diarrhea and an underdeveloped host defense system in suckling mice do not provide information about the host factors important for the secretory response. In the case of the rabbit ileal loop, the closed intestinal loop system bypasses the natural route of infection as well as several aspects of GI tract physiology, such as peristalsis. Therefore, a direct confirmation of our study awaits an improved mammalian model.

In conclusion, this study reports that SB inhibits ToxT activity in *V. cholerae*. This is the first report of direct binding of SCFA, butyrate, to a virulence regulator in *V. cholerae*. Mitigation of *V. cholerae* virulence without reducing bacterial burden may also reduce

the potential to develop unwanted antibiotic resistance. Furthermore, the homology of ToxT with other virulence regulators in different pathogenic bacteria could facilitate the development of broad-spectrum anti-virulent agents (46, 73). Such therapeutics would offer a new option to treat MDR bacterial infections.

MATERIALS AND METHODS

Computational methods

The 3D structure of the docking target ToxT was downloaded from the RCSB Protein Databank Server and visualized using UCSF Chimera version 1.11. The said protein was prepared for docking using the Yasara engine and then saved as a new PDB file using Chimera. The ligands used for docking were collected from different literature sources. Ligands were converted to the PDB file using UCSF Chimera (74, 75) and were energy minimized using universal force fields (UFF). These ligands were then docked into the binding pocket of ToxT using PyRx autodock vina, and the energy values were computed for each ligand. Ligands that fit into the binding pocket were selected and considered for further *in vitro* and *in vivo* studies.

Bacterial strains and culture conditions

Bacterial strains used in this study and their antibiotic resistance profiles are listed in Table S2. Strains were maintained at −80°C in Luria-Bertani broth (LB) containing 20% glycerol. Overnight cultures were grown for 24 h at 37°C in LB medium. Growth of the *V. cholerae* strains under toxin-inducing conditions consists of diluting overnight culture 1:1,000 in fresh AKI medium, growing them under stationary conditions for an initial 4 h, and then shifting to shaking condition for another 16 h (15). Concentrations of antibiotics used (Sigma, Saint Louis, MO) were as follows: streptomycin, 100 µg/mL, and ampicillin, 100 µg/mL.

Susceptibility testing and growth curve assay in the presence of SB

SB used in this study was purchased from Sigma-Aldrich. SB stock solution was made to 5 M in water and was stored at 4°C.

The MIC was determined following the Clinical and Laboratory Standards Institute microdilution assay using the cation-adjusted Mueller-Hinton broth (CAMHB) (76). Bacterial strains were grown on Luria agar plates (LA) at 37°C overnight. The colonies were resuspended in CAMHB to a 0.5 McFarland standard. The 100 µL of adjusted culture was further diluted with serially diluted concentrations of SB (ranging between 600 mM and 5 mM) in CAMHB in a round bottom 96-well plate to a final concentration of 5×10^5 CFU/mL. The plates were incubated at 37°C for 24 h without shaking. The concentrations of SB that did not affect the bacterial growth were selected as the sub-MICs for this study, whereas the lowest concentration that inhibited the visible bacterial growth was identified as the MIC (77). To determine the MBC values, 100 µL of each well medium with no visible growth was inoculated in Mueller-Hinton agar plates (MHA). The lowest concentration at which no colonies were identified on the plate after 24 h incubation was determined to be the MBC.

To evaluate the effect of SB on bacterial growth, the overnight bacterial cultures were diluted 1:1,000 in a flask containing 200 mL of LB broth with or without SB and incubated at 37°C with shaking at 180 rpm. A 100 µL aliquot was removed from the flask, and suitable dilutions were plated on LA plates containing antibiotics. The growth curve was determined by cell counts and is expressed in $\log_{10}$CFU/mL. Experiments were independently performed three times.

Detection of cholera toxin by ELISA

Cultures of *V. cholerae* were grown under toxin-inducing conditions in the presence or absence of SB. GM1 ganglioside enzyme-linked immunosorbent CT assays were

performed as previously described (78) on equal volumes of resulting supernatant. CT expression values were normalized to OD_{600}, and the average was calculated from triplicate experiments.

RNA isolation and qRT PCR

Cells were cultured under toxin-inducing conditions in the presence or absence of SB. RNA was harvested with Trizol (Invitrogen, Carlsbad, CA) according to the manufacturer's instructions, and DNA was removed using a DNA-free kit (Ambion, Austin, TX). RNA was converted to cDNA using the cDNA synthesis kit (Thermo Scientific, Waltham, MA). Real-time PCR was performed in the StepOnePlus real-time PCR system (Applied Biosystems, Foster City, CA) using SYBR green master mix (Applied Biosystems) according to the manufacturer's instructions. The mRNA quantity relative fold change data were calculated using standard curves (79) and normalized by the expression levels of the *recA* gene (internal reference gene) (80). The results are the averages from three biological replicates with three technical replicates per experiment. Primer sequences used in this study are listed in Table S3.

Western blot analysis

Cells were cultured under toxin-inducing conditions in the presence or absence of SB. Next, the bacterial cells were pelleted from each condition at 5,000 × *g* for 10 min. After the supernatant was decanted, the pellets were resuspended in phosphate-buffered saline (PBS). Cells were lysed by sonication for 3 min and centrifuged at 12,000 × *g* for 10 min at 4°C to remove cell debris. Then, the clear lysate was collected in a new tube, and protein concentrations were determined using a Bradford assay reagent (Thermo Scientific). Next, 20 µg of the total protein from each cell lysate was loaded and separated by 12% sodium dodecyl sulfate-polyacrylamide gel electrophoresis (SDS-PAGE). The proteins were transferred onto a polyvinylidene fluoride (PVDF) membrane (Millipore, Burlington, MA) and probed via immunoblotting. The following antibodies were used for immunoblotting: rabbit polyclonal ToxT, TcpA, and DnaK (Biobharati Life Sciences, West Bengal, IN) primary antibodies and horseradish peroxidase (HRP)-conjugated goat anti-rabbit secondary antibody (Sigma-Aldrich). Bands were observed in the ChemiDoc MP Imaging System (Bio-Rad, Hercules, CA) using chemiluminescent HRP substrate (Millipore). Relative fold changes in protein expression were measured after normalizing against DnaK using Image Lab software (version 5.2.1).

Protein purification

Nickel binding protein-recombinant protein fusion (NBP-ToxT/CytR) purification was performed as previously described using *Escherichia coli* strain BL21(DE3) with plasmid pHIS-Tev plasmid harboring the 6× His-recombinant protein fusion construct (40). Briefly, after NBP-recombinant protein fusion construct induction by Isopropyl-β-D-thiogalacto-pyranoside (IPTG), cells were lysed by sonication and loaded on top of Ni^{2+}-conjugated agarose beads. The fractions containing NBP-recombinant protein were dialyzed with 25 mM Tris (pH 8.0) and 100 mM NaCl solution. Purified protein was quantified by Bradford reagent, and the purity was confirmed by SDS-PAGE, stained with Coomassie Brilliant Blue.

Fluorescence quenching

Interaction between ToxT protein and SB was analyzed by the concentration-dependent effect of SB on the tryptophan fluorescence emission of ToxT. The emission spectra of ToxT were acquired using 0.1 µM protein dissolved in 25 mM Tris (pH 7.5) and 100 mM NaCl in the presence or absence of SB. The solution was excited at 280 nm, and the intrinsic fluorescence emissions were scanned from 300 nm to 500 nm (Hitachi

Fluorescence Spectrophotometer F-7000, Tokyo, Japan). Fluorescence quenching was analyzed by the classical Stern-Volmer equation as previously described (81).

EMSA and ChIP

The chromosomal DNA of *V. cholerae* N16961 was used as a template in the PCR process to amplify DNA fragments of size 150 bp for the *tcpA* promoter region. Then this amplified product was labeled with biotin at the 5′ end followed by purification using the Qiaquick nucleotide removal kit (QIAGEN, Hilden, Germany). EMSA of ToxT protein binding to the *tcpA* promoter region was performed as described previously (22). For the EMSA binding assay, different concentrations of purified ToxT protein (0.4, 0.6, 0.8, 1.0, 1.2, 1.4, and 1.6 µM) were mixed with fixed amounts of biotin-labeled DNA fragment P_{tcpA} (1 nM) in a binding buffer (10 mM Tris-HCl [pH 7.5], 100 mM KCl, 1 mM EDTA, 1 mM dithiothreitol, 200 µg of bovine serum albumin/mL, and 10% glycerol) and incubated for 20 min (82). To check the SB-ToxT interaction, the binding reactions were set up where different concentrations of ToxT (0.4, 0.6, 0.8, 1.0, 1.2, 1.4, and 1.6 µM) were pre-incubated with SB (20 mM) for 20 min in binding buffer, followed by the addition of DNA fragment P_{tcpA} (1 nM) and incubation continued for another 20 min. To determine the effect of increasing concentrations of SB, the binding reactions were set up where ToxT (1.0 µM) was pre-incubated with varying doses of SB (10, 20, and 40 mM) for 20 min in binding buffer, followed by the addition of DNA fragment P_{tcpA} (1 nM). To determine the specificity of SB-ToxT interaction, the binding reactions were set up where ToxT (1.0 µM) was pre-incubated with SB (40 mM) or another butyrate derivative TB (40 mM) for 20 min in binding buffer, followed by the addition of DNA fragment P_{tcpA} (1 nM). Furthermore, to check possible SB-P_{tcpA} DNA interaction, labeled P_{tcpA} DNA (0.5 nM) was pre-incubated with SB (20 and 40 mM) for 20 min in binding buffer, followed by the addition of purified ToxT protein (4 µM), and the incubation continued for another 20 min (82). To show the specificity, non-specific protein (CytR, 1.0 µM), a 70-fold molar excess of unlabeled double-stranded *tcpA* fragment, and a 70-fold molar excess of unlabeled nonspecific DNA were used as controls (Table S3). The samples were loaded on 4% native polyacrylamide gel and electrophoresed at 100 V, 4°C in 0.5× Tris-borate-EDTA buffer. DNA was then transferred from gel to charged nylon membrane for nucleic acid blotting (Millipore) followed by cross-linking using a UV Stratalinker from Stratagene and detected using LightShift Chemiluminescent EMSA Kit (Thermo Scientific).

To determine the K_d (equilibrium dissociation constant) for samples with or without SB, the percentage of labeled DNA bound to protein was determined for each lane. This was then fit to the following equation: percent bound = $B_{\max} \times [\text{protein}]^h/(K_d{}^h + [\text{protein}]^h)$, where h is the Hill coefficient and $B_{\max}$ is the amount of bound DNA at which the curve plateaus, which was set to a constraint of 100% using GraphPad Prism 9.0 software. The K_d values for each condition were compared using the extra sum of squares F test to determine if the two values were statistically different.

ChIP analysis was performed as described previously (83), with some modifications. Briefly, cells were grown in the presence or absence of SB for 4 h. After cross-linking with formaldehyde, cells were lysed and sonicated to shear the genomic DNA. Clarified lysates were incubated for 6 h at 4°C with 8 µg anti-ToxT antibody or control mouse IgG (Cell Signaling Technology). The chromatin fraction, which lacks the primary antibody, was taken as "input." After washing, the immunoprecipitated complexes were eluted, and DNA was reverse cross-linked. Real-time quantitative PCR (qPCR) and agarose PCR gel electrophoresis were used to quantitate promoter occupancy by ToxT as formerly described (84, 85) using the primers for ChIP (Table S3). The data were graphically represented as % input.

RNA sequencing and analysis

Triplicate N16961 samples were grown under toxin-inducing conditions in the presence or absence of SB. Total RNA was isolated as described above, and mRNA was selectively enriched by depleting rRNA using a Ribo-Zero rRNA removal kit (Epicentre, Madison, WI). Then, the cDNA library was constructed using a TruSeq-stranded mRNA sample kit (Illumina, San Diego, CA). RNA sequencing was done on the Illumina HiSeqX system by MedGenome Labs Ltd., Bangalore, India. The raw data were processed using the HISAT2-StringTie pipeline as described elsewhere (86). The raw sequencing reads were mapped against the genomic sequence of *V. cholerae* O1 biovar El Tor str. N16961 using the HISAT2 alignment tool. StringTie was used to assemble reads and generate FPKM (fragments per kilobase per million) values, as a normalization metric (87). After filtering undesirable contaminants (such as rRNAs), differentially expressed genes between different groups were identified by the package DESeq2 [20 mM of SB over 0 mM of SB treatment were determined as fold change (FC) by the formula log2(mean $FPKM_{test}$/mean $FPKM_{control}$)], with thresholds of adjusted *P* values at ≤0.05 and an absolute fold change ≥2. The differentially expressed genes identified among the two groups were generated in a heatmap by the CIMminer program as described previously (88). The complete list of the FPKM values, fold change values, and *P* values are provided in Data Set S1.

Cell culture experiments

Human adenocarcinoma cell line HT-29 (ATCC HTB-38) was maintained in Dulbecco modified essential medium (DMEM) (Sigma-Aldrich) supplemented with 10% fetal bovine serum (PAN Biotech, Aidenbach, BY). The cells were kept at 37°C in a humidified 5% CO_2 incubator.

Adhesion of *V. cholerae* to HT-29 cells was done according to the previously described method (80). Briefly, HT-29 cells were grown up to 80%–90% confluency. The cells were infected with bacterial suspensions in DMEM (without antibiotics) at an MOI of 100 for 2 h in the presence or absence of SB. Following incubation, the nonadherent bacteria were completely removed by washing with PBS. Cells were lysed in 0.1% Triton X-100 solution. The lysate solution was gradient-diluted and plated on LA plates, and the plates were incubated overnight at 37°C. The attachment efficiency was determined by the number of bacteria recovered on plates. At least three independent biological replicates were prepared and analyzed.

The MTT assay was performed as described previously (89). Briefly, HT-29 cells were treated with different doses of SB (5–160 mM) at 37°C. The cell viability was determined after 24 h using the Colorimetric Cell Viability Kit IV (MTT) (Promokine, Heidelberg, Germany) according to the manufacturer's guidelines. The absorbance was read at 570 nm, and % viability was calculated as described previously (26).

Suckling mice colonization assay

Four- to five-day-old suckling BALB/c mice were orogastrically inoculated with 50 µL (containing 10^5 CFU of *V. cholerae* cells) of the bacterial suspension with or without drugs. The mice were maintained at 30°C and sacrificed after 18 h. The entire intestine was removed and homogenized in PBS. Serial dilutions of the homogenates were then plated on LA plates containing antibiotics to enumerate viable *V. cholerae* cells and expressed as CFU per mouse intestine (90). The colonization experiment was performed three times independently in 3 days with at least four mice in each group, and the combined data for the three experiments were used for statistical analysis.

Rabbit ileal loop assays

Assays of fluid accumulation in rabbit ileal loops were performed as previously described (90). Each loop received 1 mL (containing 10^9 CFU of *V. cholerae* cells) of bacterial suspension with or without drugs. After 18 h, the rabbits were sacrificed, and their

intestine was dissected. The fluid accumulated within each loop was collected separately, measured, and expressed as a ratio of the amount (mL) of fluid per unit length (cm) of the loop. The amount of CT produced was assessed by CT-ELISA, and the inflammatory cytokines (IL-6, IL-8, IL-1β, and TNF-α) produced under each condition were determined by ELISA kits (Krishgen, Mumbai, India) following the manufacturer's instructions. For qRT-PCR analysis of virulence genes, bacteria were harvested from loop fluid by centrifugation and used for RNA preparation, which is further processed to qRT-PCR as described above.

The ileal loops obtained from the above procedure were analyzed for the estimation of adhered bacteria to the intestinal mucosa following the previously described protocol (91). Briefly, the fluid in the loops was taken out as outlined above. Each intestine was then excised and opened by longitudinal incision and was washed three times with PBS to remove the nonadherent or loosely adhered bacteria. After washing, the opened intestine was stretched on a wooden sheet with a luminal surface uppermost, and several circular pieces of mucosa (7 mm in diameter) were punched out. Each of the intestinal punches was then homogenized in 0.25 mL of Krebs/Ringer/Tris (KRT) buffer (pH 7.5). To determine the viable cells of *V. cholerae*, 0.1 mL of the homogenate was serially diluted in PBS and 0.1 mL of aliquots were plated onto LA plates containing antibiotics to enumerate viable *V. cholerae* cells. The adhesive ability of *V. cholerae* (adherence index) was expressed as the average number of adhered bacterial cells per punched mucosal surface.

For the histopathological study, rabbit ileal tissue samples were fixed with 10% buffered formalin, embedded in paraffin, and sliced into 4-µm-thick sections. The tissue was then deparaffinized and stained using HE and visualized using a bright field microscope for further analysis. The rabbit ileal loop experiments were performed three times independently, and the results were expressed as mean ± SD (n = 3).

Statistical analysis

Statistical analyses were carried out using the GraphPad Prism 9.0 software, and all data are denoted as mean ± standard deviation (SD) unless otherwise specified. The results were analyzed using appropriate statistical tests as indicated in figure legends.

ACKNOWLEDGMENTS

S.K. thanks the University Grants Commission (UGC). P.M. thanks the Council for Scientific and Industrial Research (CSIR), and P.H. thanks the Indian Council of Medical Research (ICMR) for supporting with fellowship. We also thank the Indian Council of Medical Research (ICMR) and Department of Health Research (DHR) for institutional funding. This work was supported by the Japan Agency for Medical Research and Development (AMED; Grant No. JP24wm0125004 (to S.-I.M.).

AUTHOR AFFILIATIONS

[1]Division of Biochemistry, ICMR-National Institute for Research in Bacterial Infections (Formerly ICMR-National Institute of Cholera and Enteric Diseases), Kolkata, India
[2]Division of Bacteriology, ICMR-National Institute for Research in Bacterial Infections (Formerly ICMR-National Institute of Cholera and Enteric Diseases), Kolkata, India
[3]Division of Pharmaceutical Sciences, Graduate School of Medicine, Dentistry and Pharmaceutical Sciences, Okayama University, Okayama, Japan

AUTHOR ORCIDs

Sushmita Kundu http://orcid.org/0009-0006-4004-8481
Suman Das http://orcid.org/0000-0003-2714-033X
Sushmita Bhattacharya http://orcid.org/0009-0001-6867-4381

FUNDING

Funder	Grant(s)	Author(s)
Japan Agency for Medical Research and Development	JP24wm0125004	Sushmita Kundu Shin-ichi Miyoshi Sushmita Bhattacharya

AUTHOR CONTRIBUTIONS

Sushmita Kundu, Conceptualization, Data curation, Formal analysis, Investigation, Methodology, Validation, Visualization, Writing – original draft, Writing – review and editing | Suman Das, Conceptualization, Data curation, Formal analysis, Investigation, Methodology, Validation, Visualization, Writing – review and editing | Priyanka Maitra, Conceptualization, Data curation, Formal analysis, Investigation, Validation, Visualization, Writing – review and editing | Prolay Halder, Data curation, Formal analysis, Investigation, Methodology, Validation, Visualization, Writing – review and editing | Hemanta Koley, Data curation, Investigation, Methodology, Supervision, Writing – review and editing | Asish K. Mukhopadhyay, Data curation, Investigation, Supervision, Writing – review and editing | Shin-ichi Miyoshi, Data curation, Funding acquisition, Investigation, Project administration, Resources, Supervision, Writing – review and editing | Shanta Dutta, Funding acquisition, Investigation, Project administration, Resources | Nabendu Sekhar Chatterjee, Conceptualization, Data curation, Formal analysis, Funding acquisition, Project administration, Resources, Supervision, Validation, Writing – review and editing | Sushmita Bhattacharya, Conceptualization, Data curation, Formal analysis, Funding acquisition, Investigation, Methodology, Project administration, Resources, Supervision, Validation, Visualization, Writing – original draft, Writing – review and editing

DATA AVAILABILITY

All raw transcriptome data have been deposited in the NCBI BioProject database under accession number PRJNA1194555.

ETHICS APPROVAL

All animal care and experimental procedures in the study were conducted in accordance with the Animal Ethics Committee for the Purpose of Control and Supervision of Experiments on Animals (CPCSEA). The protocol was also approved by the Institutional Animal Ethics Committee of the National Institute of Cholera and Enteric Diseases (registration no: 68/GO/ReBi/S/99/CPCSEA).

ADDITIONAL FILES

The following material is available online.

Supplemental Material

DATA SET S1 (mSphere00824-24-S0001.xlsx). RNA seq.
FIGURE S1 (mSphere00824-24-S0002.tif). Susceptibility testing and cytotoxicity of SB
FIGURE S2 (mSphere00824-24-S0003.tif). Effect of SB on the virulence attributes of V. cholerae.
FIGURE S3 (mSphere00824-24-S0004.tif). EMSAs demonstrating the specificity of the interactions.
FIGURE S4 (mSphere00824-24-S0005.tif). Efficacy of drugs against the virulence factors and inflammatory cytokines *in vivo*.
Supplemental material (mSphere00824-24-S0006.docx). Supplemental figure legends and tables.

REFERENCES

1. Clemens JD, Nair GB, Ahmed T, Qadri F, Holmgren J. 2017. Cholera. Lancet 390:1539–1549. https://doi.org/10.1016/S0140-6736(17)30559-7
2. World Health Organization. 2023. Cholera – global situation
3. Walton MG, Cubillejo I, Nag D, Withey JH. 2023. Advances in cholera research: from molecular biology to public health initiatives. Front Microbiol 14:1178538. https://doi.org/10.3389/fmicb.2023.1178538
4. Kim EJ, Lee CH, Nair GB, Kim DW. 2015. Whole-genome sequence comparisons reveal the evolution of *Vibrio cholerae* O1. Trends Microbiol 23:479–489. https://doi.org/10.1016/j.tim.2015.03.010
5. Muanprasat C, Chatsudthipong V. 2013. Cholera: pathophysiology and emerging therapeutic targets. Future Med Chem 5:781–798. https://doi.org/10.4155/fmc.13.42
6. Peterson KM, Gellings PS. 2018. Multiple intraintestinal signals coordinate the regulation of *Vibrio cholerae* virulence determinants. Pathog Dis 76. https://doi.org/10.1093/femspd/ftx126
7. Cho JY, Liu R, Macbeth JC, Hsiao A. 2021. The Interface of *Vibrio cholerae* and the gut microbiome. Gut Microbes. https://doi.org/10.1080/19490976.2021.1937015
8. Hsiao A, Zhu J. 2020. Pathogenicity and virulence regulation of *Vibrio cholerae* at the interface of host-gut microbiome interactions. Virulence 11:1582–1599. https://doi.org/10.1080/21505594.2020.1845039
9. Li J, Wehmeyer G, Lovell S, Battaile KP, Egan SM. 2016. 1.65 Å resolution structure of the AraC-family transcriptional activator ToxT from *Vibrio cholerae*. Acta Crystallogr F Struct Biol Commun 72:726–731. https://doi.org/10.1107/S2053230X1601298X
10. Ramamurthy T, Nandy RK, Mukhopadhyay AK, Dutta S, Mutreja A, Okamoto K, Miyoshi SI, Nair GB, Ghosh A. 2020. Virulence regulation and innate host response in the pathogenicity of *Vibrio cholerae*. Front Cell Infect Microbiol 10:572096. https://doi.org/10.3389/fcimb.2020.572096
11. Liu Z, Wang H, Zhou Z, Naseer N, Xiang F, Kan B, Goulian M, Zhu J. 2016. Differential thiol-based switches jump-start *Vibrio cholerae* pathogenesis. Cell Rep 14:347–354. https://doi.org/10.1016/j.celrep.2015.12.038
12. Yang M, Liu Z, Hughes C, Stern AM, Wang H, Zhong Z, Kan B, Fenical W, Zhu J. 2013. Bile salt-induced intermolecular disulfide bond formation activates *Vibrio cholerae* virulence. Proc Natl Acad Sci USA 110:2348–2353. https://doi.org/10.1073/pnas.1218039110
13. Pietroni MAC. 2020. Case management of cholera. Vaccine 38:A105–A109. https://doi.org/10.1016/j.vaccine.2019.09.098
14. Kühn J, Finger F, Bertuzzo E, Borgeaud S, Gatto M, Rinaldo A, Blokesch M. 2014. Glucose- but not rice-based oral rehydration therapy enhances the production of virulence determinants in the human pathogen *Vibrio cholerae*. PLoS Negl Trop Dis 8:e3347. https://doi.org/10.1371/journal.pntd.0003347
15. Anthouard R, DiRita VJ. 2013. Small-molecule inhibitors of toxT expression in *Vibrio cholerae*. MBio 4:e00403-13. https://doi.org/10.1128/mBio.00403-13
16. Mandal J, Dinoop KP, Parija SC. 2012. Increasing antimicrobial resistance of *Vibrio cholerae* OI biotype E1 tor strains isolated in a tertiary-care centre in India. J Health Popul Nutr 30:12–16. https://doi.org/10.3329/jhpn.v30i1.11270
17. Narendrakumar L, Gupta SS, Johnson JB, Ramamurthy T, Thomas S. 2019. Molecular adaptations and antibiotic resistance in *Vibrio cholerae*: a communal challenge. Microb Drug Resist 25:1012–1022. https://doi.org/10.1089/mdr.2018.0354
18. Verma J, Bag S, Saha B, Kumar P, Ghosh TS, Dayal M, Senapati T, Mehra S, Dey P, Desigamani A, Kumar D, Rana P, Kumar B, Maiti TK, Sharma NC, Bhadra RK, Mutreja A, Nair GB, Ramamurthy T, Das B. 2019. Genomic plasticity associated with antimicrobial resistance in *Vibrio cholerae*. Proc Natl Acad Sci USA 116:6226–6231. https://doi.org/10.1073/pnas.1900141116
19. Yen M, Cairns LS, Camilli A. 2017. A cocktail of three virulent bacteriophages prevents *Vibrio cholerae* infection in animal models. Nat Commun 8:14187. https://doi.org/10.1038/ncomms14187
20. Gupta SS, Bharati K, Sur D, Khera A, Ganguly NK, Nair GB. 2016. Why is the oral cholera vaccine not considered an option for prevention of cholera in India? analysis of possible reasons. Indian J Med Res 143:545–551. https://doi.org/10.4103/0971-5916.187102
21. Roca I, Akova M, Baquero F, Carlet J, Cavaleri M, Coenen S, Cohen J, Findlay D, Gyssens I, Heuer OE, Kahlmeter G, Kruse H, Laxminarayan R, Liébana E, López-Cerero L, MacGowan A, Martins M, Rodríguez-Baño J, Rolain J-M, Segovia C, Sigauque B, Tacconelli E, Wellington E, Vila J. 2015. The global threat of antimicrobial resistance: science for intervention. New Microbes New Infect 6:22–29. https://doi.org/10.1016/j.nmni.2015.02.007
22. Withey JH, Nag D, Plecha SC, Sinha R, Koley H. 2015. Conjugated linoleic acid reduces cholera toxin production *in vitro* and *in vivo* by inhibiting *Vibrio cholerae* ToxT Activity. Antimicrob Agents Chemother 59:7471–7476. https://doi.org/10.1128/AAC.01029-15
23. Mandal RS, Ta A, Sinha R, Theeya N, Ghosh A, Tasneem M, Bhunia A, Koley H, Das S. 2016. Ribavirin suppresses bacterial virulence by targeting LysR-type transcriptional regulators. Sci Rep 6:39454. https://doi.org/10.1038/srep39454
24. Zahid MSH, Awasthi SP, Asakura M, Chatterjee S, Hinenoya A, Faruque SM, Yamasaki S. 2015. Suppression of virulence of toxigenic *Vibrio cholerae* by anethole through the cyclic AMP (cAMP)-cAMP receptor protein signaling system. PLoS ONE 10:e0137529. https://doi.org/10.1371/journal.pone.0137529
25. Erfanimanesh S, Eslami G, Taherpour A, Hashemi A. 2018. Capsaicin inhibitory effects on *Vibrio cholerae* toxin genes expression. Avicenna J Phytomed 9:187–194.
26. Sarwar S, Ali A, Pal M, Chakrabarti P. 2017. Zinc oxide nanoparticles provide anti-cholera activity by disrupting the interaction of cholera toxin with the human GM1 receptor. J Biol Chem 292:18303–18311. https://doi.org/10.1074/jbc.M117.793240
27. Kumar V, Turnbull WB. 2018. Carbohydrate inhibitors of cholera toxin. Beilstein J Org Chem 14:484–498. https://doi.org/10.3762/bjoc.14.34
28. Wands AM, Cervin J, Huang H, Zhang Y, Youn G, Brautigam CA, Matson Dzebo M, Björklund P, Wallenius V, Bright DK, Bennett CS, Wittung-Stafshede P, Sampson NS, Yrlid U, Kohler JJ. 2018. Fucosylated molecules competitively interfere with cholera toxin binding to host cells. ACS Infect Dis 4:758–770. https://doi.org/10.1021/acsinfecdis.7b00085
29. Zhang L, Liu C, Jiang Q, Yin Y. 2021. Butyrate in energy metabolism: there is still more to learn. Trends Endocrinol Metab 32:159–169. https://doi.org/10.1016/j.tem.2020.12.003
30. Du K, Bereswill S, Heimesaat MM. 2021. A literature survey on antimicrobial and immune-modulatory effects of butyrate revealing non-antibiotic approaches to tackle bacterial infections. Eur J Microbiol Immunol (Bp) 11:1–9. https://doi.org/10.1556/1886.2021.00001
31. Namkung H, Yu H, Gong J, Leeson S. 2011. Antimicrobial activity of butyrate glycerides toward *Salmonella typhimurium* and *Clostridium perfringens*. Poult Sci 90:2217–2222. https://doi.org/10.3382/ps.2011-01498
32. Kennedy GM, Min MY, Fitzgerald JF, Nguyen MT, Schultz SL, Crum MT, Starke JA, Butkus MA, Bowman DD, Labare MP. 2019. Inactivation of the bacterial pathogens *Staphylococcus pseudintermedius* and *Acinetobacter baumannii* by butanoic acid. J Appl Microbiol 126:752–763. https://doi.org/10.1111/jam.14180
33. Defoirdt T, Mai Anh NT, De Schryver P. 2018. Virulence-inhibitory activity of the degradation product 3-hydroxybutyrate explains the protective effect of poly-β-hydroxybutyrate against the major aquaculture pathogen *Vibrio campbellii*. Sci Rep 8:1–9. https://doi.org/10.1038/s41598-018-25385-w
34. Zhu W, Gao J, Liu H, Liu J, Jin T, Qin N, Ren X, xia X. 2022. Antibiofilm effect of sodium butyrate against *Vibrio parahaemolyticus*. Food Control 131:108422. https://doi.org/10.1016/j.foodcont.2021.108422
35. Hotinger JA, Morris ST, May AE. 2021. The case against antibiotics and for anti-virulence therapeutics. Microorganisms 9:2049. https://doi.org/10.3390/microorganisms9102049
36. González A, Fillat MF, Lanas Á. 2018. Transcriptional regulators: valuable targets for novel antibacterial strategies. Future Med Chem 10:541–560. https://doi.org/10.4155/fmc-2017-0181
37. Morgan SJ, French EL, Thomson JJ, Seaborn CP, Shively CA, Krukonis ES. 2016. Formation of an intramolecular periplasmic disulfide bond in TcpP protects TcpP and TcpH from degradation in *Vibrio cholerae*. J Bacteriol 198:498–509. https://doi.org/10.1128/JB.00338-15
38. Mondal SI, Khadka B, Akter A, Roy PK, Sultana R. 2014. Computer based screening for novel inhibitors against *Vibrio cholerae* using NCI diversity set-II: an alternative approach by targeting transcriptional activator ToxT. Interdiscip Sci 6:108–117. https://doi.org/10.1007/s12539-012-0046-8
39. Cruite JT, Kovacikova G, Clark KA, Woodbrey AK, Skorupski K, Kull FJ. 2019. Structural basis for virulence regulation in *Vibrio cholerae* by unsaturated fatty acid components of bile. Commun Biol 2:440. https://doi.org/10.1038/s42003-019-0686-x

40. Plecha SC, Withey JH. 2015. Mechanism for inhibition of *Vibrio cholerae* ToxT activity by the unsaturated fatty acid components of bile. J Bacteriol 197:1716–1725. https://doi.org/10.1128/JB.02409-14
41. Wang BX, Takagi J, McShane A, Park JH, Aoki K, Griffin C, Teschler J, Kitts G, Minzer G, Tiemeyer M, Hevey R, Yildiz F, Ribbeck K. 2023. Host-derived *O*-glycans inhibit toxigenic conversion by a virulence-encoding phage in *Vibrio cholerae*. EMBO J 42:e111562. https://doi.org/10.15252/embj.2022111562
42. Perez-Soto N, Moule L, Crisan DN, Insua I, Taylor-Smith LM, Voelz K, Fernandez-Trillo F, Krachler AM. 2017. Engineering microbial physiology with synthetic polymers: cationic polymers induce biofilm formation in *Vibrio cholerae* and downregulate the expression of virulence genes. Chem Sci 8:5291–5298. https://doi.org/10.1039/c7sc00615b
43. Woodbrey AK, Onyango EO, Pellegrini M, Kovacikova G, Taylor RK, Gribble GW, Kull FJ. 2017. A new class of inhibitors of the AraC family virulence regulator *Vibrio cholerae* ToxT. Sci Rep 7:1–11. https://doi.org/10.1038/srep45011
44. Woodbrey AK, Onyango EO, Kovacikova G, Kull FJ, Gribble GW. 2018. A modified ToxT inhibitor reduces *Vibrio cholerae* virulence *in vivo*. Biochemistry 57:5609–5615. https://doi.org/10.1021/acs.biochem.8b00667
45. Koppolu V, Osaka I, Skredenske JM, Kettle B, Hefty PS, Li J, Egan SM. 2013. Small-molecule inhibitor of the *Shigella flexneri* master virulence regulator VirF. Infect Immun 81:4220–4231. https://doi.org/10.1128/IAI.00919-13
46. Midgett CR, Talbot KM, Day JL, Munson GP, Kull FJ. 2021. Structure of the master regulator Rns reveals an inhibitor of enterotoxigenic *Escherichia coli* virulence regulons. Sci Rep 11:15663. https://doi.org/10.1038/s41598-021-95123-2
47. Ovung A, Bhattacharyya J. 2021. Sulfonamide drugs: structure, antibacterial property, toxicity, and biophysical interactions. Biophys Rev 13:259–272. https://doi.org/10.1007/s12551-021-00795-9
48. Gheibzadeh MS, Capasso C, Supuran CT, Zolfaghari Emameh R. 2024. Antibacterial carbonic anhydrase inhibitors targeting *Vibrio cholerae* enzymes. Expert Opin Ther Targets 28:623–635. https://doi.org/10.1080/14728222.2024.2369622
49. Supuran CT. 2011. Bacterial carbonic anhydrases as drug targets: toward novel antibiotics? Front Pharmacol 2:34. https://doi.org/10.3389/fphar.2011.00034
50. Nocentini A, Capasso C, Supuran CT. 2023. Carbonic anhydrase inhibitors as novel antibacterials in the era of antibiotic resistance: where are we now? Antibiotics 12:142. https://doi.org/10.3390/antibiotics12010142
51. Ferraroni M, Cornelio B, Sapi J, Supuran CT, Scozzafava A. 2018. Sulfonamide carbonic anhydrase inhibitors: zinc coordination and tail effects influence inhibitory efficacy and selectivity for different isoforms. Inorganica Chim Acta 470:128–132. https://doi.org/10.1016/j.ica.2017.03.038
52. Recharla N, Geesala R, Shi XZ. 2023. Gut microbial metabolite butyrate and its therapeutic role in inflammatory bowel disease: a literature review. Nutrients 15:2275. https://doi.org/10.3390/nu15102275
53. Hodgkinson K, El Abbar F, Dobranowski P, Manoogian J, Butcher J, Figeys D, Mack D, Stintzi A. 2023. Butyrate's role in human health and the current progress towards its clinical application to treat gastrointestinal disease. Clin Nutr 42:61–75. https://doi.org/10.1016/j.clnu.2022.10.024
54. Canani RB, Costanzo MD, Leone L, Pedata M, Meli R, Calignano A. 2011. Potential beneficial effects of butyrate in intestinal and extraintestinal diseases. World J Gastroenterol 17:1519–1528. https://doi.org/10.3748/wjg.v17.i12.1519
55. Fang W, Xue H, Chen X, Chen K, Ling W. 2019. Supplementation with sodium butyrate modulates the composition of the gut microbiota and ameliorates high-fat diet-induced obesity in mice. J Nutr 149:747–754. https://doi.org/10.1093/jn/nxy324
56. Zhou D, Pan Q, Xin FZ, Zhang RN, He CX, Chen GY, Liu C, Chen YW, Fan JG. 2017. Sodium butyrate attenuates high-fat diet-induced steatohepatitis in mice by improving gut microbiota and gastrointestinal barrier. World J Gastroenterol 23:60–75. https://doi.org/10.3748/wjg.v23.i1.60
57. Hong J, Jia Y, Pan S, Jia L, Li H, Han Z, Cai D, Zhao R. 2016. Butyrate alleviates high fat diet-induced obesity through activation of adiponectin-mediated pathway and stimulation of mitochondrial function in the skeletal muscle of mice. Oncotarget 7:56071–56082. https://doi.org/10.18632/oncotarget.11267
58. Liu H, Wang J, He T, Becker S, Zhang G, Li D, Ma X. 2018. Butyrate: a double-edged sword for health? Adv Nutr 9:21–29. https://doi.org/10.1093/advances/nmx009
59. Birt DF, Boylston T, Hendrich S, Jane J-L, Hollis J, Li L, McClelland J, Moore S, Phillips GJ, Rowling M, Schalinske K, Scott MP, Whitley EM. 2013. Resistant starch: promise for improving human health. Adv Nutr 4:587–601. https://doi.org/10.3945/an.113.004325
60. van de Wouw M, Schellekens H, Dinan TG, Cryan JF. 2017. Microbiota-gut-brain axis: modulator of host metabolism and appetite. J Nutr 147:727–745. https://doi.org/10.3945/jn.116.240481
61. Gagliano H, Delgado-Morales R, Sanz-Garcia A, Armario A. 2014. High doses of the histone deacetylase inhibitor sodium butyrate trigger a stress-like response. Neuropharmacology 79:75–82. https://doi.org/10.1016/j.neuropharm.2013.10.031
62. Stilling RM, van de Wouw M, Clarke G, Stanton C, Dinan TG, Cryan JF. 2016. The neuropharmacology of butyrate: the bread and butter of the microbiota-gut-brain axis? Neurochem Int 99:110–132. https://doi.org/10.1016/j.neuint.2016.06.011
63. Cheng X, Zhou T, He Y, Xie Y, Xu Y, Huang W. 2022. The role and mechanism of butyrate in the prevention and treatment of diabetic kidney disease. Front Microbiol 13:961536. https://doi.org/10.3389/fmicb.2022.961536
64. Mayorga-Ramos A, Barba-Ostria C, Simancas-Racines D, Guamán LP. 2022. Protective role of butyrate in obesity and diabetes: new insights. Front Nutr 9:1067647. https://doi.org/10.3389/fnut.2022.1067647
65. Amiri P, Arefhosseini S, Bakhshimoghaddam F, Jamshidi Gurvan H, Hosseini SA. 2022. Mechanistic insights into the pleiotropic effects of butyrate as a potential therapeutic agent on NAFLD management: a systematic review. Front Nutr 9:1037696. https://doi.org/10.3389/fnut.2022.1037696
66. Chen X, Su W, Wan T, Yu J, Zhu W, Tang F, Liu G, Olsen N, Liang D, Zheng SG. 2017. Sodium butyrate regulates Th17/Treg cell balance to ameliorate uveitis via the Nrf2/HO-1 pathway. Biochem Pharmacol 142:111–119. https://doi.org/10.1016/j.bcp.2017.06.136
67. Wang F, Wu H, Fan M, Yu R, Zhang Y, Liu J, Zhou X, Cai Y, Huang S, Hu Z, Jin X. 2020. Sodium butyrate inhibits migration and induces AMPK-mTOR pathway-dependent autophagy and ROS-mediated apoptosis via the miR-139-5p/Bmi-1 axis in human bladder cancer cells. FASEB J 34:4266–4282. https://doi.org/10.1096/fj.201902626R
68. Kim SY, Chae CW, Lee HJ, Jung YH, Choi GE, Kim JS, Lim JR, Lee JE, Cho JH, Park H, Park C, Han HJ. 2020. Sodium butyrate inhibits high cholesterol-induced neuronal amyloidogenesis by modulating NRF2 stabilization-mediated ROS levels: involvement of NOX2 and SOD1. Cell Death Dis 11:469. https://doi.org/10.1038/s41419-020-2663-1
69. Jiminez JA, Uwiera TC, Abbott DW, Uwiera RRE, Inglis GD. 2017. Butyrate supplementation at high concentrations alters enteric bacterial communities and reduces intestinal inflammation in mice infected with *Citrobacter rodentium*. mSphere 2:e00243-17. https://doi.org/10.1128/mSphere.00243-17
70. Chen J, Vitetta L. 2020. The role of butyrate in attenuating pathobiont-induced hyperinflammation. Immune Netw 20:e15. https://doi.org/10.4110/in.2020.20.e15
71. Onrust L, Baeyen S, Haesebrouck F, Ducatelle R, Van Immerseel F. 2020. Effect of in feed administration of different butyrate formulations on *Salmonella enteritidis* colonization and cecal microbiota in broilers. Vet Res 51:56. https://doi.org/10.1186/s13567-020-00780-2
72. Chu B, Zhu Y, Su J, Xia B, Zou Y, Nie J, Zhang W, Wang J. 2020. Butyrate-mediated autophagy inhibition limits cytosolic *Salmonella infantis* replication in the colon of pigs treated with a mixture of *Lactobacillus* and *Bacillus*. Vet Res 51:99. https://doi.org/10.1186/s13567-020-00823-8
73. Trirocco R, Pasqua M, Tramonti A, Grossi M, Colonna B, Paiardini A, Prosseda G. 2023. Fatty acids abolish *Shigella* virulence by inhibiting Its master regulator, VirF. Microbiol Spectr 11:e00778-23. https://doi.org/10.1128/spectrum.00778-23
74. Saha K, Sarkar D, Khan U, Karmakar BC, Paul S, Mukhopadhyay AK, Dutta S, Bhattacharya S. 2022. Capsaicin inhibits inflammation and gastric damage during H pylori Infection by targeting NF-kB–miRNA axis. Pathogens 11:1–13. https://doi.org/10.3390/pathogens11060641
75. Palaniappan B, Solomon AP, C DR. 2021. Targeting AgrA quorum sensing regulator by bumetanide attenuates virulence in *Staphylococcus aureus* – a drug repurposing approach. Life Sci 273:119306. https://doi.org/10.1016/j.lfs.2021.119306
76. Clinical and Laboratory Standards Institute. 2018. Methods for dilution antimicrobial susceptibility tests for bacteria that grow aerobically

standard, Approval CDM-A. In M07 methods for dilution antimicrobial susceptibility tests for bacteria that grow aerobically
77. Fernanda dos Reis T, Augusta Crivelente Horta M, Cristina Colabardini A, Mota Fernandes M, Pereira Silva L, Bastos RW, Fonseca MV de L, Wang F, Martins C, Rodrigues ML, Silva Pereira C, Del Poeta M, Wong KH, Goldman GH. 2021. Screening of chemical libraries for new antifungal drugs against *Aspergillus fumigatus* reveals sphingolipids are involved in the mechanism of action of miltefosine. mBio 12:e01458-21. https://doi.org/10.1128/mBio.01458-21
78. Takahashi E, Ochi S, Mizuno T, Morita D, Morita M, Ohnishi M, Koley H, Dutta M, Chowdhury G, Mukhopadhyay AK, Dutta S, Miyoshi SI, Okamoto K. 2021. Virulence of cholera toxin gene-positive *Vibrio cholerae* non-O1/non-O139 strains isolated from environmental water in Kolkata, India. Front Microbiol 12:726273. https://doi.org/10.3389/fmicb.2021.726273
79. Semighini CP, Marins M, Goldman MHS, Goldman GH. 2002. Quantitative analysis of the relative transcript levels of ABC transporter Atr genes in *Aspergillus nidulans* by real-time reverse transcription-PCR assay. Appl Environ Microbiol 68:1351–1357. https://doi.org/10.1128/AEM.68.3.1351-1357.2002
80. Das S, Chourashi R, Mukherjee P, Kundu S, Koley H, Dutta M, Mukhopadhyay AK, Okamoto K, Chatterjee NS. 2021. Inhibition of growth and virulence of *Vibrio cholerae* by carvacrol, an essential oil component of *Origanum* spp. J Appl Microbiol 131:1147–1161. https://doi.org/10.1111/jam.15022
81. Tükenmez H, Sarkar S, Anoosheh S, Kruchanova A, Edström I, Harrison GA, Stallings CL, Almqvist F, Larsson C. 2021. *Mycobacterium tuberculosis* Rv3160c is a TetR-like transcriptional repressor that regulates expression of the putative oxygenase Rv3161c. Sci Rep 11:1523. https://doi.org/10.1038/s41598-021-81104-y
82. Hartsock WJ, Cohen JD, Segal DJ. 2007. Uranyl acetate as a direct inhibitor of DNA-binding proteins. Chem Res Toxicol 20:784–789. https://doi.org/10.1021/tx600347k
83. Yan J, Liu Q, Xue X, Li J, Li Y, Su Y, Cao B. 2023. The response regulator VC1795 of *Vibrio* pathogenicity island-2 contributes to intestinal colonization by *Vibrio cholerae*. Int J Mol Sci 24:13523. https://doi.org/10.3390/ijms241713523
84. Basak P, Maitra P, Khan U, Saha K, Bhattacharya SS, Dutta M, Bhattacharya S. 2022. Capsaicin inhibits *Shigella flexneri* intracellular growth by inducing autophagy. Front Pharmacol 13:903438. https://doi.org/10.3389/fphar.2022.903438
85. Goel S, Bhatia V, Kundu S, Biswas T, Carskadon S, Gupta N, Asim M, Morrissey C, Palanisamy N, Ateeq B. 2021. Transcriptional network involving ERG and AR orchestrates distal-less homeobox-1 mediated prostate cancer progression. Nat Commun 12:5325. https://doi.org/10.1038/s41467-021-25623-2
86. Pertea M, Kim D, Pertea GM, Leek JT, Salzberg SL. 2016. Transcript-level expression analysis of RNA-seq experiments with HISAT, stringtie and ballgown. Nat Protoc 11:1650–1667. https://doi.org/10.1038/nprot.2016.095
87. Liu Y, Xu T, Wang Q, Huang J, Zhu Y, Liu X, Liu R, Yang B, Zhou K. 2022. *Vibrio cholerae* senses human enteric α-defensin 5 through a CarSR two-component system to promote bacterial pathogenicity. Commun Biol 5:559. https://doi.org/10.1038/s42003-022-03525-3
88. Badal D, Jayarani AV, Kollaran MA, Prakash D, P M, Singh V. 2021. Foraging signals promote swarming in starving *Pseudomonas aeruginosa*. mBio 12:e02033-21. https://doi.org/10.1128/mBio.02033-21
89. Rai Y, Pathak R, Kumari N, Sah DK, Pandey S, Kalra N, Soni R, Dwarakanath BS, Bhatt AN. 2018. Mitochondrial biogenesis and metabolic hyperactivation limits the application of MTT assay in the estimation of radiation induced growth inhibition. Sci Rep 8:1531. https://doi.org/10.1038/s41598-018-19930-w
90. Roy S, Patra T, Golder T, Chatterjee S, Koley H, Nandy RK. 2016. Characterization of the gluconate utilization system of *Vibrio cholerae* with special reference to virulence modulation. Pathog Dis 74:1–10. https://doi.org/10.1093/femspd/ftw085
91. Alam M, Miyoshi S, Sonoda Y, Chowdhury MAR, Tomochika K, Shinoda S. 1997. Role of a protease in the adherence and enterotoxicity of *Vibrio mimicus*. World J Microbiol Biotechnol 13:37–41. https://doi.org/10.1007/BF02770805

Journal of Applied Microbiology

Journal of Applied Microbiology ISSN 1364-5072

ORIGINAL ARTICLE

Inhibition of growth and virulence of *Vibrio cholerae* by carvacrol, an essential oil component of *Origanum* spp.

S. Das[1], R. Chourashi[1], P. Mukherjee[2], S. Kundu[1], H. Koley[2], M. Dutta[3], A.K. Mukhopadhyay[2], K. Okamoto[4] and N.S. Chatterjee[1]

1 Division of Biochemistry, ICMR-National Institute of Cholera and Enteric Diseases, Kolkata, India
2 Division of Bacteriology, ICMR-National Institute of Cholera and Enteric Diseases, Kolkata, India
3 Division of Electron Microscopy, ICMR-National Institute of Cholera and Enteric Diseases, Kolkata, India
4 Collaborative Research Center of Okayama University for Infectious Diseases at NICED, Kolkata, India

Keywords
carvacrol, inhibitor, motility, pathogenesis, *Vibrio cholerae*, virulence.

Correspondence
Nabendu Sekhar Chatterjee, Division of Biochemistry, ICMR-National Institute of Cholera and Enteric Diseases, P-33, C.I.T. Road, Scheme XM, Beliaghata, Kolkata 700010, India.
E-mail: nschatterjee@rediffmail.com; chatterjeens.niced@gov.in

2021/2235: received 16 October 2020, revised 14 January 2021 and accepted 28 January 2021

doi:10.1111/jam.15022

Abstract

Aims: In the age where bacterial resistance to conventional antibiotics is increasing at an alarming rate, the use of the traditional plant, herb extracts or other bioactive constituents is gradually becoming popular as an anti-virulence agent to treat pathogenic diseases. Carvacrol, a major essential oil fraction of Oregano, possesses a wide range of bioactivities. Therefore, we aimed to study the effect of sub-inhibitory concentrations of carvacrol on major virulence traits of *Vibrio cholerae*.

Methods and Results: We have used *in vitro* as well as *ex vivo* models to access the anti-pathogenic role of carvacrol. We found that the sub-inhibitory concentration of carvacrol significantly repressed bacterial mucin penetrating ability. Carvacrol also reduced the adherence and fluid accumulation in the rabbit ileal loop model. Reduction in virulence is associated with the downregulated expression of *tcpA*, *ctxB*, *hlyA* and *toxT*. Furthermore, carvacrol inhibits flagellar synthesis by downregulating the expression of *flrC* and most of the class III genes.

Conclusions: Carvacrol exhibited anti-virulence activity against *V. cholerae*, which involved many events including the inhibition of mucin penetration, adhesion, reduced expression of virulence-associated genes culminating in reduced fluid accumulation.

Significance and Impact of the Study: These findings indicate that carvacrol possesses inhibitory activity against *V. cholerae* pathogenesis and might be considered as a potential bio-active therapeutic alternative to combat cholera.

Introduction

Vibrio cholerae is a comma-shaped, Gram-negative, facultatively anaerobic bacterium that causes severe food and waterborne diarrhoeal disease cholera. The disease cholera causes gastrointestinal ailments with characteristic non-bloody watery diarrhoea leading to the loss of body fluids and the consequent electrolyte imbalance results in the death of the individual if left untreated. Infection of *V. cholerae* in humans is caused by the ingestion of contaminated water and food (Kaper *et al.* 1995). After reaching the small intestine, *V. cholerae* confronts the thick mucus barrier of the intestine, where it penetrates the thick mucus barrier by the simultaneous action of flagellar movement and release of different proteases and chitinases. As a result, *V. cholerae* subverts the protective mucus layer and then adheres to the epithelial cell. After the adherence, colonization of *V. cholerae* occurs by forming microcolonies. *Vibrio cholerae* then produces cholera toxin (CT) and other virulence factors and cause disease (Matson *et al.* 2007; Das *et al.* 2020). WHO estimates that each year cholera infects nearly 1–4 million people worldwide and claims up to 21 000–143 000 lives (Ali *et al.* 2015).

Throughout the last decade, awareness and campaigning among the people of developing nations about the practice of proper hygiene and sanitation and the availability of uncontaminated drinking water has reduced the global burden of cholera. In 2018, total cases of cholera were reduced by 60% than the previous year (World Health Organization 2019). Typically, treatment of cholera includes electrolyte replacement therapy and sometimes antibiotics. However, the inappropriate and overuse of antibiotics through self-medication and indiscriminate access to antibiotics without prescription has led to the emergence of multidrug-resistant epidemic strains of bacteria. Among bacteria, antibiotic-resistant *V. cholerae* is becoming worryingly common across the globe (Verma *et al.* 2019). Countries reporting major drug-resistant *V. cholerae* strains are reviewed extensively by Kitaoka et al. (Kitaoka *et al.* 2011). *Vibrio cholerae* becomes drug resistant by the frequent acquisition of extrachromosomal mobile genetic elements by horizontal gene transfer from other bacterial species. (Narendrakumar *et al.* 2019; Verma *et al.* 2019; Das *et al.* 2020).

Traditional antimicrobials are usually bacteriostatic or bactericidal which may facilitate the emergence of MDR strains. Therefore, alternative novel therapeutic approaches like the use of plant or herb extracts, bioactive phytochemicals or the use of small molecules are in urgent need to fight against these pathogens by particularly targeting bacterial virulence factors. Furthermore, the use of *Bdellovibrio bacteriovorus* or *Micavibrio aeruginosavorus* as probiotic treatment has also been reported to decrease the spread of antibiotic resistance in *V. cholerae* (Dwidar *et al.* 2012; Duncan *et al.* 2018). The use of bioactive compounds from natural products such as herbs, spices, fruits and seeds has many beneficial effects on our health and possess lesser side effects.

In India, various plant parts and their derivative components have been used as Ayurvedic medicine since ancient times to treat various diseases including diarrhoea. Plant-derived essential oils possess important volatile components with diverse bioactivities including antimicrobial potential. Over the past few years, the use of essential oils from cinnamon, cardamom, red chili, white pepper, sweet fennel and ginger has been well documented (Aminzare *et al.* 2018). These bioactive compounds act against *V. cholerae* in various ways mainly by controlling virulence regulatory gene *toxT* (Virstatin) (Hung 2005; Shakhnovich *et al.* 2007), inhibiting the binding of CT to GM_1 (6-Gingerol) (Saha *et al.* 2013), disrupting the secondary structure of CT (zinc oxide nanoparticles) (Sarwar *et al.* 2017) or by showing direct antimicrobial activity against the pathogen.

Carvacrol (CV) is a naturally occurring essential oil fraction of Oregano (*Origanum vulgare*) and it exhibits antimicrobial activity against a variety of foodborne pathogens such as *Escherichia coli* O157: H7 (Obaidat and Frank 2009), *Bacillus cereus* (Ultee *et al.* 1999), *Shigella*sp. (Bagamboula *et al.* 2004), *Salmonella*sp. (Miladi *et al.* 2016), *Clostridium difficile* (Mooyottu *et al.* 2014) and also *V. cholerae* (Rattanachaikunsopon and Phumkhachorn 2010). Studies indicated that CV possesses a variety of characteristics (Ahmad *et al.* 2010; Arunasree 2010) including anti-oxidant (Slameňová *et al.* 2007; Slamenova *et al.* 2008; Aristatile *et al.* 2009), antibacterial (Nostro *et al.* 2009; Rattanachaikunsopon and Phumkhachorn 2010; Pérez-Conesa *et al.* 2011) and anti-inflammatory properties (Landa *et al.* 2009; Hotta *et al.* 2009).

Most of the studies on the effects of carvacrol on bacteria have focussed on determining the minimum inhibitory concentration (MIC) at which growth arrest of the bacterial culture occurs, or on the minimum bactericidal concentration (MBC), that is, the concentration at which >99·9% of the bacterial population are killed (van Alphen *et al.* 2012). Despite extensive research on carvacrol in recent years, there is still no report regarding the anti-virulence properties of carvacrol against *V. cholerae*. In this study, we investigated the potential effects of sub-inhibitory (sub-MIC) concentration of carvacrol on the virulence potential of *V. cholerae*. In this context, we have evaluated the activity of carvacrol on *V. cholerae* motility, transcriptional regulation of flagella synthesis genes, *in vitro* mucin penetration, adhesion to epithelial cells followed by studying the *in vivo* anti-virulence activity of carvacrol using the rabbit ileal loop models. Here, we report for the first time the anti-virulence activity of carvacrol against pathogenic *V. cholerae*. Our results indicate that at concentrations that do not affect the bacterial growth CV can inhibit *V. cholerae* motility, mucin penetration, adhesion, toxin production and virulence which may limit bacterial infection and disease pathogenesis within the human host.

Materials and methods

Ethics statement

Animal experiments were carried on following the guideline proposed by the Committee for the Purpose of Control and Supervision of Experiments on Animal (CPCSEA), Government of India. All animal experiments performed here were subjected to the approval (registration no: PRO/120/April 2016–March 2019) by the Institutional Animal Ethics Committee of the National Institute of Cholera and Enteric Diseases. For *in vivo* fluid accumulation study, New Zealand white rabbits of about 2·5 kg were used. At the time of harvesting the

intestine, animals were euthanized in the CO chamber assuring minimum pain to the animals.

Bacterial strains and culture conditions

Streptomycin-resistant O1 El Tor Inaba *V. cholerae* strain N16961 was used in all the experiments performed here. This strain was cultured in Luria–Bertani (LB) medium at 37°C with 180 rev min^{-1} constant shaking or at static conditions on Petri plates containing LB agar supplemented with appropriate antibiotics streptomycin (100 $\mu g\ ml^{-1}$). Bacteria were also cultured in AKI media containing 0·4% yeast extract (BD Difco, San Diego, CA), 1·5% Bacto peptone (BD Difco, San Diego, CA), 0·5% NaCl and 0·3% freshly prepared $NaHCO_3$ (Merck, Burlington, MA) pH 7·2 at 37°C under static condition for CT analysis.

Determination of MIC and MBC of Carvacrol

The study compound carvacrol, a major constituent of essential oil fraction of oregano (*O. vulgare*), was purchased from Sigma-Aldrich, St. Louis, MO. A stock solution of carvacrol with a concentration of 50 mg ml^{-1} was prepared by diluting it in DMSO before use. These stocks were stored at 4°C in the dark until required and diluted stocks are used for not more than 1 week.

The MIC of carvacrol was determined by the broth microdilution method according to CLSI guidelines (Clinical Laboratory Standards Institute 2012) in 96-well flat-bottomed polystyrene microtiter plates (Costar Corning, Corning, NY). Bacterial strain suspension was adjusted to optical density values 0·08–0·12 at 600 nm (equivalent to 0·5 McFarland standard turbidity) with a spectrophotometer. In total, 200 μl of cell suspensions was inoculated into the wells of 96-well microplates and carvacrol was dissolved in DMSO and then in Muller Hinton Broth (MHB) as required and transferred to the microplate well to obtain a twofold serial dilution ranging from 1200 to 1 $\mu g\ ml^{-1}$. MHB only and MHB with bacteria containing wells were used as negative and positive controls, respectively. Plates were incubated for 24 h at 37°C and bacterial growth was evaluated by the presence of turbidity and a pellet on the bottom. The MIC value was recorded as the lowest concentration of the tested compound that had no macroscopically visible growth of bacteria (Burt 2004). To determine the MBC values, 100 μl of each well medium with no visible growth was inoculated in Muller Hinton Agar plates. After 24 h of incubation at 37°C, the number of surviving organisms was determined. MBC was defined as the lowest concentration of compounds at which 99% of the bacteria were killed. Each experiment was repeated twice separately (Magina *et al.* 2009). To verify that the antimicrobial effect was from the carvacrol and not from DMSO (that was used as the solvent for carvacrol), we used DMSO as negative control and it did not inhibit bacterial growth.

Vibrio cholerae growth assay

For growth curve analysis, overnight grown log-phase cultures of *V. cholerae* N16961 were collected, centrifuged, washed in PBS, and cell number was adjusted to 1×10^9 cells per ml using LB medium. The growth curve was done in a nutrient-rich LB medium. Carvacrol was supplemented to the culture media at different concentrations (150, 75 and 37·5 $\mu g\ ml^{-1}$). A starting inoculum of 1×10^8 cells per ml was given to the fresh LB broth medium. Cultures were grown at 37°C under constant shaking at 180 rev min^{-1} for up to 24 h (Chourashi *et al.* 2016). The viable cell counts were enumerated by dilution plating of the bacterial cultures at different time points onto LB agar plates supplemented with streptomycin followed by colony count.

RNA isolation and quantitative RT-PCR

To determine the effect of carvacrol on *V. cholerae* toxin gene associated virulence gene and flagellar gene expression, total RNA was isolated from the mid-logarithmic-phase (O. D_{600} values 0·5–0·6) bacterial culture. Carvacrol-treated and -untreated bacterial cultures were harvested either from in vitro samples grown in AKI and LB broth or from *in vivo* rabbit ileal loop. After extracting the total RNA using Trizol (Invitrogen, Carlsbad, CA) method, it was dissolved in RNase-free water at −80°C until use. Contaminating genomic DNA was eliminated by DNase treatment using a DNA-free kit (Ambion, Austin, TX). 1 μg of RNA from each sample was subjected to cDNA synthesis using a Reverse Transcription kit (Promega, Madison, WI) following the manufacturer's protocol. The mRNA transcript levels were quantified by quantitative PCR (qPCR) using 2 × SYBR green PCR master mix (AB Applied Biosystems, Foster City, CA) and 0·2 $\mu mol\ l^{-1}$ of specific forward and reverse primers designed using PrimerQuest from Integrated DNA Technologies (IDT) for each transcript (Table S1). Data analysis was done using a 7500 Real-Time PCR detection system (Applied Biosystems, Foster City, CA) with 40 cycles of a two-step cycle followed by a melting curve. The relative expression of the target transcripts was calculated according to Livak's $2^{-\Delta\Delta C_T}$ method (Livak and Schmittgen 2001) using *recA* (VC_0543) as an internal control.

Mucin penetration assay

Mucin penetration study was performed according to the previously described method (Liu *et al.* 2008). In brief, mucin columns were prepared by adding 1·5% porcine mucin (Sigma-Aldrich) in 1-ml syringes. Different concentrations of carvacrol (75 and 37·5 μg ml^{-1}) were added to each of the mucin columns. The untreated mucin column was used as control. *Vibrio cholerae* was grown up to mid-log phase and the concentration was adjusted to 5×10^8 cells per ml using PBS. On top of the mucin columns, 0·1 ml of the culture was loaded and allowed to settle for 1 h at 37°C under static conditions (Chourashi *et al.* 2016). In all, 100 μl of culture fractions was collected from the bottom of the columns. Bacterial numbers were measured by serially diluting the samples and plating them onto LB agar and counting the colony forming units (CFU).

Motility assay

The surface motility of *V. cholerae* was done by the previously described method (Yeung *et al.* 2012). Bacteria were grown up to the mid-log phase in LB broth. The culture was resuspended in PBS and OD_{600} adjusted to 0·5. In total, 1 μl of this culture was spotted on soft agar plates containing different concentrations of carvacrol (75 and 37·5 μg ml^{-1}) in LB media and 0·3% bacto agar. The plates were incubated for 24 h at 37°C. Bacterial motility was analysed by measuring the diameter of the motility zone on the plate surface.

Cell culture

Human adenocarcinoma cell line HT-29 (ATCC HTB-38) was used to study the effect of carvacrol in ex vivo conditions. HT-29 cells were maintained in Dulbecco's modified Eagle's medium (DMEM) (Sigma-Aldrich, St. Louis, MO), supplemented with 10% foetal bovine serum (PAN Biotech, Aidenbach, BY), 1% non-essential amino acid (Sigma-Aldrich, St. Louis, MO) and 1% penicillin/streptomycin (Sigma-Aldrich, St. Louis, MO) mixture at 37°C under 5% CO_2 in a humidified incubator (Mondal *et al.* 2014).

Adhesion assay

Vibrio cholerae adhesion to HT-29 was done according to the method described previously (Chourashi *et al.* 2016). HT-29 cells were split into 12-well cell culture plates and grown up to 80% confluency. *Vibrio cholerae* grown till mid-log phase was taken and $1{\cdot}2 \times 10^8$ bacteria were (1 : 100 MOI) inoculated to HT-29 cells. Carvacrol at different concentrations (75 and 37·5 μg ml^{-1}) was added to the DMEM in each well. Adhesion assay was done by incubating the bacteria/cell at 37°C for 1 h. The cells were then washed three times with pre-warmed PBS pH 7·4 to remove unbound bacteria. Adhered bacteria were detached using 0·1% Triton X-100 in each treatment group and were counted after serial dilution by plating on LB agar plates supplemented with 100 μg ml^{-1} streptomycin. *In vivo* adhesion of bacterial strains with the rabbit intestinal lumen was also evaluated. Intestinal loop sections recovered 18 h after the rabbit ileal loop experiment were washed in PBS three times, homogenized and serially diluted in PBS. The adherent bacterial count was determined by plating these bacterial cultures on LB agar supplemented with 100 μg ml^{-1} streptomycin.

Ligated rabbit ileal loop assay for fluid accumulation and bacterial recovery

New Zealand white rabbit was used to study intestinal fluid accumulation assay. In total, 1 ml of 1×10^9 CFU per ml *V. cholerae* culture with or without carvacrol (at 150, 75, 37·5 μg ml^{-1}) was introduced into each ileal loop. The negative control loop was inoculated with PBS. After 18 h, the animal was sacrificed and the loops were taken out and the volume of the accumulated fluid and the length of the loops were measured. The amount of the accumulated fluid (FA) was expressed as a loop fluid volume (ml)/length (cm) ratio (Chourashi *et al.* 2016). The accumulated fluid was also used for bacterial adhesion, CT production and virulence gene expression studies.

GM1 enzyme-linked immunosorbent assay

The amount of CT in the culture supernatant was quantified by GM1 enzyme-linked immunosorbent assay (ELISA) as described by Holmgren (1973) with minor alterations (De *et al.* 2004; Patra *et al.* 2012). *Vibrio cholerae* grown in AKI media for 18 h was harvested and cell-free culture supernatant was pulled out by centrifugation. Culture supernatants were added to the wells of MaxiSorp ELISA plates (Nunc, Rochester, NY) and precoated with GM1 ganglioside (Sigma-Aldrich, St. Louis, MO). Subsequently, each well was treated with a polyclonal anti-CT antibody (Sigma-Aldrich, St. Louis, MO). In each set of assays, known amounts of purified CT were used in different concentrations to generate a standard curve. The amount of CT secreted by *V. cholerae* strains was done by extrapolating the optical density value of the samples at 450nm in the standard curve. The average of OD_{450} values obtained from triplicate wells of each experimental set was considered to estimate the amount of CT

present and expressed as ng of CT per ml. The amount of CT produced *in vivo* rabbit ileal loop culture was also measured by this method.

Transmission electron microscopy

Whole-cell mounts of *V. cholerae* were negatively stained and bacterial morphology was visualized. In brief, wild-type *V. cholerae* was grown in LB broth with or without carvacrol at different concentrations (150, 75 and 37·5 μg ml^{-1}). In total, 5 μl of bacterial suspension was gently placed on a carbon-coated 300 mesh copper grid. After about 1 min, the remaining solution on the grids was wicked away with the help of a filter paper followed by washing with two drops of distilled water. The grid was then stained with 2% (w/v) uranyl acetate and air-dried. The negatively stained cells were visualized with an FEI Tecnai 12 BioTWIN transmission electron microscope (FEI, Hillsboro, OR) at an operating voltage of 100 kV.

LDH cytotoxicity assay

The effect of carvacrol on the cytotoxicity of the HT-29 cell line was estimated by lactate dehydrogenase (LDH) release assay following the manufacturer's protocol (LDH cytotoxicity detection kit, TaKaRa Biosciences). In brief, HT-29 cells were grown in six-well cell culture plates up to 80% confluency and then co-incubation with carvacrol at different concentrations was done for 12 h at 37°C humid cell culture incubator. Cell culture supernatants were analysed for the release of LDH. The percent cytotoxicity value was calculated using the following formula:

$$\text{Cytotoxicity}(\%) = \left(\frac{\text{EX} - \text{LC}}{\text{HC} - \text{LC}} - \text{BC}\right) \times 100,$$

where EX is the experimental value, LC the low control or spontaneous LDH release from the untreated normal HT-29 cells, HC the high control or maximum releasable LDH in the HT-29 cells by the addition of 1% Triton X-100 and BC the background control or LDH activity in the assay medium. Treatment with 1% (v/v) Triton X-100 represented maximum LDH release, hence represented 100% cytotoxicity.

Cell staining and fluorescence microscopy

The effect of carvacrol on human adenocarcinoma cell line HT-29 was visualized by fluorescence microscopy. HT-29 cells were seeded on sterile borosilicate cover glass (Blue star, Mumbai, MH) in six-well cell culture plates. Upon reaching 80% confluency, HT-29 cells were incubated in serum-free DMEM and carvacrol treatment at different concentrations (0–250 μg ml^{-1}) was done for 4 h. After removing the media, HT-29 cells were washed in PBS and stained with Hoechst 33342 (5 μg ml^{-1}) (Sigma-Aldrich) for 10 min. Cells were then washed in PBS twice and subsequently counterstained and mounted with PI containing mounting medium (VectaShield, Vector Laboratories, Burlingame, CA). Both carvacrol-treated and -untreated cells were visualized under a confocal laser scanning microscope. Propidium iodide (PI) is a membrane impermeant dye, whereas Hoechst H33342 is a membrane-permeable stain; therefore, HT-29 cells exhibiting membrane permeability upon carvacrol treatment display red (PI) intensity.

Statistical analysis

All the experiments were performed independently in triplicates, and the data obtained were analysed by Student's *t* test. Data were represented as mean ± standard error of mean (SEM). A $P < 0{\cdot}05$ was considered as statistically significant.

Results

Determination of MIC and growth of *V. cholerae* at sub-MIC concentrations of carvacrol

The antibacterial activities in terms of MIC of carvacrol against *V. cholerae* were found to be 150 μg ml^{-1}. In this concentration of carvacrol, no visible growth of *V. cholerae* was seen in the broth dilution assay. Also, in line with the definition of MBC (Helander *et al.* 1998), its value was found to be the same as MIC, as no viable bacteria were found in this concentration of carvacrol. Furthermore, all the experiments of this study were performed at sub-MIC concentrations of carvacrol (at ½ MIC (75 μg ml^{-1}) and ¼ MIC (37·5 μg ml^{-1})). MIC of carvacrol was also used in some experiments to compare the effect with other treatment groups. The effect of carvacrol on *V. cholerae* growth in a time-dependent manner was examined by counting the viable cells on the plates. The growth rate of *V. cholerae* was measured in LB medium along with exogenously added MIC and sub-MIC concentrations of carvacrol. The result indicated that *V. cholerae* growth was completely inhibited at MIC (150 μg ml^{-1}). No bacteria were recovered after 2 h of initial inoculum at MIC. At ½ MIC (75 μg ml^{-1}), the viable count of the bacteria was reduced to 60% 1 h post-initial inoculum. Within the initial 8 h, the viable count of the bacteria reduced gradually to 20%. At 24 h, the growth of the *V. cholerae* starts resuming to a lesser extent and reaches up to 37% viability of the initial bacterial population. On the contrary, carvacrol treatment at

¼ MIC (37·5 μg ml^{-1}) resulted in a reduction in the bacterial population to 60% within 2 h of the initial inoculum. After that *V. cholerae* resumes growth and at 24 h, the viable count of the bacteria exceeds more than five times the initial inoculum (Fig. 1). At the initial phase of the sub-MIC treatment, carvacrol showed the bactericidal effect on *V. cholerae*; subsequently, it remained bacteriostatic for the remaining viable bacteria. This suggests that *V. cholerae* remained viable and continued to grow even upon carvacrol treatment at sub-MIC concentrations.

Swarming motility and mucin penetrating ability of *V. cholerae* is reduced by carvacrol

The ability of *V. cholerae* to penetrate the mucin layer *in vitro* in the presence of carvacrol was investigated. It was found that *V. cholerae* mucin penetration decreased significantly upon carvacrol treatment. Out of a total of 5×10^8 CFU per ml bacteria loaded on top of the 1·5% mucin column, 100 μl of 43×10^3 CFU per ml bacteria was recovered after 1 h from the bottom of the column (Fig. 2a). In case of CV treatment at ¼ MIC (37·5 μg ml^{-1}) and ½ MIC (75 μg ml^{-1}), a total of 8×10^2 and $3{\cdot}5 \times 10^2$ bacteria were recovered from the bottom of the column, respectively, which seems to have caused a 5·2-fold and 12·3-fold reduction in mucin penetration, respectively. Because CV at both sub-MIC concentrations reduced the viable count of the bacteria by 40% in the initial 1 h of growth, we can say that the viable count of the bacteria must be $25{\cdot}8 \times 10^2$ in the bottom 100 μl fraction of the CV-treated columns. Compared to that, ¼ MIC of CV treatment showed 3·2-fold and ½ MIC of CV treatment showed a 7·4-fold reduction. We have also investigated the surface motility of *V. cholerae* on soft agar LB plates (Fig. 2b). We found that in the CV-untreated plate V. *cholerae* showed a motility zone of 7 ± 0·3 cm and the addition of CV resulted in complete inhibition of swarming motility after 24 h of incubation.

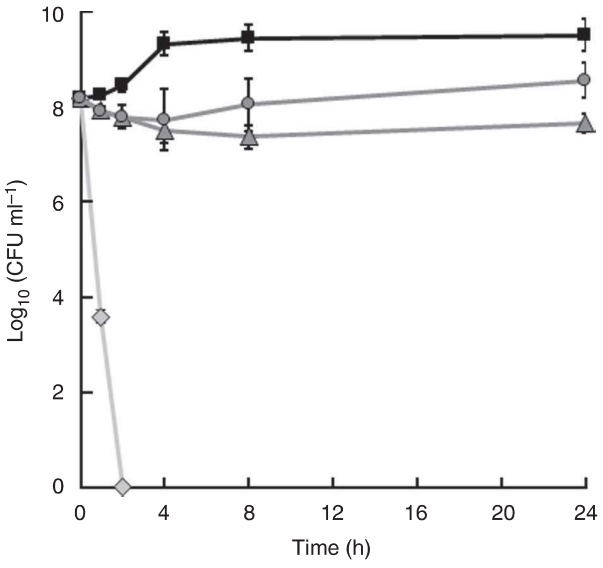

Figure 1 Effect of carvacrol on *Vibrio cholerae* growth at MIC and sub-MICs. Wild-type *V. cholerae* N16961 were grown in LB broth along with carvacrol at MIC (150 μg ml^{-1}), CV 150 (◇); ½ MIC (75 μg ml^{-1}), CV 75 (△); ¼ MIC (37·5 μg ml^{-1}), CV 37·5 (○) along with the untreated control, CV 0 (□). The viable bacterial counts in CFU per ml detected by the plate count method were represented graphically. Each experiment was repeated three times (n = 3) and the data were expressed as mean ± SEM.

Adhesion to epithelial cells is affected by carvacrol

The effect of carvacrol on *V. cholerae* adherence to rabbit ileum epithelial cells was tested. The result suggested that $3{\cdot}37 \times 10^7$ CFU per ml adherent *V. cholerae* was present in the untreated condition (Fig. 3a). In contrast, there was only $8{\cdot}7 \times 10^6$ CFU per ml and 21×10^6 CFU per ml of adherent bacteria at ½ MIC (75 μg ml^{-1}) and ¼ MIC (37·5 μg ml^{-1}) of carvacrol treatment, respectively. We have also checked the bacterial load in each of the ileal loop samples. $1{\cdot}98 \times 10^9$ CFU per ml, $2{\cdot}08 \times 10^9$ CFU per ml and $1{\cdot}59 \times 10^9$ CFU per ml bacteria were recovered from the CV-untreated, ¼ MIC of CV-treated and ½ MIC of CV-treated ileal loop samples (Fig. 3b). This study exhibits that only 1·7% of the total *V. cholerae* adhered to the epithelium in the absence of CV. Whereas 0·5% out of total *V. cholerae* was adhered to the epithelium in the presence of ½ MIC of CV treatment, showing three times less adherence capability of *V. cholerae*. Furthermore, the adherence capability of *V. cholerae* to the HT-29 intestinal epithelial cell line was also studied comparing with the recovered viable bacteria from treated and untreated culture samples. In the absence of CV, 1·47% out of total bacteria adhered to the HT-29. Whereas only 0·12 and 0·04% bacteria out of total viable bacteria adhered at ¼ and ½ MIC of carvacrol treatment (Fig. 3c,d). Therefore, the effect of carvacrol on *V. cholerae* is more pronounced in cell culture conditions although we found significant results *in vivo* treatment.

Vibrio cholerae show less fluid accumulation upon carvacrol treatment

Next, the effect of carvacrol in fluid accumulation in ligated rabbit ileal loop model was studied. The amount of fluid accumulated per unit length (FA ratio) in each loop was measured 18 h post-infection with or without carvacrol-treated *V. cholerae* culture (Fig. 4a). When quantified, the FA ratio of CV treatment showed

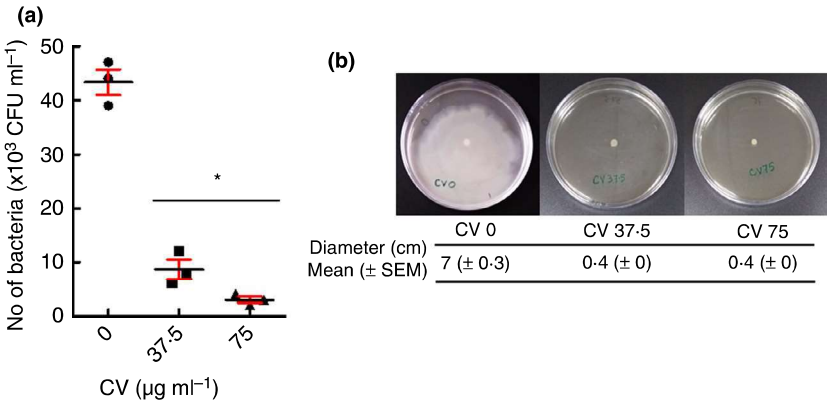

Figure 2 Effect of carvacrol on motility of *Vibrio cholerae*. (a) Mucin penetration was performed in a 1·5% mucin column in the presence of different concentrations of carvacrol at ½ MIC (75 μg ml^{-1}) and ¼ MIC (37·5 μg ml^{-1}). Please see Materials and methods for details. Bacterial numbers eluted were counted and graphically represented. (b) Representative plates showing the motility zone of *V. cholerae* on 0·3% agar plates under different treatment conditions. Each of the experiments was repeated three times (n = 3) and the data were expressed as mean ± SEM. *P < 0·05.

complete obliteration of fluid accumulation upon treatment with MIC of carvacrol (i.e. 150 μg ml^{-1}). At ½ MIC (75 μg ml^{-1}), a 3·7-fold decrease in fluid accumulation was observed compared to the control (Fig. 4b). At ¼ MIC (37·5 μg ml^{-1}) of carvacrol, the FA ratio was found to be similar to the untreated one.

CT production and virulence gene expression is decreased by carvacrol

CT production in the rabbit ileal loop sample, which is primarily responsible for fluid accumulation, was measured by GM_1-CT ELISA. Experimental results suggested that *V. cholerae* produced 666 ng ml^{-1} of CT in the untreated ileal loop. At ½ MIC (75 μg ml^{-1}) of carvacrol treatment, CT production was measured to be 106·6 ng ml^{-1} resulting in 6·3-fold reduced production of CT compared to the untreated control loop (Fig. 5a). Fluid from ¼ MIC (37·5 μg ml^{-1}) carvacrol-infected loop showed almost similar CT production (612 ng ml^{-1}) compared to the control loop. The expression of different virulence genes (*toxT*, *hlyA*, *tcpA* and *ctxB*) was also measured by qPCR. It was found that the expression of these genes was significantly reduced by twofold, 2·3-fold, 4·4-fold and 4·2-fold, respectively, in ¼ MIC carvacrol (37·5 μg ml^{-1})-infected ileal loop samples relating to the infection with only *V. cholerae* (Fig. 5b). At ½ MIC (75 μg ml^{-1}) of carvacrol treatment, expression of these genes was greatly reduced compared to the control gene at the control condition. Carvacrol also reduced CT production as well as the expression of virulence genes *in vitro* AKI media (Fig. S1).

Negligible cytotoxic effect was seen at sub-MIC concentrations of carvacrol

Cytotoxicity of the HT-29 cell line upon carvacrol treatment was measured by LDH release assay. Different doses of carvacrol were used to treat HT-29 cells and after 12 h the supernatants were collected and assessed for the release of LDH. HT-29 cell treatment with triton X-100 showed maximum membrane damage, hence considered to possess 100% cytotoxicity. The experimental result obtained here showed that carvacrol exerts 9% and <1% cytotoxicity at MIC and ½ MIC (75 μg ml^{-1}), respectively, compared to the triton X-100 treated cell (Fig. 6a). So, no substantial membrane damage upon treatment at MIC (150 μg ml^{-1}) and sub-MIC concentrations carvacrol is observed. Although at higher concentration (250 μg ml^{-1}), carvacrol exhibited noteworthy spillage of LDH resulted in 58% cytotoxicity. Confocal microscopy images also revealed that at MIC and sub-MIC treatment of carvacrol, the permeability of PI to HT-29 cell line was very less compared to the Triton-X 100 treatment (Fig. 6 b). The above results led to the conclusion that carvacrol at sub-MIC is safe and does not cause human epithelial cell damage.

Morphology and flagellar synthesis in *V. cholerae* is affected by carvacrol

Changes in bacterial morphology were observed by transmission electron microscopy upon carvacrol treatment. As shown in Fig. 7, carvacrol treatment at MIC (150 μg ml^{-1}) showed altered morphology with distorted shape and damaged cell membranes, whereas lower

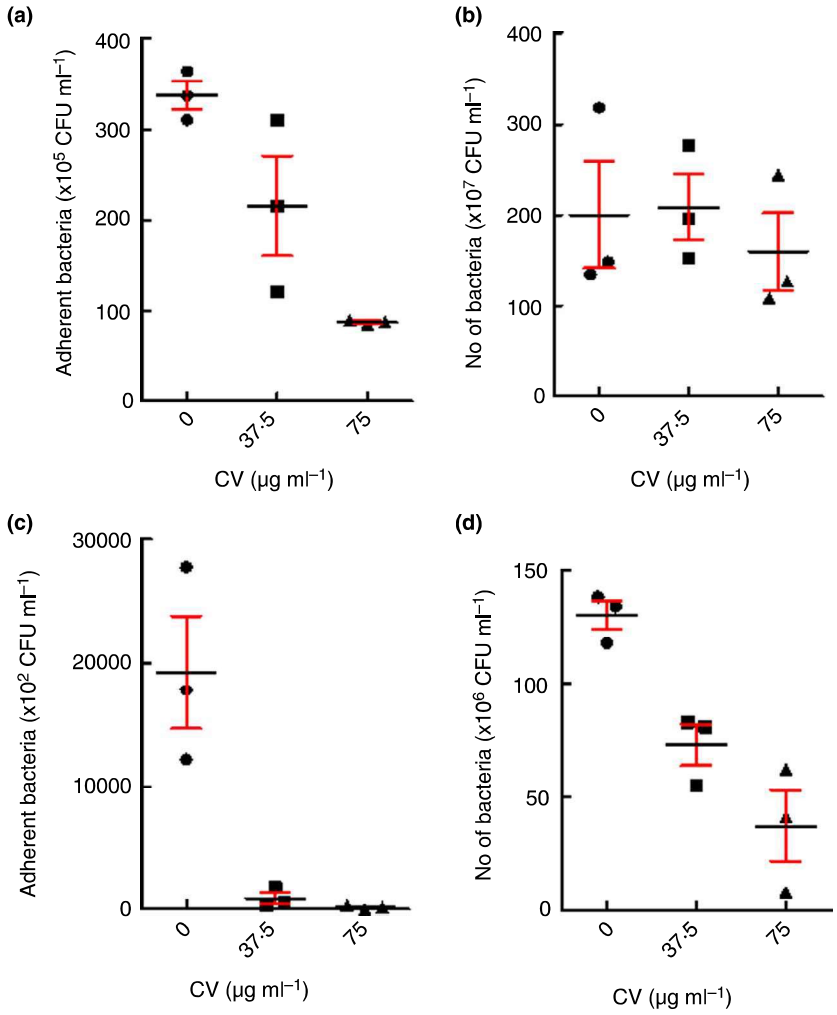

Figure 3 Effect of carvacrol on the adhesion of *Vibrio cholerae* to the epithelial cells. Carvacrol at ½ MIC (75 μg ml^{-1}) and ¼ MIC (37·5 μg ml^{-1}) were used in treating both rabbit intestine and cell culture conditions. (a) Adhered *V. cholerae* in the rabbit ileal loop tissue samples. (b) Total number of *V. cholerae* count in each of the rabbit ileal loops. (c) Adhered *V. cholerae* with the HT-29 cell line. (d) Total number of *V. cholerae* count in each HT-29 culture samples. The result is shown as the mean ± SEM of three biological replicates (n = 3).

concentrations of carvacrol showed the normal shape of the bacteria. Although flagella in each of the treatments was not observed in *V. cholerae*. Compared to that untreated *V. cholerae* showed a normal shape and single polar flagellum (Fig. 7). Flagella-driven bacterial motility is an important virulence trait of *V. cholerae*. Reduced mucin penetration and absence of flagella by microscopic analysis upon carvacrol treatment raised interest in whether carvacrol has any effect on flagella synthesis. Therefore, the effect of the sub-inhibitory concentration of carvacrol on *V. cholerae* flagella synthesis was assessed by measuring the transcription of flagella synthesis genes by qRT-PCR. The analysis revealed that at ¼ MIC (37·5 μg ml^{-1}) of carvacrol treatment, there was a fourfold decreased expression of *flrC*, a response regulator ($P < 0{\cdot}05$) (Fig. 8). Transcriptional expression of master regulator *flrA*, histidine kinase *flrB* and *fliF* (MS ring structure forming unit) was not significantly changed upon carvacrol treatment ($P > 0{\cdot}05$). On the other hand, alternate sigma factor *fliA* (σ^{28}), *flgM* and *RpoN* (σ^{54}) expressions were downregulated by 2·5-fold, 2·9-fold, and 3·5-fold, respectively. Furthermore, downregulation of *motY* (T-ring motor protein), *flaA* (main flagellin subunit), *flgP* (H-ring-associated protein), *flgT* (H-ring component), *flgK* (hook filament junction protein), *flgG* (distal rod) and *flgB* (proximal rod) all of which belong to Class III flagellar synthesis genes were downregulated by 10·5-fold, 7·1-fold, 3·8-fold, 6·6-fold, 33·3-fold, 5-fold

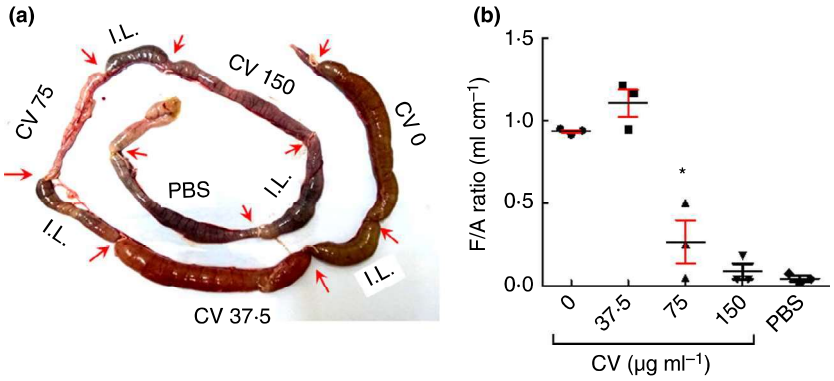

Figure 4 Effect of carvacrol in fluid accumulation in rabbit intestine. (a) Representative image of retrieved rabbit intestinal portion showing infected loop 18 h post-infection. The negative control loop was inoculated with PBS. Arrow showing the location of ligations in the loop. I.L., Inter Loop. (b) Fluid accumulation ratio in the rabbit intestine of three different experiments was measured and represented graphically as mean ± SEM. *$P < 0{\cdot}05$.

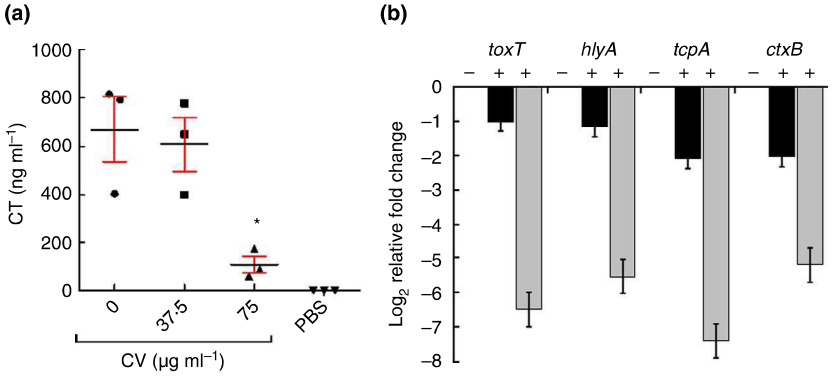

Figure 5 Effect of carvacrol on cholera toxin (CT) production and virulence gene expression. (a) *In vivo* CT production was measured by ELISA from the accumulated fluid samples of carvacrol treated (with ½ MIC (75 μg ml^{-1}), ¼ MIC (37·5 μg ml^{-1})) and untreated ligated rabbit ileal loops. (b) Relative expression of *Vibrio cholerae* virulence genes by real-time PCR. RNA was isolated from the untreated (–) or carvacrol treated (+) (¼ MIC (37·5 μg ml^{-1}) CV, (□) and ½ MIC (75 μg ml^{-1}), (□)) ileal loop bacterial samples. *recA* was used as an internal control gene. Data showed here as the $\log_2$-transformed values of relative fold change. Each of the experiments was repeated three times ($n = 3$) and the data were expressed as mean ± SEM.

and 3·2-fold, respectively, upon ¼ MIC (37·5 μg ml^{-1}) of carvacrol treatment. However, inconspicuous change in the expression pattern of these flagellar synthesis genes was noticed when *V. cholerae* culture was treated with even higher sub-inhibitory concentration, that is, ½ MIC (75 μg ml^{-1}) of carvacrol.

Discussion

Preceding the age of antibiotic discovery, traditional knowledge of herbal extracts was widely practiced as remedies to treat certain diseases around the world. However, in this antibiotic era, bacteria with resistance to various antibiotics are emerging increasingly, along with the declined rate of development of new antibiotics during the last decade compelled researchers to look for alternative approaches to treat pathogenic infections (Bassetti *et al.* 2013; Sharifi-Rad *et al.* 2018). After an extensive literature survey, Carvacrol (CV), an essential oil fraction of oregano, was selected for the study possessing several bioactive properties on various organisms.

In this study, we have investigated the effect of the sub-inhibitory concentration of CV on *V. cholerae* to access the spectrum of biological activities under pathogenic conditions. Our experimental result from the present study suggests that CV possesses bacteriostatic as well as the bactericidal effect on *V. cholerae* at MIC. These findings are in accordance with the previous study, although a minor difference in MIC was also observed (Rattanachaikunsopon and Phumkhachorn 2010; Magi

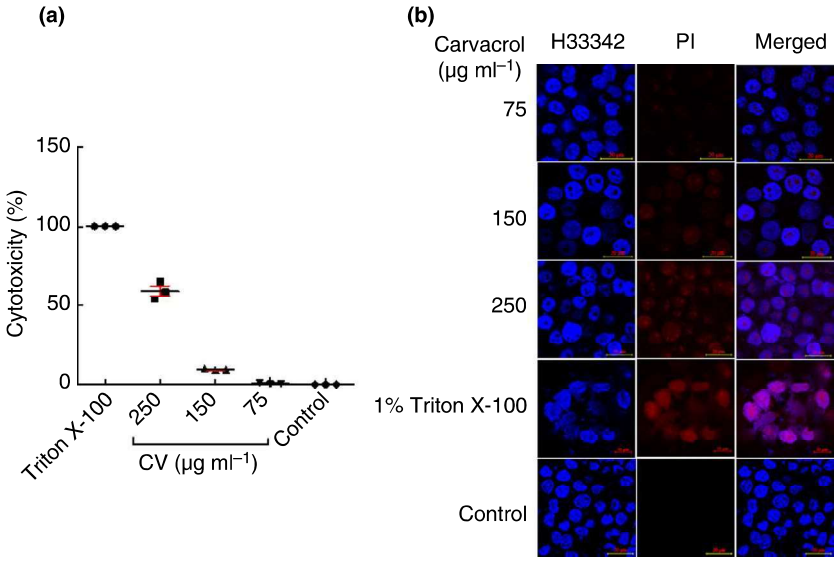

Figure 6 Cytotoxic activity of carvacrol in the HT-29 cell line. (a) The cytotoxic effect of carvacrol at different concentrations was measured by LDH release assay in HT-29 cells and graphically represented as percent cytotoxicity. Triton X-100 treated cell's LDH release as a positive control. (b) Confocal images of HT-29 cells treated with different concentrations of carvacrol. Cells were stained with Hoechst 33342 (Blue) and counter-stained with propidium iodide (Red).

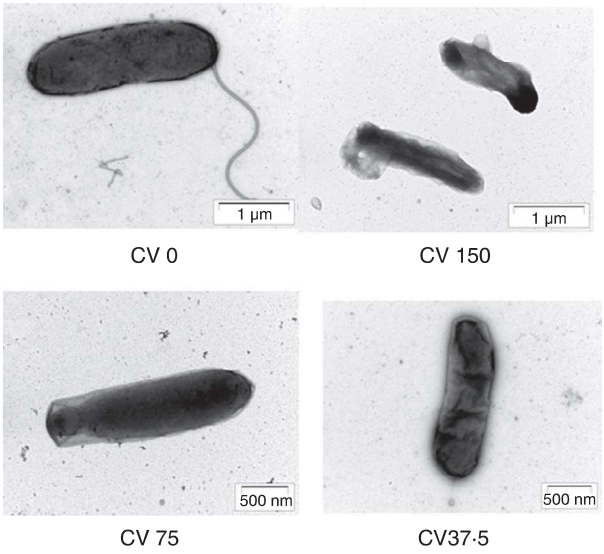

Figure 7 Effect of carvacrol on *Vibrio cholerae* morphology. Transmission electron micrographs of negatively stained *V. cholerae* in the absence and presence of different concentrations of carvacrol.

et al. 2015). To find out the anti-pathogenic role of CV against *V. cholerae*, we determined that ½ MIC is the highest concentration of CV that does not inhibit the growth of *V. cholerae* and it remained viable. Therefore, the concentration of ½ MIC and lower was used to assess the inhibitory effect of carvacrol on the different virulence and pathogenic attributes of *V. cholerae*. We have also ensured that at a particular optical density of CV-treated or -untreated *V. cholerae* cultures possess equal viable bacteria, thereby eliminating the possibility of unfair analysis of the experimental results (Preliminary observation).

Transmission of *V. cholerae* in humans involves the faecal-oral route. After reaching the small intestine, *V. cholerae* need to penetrate through the thick mucus layer to successfully colonize the underlying enterocytes (Jordan *et al.* 1998). We found that CV at sub-MIC inhibited *V. cholerae* mucin penetrating ability in a dose-dependent manner. *Vibrio cholerae* motility and mucin penetration are mediated by the rotation of its monotrichous polar flagellum and is considered as a significant virulence factor for the bacteria (Silva 2003; Mewborn *et al.* 2017). Our findings are also in line with previous studies where various bioactive phyto-chemicals or their derivatives produce anti-virulence effect against different pathogenic micro-organisms by diminishing bacterial motility and flagellar protein expression (Liu *et al.* 2017). It was also previously reported that the polyphenolic fraction of Kombucha was able to inhibit the motility of *V. cholerae* as a result of the disruption in flagellar gene biosynthesis (Bhattacharya *et al.* 2020). Furthermore, two separate studies showed swarming motility of *Pseudomonas aeruginosa* was inhibited by tea polyphenols and cranberry proantocyanidins (O'May and Tufenkji 2011; Yin *et al.* 2015).

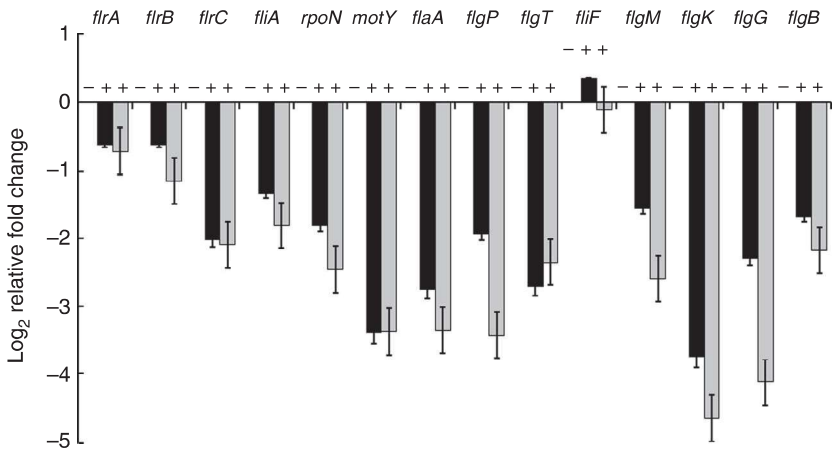

Figure 8 Effect of carvacrol in *Vibrio cholerae* flagellar gene synthesis. Mid-log-phase bacterial cultures in the presence (+) (¼ MIC (37·5 μg ml^{-1}), (□) and ½ MIC (75 μg ml^{-1}) (□)) or absence (–) of carvacrol were subjected to RNA isolation using the TriZol method and mRNA transcript levels were analysed by qRT PCR and graphically represented, using *recA* as an internal control gene. Data showed here as the $\log_2$-transformed values of relative fold change. Each of the experiments was repeated three times (n = 3) and the data were expressed as mean ± SEM.

Transmission electron microscopy reveals that sub-MIC treatment of CV causes *V. cholerae* to become aflagellate, which further explains the rationale behind the reduced motility. RT-PCR results showed that the sub-inhibitory concentrations of CV had a significant ($P < 0·05$) downregulatory effect on *flrC*, which is a cytosolic response regulator and belongs to the Class II flagellar synthesis genes. *flrC* along with the histidine kinase *flrB* regulates the synthesis of Class III flagellar gene which are mostly associated with the synthesis of flagellin proteins as well as the structural units of the flagellar basal body (Klose and Mekalanos 1998; Echazarreta and Klose 2019). We have also found that sub-MIC of CV downregulates the expression of class III genes. These genes primarily include *motY*, *flaA*, *flgP*, *flgT*, *flgK*, *flgG* and *flgB*. Therefore, we speculate CV at sub-MIC inhibits the synthesis of class III genes directly by regulating their expression or by specifically modulating the expression of class II component *flrC*. Although further research is a prerequisite to gain a better insight into this mechanism. The swarming motility and mucin penetrating ability of *V. cholerae* also get inhibited by CV. Therefore, the inability to swim and penetrate the mucin layer can be explained by the absence of flagella.

After penetrating the thick mucus layer, *V. cholerae* adheres to the brush borders of epithelial cells for colonization. We found that CV reduced adherence of *V. cholerae* to the epithelial cells. Although to attain a significant effect under *in vivo* conditions, a higher dose of CV was needed, probably due to the lesser bioavailability. Furthermore, reduced expression of toxin co-regulated pilus A (*tcpA*), one of the major adhesin of *V. cholerae*, might explain the possible reason behind decreased adhesion of *V. cholerae* to the epithelium. After adhering to the intestinal brush border epithelium, *V. cholerae* starts secreting CT. Fluid accumulation as a result of CT production is the primary determinant of cholera pathogenesis. In the rabbit ileal loop model, we have found a significant reduction in fluid accumulation upon CV treatment. This observation also corroborates with earlier works where CV treatment at 60 μg ml^{-1} has been reported to reduce 80% diarrhoeal toxin production by *B. cereus* (Ultee and Smid 2001).

To analyse the inhibitory mechanisms of CV on CT production in *V. cholerae*, quantitative RT-PCR of major virulence genes including *toxT*, *ctxB*, *tcpA* and *hlyA* were performed. In this context, we found a significant decline in all of the virulence genes by more than twofold at sub-MIC. In *V. cholerae*, expression of CT and TCP is activated by the expression of ToxT, the master virulence regulator, which, in turn, is controlled by upstream regulators such as TcpP/TcpH and ToxR/ToxS (Matson *et al.* 2007). Therefore, we assume that the reduction in transcription of *ctxB*, *tcpA* genes upon sub-MIC treatment of CV may be due to the inhibitory effect of CV on *toxT*. Notably, CV might also be involved in the regulation of the transcription of *toxT*, *tcpA*, *ctxB* and *hlyA* by either a direct or an indirect mechanism, although further study regarding the mechanism is needed for a complete understanding of this process.

The phenolic group of CV causes bacterial membrane damage and results in increased membrane fluidity (Weber and De Bont 1996) and loss of protons and bigger ions (Langeveld *et al.* 2013). TEM micrographs

demonstrated that CV at MIC caused severe damage to the surface of *V. cholerae* and altered the bacterial morphology. At sub-MIC, membrane impairment was not noticed but as stated earlier it lacks the presence of flagella. It is evident that CV at MIC causes membrane disruption and affects *V. cholerae* survival and growth, but at sub-MIC *V. cholerae* can retain its membrane integrity and shape. This also supports the previous report where *B. cereus* was found to adapt to the non-lethal concentrations of CV (Ultee *et al.* 2000). Altogether, these data indicated that CV exhibited a dose-dependent virulence inhibitory effect on *V. cholerae*.

Bioactive phytochemicals possess many beneficial effects. Besides these properties, they might also have potential cytotoxic effects on the host cells (Llana-Ruiz-Cabello *et al.* 2015), which is needed to be evaluated. We have tested the cytotoxic activity of CV on the human cell line HT-29 and CV showed minimum membrane damage. Even after 48 h, ½ MIC of CV showed 5·12% cytotoxicity. Therefore, it is expected that the use of CV at sub-MIC may not pose any harm to the human intestinal cells. Fluorescence microscopy also supports this observation. Earlier studies have also suggested that CV is usually nongenotoxic to the living cells (Bakkali *et al.* 2008) and shown to be safe for 24 h on HepG2 cell-line (Palabiyik *et al.* 2016).

In conclusion, the present study shows for the first time that the sub-inhibitory concentrations of CV inhibit growth and virulence in *V. cholerae*. CV treatment suppressed *V. cholerae* flagellar synthesis, thereby inhibiting the bacterial motility through the thick mucus layer followed by reduced adhesion to the intestinal epithelium and finally reduced expression of CT and other virulence-associated genes. These events finally lead to reduced fluid accumulation in the rabbit intestine. To understand the pleiotropic effect of CV on such a wide range of virulence genes, it is possible that CV could act on a global regulator. Repression of the CT production and virulence gene transcription is affected by natural compounds (Hyldgaard *et al.* 2012). One such example includes capsaicin, a red chili extract that reduced the virulence of *V. cholerae* by regulating the expression of *hns* (Yamasaki *et al.* 2011). Future study is needed to identify the global regulator and understand the cascade of the inhibitory mechanism. A previous study demonstrated that the use of CV to be safe for human use and we have also showed that it has a negligible cytotoxic effect at sub-MIC up to 12 h. We have also checked the long exposure of CV to HT-29 cell line and it showed around 5% cytotoxicity at ½ MIC after 48 h (Preliminary observation). The findings of the present study highlight the promising role of CV as a novel anti-virulent compound and can be promoted as a therapeutic agent to treat *V. cholerae* infection.

The findings of the present study highlight the promising role of CV as a novel anti-virulent compound and can be promoted as a therapeutic agent to treat *V. cholerae* infection. Further experiments on the detailed pharmacokinetics relating to human evidence may be worthy of evaluation before CV administration. Although CV has been categorized as a Generally Recognized As Safe (GRAS) compound and approved for safe use (U.S. Food and Drug Administration 1998; Hyldgaard *et al.* 2012), its poor solubility and bioavailability remain a problem (Suntres *et al.* 2015). So, the advancement of the delivery systems needs to be developed in parallel which will improve the solubility, stability and bioavailability of this compound.

Acknowledgements

Our research was supported in part by Japan Initiative for Global Research Network on Infectious Diseases (J-GRID) and from the Ministry of Education, Culture, Sports, Science and Technology in Japan, and Japan Agency for Medical Research and Development (AMED), and Indian Council of Medical Research, Government of India. S. D. was supported by a fellowship from the Indian Council of Medical Research (3/1/3/JRF-2015/HRD-LS/106/60046/56), dated-10/09/15, Government of India.

Author contributions

SD, RC and NSC conceptualized the study. SD, RC, PM, SK, HK and MD performed the experiments. SD, AKM and NSC prepared the original draft of the manuscript. AKM and KO collaborated with this study. All authors did data analysis, draft review, editing and approval.

Conflict of Interest

The authors declare that they have no competing interests.

References

Ahmad, A., Khan, A., Akhtar, F., Yousuf, S., Xess, I., Khan, L.A. and Manzoor, N. (2010) Fungicidal activity of thymol and carvacrol by disrupting ergosterol biosynthesis and membrane integrity against Candida. *Eur J Clin Microbiol Infect Dis* **30**, 41–50.

Ali, M., Nelson, A.R., Lopez, A.L. and Sack, D.A. (2015) Updated global burden of cholera in endemic countries. *PLoS Negl Trop Dis* **9**, e0003832.

van Alphen, L.B., Burt, S.A., Veenendaal, A.K.J., Bleumink-Pluym, N.M.C. and van Putten, J.P.M. (2012) The natural

antimicrobial carvacrol inhibits *Campylobacter jejuni* motility and infection of epithelial cells. *PLoS One* **7**, e45343.

Aminzare, M., Hashemi, M., Abbasi, Z., Mohseni, M. and Amiri, E. (2018) Vibriosis phytotherapy: a review on the most important world medicinal plants effective on Vibrio spp. *J Appl Pharm Sci* **8**, 170–177.

Aristatile, B., Al-Numair, K.S., Veeramani, C. and Pugalendi, K.V. (2009) Effect of carvacrol on hepatic marker enzymes and antioxidant status in d-galactosamine-induced hepatotoxicity in rats. *Fundam Clin Pharmacol* **23**, 757–765.

Arunasree, K.M. (2010) Anti-proliferative effects of carvacrol on a human metastatic breast cancer cell line, MDA-MB 231. *Phytomedicine* **17**, 581–588.

Bagamboula, C.F., Uyttendaele, M. and Debevere, J. (2004) Inhibitory effect of thyme and basil essential oils, carvacrol, thymol, estragol, linalool and p-cymene towards *Shigella sonnei* and *S. flexneri*. *Food Microbiol* **21**, 33–42.

Bakkali, F., Averbeck, S., Averbeck, D. and Idaomar, M. (2008) Biological effects of essential oils – a review. *Food Chem Toxicol* **46**, 446–475.

Bassetti, M., Merelli, M., Temperoni, C. and Astilean, A. (2013) New antibiotics for bad bugs: where are we? *Ann Clin Microbiol Antimicrob* **12**, 22.

Bhattacharya, D., Sinha, R., Mukherjee, P., Howlader, D.R., Nag, D., Sarkar, S., Koley, H., Withey, J.H. *et al.* (2020) Anti-virulence activity of polyphenolic fraction isolated from Kombucha against *Vibrio cholerae*. *Microb Pathog* **140**, 103927.

Burt, S. (2004) Essential oils: their antibacterial properties and potential applications in foods—a review. *Int J Food Microbiol* **94**, 223–253.

Chourashi, R., Mondal, M., Sinha, R., Debnath, A., Das, S., Koley, H. and Chatterjee, N.S. (2016) Role of a sensor histidine kinase ChiS of *Vibrio cholerae* in pathogenesis. *Int J Med Microbiol* **306**, 657–665.

Clinical and Laboratory Standards Institute. (2012) Methods for Dilution Antimicrobial Susceptibility Tests for Bacteria That Grow Aerobically; Approved Standard—Ninth Edition, pp. 1–68, Vol. **32**, M07-A9. Wayne, PA: Clinical and Laboratory Standards Institute. www.clsi.org

Das, B., Verma, J., Kumar, P., Ghosh, A. and Ramamurthy, T. (2020) Antibiotic resistance in *Vibrio cholerae*: understanding the ecology of resistance genes and mechanisms. *Vaccine* **38**, 83–92.

Das, S., Chourashi, R., Mukherjee, P., Gope, A., Koley, H., Dutta, M., Mukhopadhyay, A.K., Okamoto, K. *et al.* (2020) Multifunctional transcription factor CytR of *Vibrio cholerae* is important for pathogenesis. *Microbiology* **166**, 1136–1148.

De, K., Ramamurthy, T., Faruque, S.M., Yamasaki, S., Takeda, Y., Nair, G.B. and Nandy, R.K. (2004) Molecular characterisation of rough strains of *Vibrio cholera* isolated from diarrhoeal cases in India and their comparison to smooth strains. *FEMS Microbiol Lett* **232**, 23–30.

Duncan, M.C., Forbes, J.C., Nguyen, Y., Shull, L.M., Gillette, R.K., Lazinski, D.W., Ali, A., Shanks, R.M.Q. *et al.* (2018) *Vibrio cholerae* motility exerts drag force to impede attack by the bacterial predator *Bdellovibrio bacteriovorus*. *Nat Commun* **9**(1), 1–9.

Dwidar, M., Monnappa, A.K. and Mitchell, R.J. (2012) The dual probiotic and antibiotic nature of *Bdellovibrio bacteriovorus*. *BMB Rep* **45**, 71–78.

Echazarreta, M.A. and Klose, K.E. (2019) Vibrio flagellar synthesis. *Front Cell Infect Microbiol* **9**, 1–11.

Helander, I.M., Alakomi, H.-L., Latva-Kala, K., Mattila-Sandholm, T., Pol, I., Smid, E.J., Gorris, L.G.M. and von Wright, A. (1998) Characterization of the action of selected essential oil components on gram-negative bacteria. *J Agric Food Chem* **46**, 3590–3595.

Holmgren, J. (1973) Comparison of the tissue receptors for *Vibrio cholerae* and *Escherichia coli* enterotoxins by means of gangliosides and natural cholera toxoid. *Infect Immun* **8**, 851–859.

Hotta, M., Nakata, R., Katsukawa, M., Hori, K., Takahashi, S. and Inoue, H. (2009) Carvacrol, a component of thyme oil, activates PPARα and γ and suppresses COX-2 expression. *J Lipid Res* **51**, 132–139.

Hung, D.T. (2005) Small-molecule inhibitor of *Vibrio cholerae* virulence and intestinal colonization. *Science* **310**, 670–674.

Hyldgaard, M., Mygind, T. and Meyer, R.L. (2012) Essential oils in food preservation: mode of action, synergies, and interactions with food matrix componetns. *Front Microbiol* **3**, 1–24.

Jordan, N., Newton, J., Pearson, J. and Allen, A. (1998) A novel method for the visualization of the in situ mucus layer in rat and man. *Clin Sci* **95**, 97.

Kaper, J.B., Morris, J.G. and Levine, M.M. (1995) Cholera. *Clin Microbiol Rev* **8**, 48–86.

Kitaoka, M., Miyata, S.T., Unterweger, D. and Pukatzki, S. (2011) Antibiotic resistance mechanisms of *Vibrio cholerae*. *J Med Microbiol* **60**, 397–407.

Klose, K.E. and Mekalanos, J.J. (1998) Distinct roles of an alternative sigma factor during both free-swimming and colonizing phases of the *Vibrio cholerae* pathogenic cycle. *Mol Microbiol* **28**, 501–520.

Landa, P., Kokoska, L., Pribylova, M., Vanek, T. and Marsik, P. (2009) In vitro anti-inflammatory activity of carvacrol: inhibitory effect on COX-2 catalyzed prostaglandin E2 biosynthesisb. *Arch Pharm Res* **32**, 75–78.

Langeveld, W.T., Veldhuizen, E.J.A. and Burt, S.A. (2013) Synergy between essential oil components and antibiotics: a review. *Crit Rev Microbiol* **40**, 76–94.

Liu, Y., McKeever, L.C. and Malik, N.S.A. (2017) Assessment of the antimicrobial activity of olive leaf extract against foodborne bacterial pathogens. *Front Microbiol* **8**, 1–8.

Liu, Z., Miyashiro, T., Tsou, A., Hsiao, A., Goulian, M. and Zhu, J. (2008) Mucosal penetration primes *Vibrio cholerae* for host colonization by repressing quorum sensing. *Proc Natl Acad Sci USA* **105**, 9769–9774.

Livak, K.J. and Schmittgen, T.D. (2001) Analysis of relative gene expression data using real-time quantitative PCR and the 2−ΔΔCT Method. *Methods* **25**, 402–408.

Llana-Ruiz-Cabello, M., Pichardo, S., Maisanaba, S., Puerto, M., Prieto, A.I., Gutiérrez-Praena, D., Jos, A. and Cameán, A.M. (2015) In vitro toxicological evaluation of essential oils and their main compounds used in active food packaging: a review. *Food Chem Toxicol* **81**, 9–27.

Magi, G., Marini, E. and Facinelli, B. (2015) Antimicrobial activity of essential oils and carvacrol, and synergy of carvacrol and erythromycin, against clinical, erythromycin-resistant Group A Streptococci. *Front Microbiol* **6**, 1–7.

Magina, M.D.A., Dalmarco, E.M., Wisniewski, A., Simionatto, E.L., Dalmarco, J.B., Pizzolatti, M.G. and Brighente, I.M.C. (2009) Chemical composition and antibacterial activity of essential oils of Eugenia species. *J Nat Med* **63**, 345–350.

Matson, J.S., Withey, J.H. and DiRita, V.J. (2007) Regulatory networks controlling *Vibrio cholerae* virulence gene expression. *Infect Immun* **75**, 5542–5549.

Mewborn, L., Benitez, J.A. and Silva, A.J. (2017) Flagellar motility, extracellular proteases and *Vibrio cholerae* detachment from abiotic and biotic surfaces. *Microb Pathogenesis* **113**, 17–24.

Miladi, H., Zmantar, T., Chaabouni, Y., Fedhila, K., Bakhrouf, A., Mahdouani, K. and Chaieb, K. (2016) Antibacterial and efflux pump inhibitors of thymol and carvacrol against food-borne pathogens. *Microb Pathogenesis* **99**, 95–100.

Mondal, M., Nag, D., Koley, H., Saha, D.R. and Chatterjee, N.S. (2014) The *Vibrio cholerae* extracellular chitinase ChiA2 is important for survival and pathogenesis in the host intestine. *PLoS One* **9**, e103119.

Mooyottu, S., Kollanoor-Johny, A., Flock, G., Bouillaut, L., Upadhyay, A., Sonenshein, A. and Venkitanarayanan, K. (2014) Carvacrol and trans-cinnamaldehyde reduce *Clostridium difficile* toxin production and cytotoxicity in vitro. *Int J Mol Sci* **15**, 4415–4430.

Narendrakumar, L., Gupta, S.S., Johnson, J.B., Ramamurthy, T. and Thomas, S. (2019) Molecular adaptations and antibiotic resistance in *Vibrio cholerae*: a communal challenge. *Microb Drug Resist* **25**, 1012–1022.

Nostro, A., Marino, A., Blanco, A.R., Cellini, L., Di Giulio, M., Pizzimenti, F., Roccaro, A.S. and Bisignano, G. (2009) In vitro activity of carvacrol against staphylococcal preformed biofilm by liquid and vapour contact. *J Med Microbiol* **58**, 791–797.

O'May, C. and Tufenkji, N. (2011) The swarming motility of *Pseudomonas aeruginosa* is blocked by cranberry proanthocyanidins and other tannin-containing materials. *Appl Environ Microb* **77**, 3061–3067.

Obaidat, M.M. and Frank, J.F. (2009) Inactivation of *Escherichia coli* O157:H7 on the intact and damaged portions of lettuce and spinach leaves by using allyl isothiocyanate, carvacrol, and cinnamaldehyde in vapor phase. *J Food Protect* **72**, 2046–2055.

Palabiyik, S., Karakus, E., Halici, Z., Cadirci, E., Bayir, Y., Ayaz, G. and Cinar, I. (2016) The protective effects of carvacrol and thymol against paracetamol-induced toxicity on human hepatocellular carcinoma cell lines (HepG2). *Hum Exp Toxicol* **35**, 1252–1263.

Patra,T.,Koley,H.,Ramamurthy,T.,Ghose,A.C.andNandy,R.K. (2012)TheEntner-Doudoroffpathwayisobligatoryfor gluconateutilizationandcontributestothepathogenicityof *Vibriocholerae.JBacteriol***194**,3377–3385.

Perez-Conesa, D., Cao, J., Chen, L., McLandsborough, L. and Weiss, J. (2011) Inactivation of *Listeria monocytogenes* and *Escherichia coli* O157:H7 biofilms by micelle-encapsulated eugenol and carvacrol. *J Food Protect* **74**, 55–62.

Rattanachaikunsopon, P. and Phumkhachorn, P. (2010) Assessment of factors influencing antimicrobial activity of carvacrol and cymene against *Vibrio cholerae* in food. *J Biosci Bioeng* **110**, 614–619.

Saha, P., Das, B. and Chaudhuri, K. (2013) Role of 6-gingerol in reduction of cholera toxin activity in vitro and in vivo. *Antimicrob Agents Chemother* **57**, 4373–4380.

Sarwar, S., Ali, A., Pal, M. and Chakrabarti, P. (2017) Zinc oxide nanoparticles provide anti-cholera activity by disrupting the interaction of cholera toxin with the human GM1 receptor. *J Biol Chem* **292**, 18303–18311.

Shakhnovich, E.A., Hung, D.T., Pierson, E., Lee, K. and Mekalanos, J.J. (2007) Virstatin inhibits dimerization of the transcriptional activator ToxT. *Proc Natl Acad Sci USA* **104**, 2372–2377.

Sharifi-Rad, M., Varoni, E.M., Iriti, M., Martorell, M., Setzer, W.N., del Mar Contreras, M., Salehi, B., Soltani-Nejad, A. *et al.* (2018) Carvacrol and human health: a comprehensive review. *Phytother Res* **32**, 1675–1687.

Silva, A.J. (2003) Haemagglutinin/protease expression and mucin gel penetration in El Tor biotype *Vibrio cholerae*. *Microbiology* **149**, 1883–1891.

Slameňová, D., Horváthová, E., Šramková, M. and Maršálková, L. (2007) DNA-protective effects of two components of essential plant oils carvacrol and thymol on mammalian cells cultured in vitro. *Neoplasma* **54**, 108–112.

Slamenova, D., Horvathova, E., Marsalkova, L. and Wsolova, L. (2008). Carvacrol given to rats in drinking water reduces the level of DNA lesions induced in freshly isolated hepatocytes and testicular cells by H_2O_2. *Neoplasma*, **55**, 394.

Suntres, Z.E., Coccimiglio, J. and Alipour, M. (2015) The bioactivity and toxicological actions of carvacrol. *Crit Rev Food Sci* **55**, 304–318.

U.S. Food and Drug Administration (1998). EAFUS: a food additive database. pp. 1–153. http://www.usc.es/caa/EdulcWeb/EAFUS

Ultee, A., Kets, E.P.W. and Smid, E.J. (1999) Mechanisms of action of carvacrol on the food-borne pathogen *Bacillus cereus*. *Appl Environ Microb* **65**, 4606–4610.

Ultee, A., Kets, E.P.W., Alberda, M., Hoekstra, F.A. and Smid, E.J. (2000) Adaptation of the food-borne pathogen *Bacillus cereus* to carvacrol. *Arch Microbiol* **174**, 233–238.

Ultee, A. and Smid, E.J. (2001) Influence of carvacrol on growth and toxin production by *Bacillus cereus*. *Int J Food Microbiol* **64**, 373–378.

Verma, J., Bag, S., Saha, B., Kumar, P., Ghosh, T.S., Dayal, M., Senapati, T., Mehra, S. *et al.* (2019) Genomic plasticity associated with antimicrobial resistance in *Vibrio cholerae*. *Proc Natl Acad Sci USA* **116**, 6226–6231.

Weber, F.J. and de Bont, J.A.M. (1996). Adaptation mechanisms of microorganisms to the toxic effects of organic solvents on membranes. *Biochimica et Biophysica Acta (BBA) – Reviews on Biomembranes* **1286**, 225–245.

World Health Organization (2019). Weekly epidemiological record – cholera 2018. pp. 561–580. https://www.who.int/wer/2019/wer9448

Yamasaki, S., Asakura, M., Neogi, S.B., Hinenoya, A., Iwaoka, E. and Aoki, S. (2011) Inhibition of virulence potential of *Vibrio cholerae* by natural compounds. *Indian J Med Res* **133**, 232–239.

Yeung, A.T.Y., Parayno A. and Hancock, R.E.W. (2012) Mucin promotes rapid surface motility in Pseudomonas aeruginosa. *mBio* **3**(3), 1–12.

Yin, H., Deng, Y., Wang, H., Liu, W., Zhuang, X. and Chu, W. (2015) Tea polyphenols as an antivirulence compound disrupt quorum-sensing regulated pathogenicity of *Pseudomonas aeruginosa*. *Sci Rep UK* **5**, 1–11.

Supporting Information

Additional Supporting Information may be found in the online version of this article:

Figure S1. Effect of carvacrol on cholera toxin (CT) production and virulence gene expression.

Table S1. List of primers used in quantitative real time PCR experiment.